UNIVERSITY OF LEEDS

Seasonal prediction of wind and solar PV generation in India during the western summer monsoon

James Norman

Submitted in accordance with the requirements for the degree of Doctor of Philosophy

The University of Leeds

School of Earth and Environment

April 2024

Declaration

I confirm that the work submitted is my own, except where work which has formed part of jointly authored publications has been included. My contribution and the other authors to this work has been explicitly indicated below. I confirm that appropriate credit has been given within the thesis where reference has been made to the work of others.

The first and fourth results chapters form the basis for a paper that has already been peer reviewed and published. Content from the second and third results chapters is being prepared in a manuscript for submission to a suitable journal.

Work from the publication Norman, J., Maycock, A.C., Troccoli, A. and Dessai, S., 2024. The role of repowering India's ageing wind farms in achieving net-zero ambitions. Environmental Research Letters, 19(3), p.034031. DOI 10.1088/1748-9326/ad28db is included in the first and fourth results chapters. The text of the publication was solely written by James Norman, with comments from co-authors. The candidate performed the data analysis and produced all the figures. A.C. Maycock, A. Troccoli and S., Dessai contributed to the interpretation of the results.

Abstract

India's ambitious net-zero climate goals include plans for significant increases in wind and solar photovoltaic (PV) energy generation by 2030. Despite the importance of these two sources in India's future energy mix, few studies have estimated the magnitude of interannual generation variability that results from such expansion. Furthermore, there is little understanding of the meteorological drivers of wind and solar PV generation on seasonal timescales, nor any documented attempts to use dynamical seasonal forecasts to predict seasonal generation anomalies.

This thesis explores interannual variability in India's wind and solar PV generation, focusing on the summer monsoon season (June, July, August, and September). An atmospheric reanalysis is used to create synthetic wind and solar PV generation time series for India to study variability. And data outputs from a seasonal forecasting system are used to test seasonal generation predictions for wind and solar PV.

The generation timeseries wind and solar PV were found to be an accurate means of representing observed generation variability on a range of timescales. Relationships between anomalies in the multi-decadal generation syntheses and meteorological drivers were investigated. The western North Pacific Monsoon and Indian summer monsoon circulations were found to be responsible for the majority of observed interannual variability in wind and solar PV generation in summer, respectively. Skilful forecasts of summer season wind and solar PV generation at a one-month lead time are possible using seasonal climate forecasts initialised in May.

The generation syntheses were found to be sensitive to the technology parameterisations of wind turbines and solar arrays. Additional generation syntheses that used state-of-the-art turbine and solar array parameterisations appreciably increased the capacity factors of both technologies when rolled out nationwide. This suggests that less installed capacity is required to achieve specific generation outcomes than previously estimated.

Publications

The research in chapters 4, and 7 of this thesis has been published in the article:

Norman, J., Maycock, A.C., Troccoli, A. and Dessai, S., 2024. The role of repowering India's ageing wind farms in achieving net-zero ambitions. *Environmental Research Letters* DOI 10.1088/1748-9326/ad28db.

Acknowledgements

Firstly, I would like to thank my supervisors, Amanda Maycock, Suraje Dessai, Alberto Troccoli, and Marta Bruno Soares. Over the course of my PhD project, their advice, input, and guidance have been greatly appreciated. I certainly could not have learned or achieved as much without them.

Secondly, many thanks to my family for supporting me throughout a long PhD process, not least Andrea and Nico, who were always there for me.

And numerous additional thanks (too many to list here) are required to friends, co-workers, workshop attendees, anonymous manuscript reviewers, and open data initiatives!

Contents

Chapter 1

Introduction

1.1 Motivation

Climate change mitigation efforts rely on significant and timely reductions of greenhouse gas emissions (GHG) from the energy sector (Riahi, Schaeffer, et al., 2022). The growth of renewable energy sources within the energy supply mix is a crucial source of mitigation potential (Clarke et al., 2022). Recent assessments of viable technology pathways toward ambitious climate goals have highlighted the importance of wind and solar photovoltaic (PV) technologies in achieving rapid and deep decarbonisation of energy supply (Clarke et al., 2022).

Of the hundreds of technology pathways that keep end-of-century global average temperature increases to below 2°C above preindustrial levels, considered as part of the 6th Assessment Report (AR6) of the Intergovernmental Panel on Climate Change (IPCC), the median value of global electrical energy supplied by wind and solar PV technologies is 59% in the year 2050 (10th-90th percentile range is 28 to 87%, Clarke et al. (2022). This amount of generation from wind and solar PV would require an approximate fourteen-fold increase in current generation levels globally from the two sources (IRENA, 2023a).

Although this level of scale-up is unprecedented, recent trends within the energy sector underscore the favourability of wind and solar PV technologies and their anticipated dominance within new power installations for the coming decades (Pan et al., 2021). Most notable are the sustained cost reductions of these two technologies, some 88% and 68% in the past ten years for utility-scale solar PV and onshore wind (IRENA, 2022), respectively, meaning both technologies offer cheaper generation than conventional power sources in many regions. Furthermore, ancillary technologies that support wind and solar PV, namely battery storage technologies and electrified end-use technologies (e.g. electric vehicles), have also seen significant cost reductions. Although the rate of recent wind and solar PV installations tracks below the trajectories re-

quired in ambitions decarbonisation pathways, these two technologies dominate recent growth in the power sector, registering record deployment in 2023, and are anticipated to account for 95% of renewable capacity additions globally in the coming five years (IEA, 2023).

Large-scale expansion of weather-dependent wind and solar energy generation presents integration challenges for existing electricity networks and power markets, as these systems are primarily designed to accommodate controllable sources of energy, such as natural gas and coal (Hill et al., 2012). To successfully integrate wind and solar energy sources, their variable and weather-dependent output must be managed to reliably meet the demand for electrical power while avoiding curtailment of excess generation and minimising system costs (Sims et al., 2011). Without successful integration, the cost of transitioning to a low-carbon energy system will increase, and the rate and extent of change will slow (Clarke et al., 2022).

Numerous technological solutions exist or have been proposed for integrating very high shares of wind and solar capacity into energy systems (Bistline, 2021), and multiple studies have demonstrated the technical feasibility of high-share renewable energy systems that use such technologies (e.g., Hansen et al., 2019). However, much of this work has focussed on managing variability in generation over short timescales, particularly rapid demand ramps and diurnal mismatches between energy supply and demand, with substantially fewer studies addressing prolonged periods of generation surplus and/or deficit (Denholm and Mai, 2019). Furthermore, existing variability studies are limited in geographical scope (primarily focussed on countries or regions with historically large shares of wind and/or solar PV capacity) and rarely validate model-based estimates of generation or correct for known biases in meteorological input data (e.g., Staffell and Pfenninger, 2016). Furthermore, existing works typically consider ad-hoc, hypothetical modifications to power systems or future deployment based on an arbitrary scaling of current capacity and technologies rather than spatially explicit scenarios founded on the planned development of existing systems, subject to physical constraints and technology trends (e.g., Jerez et al., 2015; Ryberg et al., 2019).

As the likelihood of prolonged periods of generation surplus and deficit increase at greater levels of wind and solar deployment, so too does the need to characterise and anticipate variability in generation on longer timescales. Quantifying long-duration variability in generation, in the order of weeks to seasons, will inform the strategic design of the power system, such as the required scale of controllable generation, demand-side response and energy storage (Bistline

et al., 2021). Additionally, the ability to anticipate variability in generation over these longer timescales will enable operational measures necessary for ensuring security of supply in the power system, such as the availability and scheduling of controllable generation and storage (Troccoli, 2018).

In this thesis, India is chosen as a highly relevant country case study. India became the world's most populous country in spring of 2023 (UN-DESA, 2023) and is anticipated to become the third-largest economy by 2030 (IMF, 2020). Such growth could double per capita energy use in India and drive the largest increase in energy needs of any country globally over the next decade (IEA, 2022a). Already the third-largest GHG emitter globally (Gütschow et al., 2021), the rate and scale at which India shifts to low-carbon energy supply will significantly affect the success of global climate change mitigation goals.

India's ambitious climate goals, namely reaching net-zero emissions by 2070 and meeting half of its electricity requirements from renewable energy sources by 2030, indicate the political support for meeting much of the increased energy demand with low-carbon technologies, notably wind and solar PV technologies. The scale of this ambition for wind and solar, as stated within the National Electricity Plan of India (NEP), is 121GW of wind and 365GW of solar PV by 2032 (PIB, 2023a). These figures would see wind and solar PV constitute 54% of nationwide power capacity in 2032, providing 30% of all electrical energy needs. Anticipating how these energy sources perform within India's monsoonal climate will be of great importance for the national and global energy transition.

Within this Indian context, existing studies of wind and solar PV generation variability are lacking in several regards:

1. A lack of long-term observed generation data from wind and solar PV sources and detailed farm-specific technical and location data.
2. Limited understanding of meteorological drivers of wind and solar PV generation variability in India.
3. No known applications of seasonal climate predictions within a wind or solar PV generation context in India.

The investigation presented in this thesis offers original contributions to the academic literature that address each of the three limitations identified above. Firstly, this thesis presents the first

known example of a validated synthetic generation timeseries for wind and solar PV generation in India using an atmospheric reanalysis and a detailed description of existing wind and solar farms. Previous studies in this field lack adequate characterisation of existing wind and solar PV technologies and avoid validation against observed generation to correct for known biases in meteorological input data (e.g., Deshmukh et al., 2019; Gulagi et al., 2022).

Existing studies offer a degree of insight into wind and solar PV generation variability over a range of timescales, e.g., high frequency (Palchak et al., 2017), diurnal (Gangopadhyay et al., 2023), intraseasonal (Dunning et al., 2015), and seasonal cycle (Hunt and Bloomfield, 2023). However, treatment of interannual variability remains limited. This thesis offers the first detailed characterisation of interannual variability and associated meteorological drivers of wind and solar PV generation focusing on the Indian summer monsoon season.

Thirdly, despite the long pedigree of seasonal climate forecasting (SCF) in South Asia, with much attention devoted to Indian summer monsoon rainfall, little work considers SCF applications to energy generation in India. At the time of writing, just a single article exists in the academic peer-reviewed literature, which provides a cursory indication of forecast skill in area-averaged values of energy-relevant variables (Das and Baidya Roy, 2021). This thesis offers a considerable extension to existing work by demonstrating the use of generation syntheses for wind and solar PV in India to calibrate SCFs of relevant predictor variables and yield skilful generation forecasts.

1.2 Aims and Objectives

The principal aim of this thesis is:

Identify the driver(s) of interannual variability in wind and solar PV generation in India during the summer monsoon season and test the ability to skilfully forecast anomalous generation in this season based on the outputs of a dynamical SCF system.

Several separate objectives underpin the fulfilment of this overarching aim, as set out below (with corresponding Results Chapter numbers in brackets).

1. Develop a model synthesis of wind and solar PV generation in India that includes geolocated farms and technology characteristics that can be calibrated with observed generation

data (4).

2. Characterise and quantify the impact of meteorological drivers on wind and solar PV generation variability in boreal summer (5).

3. Test the predictability of wind and solar PV generation at a one-month lead time based on an operational SCF system (6).

4. Test the sensitivity of the wind and solar generation synthesis for India to technological parameterisations and future deployment scenarios (7).

Findings from each of the results Chapters are interlinked, with these links highlighted within each Results Chapter's summary section. The fulfilment of these four objectives contributes to the relatively limited literature on the influence of weather and climate variability on energy systems in India. Furthermore, the analysis in this thesis provides methodologies, guidance, and insights relevant to the operational, planning, and strategic requirements of existing and future electricity systems.

1.3 Thesis structure

The investigation documented in this thesis is laid out as follows:

- Chapter 2 presents a Background Literature review covering the role of wind and solar PV in global and Indian mitigation efforts, integration challenges of high renewable shares, and existing energy meteorology work relevant to the Indian case.

- Chapter 3 details the Data and Methods used in each of the four results chapters. These include a description of input datasets and the method used to create a wind and solar PV generation timeseries for India used in Chapter 4. Next, is a description of the climate datasets and techniques used to describe meteorological drivers of interannual variability in the boreal summer season (Chapter 5). The description of relevant data methods for Chapter 6 covers the SCF system, hindcast dataset, statistical downscaling methods and verification metrics. And finally, a description of future scenario data used in Chapter 7.

- Chapter 4 provides an exposition of the generation syntheses performance, key sensitivities, and the annual and interannual variability profiles.

- Chapter 5 explores meteorological drivers of wind and solar PV generation variability, with

a particular focus on the boreal summer season (months of July to September inclusive).

- Chapter 6 tests the performance of various candidate climate predictor variables for generation anomalies and tests their representation within a SCF system using a range of verification metrics.
- Chapter 7 further investigates sensitivities of the generation synthesis in terms of technological parametrisations and near-term capacity deployment.
- Finally, Chapter 8 review the main findings of the investigation, offers a critical reflection on the wider implications for the Indian energy system, and provides suggestions for future work.

Chapter 2

Background Literature

This review of the current literature begins with a top-down view of climate action and the implications for energy sector transition, beginning at a global level and then down to the level of India.

2.1 Global climate action

In December 2015, the Paris Climate Change Agreement was adopted by parties to the United Nations Framework Convention on Climate Change (UNFCCC) at the 21st Conference of Parties (COP). The main aim of the Paris Agreement is to limit "the increase in the global average temperature to well below 2°C above pre-industrial levels and to pursue efforts to limit the temperature increase to 1.5°C above pre-industrial levels" (UNFCCC, 2015). Ultimately, this aim upholds the overarching objective of the UNFCCC, to "prevent dangerous anthropogenic interference with the climate system" (UNFCCC, 1992). The climate targets specified in the Paris Agreement result from over two decades of political dialogue, informed by multiple coordinated syntheses of the scientific literature. The 2°C warming target gained widespread acceptance at previous COP sessions in Copenhagen (COP-15) and Cancun (COP-16), becoming recognised as a 'guard-rail' to prevent dangerous interference with the climate system (UNFCCC, 2010).

Recent evidence shows that adherence to specific global warming targets implies a corresponding finite carbon budget (Gillett et al., 2013; Canadell et al., 2021). Although estimates of how the climate responds to cumulative carbon emissions are subject to uncertainty, the coordinated syntheses of the scientific literature in the Sixth Assessment Report (AR6) of the Intergovernmental Panel on Climate Change (IPCC) is unequivocal about the need for a net zero emissions rate in order to meet a specified global warming limit (N.B. net-zero emissions refers to the situation where anthropogenic carbon dioxide (CO_2) emissions are equal to or less than anthropogenic CO_2 removals).

For a given carbon budget, there exist numerous possible annual emission rate trajectories towards net zero emissions. The necessary socioeconomic and technological changes consistent with these emission trajectories have been extensively explored by model-based studies, most notably, the Integrated Assessment Model (IAM) simulations, which contributed to AR5 and AR6 (Clarke et al., 2014), as well as the IPCC Special Report on 1.5°C (Rogelj et al., 2015; Van Vuuren et al., 2018). Although other model and non-model-based approaches to defining decarbonisation strategies exist, only IAMs provide the global scope and detailed treatment of emission categories to provide the necessary information for an assessment of the net global warming effect of future transitions (Riahi, Schaeffer, et al., 2022). As tools for informing climate policy, IAMs and the 'decarbonisation pathways' they produce have gained prominence in recent years (CarbonBrief, 2015; Van Beek et al., 2020; IPCC, 2022) and have been fundamental in shaping global climate policy by providing "politically powerful visions of actionable futures" (Beck and Mahony (2018), p.1). The following section reviews the role of two key technologies within decarbonisation pathways: wind and solar photovoltaics (PV).

2.2 The role of wind and solar PV technologies

Common features of decarbonisation pathways consistent with an end-of-century global warming outcome of less than 2°C above pre-industrial levels include improved energy efficiency, electrification of the energy system, decarbonisation of energy supply and, in numerous cases, the use of carbon dioxide removal (CDR) technologies (e.g. carbon capture and storage, Luderer et al., 2022). Figure 2.1 shows some of these key features at the global level across 1202[1] decarbonisation pathways in the Working Group III database (Byers et al., 2022) collated as part of the AR6 (Riahi, Schaeffer, et al., 2022), and are categorised into eight categories of end-of-21st century climate response.

Though much diversity exists regarding the exact combination of supply and demand-side technologies, Figure 2.1a shows how renewable technologies, including wind, solar PV, concentrated solar, hydropower and biomass with CCS, generally feature significantly across low-warming pathways. The median share of renewables in primary energy reaches 53% by 2050. Specific to wind and solar PV technologies, pathways consistent with a global average temperature change of likely below 2°C generally involve greater amounts of each technology, with the median value

[1]The 1202 pathways that have sufficient emissions species and projection timeframe to be considered for climate assessment with climate response emulators.

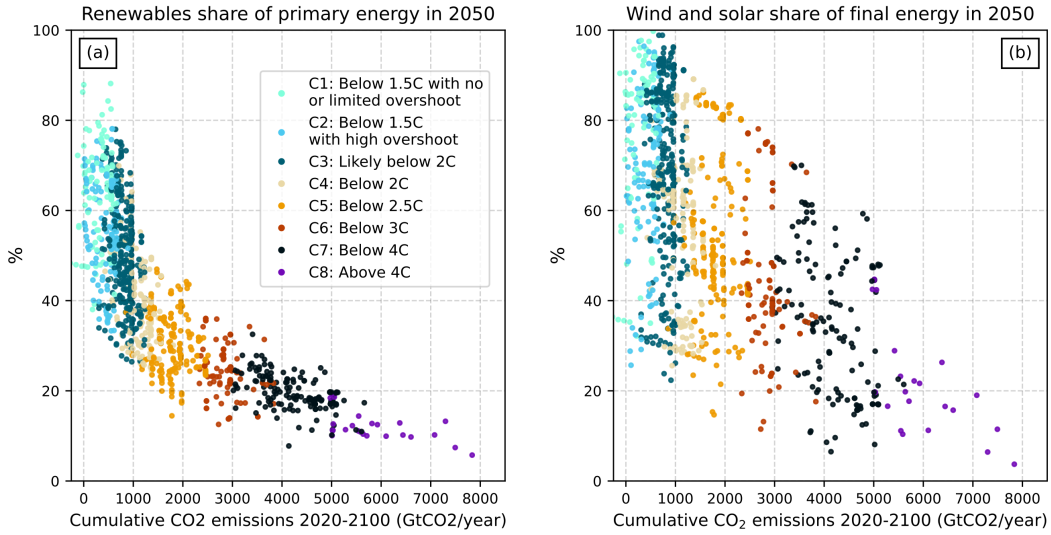

Figure 2.1: IPCC AR6 decarbonisation pathway (n=1202) data, where each point represents a single pathway, coloured by end-of-21st century warming outcome (see inset in panel (a) for colouring key). Panels a and b show selected results as a function of cumulative CO2 emissions for the period 2020 to 2100: (a) total primary energy supply from renewable sources (wind, solar, biomass, hydro, geothermal) as a percentage of total primary energy supply in 2050; and (b) final energy from wind and solar PV and a percentage of total final energy demand in 2050.

of the wind and solar PV share in final energy at 59% in 2050 (Figure 2.1b).

All levels of generation sourced from wind and solar PV in pathways consistent with global average temperature change of likely below 2°C mark a significant increase over present-day levels. The magnitude of these increases for selected countries is shown in Table 2.1, where recent historical generation from wind and solar PV are compared to equivalent IPCC AR6 pathway data. A factor five scale-up for wind and factor-ten scale up for solar PV is common across most countries with already sizable renewables deployment (e.g., United States, China, and the European Union).

The investigation takes a specific focus on wind and solar PV technologies and the country case of India. The following section provides a brief overview of India's national climate policy development, the domestic wind and solar PV deployment status, and the possible outlooks for these two technologies.

2.3 The Indian case

India currently has the third-largest annual greenhouse gas (GHG) emissions, after China and the United States, and is in third place globally for cumulative historical emissions with a

	Wind generation (TWh)			Solar PV generation (TWh)		
Country	2021	2050	Scale up factor	2021	2050	Scale up factor
China	657	3613	5	328	3028	9
European Union	469	1960	4	170	1301	8
United States	383	2185	6	148	1584	11
India	63	1907	30	66	1855	28
Japan	9.4	228	24	86	160	2
Brazil	72	320	4	17	135	8
Canada	35	254	7	6	131	22
Mexico	21	188	9	20	174	9
South Korea	3	169	56	23	154	7
South Africa	0.3	157	523	7	97	14
Russia	3	241	80	1	216	216
Indonesia	0.01	112	11200	0.2	307	1535

Table 2.1: Generation from wind and solar PV in 2021 (IRENA, 2023a) for selected countries and median values for equivalent IPCC AR6 pathway data in end-of-21st century warming outcomes of 2°C and below, by the year 2050.

share estimated at 7-8% (Gütschow et al., 2021). At COP26, held in Glasgow October 2021, Prime Minister Narendra Modi announced a package of climate pledges, most notably a net-zero emissions target by 2070, sourcing 50% of energy from renewable sources by 2030, and a non-fossil fuel energy capacity of 500 GW by 2030, the majority of which would come from wind and solar PV (ASPI, 2022). The pledges were reiterated within an updated Nationally Determined Contribution (NDC) submission at COP27 (MoEFCC, 2022). And in 2023, updated National Electricity Plan of India (NEP) proposes 121GW (258TWh) of wind and 365GW (658TWh) of solar PV by 2032 (together ∼90% of the 500GW target) (PIB, 2023a). The NEP figures mark a three-fold increase in wind capacity (40.8GW) and six-fold increase in solar PV capacity (57.7GW) compared to total installed capacity in 2022 (CEA, 2023).

Figure 2.2 compares historical wind and solar PV generation in India and AR6 data for pathways that achieve end-of-21st-century warming outcomes of 2°C and below. The NEP targets for 2032 fall in the middle of the range of AR6 pathways for solar PV generation and at approximately the 25th percentile for wind. Recent rates of increase in generation sourced from wind and solar require a boost to meet the NEP targets. However, a new Renewables Purchasing Obligation (RPO) that obliges Indian states to meet a certain percentage of electricity requirements through specific renewable sources, and a large tendering schedule for renewable energy projects indicates that the NEP targets for 2032 will likely be fulfilled (PIB, 2023a).

So far, this Chapter has made the case for rapid and deep reductions in GHG emissions, pri-

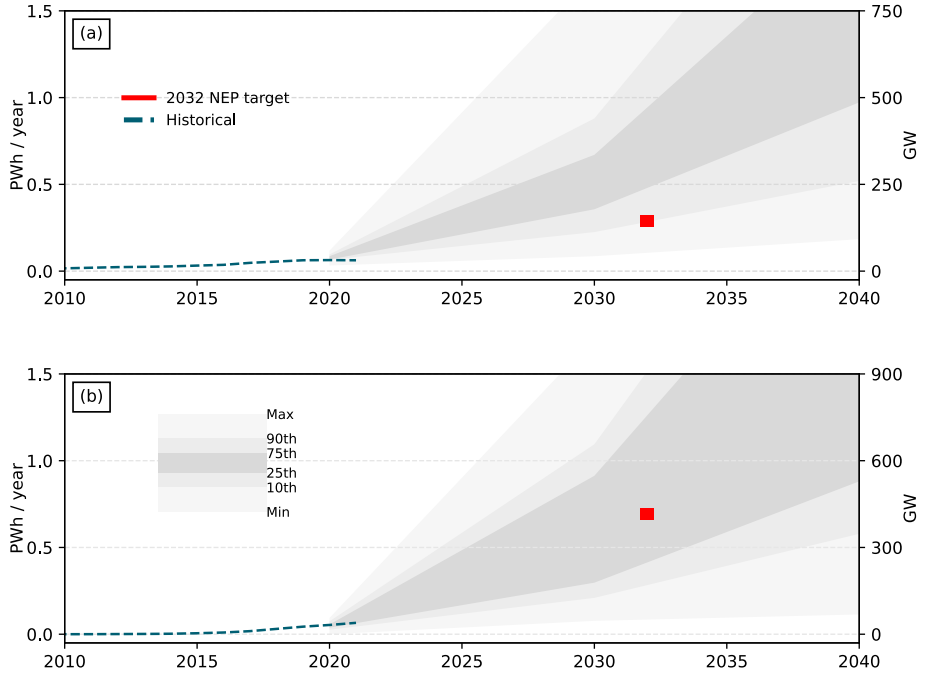

Figure 2.2: Historical wind (a) and solar PV (b) generation (dashed lines) for India (IRENA, 2023a)). Future projected generation (grey shaded region) from AR6 decarbonisation pathways for India that achieve an end of 21st-cenurty warming outcome of less than 2°C with greater than 67% likelihood (i.e., C1-3 pathways, n=338 wind; n=368 solar PV). Shading reflects percentiles and full range of generation envisaged in AR6 pathways. Indian National Electricity Plan targets shown as red bars. Indicative figures for corresponding wind and solar PV capacity shown on secondary y-axis, estimated from median wind/solar PV capacity per unit generation in 2040 across AR6 India-only pathways.

marily achieved by transitioning from carbon-intensive energy sources to lower-carbon alternatives. Weather-tied variable renewable energy (VRE) sources are vital amongst these alternative sources, most notably wind and solar PV technologies. The integration challenges that arise in high VRE electricity systems are address in the following section.

2.4 Integration challenges of high VRE shares

The following addresses essential aspects of the VRE integration challenge and available technological solutions. The role of quantifying meteorological generation variability is highlighted as a key step towards successfully implementing technological solutions. Finally, past studies of weather variability impacts on the VRE generation are reviewed, focusing on existing research gaps for the case study of India.

2.4.1 Electricity system basics

Greater electrification of the energy system (such as transport and space heating) implies a central role for electricity networks (Hansen et al., 2019). These networks comprise multiple generator sources (e.g., a gas-fired power plant) connected with numerous demand sinks (e.g., households) using a grid infrastructure. This grid includes high-voltage transmission lines, transporting large power volumes over long distances. Voltages are then stepped-down from the transmission to regional and local distribution networks to disseminate power to consumers and connect smaller-scale, distributed generators (generally, renewable sources of low capacity) (Bergen, 2009). Electricity networks vary considerably in size, ranging from neighbourhood micro-grids to continental-scale transmission systems. Most counties operate a national power network comprising 10^2-10^4 generators and up to several million demand sinks, often with some degree of interconnection with the national electricity networks of neighbouring countries. All power networks have a common function of providing dependable and cost-effective access to electrical power. As electrical energy services are vital to the economy and livelihoods, the continual functioning of electricity grids is imperative (Modi et al., 2005).

2.4.2 Impacts of VRE integration

Integrating greater shares of weather-dependent energy generation into existing electricity networks and power markets presents multiple challenges, as these systems have primarily been designed to accommodate controllable sources of energy, such as natural gas and coal (Hill et al., 2012). The key integration challenges stem from 1) the relative unpredictability of VRE, particularly wind and solar resources; (2) the limited flexibility of most electricity systems to respond to unanticipated changes in generation; (3) the relatively high cost or limited use of technical solutions (e.g. expensive energy storage options and limited uptake of smart appliances); and (4) the requirement for continual balance between electrical energy supply and demand on all timescales (Dubus et al., 2018).

Modern electricity networks already manage a degree of variability in the demand for electrical energy and some variation in supply. For example, the demand profile follows a characteristic diurnal pattern when aggregated across a region or country: lowest at night, reaching peak levels during daytime working hours, with reductions on weekends and holidays (Taylor and Buizza, 2003). Demand also tends to track the annual cycle in temperature within temperate regions.

Most electricity networks manage variability primarily through redundancy, whereby conventional controllable generators are held at various readiness levels, with a generation capacity greater than the magnitude of variability (responding on timescales of hours to months) (Milligan et al., 2015). Additional options capable of rapidly reducing demand or increasing supply are also available to balance short-term mismatches between supply and demand (responding on timescales of milliseconds to hours).

Examples of variation in supply from wind and solar PV are already available within several national and regional electricity systems which include significant shares of one or both technologies (e.g., Denmark: 60% annual electricity generation, and the United Kingdom: 29% IEA, 2024). However, few existing energy systems currently make use of wind and solar PV at the levels required by ambitious mitigation scenarios. Even in regions with high relative shares of wind and/or solar PV today, the absolute level of capacity is set to increase considerably should long-term climate strategies be realised. Such levels of VRE will stretch existing responses to managing electricity supply balance and challenge reliable, cost-effective operation of the electricity grid (IEA, 2020).

Greater flexibility of the electricity network is, therefore, seen as imperative to manage increased demand and supply variability in a decarbonised energy system (Strbac et al., 2020). Such flexibility will rely on particular technologies, namely energy storage technologies (mainly providing electrical energy storage), responsive demand (e.g. smart appliances and two-way electric vehicle (dis)charging), and greater levels of interconnection between electricity networks (Bistline et al., 2021). Despite these various means of managing variable supply of and demand for electrical energy, networks will become ever more weather-tied, with the impacts of meteorological variability on wind and solar PV generation increasing (Pfenninger et al., 2014). The exact form and scale of technological solutions and management responses will be guided by understanding supply-side variability, which could conceivably originate primarily from wind and solar PV sources in aggressive mitigation pathways. The following section considers existing work that has characterised wind and solar PV generation variability.

2.5 Quantifying weather and climate-related variability

2.5.1 Existing energy meteorology work on weather timescales

Numerous studies have considered integration challenges posed by VRE by examining the magnitude and pattern of variability in renewable generation. Many studies consider only the observed variability in underlying meteorological variables relevant to VRE. The review from Widén et al. (2015) and a meta-analysis from Engeland et al. (2017) have both shown how short-term (hours - 1-day), regional (1-100km) scales make up the majority of work studying space-time energy variability due to meteorological variables. The literature which uses either observed or simulated wind and solar PV generation provides a regional focus on short-term, hour-to-hour fluctuations (Sinden (2007), Kiss et al. (2009), Hawkins et al. (2011), Olauson and Bergkvist (2015), Staffell and Pfenninger (2016), Elliston et al. (2012), Juruš et al. (2013), Ueckerdt et al. (2015), Pfenninger and Staffell (2016), and Fattori et al. (2017); and reviewed in Ringkjøb et al. (2018)), or aggregate wind and solar generation net of electricity demand (Holttinen, 2005; Holttinen et al., 2011; Joskow, 2011; Huber et al., 2014; Cannon et al., 2015; Olauson et al., 2016; Santos-Alamillos et al., 2017; Staffell and Pfenninger, 2018; Shaner et al., 2018). The emphasis on quantifying variability on short time horizons is, in large part, due to the imperative for maintaining a real-time balance between electrical energy supply and demand over the network (Holttinen et al., 2011; Holttinen et al., 2021), and because the majority of operational (e.g., unit commitment) and power market trading decisions occur on these timescales (Foley et al., 2012; Inman et al., 2013; Okumus and Dinler, 2016).

However, as the likelihood of prolonged periods of generation surplus and/or deficit is expected to increase at greater levels of wind and solar deployment, so too does the need to quantify variability in generation on longer timescales. Quantifying variability on longer timescales provides several insights which can help inform operational and strategic measures necessary for ensuring security of supply in the power system. First, quantifying the magnitude of variability can help inform the amount of controllable generation required to maintain adequate power generation resource or the dimensioning of energy storage systems (IEA, 2022b). Second, estimating the frequency, duration, and timing of prolonged variations in wind and solar generation, such as the coincidence of extreme low generation events with periods of heightened demand, indicates the likelihood of system pressure points. Thirdly, studying the variability of prolonged wind

and solar PV generation anomalies is relevant to assessing possible complementarity or anti-phasing between sources (Holttinen et al., 2021). As wind and solar PV installations are often geographically dispersed, it is also relevant to consider the spatial dependence of variability in generation to identify the likely coincidence of surplus/deficit generation across a wider region and the possible effects of greater interconnection (Mills, 2010).

Variation between years in periods of generation surplus and/or deficit lasting weeks to months would be particularly challenging for electricity system operation, especially if extending over wider regions and affecting more than one VRE source. Energy system modelling attempting to optimise future energy systems often lacks adequate representation of interannual climate variability (Hilbers et al, 2019). However, the importance of multi-year wind and solar PV generation profiles is an increasingly recognised within studies of electricity system resilience (Bloomfield et al., 2016; Collins et al., 2017; Pfenninger, 2017; Coker et al, 2020). Variability on this interannual timescale is also relevant to individual wind and solar PV plant owners/-operators, who contend with uncertainty in this variability in measurement campaigns used to estimate profitability and the allowable project debt burden (Carta et al., 2013; Rose and Apt, 2015a).

The following section focuses on work that has quantified generation wind and solar PV variability on interannual timescales.

2.5.2 Existing energy meteorology work on interannual timescales

Existing work concerned with wind and solar PV variability on interannual timescales has considered observed space-time variability of meteorological variables, such as met mast wind speed observations (Sinden, 2007; Earl et al., 2013), while others consider space-time variability in modelled synthetic generation output, often derived from meteorological reanalyses (Staffell and Pfenninger, 2016) and mesoscale dynamical models (Hawkins et al., 2011). The development of long timeseries of synthetic wind and solar PV generation data often yields accurate reproduction of high frequency (e.g., hourly and daily) observed generation at the scale of national power networks and provides sufficiently long datasets to quantify characteristic generation profiles and rare generation events (Kies et al., 2021). For example, Cannon et al. (2015) used reanalysis data to estimate the frequency of extreme wind power events in a static UK wind power fleet. They find that the average occurrence of low or high-generation events decreases

approximately exponentially with increasing event duration and that the extremity of lulls in summer is more pronounced than in winter. Interannual variability in these extreme events is pronounced, with differences between the most and least extreme years exceeding the mean occurrence of extreme events.

A growing body of literature considers the implications of greater shares of weather-dependent energy generation at the level of a continental-scale electricity network (Grams et al., 2017; Santos-Alamillos et al., 2017). Most of these studies seek to quantify how much weather-driven variation a renewable-powered energy system would experience to assess wind resources' dependability and ability to displace other power sources. These studies complement traditional energy system modelling studies, which have predominantly considered centralised electricity production from large conventional generators, often without temporally explicit treatment of VRE generation variability. Often, these studies also consider residual demand for electricity energy, so-called demand net of VRE, which exhibits climate-related variability using historic demand levels (Olauson et al., 2016) and estimated levels of future demand (Staffell and Pfenninger, 2018). As the smoothing effect of interconnected wind and solar generation is well evidenced in the literature (Engeland et al., 2017), several studies have hypothesised wide-scale interconnection to mitigate variability at various timescales (Archer and Jacobson, 2007; Kempton et al., 2010; Wohland et al., 2020; Jerez et al., 2023).

In addition to developing and studying generation syntheses, a related grouping of studies seeks to understand the relationships between underlying climatic drivers of interannual variability and wind and solar PV generation. Internal modes of slow-paced climate variability, such as the El Niño Southern Oscillation (Trenberth, 1997), can affect remote changes in surface-level meteorological variables relevant to wind and solar PV via teleconnections. How such modes of internal climate variability impact renewable generation has historically focused on regions of high installations, such as the well-established influence of the North Atlantic Oscillation (NAO) in the Euro-Atlantic sector, particularly the wintertime effect over Western Europe (François, 2016). For example, Brayshaw et al. (2011) evidenced the impact of NAO phase on wind speeds during an extended winter season at point locations in the United Kingdom. They demonstrated the potential for a +/-10% change in mean wind power output with a +/- unit change in NAO index. Ely et al. (2013) studied the impact of the NAO phase on an interconnected UK-Norway power system, highlighting the considerable impact of the NAO

state on demand net of wind power output and the concomitant impact on hydropower reserves in early spring. Using a synthetic time series of wintertime NAO phase and an economic dispatch model of the Irish power system, Curtis et al. (2016) demonstrated how a difference of 12% in wind power generators' revenue could arise as a consequence of contrasting NAO phases. Several other studies have further investigated the role of NAO in modulating wind power in Europe – e.g. François (2016), Commin et al. (2017), and Cradden et al. (2017).

Recognising the impact of NAO phase on storm track location and cloud cover, several studies have evidenced the covariance of winter surface irradiance and indices of NAO strength, with a positive correlation found in Southern Europe and vice versa in Northern Europe (Pozo-Vázquez et al., 2004; Chiacchio and Wild, 2010; Colantuono et al., 2014). Corresponding effects on observed and simulated (Jerez and Trigo, 2013) solar power output itself have subsequently been quantified over the Iberian peninsula, showing a particularly pronounced effect during a negative NAO phase, where incoming shortwave solar at the surface is reduced by ∼10–20%. Similar behaviour of an opposite sign has been evidenced in a study of wind and solar climatologies in the UK, with the lower tercile of surface irradiance values corresponding with sea-level pressure anomalies reminiscent of a positive NAO phase (Bett and Thornton, 2016).

Over North America, Klink (2007) showed that after removing the effect of the north-south pressure gradient on hub-height wind speeds, between 6%-15% of the remaining wind speed variation is attributable to the combined effect of Arctic Oscillation (AO) and El Niño, implicating these modes as sources of long lead time predictability. Focussing on the Great Lakes region of North America, Li et al. (2010) identify lower mean wind speeds and more frequent occurrences of still periods during strong El Niño years in 30 years of meteorological reanalysis data. ENSO teleconnections to renewable energy generation have been further evidenced over the North American continent (Hamlington et al., 2015; Yu et al., 2015). Keellings et al. (2015) find that cloudier conditions and reduced solar power potential persist over the entire state of Florida during El Niño, whereas clearer conditions are more likely in the North of the state during a positive phase of the Atlantic Multidecadal Oscillation (AMO).

Outside of Europe and North America, studies considered the impact of other major atmospheric phenomena on generation from wind and solar technologies are less numerous, although examples exist for China (Sherman et al., 2017; Yu et al., 2020), Latin America (Henao et al., 2020; Bianchi et al., 2022), Africa (Fant et al., 2016; Bloomfield et al., 2022), and Oceania (Davy

and Troccoli, 2012; Poletti and Staffell, 2021). For example, Changes of up to 10% in mean austral winter global horizontal solar irradiance (GHI) between opposite phases of ENSO have been found in Eastern Australia (Davy and Troccoli, 2012). However, enhanced variability in GHI was found in several Eastern Australia coastal regions during El Niño, potentially limiting predictability on a seasonal timescale. The effect on GHI was non-significant outside of austral winter or in other regions of mainland Australia, indicating a level of predictability derived from the seasonal cycle alone.

This review of energy meteorology work on weather to interannual timescales shows existing studies focussed mainly on countries or regions with larger shares of wind and/or solar PV capacity (notably, Europe and North America). Despite the commonalities amongst existing works in terms of methods for constructing synthetic wind/solar generation time series and analytical approaches to linking observed generation anomalies to larger-scale climate drivers, most works employ a bespoke analytical approach (e.g., composites, clustering, weather-typing, etc.) and calibration depending on the region and energy source (e.g., bias correction, validation, etc.). The following section reviews energy meteorology works specifically focussing on India.

2.6 Existing energy meteorology work in India

As in other regions, existing work focussed on India considering wind and solar generation variability has emphasised short time horizons. Numerous studies use detailed energy system models of the Indian electricity system to assess the operational reliability of electricity provision, consistent with the expanded use of wind and solar PV (Palchak et al., 2017; Rose et al., 2020; CEA, 2023; Lu et al., 2020; Gulagi et al., 2022; Bhattacharya et al., 2024). These works evidence key features of a least-cost electricity system, such as optimal generation mix and energy storage requirements, however the focus is short-term balancing aspects of variability, employing generation syntheses for representative years.

Resource potential is another energy-meteorology crossover topic frequently found in the literature focussing on India. Multiple studies have assessed nationwide wind and solar resources from the point of view of meteorological variables only (e.g., Satyanarayana Gubbala et al., 2021; Ramachandra et al., 2011). Several studies consider long-term trends in underlying variables (e.g., Jaswal and Koppar, 2013; Padma Kumari et al., 2007). Work concerned with the resource potential of wind and solar PV in India has typically estimated the upper limit for

capacity average or generation. For example, official government agency estimates put India's total wind and solar PV potential at 302GW and 748GW, respectively (MOSPI, 2021). Other studies have given significantly higher estimates which have generally increased over time (for onshore wind only: 45GW (Hossain and Raghavan, 2021); 1549 GW (Phadke et al., 2012); 4250 GW (Hossain et al., 2011); 2959MW (CSTEP, 2016); 850-3400GW (Deshmukh et al., 2019); for combined on and offshore wind: 5781GW (Chu and Hawkes, 2020); and for solar PV: 6000GW (Mahtta et al., 2014); 1300-8900GW (Deshmukh et al., 2019).

Few studies in this resource assessment category quantify spatio-temporal aspects of wind and solar PV generation variability in India on longer-term time scales. Jain et al. (2021) provide one of the few examples quantifying the year-round performance of very high share (1000GW+) wind and solar PV deployments. The study notes significant month-long mismatches between supply and demand for electrical energy could arise, particularly under wind-heavy deployment scenarios, with a requirement for seasonal-scale storage to cover early winter months with monsoon period surplus. Gulagi et al. (2020) claim the first study with a specific focus on the effect of the monsoon system on a fully 100% renewably powered electricity system and show how reduced solar PV generation during the summer monsoon period can be compensated by increased wind generation when suitably redistributed via the transmission grid. The advantageous phasing of the annual cycle of wind and solar PV generation in the South of India was also highlighted by Hunt and Bloomfield (2023), while spatial heterogeneity in the wind diurnal cycle was shown to offer a source of geographical smoothing over the day by Gangopadhyay et al. (2023).

Despite the vast literature on the Asian and Indian summer monsoons, few examples linking generation anomalies with meteorological drivers in India exist in the academic or grey literature. Within the southwestern summer monsoon season in India, studies of intra-seasonal variability in wind generation point to the anti-phasing of generation with demand for electricity during active and break phases (Dunning et al., 2015; Kulkarni et al., 2018). The reduced temperatures and increased wind speed, which prevail during the active phases of the monsoon, lead to a supply surplus. In contrast, lower wind speeds during break phases create the conditions for a supply deficit when cooling demand and agricultural activity increase electricity demand. Focussing on long-term trends in wind power potential in India, the study from Gao et al. (2018) identified the summer monsoon months as the period of greatest interannual variability in wind generation

potential. They also identified a simple statistical relationship between an index of potential wind electricity generation for India and differences in low-pressure regions over peninsular India and high-pressure regions over the Indian Ocean. However, their work was focused on reproducing historical declining trends in wind speeds rather than investigating the causes of anomalous seasons or years. Concerns within the energy sector over anomalous generation years were heightened in response to the extreme wind drought conditions experienced in the summer of 2020, where generation through June and July was 24% below climatology (Shekhar et al., 2021).

This review of energy meteorology work in India highlights the need for further work to quantify the magnitude and frequency of prolonged periods of anomalous generation resulting from the existing and future wind and solar fleet. The insights provided by such an investigation support the appraisal of electricity systems compatible with international climate goals. Furthermore, a statistical description of the impacts of specific meteorological phenomena on weather-dependent generation can provide a basis for the statistical downscaling of meteorological forecasts and potentially aid the targeted improvement of generation forecasts over a range of timescales (Doblas-Reyes et al., 2013; Torralba et al., 2017b; Clark et al., 2017; Baker et al., 2018; De Felice et al., 2019).

The following section of this Background chapter builds the case for predictions of energy generation on seasonal timescales and reviews existing energy meteorology work.

2.7 Basis for seasonal predictions

Seasonal climate forecasts (SCF) span the time period between the deterministic limit of numerical weather prediction (∼10 days) and decadal to multi-decadal climate projections (1-100 years). As such, SCF is described as both an initial condition and boundary condition problem, where the current state of the climate system and future levels of external forcing contribute to predictive skill (Doblas-Reyes et al., 2013). Sources of predictability on seasonal timescales arise from the response of the atmosphere to slow-paced, predictable changes in boundary conditions, including sea surface temperatures (SSTs), sea ice, snow cover, and soil moisture (Wang et al., 2006), with ENSO providing a major source of predictability for SCF (Cane et al., 1986). Within the tropical Pacific, ENSO results in a significant displacement to rainfall patterns and associated remote effects through atmospheric teleconnections (Alexander et al., 2002). Be-

yond the tropical Pacific, SSTs in the Indian and Atlantic Oceans have a major role in regional climate variability, particularly on tropical monsoonal rain (Goddard et al., 2001). Modes of climate variability in these basins, such as the Indian Oceanic Dipole, can potentially contribute to long lead-time predictability with regional impacts on monsoonal flows and remote impacts on extratropical climate variability (Saji et al., 1999; Zhao and Hendon, 2009). Stratospheric anomalies are an important source of seasonal predictability in winter and spring outside of the tropics (Ineson and Scaife, 2009). Changes in radiative forcing originating from GHG and aerosol concentrations can also impart predictability on seasonal timescales (Doblas-Reyes et al., 2006).

SCFs can be based on statistical methods, dynamical models or a combination of both approaches. A range of statistical-empirical approaches have been used to exploit observed dependencies between climate indices and predictands, demonstrating skill in both tropical (Hastenrath and Druyan, 1993) and extratropical regions (Wang et al., 2017). Statistical-empirical approaches are limited by the availability of relevant predictor variables and out-of-sample climate responses. Nevertheless, these approaches have proved useful in identifying potentially predictable phenomena and serve as a benchmark for comparison with alternative prediction methods. Numerical SCF models use atmosphere-ocean or global climate models with prescribed boundary conditions in a dynamically coupled set-up, incorporating observations from a range of ocean and atmosphere analyses (Doblas-Reyes et al., 2013). Similar to numerical modelling of weather and climate at other timescales, model error (structural and parameter) and imperfect knowledge of the initial climate state are the two primary sources of uncertainty in SCF (Palmer, 2000). Multi-model and perturbed parameter ensemble approaches aim to quantify the first source of error, whereas initial condition ensemble techniques can help establish the impact of uncertain initial conditions (Slingo and Palmer, 2011).

Typically, raw model output from a SCF system is post-processed to correct systematic bias and statistical features that depart from those found in an observational reference period. To determine the optimum bias correction and to evaluate the performance of SCFs, retrospective forecasts are typically performed and systematically compared with observations. Numerous measures are employed to assess various aspects of forecast quality, including the accuracy of the forecast (error relative to observations), the relative improvement of the forecast over another prediction (forecast skill, usually relative to climatology) and the mean agreement between the

frequency of observed events and the probability of those events indicated by the forecast (i.e. the reliability) (Wilks, 2011). Forecast quality metrics provide a reproducible and objective means of quantifying aspects of forecast performance across different SCF systems (WMO, 2020). The World Meteorological Organisation (WMO) has designated 14 global centres that produce SCFs, known as the Global Producing Centres for Long-Range Forecasts (GPCs-LRF), and several centres contribute to operational multi-model seasonal forecasting systems (Bojovic et al., 2022)

2.8 Seasonal climate forecasting of energy variables

To date, forecasts of near-surface wind speeds and wind power output have predominantly focussed on immediate and near-term horizons of minutes to days (Marquis et al., 2011; Foley et al., 2012). This attention on the near-term arises because most operational and power-trading decisions occur on these timescales. For example, electricity system operators primarily use forecasts of wind speeds and wind power output 1-72 hours ahead in planning and implementing the least-cost power generation mix (unit commitment and dispatch) and by power traders to inform power supply contract trading and hedging activities. Forecasting initiatives on comparable time scales for similar purposes have been developed for solar irradiance and solar PV power output, with additional focus on short (sub-hourly to hourly) timescales, primarily using a wide range of statistical modelling tools (Inman et al., 2013).

Although the utility of long-range meteorological forecasts for the energy sector has long been recognised (WMO, 1979; Brown Weiss, 1982; Knox et al., 1985), examples of their application and use have historically been relatively limited (Soares and Dessai, 2015; White et al., 2017). Use cases appear more numerous as forecast skill was demonstrated beyond the tropics and into regions with significant, weather-dependent energy demand and supply (Livezey, 1990; Changnon et al., 1995; García-Morales and Dubus, 2007; Changnon and Changnon, 2010; Troccoli, 2010). In recent years, demonstration of forecast skill on subseasonal-to-seasonal timescales for climate modes active in the Euro-Atlantic sector (Doblas-Reyes et al., 2013; Scaife et al., 2014; Smith et al., 2016; Dunstone et al., 2016) has further stimulated applications within the energy sector (Orlov et al., 2020; White et al., 2022).

Lynch et al. (2014) assessed forecast skill in surface wind speeds on sub-seasonal timescales using the ECMWF 32-day forecast system. The authors demonstrate significant predictive skill

in the ensemble mean of operational forecasts and hindcasts of weekly mean wind speed at lead times of two weeks ahead, as well as positive skill in probabilistic measures. By exploiting an observed correlation between air temperature and electricity demand in Italy, De Felice et al. (2015) demonstrate the use of ECMWF System 4 seasonal forecasts of surface air temperature in deterministic and probabilistic estimates of regional and national electricity load. Their analysis shows how forecasts initialised in May provide positive and significant skill scores for predictions of upper/lower tercile exceedance in average electricity demand for June and July. The seasonal forecast system of the UK Met Office (GloSea5) was shown by Clark et al. (2017) to provide accurate deterministic reproduction of the observed relationship between NAO on near-surface wind speed and temperature over the Euro-Atlantic sector in wintertime. Generally, the use of monthly mean outputs from SCF systems, either directly correlated with energy variables (e.g., Thornton et al., 2019; Bett et al., 2022) or in statistical-empirical hybrid predictions (e.g., Ramon et al., 2021; Lledó et al., 2022), is more common than the use of native model outputs (Lledó et al., 2019). Studies of solar PV predictability and forecast skill are less numerous than for wind (e.g., De Felice et al., 2019).

Despite the focus of SCF applications to the energy sector in Europe (Troccoli, 2018), examples can also be found in China (e.g., Lockwood et al., 2019) and North America (e.g., Torralba et al., 2017b). Bett et al. (2017) assess the performance of GloSea5 with a specific regional focus on mainland China and the South China Sea. They identify limited predictive skill, with several region-specific exceptions: winter wind speeds in the South China Sea, winter solar irradiance in eastern/southern China, and summer temperatures across the majority of mainland China (though the skill was due to almost entirely to the observed trend).

The studies mentioned above treat systematic forecast bias by either subtracting a leadtime-dependent climatology, the seasonal mean climatology, or using direct model correlations with impact variables. Recognising systematic forecast bias as a key barrier to using surface wind fields in industry, Torralba et al. (2017b) demonstrate two more sophisticated approaches to bias correction within seasonal wind speed forecasts. The first makes an anomaly bias correction and variance adjustment. In contrast, the second corrects variance such that the probability of category forecast matches the frequency of historical events – i.e. increasing the forecast reliability. Further details of the relative merits of different approaches to forecast bias correction are provided in Section 3.4.2.

2.9 Seasonal climate forecasting in India

Seasonal climate forecasting has a long pedigree in South Asia (Blanford, 1884), with much attention devoted to Indian Summer Monsoon rainfall (ISMR). Given the importance of ISMR and its prediction for the region, the following briefly reviews of the wider Asian monsoon and South Asian regional sub-system.

2.9.1 The South Asian monsoon

The Asian monsoon is the greatest monsoon system globally in terms of spatial extent and population affected (Clift and Plumb (2008); pp. vii-ix). It is made up of three sub-systems: the western North Pacific summer monsoon, the East Asian summer monsoon and the South Asian Monsoon (Wang et al., 2005). The South Asian Monsoon operates over India and consists of two parts: the southwest monsoon (or Indian Summer Monsoon), which brings heavy rains from June to September, and the northeast monsoon, which occurs from late October to December (Gadgil, 2003). These names refer to the direction of the prevailing winds. The southwest summer monsoon is responsible for over 80% of the annual rainfall in northern and central regions of India. In contrast, the northeast winter monsoon mainly contributes rainfall to the southeastern part of the country (Wang, 2006).

Traditional theories of the Indian Summer Monsoon (ISM) have stressed the importance of the faster rate of heating during boreal spring over land compared to surrounding tropical oceans, which forms a large-scale land-sea temperature gradient and drives large-scale wind reversal (Halley, 1753; Hadley, 1735). Later works describe the ISM as a seasonal migration of the Inter-Tropical Convergence Zone (ITCZ) that shifts north during boreal summer, following the region of maximum solar heating (Charney, 1969). The monsoon trough, which establishes over peninsular India during the southwest monsoon, shares many features of the ITCZ, namely low-level convergence, cyclonic vorticity above the boundary layer, and organized deep convection Sikka and Gadgil (1980).

The large-scale circulation of the ISM is characterised by south-westerly surface flow that is joined upstream with a cross-equatorial low-level flow (and upper-tropospheric cross-equatorial return flow) (Krishnamurti and Bhalme, 1976). The combined effect of the East African Highlands (Slingo et al., 2005) and Coriolis force serve to channel this surface flow across the Arabian

Sea, forming the Somali or Findlater Jet (Findlater, 1969). These winds transport moisture evaporated from the warm Indian Ocean to converge on the mountainous Western Ghats region that spans the west coast of India, where orographic lifting generates substantial rainfall, with a rain shadow to the east (Gadgil, 2003). Continuing eastwards to the Bay of Bengal, the winds turn north around the low-pressure monsoon trough (large-scale cyclonic vorticity extending from BOB to northwest India), in which most monsoon rainfall occurs (Rajeevan et al., 2010).

Rainfall during the ISM is not continuous but instead shows considerable spatial and temporal variability (Gadgil, 2003). On a synoptic scale, cyclonic low-pressure systems (LPS) dominate and typically form over the northern Bay of Bengal before travelling inland northwest over India, lasting 3-7 days (Sikka and Gadgil, 1978). Beyond the synoptic scale variability associated with individual LPS, longer-lived modes of intra seasonal variability are present within the ISM (Krishnamurti and Bhalme, 1976; Murakami, 1976; Yasunari, 1979; Sikka and Gadgil, 1980; Lau and Chan, 1986). These variations exhibit two non-periodic yet distinct time scales in the range of 10-20 and 30-60 days (Annamalai and Slingo, 2001). The shorter quasi biweekly period is associated with westward-propagating clusters of synoptic-scale convective systems that originate over the northwest tropical Pacific and propagate inland over Northern India via the Bay of Bengal (Hoyos and Webster, 2007). The longer period oscillations have a north–south dipole structure, are tied to the phase and magnitude of the Madden Julian Oscillation (MJO) (Singh et al., 2019) and are typically considered as a manifestation of the Tropical Convergence Zone alternating position between the tropical Indian Ocean and the Indo-Gangetic plain (Gadgil, 2003).

Together, intra seasonal oscillations on the two timescales are considered to represent so-called active and break phases of the monsoon (although intraseaonal oscillations on other time periods have been identified, active and break phases are typically considered as the superposition of these modes, with the amplitude of 30–60-day mode dominating (Krishnamurthy and Shukla, 2007). Active phases typically herald time-clustered monsoon depression activity, reduced surface pressure across central India and monsoon trough zone, anomalous cyclonic vorticity, enhanced low-level westerlies and periods of heavy rainfall in eastern and central India (Krishnamurthy and Shukla, 2000; Rajeevan et al., 2010). Break phases see a southward shift of the main zone of convective activity, positive surface pressure anomalies over peninsular India, weakened low-level westerlies, and a dry interval persists over much of peninsular India

(Blandford, 1886; Ramamurthy, 1969; Lau et al., 2012).

The ISM also exhibits considerable variability on interannual timescales. Although total summer rainfall for India varies by only+/-10% between years, differences at the finer scale are more pronounced, with a coefficient of variation of 35% in the core central region of monsoon rainfall (Moron et al., 2012). This interannual variability results from internal variability (i.e. intraseasonal scale oscillations) and external forcings with a time period greater than the ISM.

Of the external forcings that contribute to interannual variability in the ISM, tropical Pacific Ocean SST anomalies associated with the El Niño Southern Oscillation (ENSO) dominate, accounting for around one-third of interannual variability in ISM rainfall totals (Kulkarni et al., 2021). ENSO describes an internal mode of variability in the tropical Pacific that couples ocean and atmosphere and produces remote impacts on weather across the globe (Shukla, 1987). ENSO includes the El Niño warming phase, with positive SST anomalies in the central and eastern tropical Pacific, and the opposite sign La Niña cooling phase. ENSO phases exhibit a semi-regular time period between 2 to 7 years, and each ENSO event usually persists for 9 to 12 months, with peak SST anomalies typically arising in boreal winter (McPhaden et al., 2006).

ENSO phases and associated SST anomalies bring about the so-called Southern Oscillation, a large-scale alternation in surface pressure between the Pacific and Indian Ocean basins (Bjerknes, 1969; Rasmusson and Carpenter, 1982). ENSO SST anomalies can affect the zonal overturning circulation in the Indo-Pacific region, i.e. the Walker circulation, with the usual ascending (descending) branch over the western (eastern) Pacific Ocean shifting eastward (westward) during El Niño (La Niña) (Walker and Bliss, 1932; Sikka, 1980). The anomalous subsidence over the South Asian region that results from this displacement during El Niño conditions tends to suppress convention, while enhanced convection is favoured during La Niña (Webster et al,1998). These changes in the monsoon circulation often materialise as a decrease (increase) in ISMR El Niño (La Niña) (Pant and Parthasarathy, 1981; Rasmusson and Carpenter, 1983; Mooley and Parthasarathy, 1983). Aside from influencing the ISMR via changes to large-scale circulation over the Indo-western Pacific, ENSO modulates the ISMR via various indirect physical processes, including impacts on the meridional temperature gradient over South Asia (Yang and Lau, 1998; Goswami and Xavier, 2005), the India ocean sea surface temperatures and moisture content of the atmosphere over the region (Ashok et al., 2004; Wu and Kirtman, 2004).

Aside from ENSO, a second major driver of interannual variability in ISMR is the Indian Ocean

Dipole (IOD), which describes the east-west gradient in SST within the equatorial Indian Ocean (Saji et al., 1999). The positive phase of IOD coincides with positive (negative) SST anomalies in the west (southeast) Indian Ocean and is associated with increased (decreased) IMSR over central (central and eastern) India (Ashok et al., 2001). Additional remote drivers of ISMR include springtime snow depth in the Himalayan mountains (Hahn and Shukla, 1976), aerosols (Ramanathan et al., 2005) and North Atlantic Ocean seas surface temperature anomalies (Pai and Rajeevan, 2006). Although ENSO and IOD remain the most influential sources of predictability on seasonal timescales (Johnson et al., 2017).

2.9.2 Seasonal forecast skill in India

Early ISMR predictions relied entirely on statistical models (e.g., Walker and Bliss, 1932; Rajeevan and Francis, 2007), but progressive improvements to general circulation models (GCMs), notably coupled atmosphere–ocean schemes, led to improvements in dynamical seasonal forecasting systems (Charney and Shukla, 1981; Webster et al., 1998; Preethi et al., 2010; Saha et al., 2014; Jain et al., 2019). Current operational seasonal forecasting systems demonstrate varying levels of deterministic skill in IMSR predictions, generally with an r value for seasonal mean rainfall of 0.35-0.60, though assessments are sensitive to the hindcast period considered and observational reference dataset (Rajeevan et al., 2012a; Jain et al., 2023; Chevuturi et al., 2021). Common amongst forecast systems is limited grid-scale forecast skill, which improves when considering areal averages spanning the Indian subcontinent, albeit with wet bias a common issue (Jain et al., 2019). Few models attain skill levels approaching potential predictability, which is typically estimated with an upper limit of 0.7-0.8 (Krishna Kumar et al., 2005; Saha et al., 2019).

The Indian Meteorological Department (IMD) currently issues seasonal rainfall forecasts operationally using a version of the Climate Forecast System version 2 (CFSv2) (Saha et al., 2014) with several ISM-specific parameterisations. A recently upgraded version of the IMD system that includes a higher resolution atmospheric module achieves the highest reported deterministic forecast skill of ISMR from a dynamical model (0.63-0.72, depending on the rainfall dataset used for verification, Jain et al. (2023)). Despite the improvements in ISM prediction, almost no examples of SCF applications to energy generation in India exist within the peer-reviewed or grey literature. Only a single study from Das and Baidya Roy (2021) provides any insight into the seasonal forecast skill of energy-relevant variables. They assess area-averages of four

energy-relevant variables across six operational forecasting models and find generally modest skill, with ECMWF System 5 performing best for all variables. India's current National Climate Research Agenda identifies improved forecasting capabilities and climate services for the renewables sector as key development priorities (PIB, 2023b). Although more than a dozen Renewable Energy Management Centres currently operate within national and regional load dispatch centres, forecasting capabilities only include near-term horizons out to one week (Joshi and Inskeep, 2023)

2.10 Chapter summary

This Chapter has reviewed the role of wind and solar PV technologies in global and Indian energy transition plans, noted the integration challenges that arise with high shares of weather-tied generation, and has covered the role of quantifying and anticipating generation variability in the operational and strategic management of electricity systems. A focus on interannual generation variability and prediction on seasonal timescales within India has highlighted several research gaps:

1. Limited analysis of observed wind and solar PV generation variability (i.e., analysis of historical data) in India, likely due to limited data records on generation and existing renewables fleet.

2. Existing examples of synthetic wind and solar PV generation in India (e.g., Palchak et al., 2017; Gao et al., 2018; Deshmukh et al., 2019) lack one or more of the following: (1) a detailed description of existing farms in terms of location, turbine/array model, and commissioning date; (2) verification against observed historical generation records; (3) calibration/bias correction against observed historical generation records; and (4) multi-decadal meteorological input data.

3. No known examples of studies linking meteorological drivers to seasonal wind or solar PV generation anomalies in India.

4. No known studies demonstrating seasonal forecast skill of generation in India.

5. Most work considering future renewables deployment in India considers ad-hoc, hypothetical modifications to power systems, future deployment based on an arbitrary scaling of current capacity, or generic region-wide synthesis datasets, rarely founded on either the

planned development of existing systems or physical constraints (e.g., Ryberg et al., 2019; Jerez et al., 2015).

The objectives of this thesis, as set out in the previous chapter, seek to address these existing research gaps. The methods and data sources used to undertake the investigation are laid out in the following chapter.

Chapter 3

Data and Methods

3.1 Overview

The set of methods and supporting data that accompany each of the four results chapters are detailed in the following sections.

Section 3.2 summarises the methodological approach for the first results chapter (Chapter 4), which includes creating a database of all wind and solar PV farms in India, estimating generation from these installations for the years 2017 to 2021 using meteorological reanalysis data and subsequently calibrating against daily generation records for state and regional groupings.

Section 3.3 summarises the methodological approach for the second results chapter (Chapter 5) and details the various observational datasets and associated climate indices used to assess candidate drivers of interannual variability in wind and solar PV generation syntheses for the JJAS season.

Section 3.4 summarises the methodological approach for the third results chapter (Chapter 6) and includes details of the seasonal forecasting system used to derive wind and solar PV generation forecasts for JJAS and specifics on the hindcast set, calibration and verification techniques used.

Section 3.5 summarises the methodological approach for the fourth results chapter (Chapter 7), specifically two scenarios for near-term capacity and technology development for wind in India.

3.2 Data and Methods: First Results Chapter

The following details the methodology to produce synthetic wind and solar PV generation timeseries for present-day installations in India, and comprises the following processing steps:

1. Populate a geospatial database of wind farm and solar PV installations in India with available technical data (turbine model and hub height in the case of wind) and commissioning dates.
2. Transform surface winds speeds into estimates of wind generation for existing wind farms using a modified wind farm power curve.
3. Transform irradiance and temperature fields into estimates of solar PV generation for existing solar farms.
4. Construct a time series of wind and solar PV generation for the years 2017 to 2020, aggregated for selected states and regions in India.
5. Validate generation synthesis based on observed historical generation and determine suitable bias correction method.
6. Construct a time series of wind and solar PV generation for selected states and regional aggregates in India using the entire span of the reanalysis dataset (1979 to 2021).

The following sections describe each of these processing stages in detail.

3.2.1 Installation locations and technical characteristics

Spatially explicit synthesis of wind and solar PV generation is limited by the availability of suitable geo-referenced datasets with sufficient farm-level technical data (e.g. turbine model for wind or array tilt for solar PV). This lack of suitable data represents a recognised impediment to studies of renewable energy generation (Pfenninger et al., 2017). Few renewable energy datasets maintained by national governments contain complete information on installation location and technical characteristics. Several industry organisations and market intelligence firms maintain similar databases. However, these are typically cost-prohibitive for researchers (e.g., the 'GlobalData'[1] product from market intelligence firm Energy Monitor) or lack sufficient detail (e.g. the wind farm database from market intelligence firm 'thewindpower.net'[2] is often used in research initiatives of wind generation but lacks information on location, commissioning date and turbine specifications for over 90% of total wind capacity in India). Several academic exercises have sought to compile complete global inventories of wind and/or solar PV generator locations using automated compilation techniques (e.g., Dunnett et al., 2020) or satellite imagery (e.g.,

[1]GlobalData: www.energymonitor.ai/companies/globaldata-energy
[2]thewindpower.net: www.thewindpower.net

Zhang et al., 2021). However, such datasets are again insufficient in technical detail or coverage for India (location and estimated capacity data only).

3.2.2 Compiling data for existing wind farms

A comprehensive dataset of existing installed capacity for wind in India was compiled by combining previously disconnected national government and industry datasets. Specifically, the Central Electricity Agency (CEA) of India maintains a list of all wind installations nationally, broken down by the project investor name and installation location, with additional information on the commissioning date (CEA, 2022). The Geospatial Energy Map of India, produced by the National Institution for Transforming India (NITI Aayog), provides location data for wind installations nationally, down to the level of the nearest village settlement to the installation (NITI Aayog, 2022). The NITI Aayog dataset also provides the investor name per installation, thus providing a common attribute to join with the CEA dataset. Finally, the specific turbine model used at each installation was obtained from the Indian market intelligence firm Consolidated Energy Consultants Limited (CECL) via their annual Directory of Indian Windpower publication (CECL, 2020; CECL, 2022).

The compiled wind database was cross-referenced against independent (yet incomplete) datasets of wind installations in India to gain confidence in the data compilation process. Many early renewable energy projects in India were commissioned under the Clean Development Mechanism (CDM) scheme. So, full project details can be found within the Institute for Global Environmental Strategies (IGES) CDM database (IGES, 2022). Where the project name in the IGES CDM database included the investor name, a match could be made with the compiled wind database, and the project details (location, commissioning date, turbine model in the case of wind) cross-checked. Additionally, the independent research and advocacy organisation Global Energy Monitor[3] maintains global inventories of wind installation locations. Although only a small number of geolocated entries exist for India (∼6% of capacity in 2021 accurately geolocated), further cross-referencing of the compiled wind database was possible. Finally, the wind farm database from market intelligence firm 'thewindpower.net' provides project details (location, commissioning date, turbine model in the case of wind) for approximately 10% of wind capacity in India, providing a further source cross-referencing. In all cases, the compiled wind database provides an advancement on existing sources in terms of detailed project

[3]Global Energy Monitor wind tracker: https://globalenergymonitor.org/projects/global-wind-power-tracker/

data (proximate geographical location, commissioning date, and turbine model in the case of wind). Commissioning dates were not available pre-2016 for the Indian states of Gujarat and Tamil Nadu, and so dates were gap-filled with available information from the above sources and estimates based on CECL (2020) and CECL (2022).

3.2.3 Compiling data for existing solar PV installations

The same method used to compile the wind data is also applicable for solar PV, namely the reconciliation of CEA and NITI Aayog sources. However, the coverage of installed capacity is less than 50% of the cumulative total in 2021 for solar PV in the CEA source. No additional data sources on solar PV in India were found to complement information on either installed capacity, commissioning date, or location. As such, the pre-existing dataset of utility-scale solar installations maintained by Global Energy Monitor[4] was used. This dataset covers virtually all utility-scale capacity and includes proximate geographical locations. The main drawback of this dataset is the commissioning date information, which is at annual resolution only. Some inaccuracies in the solar PV generation synthesis will arise due to the misalignment of observed and synthesised generation, which are caused by the uncertainty over the exact date solar farms were installed. However, most solar PV farms have historically been installed in the first three months of the year, possibly reflecting easier working conditions outside the summer monsoon season or a rush to finalise projects before the financial year-end. (March 31st). Setting commissioning dates in the GEM database for solar PV to January 1st for the available information on the commissioning year is considered a reasonable approximation given the available data.

A second drawback of the chosen solar PV dataset is a lack of rooftop solar PV coverage. However, rooftop solar PV (installations less than 1MW capacity) represented 10.9% of total solar PV capacity in India in 2021 (BridgetoIndia, 2022), and respective generation is not monitored centrally, preventing any validation of generation estimates made for rooftop solar PV. Therefore, the exclusion of rooftop solar in this analysis is a reasonable omission.

Modelling generation from the utility-scale solar PV segment considered in the investigation requires several assumptions over technical characteristics. Firstly, the parameterisation of module conversion efficiency (explained in the following section) is set equal to present-day

[4]Global Energy Monitor solar tracker: https://globalenergymonitor.org/projects/global-solar-power-tracker/

values of multi-crystalline silicon wafer-based cells. Although various photovoltaic cell technologies exist, crystalline silicon wafer-based cells have dominated in recent years and made up 95% of the global market share in 2021 (VDMA, 2022). The recent deployment of solar PV has favoured the relatively higher efficiency of mono-crystalline silicon wafer-based cell designs (84% of the global market in 2021) over the previously prevalent multi-crystalline silicon designs (VDMA, 2022). However, due to domestic manufacturing constraints, the Indian solar market has favoured multi-crystalline silicon designs (TERI, 2019; IEEFA, 2021).

Second, ubiquitous fixed tilt designs are assumed across India in the analysis presented in this thesis, with fixed equatorward orientation. Globally, the utility-scale segment of the solar PV market has been dominated by single-axis tracking designs in recent years (VDMA, 2022). However, due to a combination of the domestic market and local siting factors, utility-scale solar PV installations in India have made almost exclusive use of fixed-angle designs (TATA, 2017). Industry reports suggest that only fixed-angle designs were used before the year 2017 and have since struggled to gain a foothold in the domestic market, representing a minor share of installations since (Bridge to India, 2018). India's leading solar tracker supplier reported that the share of tracking designs in cumulative utility-scale solar PV in 2022 was 13% (Arctech, 2022). In the absence of project-specific details on the use/non-use of tracking designs, the simplifying assumption of ubiquitous fixed tilt designs with array tilt and orientation is considered adequate (a later section provides further details on the solar module parameterisation).

The resulting database of wind and solar farms is named the Indian Wind and Solar Database (IWSD) in the following sections. Table 3.1 shows the column headers for the IWSD that are common to both wind and solar PV. For wind, the turbine hub height was taken from the average value per turbine model, referring to the turbine model dataset from 'thewindpower.net'. The installed capacity in Mega Watts (MW) refers to the direct current (DC) rating of the wind and solar PV generators before any modification by an electrical inverter (i.e., following conventional capacity reporting standards (IEA, 2021)). Figure 3.1 shows the locations of wind and solar PV installatons contained in the IWSD.

Headers	Wind	Solar PV
village	X	
district	X	
state	X	X
installed_capacity_mw	X	X
latitude	X	X
longitude	X	X
commissioning_date	X	X
number_of_turbines	X	
turbine_power_mw	X	
turbine_model	X	
turbine_manufacturer	X	

Table 3.1: Column headers for the IWSD common for wind and solar PV technologies

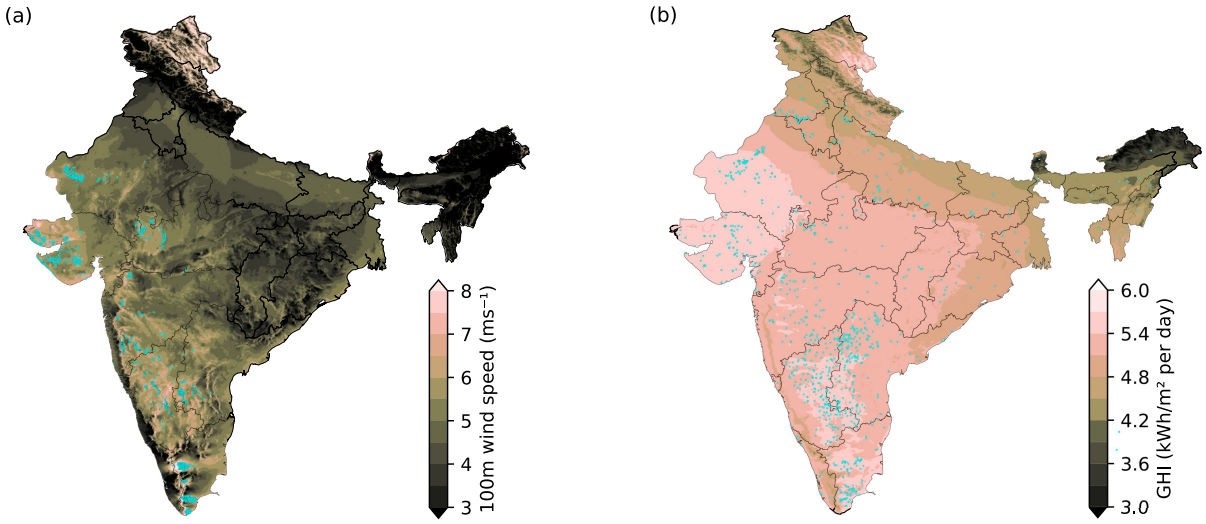

Figure 3.1: (a) Wind farm locations (blue points) in the compiled Indian wind farm dataset, with shading representing 100m mean wind speeds (using data from the Global Wind Atlas developed by the Danish Technical University (DTU-GWA) described in Section 3.2.11). (b) solar PV farm locations (blue points) from GEM, with shading representing mean daily GHI (using data from the Global Solar Atlas (GSA) product described in Section 3.2.11).

Having described the underlying data and assumptions for the Indian Wind and Solar Database (IWSD), the following sections detail the meteorological data fused to produce the generation syntheses.

3.2.4 Reanalysis Data

The temporal and spatial consistency, global coverage, multi-decadal length, and public availability of atmospheric reanalysis datasets make them well-suited to regional-scale analysis of weather-dependent energy resources (Rose and Apt, 2015b; Frank et al., 2018). Despite known

biases and uncertainties within reanalysis datasets (Decker et al., 2012; Zhang et al., 2016), the data have been employed in studies of global, national and site-specific wind and solar PV generation (Lu et al., 2009; Hoogwijk, 2004; Juruš et al., 2013; Drew et al., 2015), as well as applications within industry, most frequently for calibration of local wind resources (Olauson et al., 2017; Davidson and Millstein, 2022).

Reanalysis describes the process of assimilating various observational measurements of the climate state into a model scheme to provide a dynamically consistent approximation of meteorological variables (Trenberth et al., 2008). Modern reanalysis data products use high-resolution global climate model systems, thus providing meteorological information at all locations globally, at regular time intervals, with a standardised gridded data format. Here, the primary data source for atmospheric variables used in the synthesis of wind and solar PV generation is the fifth-generation reanalysis product produced by the European Centre for Medium-Range Weather Forecasts (ECMWF). ERA5 data is publicly available via the C3S Climate Data Store (CDS) (Buontempo et al., 2022). The model core of the ERA5 reanalysis is a variant of the ECMWF operational medium-range forecasting system (Integrated Forecasting System (IFS) Cycle 41r2), which incorporates several enhancements in model parameterisations (e.g. convection and microphysics), as well as the data assimilation method. Furthermore, this latest reanalysis has a significant increase in the horizontal resolution over the ERA-Interim reanalysis that ERA5 supersedes ($0.25° \times 0.25° \sim 31$km at the equator compared to 80km for ERA-Interim) and over twice the number of model levels in the vertical (137 versus 60) (Hersbach et al., 2020)). ERA5 also provides more output fields (including the 100m wind variable) at hourly frequency, extending back to the year 1940 rather than the 6-hourly frequency in ERA-Interim, back to 1979.

ERA5 assimilates synoptic observations at an average rate of approximately 0.75 million per day in 1979, increasing to an average of 24 million per day by the end of 2018, with satellite radiance measurements as the main data sources throughout the reanalysis period (ECMWF, 2019). Observational data inputs to the pre-satellite era of the ERA5 data product (i.e., the period 1950-1979, recently extended back to 1940 in 2023) are far less numerous, averaging approximately 53,000 observational inputs per day, sourced from conventional surface and upper air instruments only (Bell et al., 2021). This lack of observational data inputs in the early period of the ERA5 reanalysis leads to greater uncertainty and lower accuracy in the model

representation of the climate. For this reason, this investigation mainly focuses on the post-1979 period.

The analysis presented in this thesis makes use of a selection of meteorological variables from the ERA5 reanalysis product, which are further described in the following sections.

3.2.5 Wind speed data

ERA5 was selected as the source of hourly wind speed data in this study as the product has proved better able to represent observed surface wind speeds compared to other operational reanalyses (Cionni et al., 2017; Gualtieri, 2022) and has also outperformed the MERRA2 reanalysis in a simulation of national wind power generation (Olauson, 2018). Generally, the ERA5 representation of surface wind speeds has performed well in various geographies (e.g, Molina et al. (2021); Belmonte Rivas and Stoffelen (2019); Hoffmann et al. (2019)). In the case of wind, higher-resolution reanalysis products may offer a more accurate representation of surface wind speeds. Two candidate products are ERA5-Land or the IMDAA reanalysis (Rani et al., 2021), although both products lack the 100m wind speed variable and would depend more on accurate vertical extrapolation of surface wind.

Specific to India, daily mean ERA-Interim surface wind speeds have been evaluated against automated weather stations maintained by the Indian Space Research Organisation (ISRO) and wind farm met mast data maintained by the National Institute of Wind Energy (NIWE), generally showing high agreement (r values >0.8) and modest positive bias (ERA-Interim $\sim$ +10% (Satyanarayana et al., 2019; Satyanarayana Gubbala et al., 2021). The ISRO and NIWE wind speed data are not publicly available, preventing a similar comparison with ERA5 values in this thesis. However, replicating the assessment with ERA5 daily mean 10m winds against observed equivalents from the publicly accessible Global Surface Summary of the Day (GSOD)[5] data provided by the US National Centres for Environmental Information (NCEI) shows similar levels of agreement to the studies using ERA-Interim. Figure 3.2 summarises the generally high agreement between ERA5 and the observed 10m wind speed data from 106 met stations with more than five years of data records (r values generally >0.8). However, compared to the bias values reported in the studies of ERA-Interim, both positive and negative biases of greater magnitude are found in this ERA5 comparison (median bias ratio on 1.06, 25th/75th quantiles

[5]GSOD access: https://www.ncei.noaa.gov/metadata/geoportal/rest/metadata/item/gov.noaa.ncdc:C00516/html

0.72 and 1.49, respectively).

Without quality-controlled wind speed observations (like the ISRO and NIWE sources), it is difficult to ascertain whether the variable and often large bias seen in Figure 3.2 is a genuine feature of ERA5 or an outcome of the GSOD observed wind speeds. The expectation is that the generally poor quality of the GSOD data over India is the source of the discrepancy. Indeed, most GSOD data over India was discarded in the comparison, with 354 station records discarded due to sporadic or incomplete data records. Poor data completeness has been identified in other studies of the GSOD dataset, with additional data artefacts causing spurious wind speed trends over the past decade (Dunn et al., 2022). Furthermore, a recent study of surface wind speeds recorded by met stations maintained by the Indian Meteorological Department over India noted that the standard measurement height of 10m was not consistent across all stations, possibly resulting in mean biases due to vertical wind shear (Satyanarayana Gubbala et al., 2021). Ultimately, this comparison between reanalysis and available observed wind speed data underlines the caveat that must accompany the use of modelled data: that locally variable parameters (i.e., wind speed) are only approximated at a coarse scale, subject to assimilated observed values.

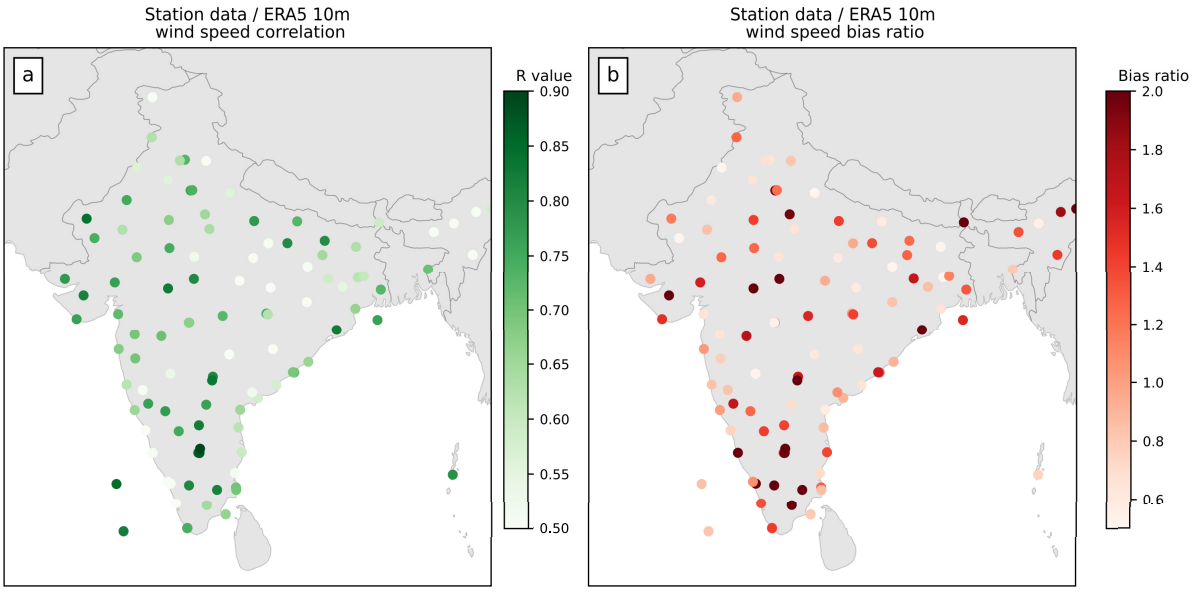

Figure 3.2: Correlation between daily mean 10m wind speed data from 106 met stations (ISD-NOAA) and equivalent ERA5 windspeeds for nearest grid cell (a). Bias ratio between daily wind speed from station data and ERA5 wind speeds (i.e., ratio of station data and ERA5 value) for nearest grid cell (b).

As the wind speed data available in ERA5 is only available at certain fixed heights that do

not necessarily correspond with a particular turbine hub height, vertical interpolation or extrapolation of wind speeds is necessary. The simplified Power-law model of vertical wind shear ($v_2 = v_1(h/100\alpha)$) is used as a means of vertical interpolation/extrapolation of ERA5 100m wind speeds, v_1, to wind speeds, v_2, at a certain hub height, h (Schallenberg-Rodriguez, 2013). The parameter α was defined empirically per grid cell using hourly 10m and 100m wind speed data and then averaged over the hour-of-the-day (n=24) and month-of-the-year (n=12) to create 288 (n=12x24) unique α values per grid cell. This scale parameter value can then be used to determine the wind speed at the hub height of a turbine at the nearest neighbouring ERA5 grid cell of the farm for the corresponding hour of day and month of the year.

Figure 3.3 shows the profile of this variable α value by averaging across all wind farms. A strong diurnal cycle is apparent, with peak values in the afternoon and evening hours. As vertical wind shear is strongly related to the thermal stratification of the boundary layer, warmer ambient air temperatures and a warmer surface promote unstable conditions and reduce vertical wind shear (and alpha exponent value) through enhanced turbulent mixing (Mahrt, 1999). The greater diurnal temperature range outside of summer months leads to a greater range in alpha exponent values. While in the period May-September, increased cloud cover acts to cool the land surface and likely contributes to higher alpha values in the midday minima.

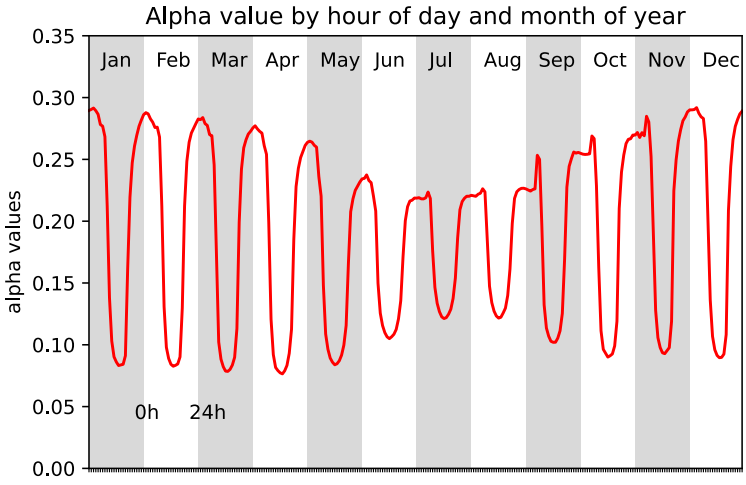

Figure 3.3: Empirically defined values for the scale parameter α by hour of and month of year, averaged over all Indian wind farms.

Alternative simple parameterizations of vertical wind shear within the boundary layer are found within the scientific literature, notably, the 'log-law' relationship derived from Monin–Obukhov

similarity theory, with either simplified assumptions of neutral atmospheric stratification or elaborated versions with a variable wind shear parameter to account for nonneutral conditions (Emeis, 2018). Such a parameterization may be more suitable for reanalyses or observations where only a surface 10m variable is available. However, the availability of the 100m wind speed parameter in ERA5 obviates the need for the log-law approach, with its requirement for further assumptions over surface roughness and atmospheric stability. Although the power law only offers a simplified description of boundary layer structure and an approximation of vertical wind shear, it is judged adequate given the available data and application (i.e., state-aggregated wind).

3.2.6 Irradiance and temperature data

The parameterisation of solar PV module performance (described in the following section) requires data inputs of direct and diffuse irradiance components. The accumulated parameter 'surface solar radiation downwards' (SSRD) [J/m2/s] in the ERA5 reanalysis was used to represent surface irradiance (i.e., the radiant flux) on a horizontal plane (ECMWF, 2015). In other works, SSRD is also termed global horizontal irradiance (GHI) and is the sum of direct and diffuse irradiance components. The accumulated parameter 'direct solar radiation at the surface' (FDIR – acronym in ERA5 signifying 'forward', i.e., downward direction of flux) [J/m2/s] in the ERA5 reanalysis was used to represent the direct irradiance component. The diffuse component is taken as SSRD minus FDIR. Dividing ERA5 irradiance values by 3600 (i.e., seconds per hour) provides hourly mean surface irradiance values in Watts per square metre (W/m2). ERA5 was selected as the source of GHI values in this study as the product has been shown to outperform other operational reanalyses when validated against ground observations (Urraca et al., 2018; He et al., 2021) and has also been shown to outperform the MERRA2 reanalysis in a simulation of national solar power generation (Camargo and Schmidt, 2020).

3.2.7 Energy conversion process

The use of reanalysis data in the estimation of wind and solar generation has a heritage in the scientific literature (see Background Literature Section 2.5), and the analysis presented here brings together key methodological developments from the literature for synthesising wind (Staffell and Pfenninger, 2016; Gonzalez-Aparicio et al., 2017) and solar PV generation (Šúri et al., 2007; Pfenninger and Staffell, 2016). The exact methods for transforming reanalysis data

into generation estimates for wind and solar PV are described in the following sections.

3.2.8 Wind turbine power curve

Manufacturer-specified power curves are typically used to relate wind speeds to power output. The power curve defines instantaneous power output as a function of tangential wind speed at hub height for a given turbine model. The characteristic power curve profile is broadly similar across different turbine designs (Figure 3.4). However, significant differences in power output are seen in the ramping segment of the power curves, with capacity factors ranging from 40% to 100% of rated power output for a wind speed of 10m/s. Turbines installed as part of a wind farm project are typically all the same model and so can be described by a single power curve. However, the diversity of wind speeds across a given wind farm causes the aggregate power output of all turbines within a wind farm to deviate from the idealised power curve of a single turbine (Barthelmie and Jensen, 2010).

A power curve adjustment is employed to account for this deviation effect, which is similar to the method of deriving aggregate turbine response first described by Norgaard and Holttinen (2004) and subsequently implemented by Staffell and Pfenninger (2016) in their syntheses of national-scale wind power generation. Each wind farm's adjusted power curve ($PC_{adj.}$) is derived by applying a Gaussian kernel filter operator, O, to the respective manufacture-specified power curve ($PC_{manu.}$) for a single turbine. Given that modern wind farms vary in size (1-100+ turbines per farm in India), an additional parameter is included such that standard deviation also scales with farm capacity. The operator, (O), is normally distributed around zero with a standard deviation given by (σ=(log10(C).v)/17.5), where C is the farm capacity in KW, v is the wind speed at hub height, and constants are defined by tuning such that correlation in daily synthetic capacity factors is maximised across the regions considered in the analysis (prior to bias correction, see Section 3.2.11). The aggregate power curve at v is, therefore, the sum of the manufacture-specified power multiplied by O, evaluated across the range v^*, which spans +/- four standard deviations, as shown by Equation (3.1).

$$PC_{agg}(C, v, \sigma) = \sum_{v^*=-4\sigma}^{4\sigma} P_{manu.}(v - v^*)O(v^*\sigma) \tag{3.1}$$

Further demonstration of this power curve deviation and adjustment method is demonstrated

in Figure (3.4a), which plots the observed aggregate generation[6] of 140 turbines at the Greater Gabbard 504MW offshore wind farm, off the East coast of England, against contemporaneous wind speed observations[7] from a met mast positioned at the approximate centre of the wind farm (Argyle et al., 2018). This particular location is used as an example due to the availability of farm-level generation data and co-located met-mast data. The aggregate power response (scatter points in Figure (3.4b)) deviates from the manufacturer curve for a single turbine (red line in Figure (3.4b)); a consequence of the combined effect of the distribution of wind speed across the farm area, turbine wake effects, as well as additional deviations attributed to directional and turbulence effects (Lydia et al., 2014; Barthelmie et al., 2012). Further losses resulting from inefficiencies in voltage transformation and turbine availability (i.e., the percentage of time a turbine is available to operate outside of maintenance periods) range from 2-3% and 2-7%, respectively (Arwade et al., 2011; Faulstich et al., 2011; Lumbreras and Ramos, 2013; Carroll et al., 2017). Turbine ageing also undermines performance through mechanical deterioration and has been shown to reduce capacity factors in the United Kingdom by an average of 0.44% per year (Staffell and Green, 2014). Here, the effect of the distribution of wind speeds across the farm area is accounted for by the power curve adjustment method (blue line in Figure (3.4b)), and additional losses are accounted for by a single fixed multiplicative term of 13% (green curve in Figure (3.4b).

Synthesis of wind generation was conducted per wind farm in the IWSD, using the corresponding adjusted wind farm power curve and wind speed from the nearest grid cell centroid. This nearest-neighbour approach to estimating point location wind speeds from a gridded product has proved comparable to other interpolation methods when estimating point location wind speeds (Cionni et al., 2017) and has shown minimal impact compared to bilinear interpolation when synthesising national aggregate wind generation (Gruber et al., 2019).

3.2.9 Solar PV array parameterisation

The lack of array-specific technical characteristics, such as array orientation or panel model, in the solar PV arrays considered in this analysis (see Section 2.1.1) necessitates a parsimonious method and simplifying assumptions to transform irradiance values to solar PV generation.

[6]Generation data obtained from The Balancing Mechanism Reporting Service (BMRS) provided by Elexon, the company responsible for administrating power contract settlement in the UK electricity market (https://www.elexon.co.uk/data/balancing-mechanism-reporting-agent/).

[7]Wind speed data from the IGMMZ met mast for the period June 2012 to June 2014 and is provided by the Crown Estate Marine Data Exchange (http://www.marinedataexchange.co.uk/wind-data.aspx).

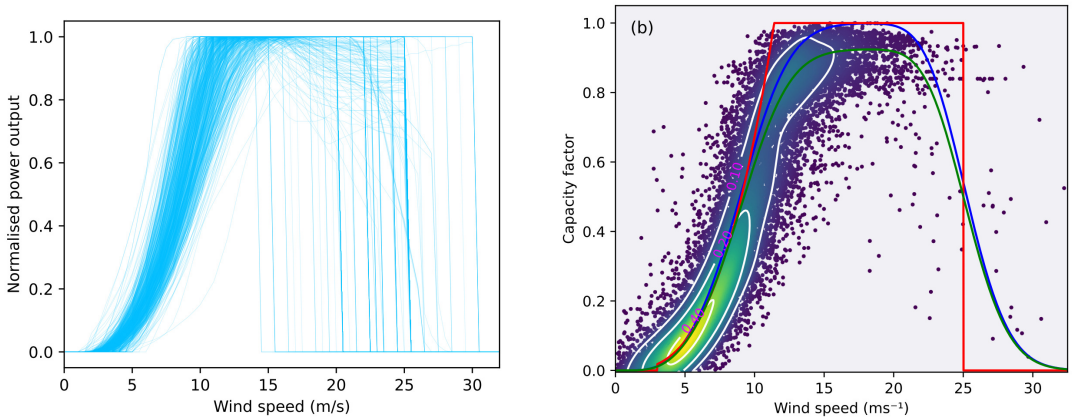

Figure 3.4: (a) Manufacturer power curves from thewindpower.net (n==805), (b) manufacturer power curve for Siemens SWT3.6–107 turbine (red line), smoothed power curve (blue line); smoothed power curve +13% loss term (green line); and hourly hub height wind speeds versus hourly power output from the 140 SWT3.6–107 turbines at the Greater Gabbard wind farm, located off the east coast of England (as scatter points with contours representing the 0.1, 0.2 and 0.4 levels of a Gaussian kernel density estimate)

The physically founded empirical relationship developed by Huld et al. (2008) for the energy rating (actual performance of a PV module relative to standard test conditions (STC)) of an archetypal multi-crystalline silicon photovoltaic module, as a function of ambient temperature and irradiance, is well-suited to this case and has proven adequate in representing solar PV generation over country scales (Huld and Gracia Amillo, 2015; Frank et al., 2021). This relationship defines solar array capacity factor (CF_G) (actual power output from a PV array relative to STC (P_G/P_{STC}) as:

$$CF_G = \frac{P_G}{P_{STC}} = \frac{G}{G_{STC}}\eta_{rel}(G,T) \tag{3.2}$$

where G is the total irradiance incident upon the array in the same plane in which the array is tilted (in-plane irradiance), G_{STC} the STC value of G, nominally 1000W/m2, and $\eta_{rel}(G,T)$, the relative energy conversion efficiency term, or the ratio of the array efficiency with values of G and T to the efficiency at STC. The relative energy conversion efficiency term describes the real-world performance of the array and takes the form:

$$\eta_{rel}(G,T) = 1 + k_1 ln(\frac{G}{G_{STC}}) + k_2 \left(ln(\frac{G}{G_{STC}}) \right)^2 + k_3 \Delta T + k_4 \Delta T ln(\frac{G}{G_{STC}}) + k_5 \Delta T \left(ln(\frac{G}{G_{STC}}) \right)^2 + k_6 \Delta T \tag{3.3}$$

where the empirically defined coefficients ($k_1 ... k_6$) have previously been determined through a least-square fit to operational solar PV[8] and ΔT represents the difference between the PV module temperature, T_{mod}, and a STC module temperature of 25°C. Module temperature (T_{mod}) scales as a function of G following the empirical relationship:

$$T_{mod} = T_{amb} + (T_{nom} - T_0) \frac{G}{G_{STC}} \tag{3.4}$$

where T_{amb} represents ambient air temperature, taken as 2m air temperature from ERA5, T_{nom}, and T_0 represent nominal operating module temperature and nominal ambient air temperature respectively and take the values of 48°C and 20°C. Total in-plane irradiance (G) is approximated using the isotropic sky model. This simple irradiance model assumes that diffuse irradiance is uniform within the celestial hemisphere and that reflection from a ground surface of known albedo is diffuse (Loutzenhiser et al., 2007). Total in-plane irradiance (G) is, therefore, the sum of direct and diffuse components, given by:

$$G = DNI.cos(aoi) + DHI \left(\frac{1 + cos(\theta)}{2} \right) + GHI.\alpha \left(\frac{1 + cos(\theta)}{2} \right) \tag{3.5}$$

where the first term represents in-plane direct irradiance, given by direct normal irradiance (DNI, or FDIR in ERA5) weighted by the cosine of the beam-array angle of incidence (considering the geometric position of the Sun and the array tilt[9]). The second term represents in-plane diffuse irradiance and is a weighted fraction of diffuse horizontal irradiance (DHI, or SSRD minus FDIR in ERA5), with θ representing array tilt relative to horizontal. The third term represents in-plane ground-reflected diffuse irradiance, and is a weighted fraction of GHI, with an albedo value (α) taken from the ERA5 variable 'forecast albedo'. This value is in the range of 0.15-0.25 throughout the Indian subcontinent, with slightly higher values (0.3) in the

[8] Coefficient values from Huld et al. (2011).

[9] All solar geometry calculations made use of the open source Python package PyEphem (Rhodes, 2011).

Thar desert region, located in the Northern state of Rajasthan.

Without array-specific technical information on orientation, it is assumed that all existing solar PV sites are installed perpendicular to and facing the equator. As previously described, fixed-tilt designs are assumed for all installations when making the generation synthesis. Regarding the tilt angle of the arrays, various methods exist for defining the exact inclination, ranging from simple latitude-based approximations to more complex solutions that account for local climate and terrain shading effects (Yadav and Chandel, 2013). The PVGIS initiative[10] is an example of the latter approach to defining optimal tilt angles. It uses satellite irradiance data and a high-resolution digital elevation map with near-global coverage to determine yield-maximising array inclination (Huld et al., 2012). Figure 3.5 shows the zonal average (i.e. averaged East-West globally) of optimal tilt angles using data from PVGIS as a function of latitude (green curve in Figure 3.5). However, real-world installations often deviate from theoretical optimum angles, usually due to on-site practicalities (e.g., rooftop slope, the shading effect of neighbouring modules due to high tilt angles, height restrictions or system layout constraints). Saint-Drenan et al. (2018) found that tilt angles for an extensive database (n=35,000) of fixed-angle solar PV installations in Germany were between 60-70% of the local optimal tilt angle as defined by PVGIS (Saint-Drenan et al., 2018). However, their dataset did include many rooftop installations, which are not considered in the analysis of India presented in this thesis.

Yet, an analysis of the United States Energy Information Administration (EIA) Annual Electric Generator Report shows a similar non-optimal inclination in utility-scale installations. Figure 3.5 also depicts the tilt angle of ∼2600 fixed-angle solar PV installations in the United States of America (U.S.A.) (grey scatter points in Figure 3.5, with data from EIA (2021)). The sample of installations from the U.S.A. show considerable spread in tilt angles amongst installations of similar latitude. However, the average tilt angle per latitude bin (orange points in Figure 3.5) is approximately in line with the 70% scaling of the local optimal tilt angle, as shown by the blue line in Figure 3.5, which represents a 0.7 scaling of a quadratic fit through PVGIS zonally averaged optimal tilt angle. This 0.7 scaling of the quadratic fit is used to define tilt angles for non-tracking array designs in this analysis based on the latitudinal position of each solar PV installation.

Although a fixed tilt angle is the base assumption in the production of the synthetic solar

[10] https://ec.europa.eu/jrc/en/pvgis

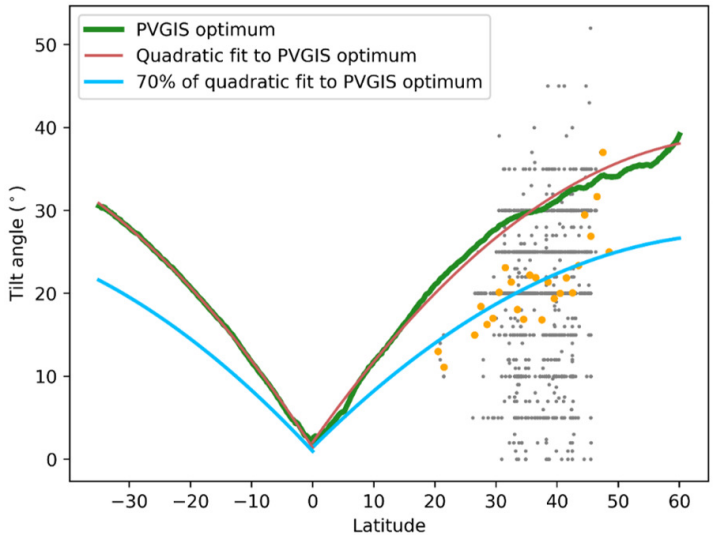

Figure 3.5: Zonally averaged optimum array tilt angles as a function of latitude using data from PVGIS (green curve) and quadratic line of best fit to PVGIS values (red curve). Actual tilt angles for fixed-tilt utility-scale solar PV installations in the United States (grey scatter points, with data from EIA) and average tilt angle per latitude bin for U.S.A installations (orange points). Blue curve represents 70% of the value of the quadratic line of best fit to PVGIS values.

PV generation, a sensitivity test is conducted with all installations representative of current state-of-the-art single-axis designs that use mono-crystalline silicon wafer-based cell designs. The single-axis tracking module of the PV-LIB Python package, itself an implementation of Holmgren et al. (2018), is used to determine the array tilt-angle that minimises the angle of incidence of incident shortwave irradiance for a given solar zenith (i.e., the array tilt for each hour of the day, for all hours of the year). This implementation mimics real-world single-axis trackers that follow the daily east-west passage of the sun.

As with the synthesis of wind generation, solar PV generation synthesis was conducted per solar farm in the IWSD, using meteorological data from the nearest grid cell centroid. Energy conversion losses, primarily attributed to electrical resistance and DC/AC inverter efficiency, are assumed to result in a fixed 10% reduction in solar PV generation (Pfenninger and Staffell, 2016).

Having described the data and processing steps involved in the construction of synthetic wind and solar PV generation data, the following sections describe the historical records of actual wind and solar generation in India used to validate and bias correct the resulting timeseries.

3.2.10 Verification data

To validate the synthetic wind and solar PV generation method, the resulting generation time-series aggregated to state, regional and national values are compared to historical records of actual wind and solar generation in the corresponding regions of India. The national electricity grid of India is overseen by Grid-India (formerly the Power System Operation Corporation Limited (POSOCO)). Five regional subdivisions of the national grid (Northern, Eastern, Western, Northeastern and Southern regional grids) are overseen by Regional Load Despatch Centres (RLDCs)[11], which coordinate operations within the regional grid zones, as well as intra/inter-regional and trans-national interconnector flows. Figure 3.6 shows the regional subdivisions RLDCs represent, with green borders signifying state groupings for the five-mainland interconnected regional electricity grids. Colour shading in Figure 3.6 indicates installed wind and solar PV capacity per state at the end of 2021. Wind installations are concentrated in the country's west, with the seven numbered states comprising 99.5% of the total installed wind capacity. The states of Gujarat in the west and Tamil Nadu in the south are states of considerable wind installations ($\sim$10GW). For solar PV, a similar concentration of installed capacity to that of wind is seen, with limited capacity in northern and eastern states. However, the northern-region state of Rajasthan houses considerable solar PV capacity $\sim$14GW).

These RLDCs have maintained an archive of daily generation and installed capacity since the year 2016. However, data before 2017 is sporadically achieved, and so ignored from the analysis. The generation values are available for the individual states of each RLDC and the regional aggregate. Daily capacity factor values (ratio of actual daily generation to maximum attainable generation for installed capacity over 24 hours) for the period 2017 to 2021 were calculated from these records and are hereafter referred to as 'observed' generation values.

RLDCs also archive demand for electrical energy within the regional electricity grid. Here, a portion of this historical archive of daily electricity demand is used to define an annual demand cycle for comparison with the annual cycle of wind and solar PV generation. Specifically, an annual cycle for electricity demand per region is defined using data from the years 2014-2019 inclusive, with the linear trend first removed before taking the median value per day of the year and normalising by the maximum value. Consistent growth in electricity demand is

[11]Data originally taken from 5 RLDC websites. The websites have since been discontinued. Alternative data source from Grid-India: `https://report.grid-india.in/index.php?p=Daily+Report%2FPSP+Report`

seen throughout this 2014-2019 period, whereafter, the dual effects of a nationwide economic slowdown and the COVID-19 pandemic abated this increase (Bhattacharya et al., 2022). Using the earlier 2014-2019 time period allows for the definition of a simple characteristic annual cycle of electricity demand during normal economic conditions.

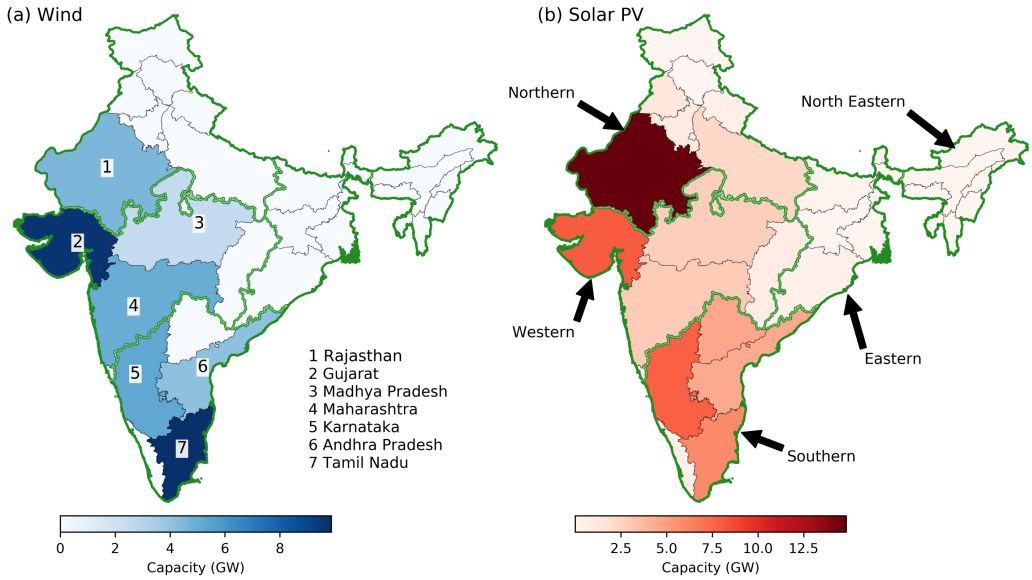

Figure 3.6: Study regions for wind (a) and solar PV (b) in India. Coloured shading signifies installed capacity for wind (a) and solar PV (b) by Indian state as of year end 2021 (MNRE, 2022b). Green borders represent India's 5 mainland regional electricity grid regions, with region labels shown in (b). Numbering denotes individual states with significant wind capacity

3.2.11 Bias correction

Synthesis of wind and solar PV generation by transforming reanalysis data can result in bias relative to equivalent observed values (McKenna et al., 2022). The origin of this bias could stem from the atmospheric variables (e.g., uncaptured orographic effects on winds at the scale of individual wind farms), the energy transformation model (e.g. incorrect specification of turbine power curve), the validation data (e.g. uncertainty over the coverage of centrally collected data from a grid operator – i.e. net of system losses, inclusive of embedded generation, etc.), or any combination of these factors. Here, it is assumed that available records of actual generation are accurate and representative of generation net of losses from transmission-connected wind and solar PV generation. With limited information on farm-level or array-specific technical characteristics, options for further refining the process from transforming reanalysis data remain limited. Therefore, the bias correction procedure used here only considers alterations to wind speed and irradiance.

Two forms of simple bias correction are trialled in the analysis presented in this thesis. The first form of bias correction relies on additional meteorological data to adjust wind speed and irradiance from the reanalysis. In the case of wind speeds, bias correction was performed using 100m wind speeds from Version 3.0 of the Global Wind Atlas developed by the Danish Technical University (DTU-GWA). The DTU-GWA Version 3.0 provides a simulated global micro-scale wind climate on a $\sim 0.3 \times 0.3$km ($0.0025° \times 0.0025°$) scale for all land areas, plus a 200km offshore buffer (Badger et al., 2015). The DTU-GWA simulation involves multiple stages of dynamical and statistical downscaling, beginning with large-scale winds from 10-years of ERA-5 atmospheric re-analysis data used to force a WRF mesoscale model with a horizontal grid spacing of 3-km. This mesoscale wind climate is used as an input to the microscale Wind Atlas Analysis and Application Program (WASP) to calculate local wind climates on a 250m horizontal grid, at several heights above the surface. The DTU-GWA has primarily been validated against synthetic aperture radar ocean derived winds and multiple field measurement campaigns. The DTU-GWA wind speed climatology is a product of a simulation spanning the period 2008-2017, and the average over this period is added to ERA5 wind speeds prior to conducting the generation synthesis (i.e., a mean bias correction). The mean bias correction was applied to both 10m and 100m windspeeds using DTU-GWA data at corresponding heights so that the generation synthesis methodology could be applied.

In the case of solar PV, bias correction of ERA5 irradiance data was performed using equivalent values from Version 2.0 of the Global Solar Atlas (GSA) 2.0. The GSA is a publicly available solar irradiance web-application that provides output from a satellite-based irradiance model, developed by the company Solargis on behalf of the World Bank Group[12]. It is assumed that the long-term average irradiance values provided by the GSA have been calculated for the same period for which input satellite data is available, i.e. mid-to-late 1980s to present (satellite radiation products such as the Satellite Application Facility on Climate Monitoring (CMSAF) and Surface Solar Radiation Data Set-Heliosat (SARAH) datasets cover this period). So, the difference in ERA5 average irradiance values (both diffuse and direct components are available from the GSA) for the period 1985-2019 is added to ERA5 irradiance values prior to conducting the generation synthesis.

The second approach to bias correction takes the form of a multiplicative adjustment factor

[12]https://globalsolaratlas.info

(AF), which is applied to wind speed and irradiance data at all wind/solar farms within respective states. The particular AF that minimises mean bias in synthetic capacity factors (AF_{min}) over the verification period is found iteratively applying a range of AF values to meteorological data. AF_{min} is identified by the point at which the ratio of observed to synthetic average capacity factor equals one.

3.2.12 Perfomance metrics

The performance of the generation syntheses is assessed relative to observations from the RLDCs using three metrics:

1. Normalised mean bias refers to the mean observed capacity factor value for a given region and technology divided by the corresponding synthetic value. A normalised mean bias value greater than 1 suggests that the synthesis underestimates generation on average through the five years considered.
2. Mean absolute error (MAE) refers to the absolute value of the observed capacity factor minus the synthetic capacity factor.
3. Correlation expressed as an r value (i.e., the Pearson correlation coefficient).

This concludes the Data and Methods section on the construction of the synthetic wind and solar PV generation timeseries. Chapter 4 presents the results associated with this methods section, the first of four results-focused chapters.

3.3 Data and Methods for Chapter 5

The analysis presented in Chapter 5 uses the wind and solar energy generation synthesis dataset described in Section 3.2 as well as various other meteorological fields and climate indices. The following sections described these meteorological variables and the approach for performing composite, correlation and empirical orthogonal function analyses.

3.3.1 ERA5 meteorological fields and derived indices

Additional ERA5 fields used in Chapter 5 include monthly mean 850hPa winds, total cloud cover (i.e., the proportion of a model grid cell covered by cloud, summed across all vertical levels), sea surface temperature (SST) and mean sea-level pressure (MSLP). Indices based on ERA5

monthly SST fields include the Dipole Mode Index (DMI) and the Equatorial Indian Ocean Oscillation index (EQWIN), which are both standardised anomalies of spatially averaged SSTs (exact region definition described in the Chapter 5 text).

Indices based on ERA5 monthly 850hPa wind fields include two Wang-Fan indices. These indices describe regional monsoon circulations over India and the Northwest Pacific. The indices follow the physically motivated definitions first described by Wang and Fan (1999) and capture observed relationships between the two major convective heat sources that energise regional manifestations of the wider Asian summer monsoon system. The dynamically-based index of the Indian summer monsoon, termed ISMi in this thesis, is defined as the difference between the 850hPa zonal wind in a southern region (0°-15°N, 35°-65°E) located over the climatological position of the Somali Jet (westerlies) and a northern (20°-30°N, 60°-80°E) region co-located with the monsoon trough (easterlies - see Figure 3.7a). The ISMi captures the strength of monsoon westerlies and is indicative of anomalous lower-tropospheric vorticity that causes the monsoon trough (Wang et al., 2001). Lower tropospheric vorticity and monsoon westerlies are strongly tied to boundary layer moisture convergence, so the ISMi is highly correlated with summer monsoon rainfall anomalies.

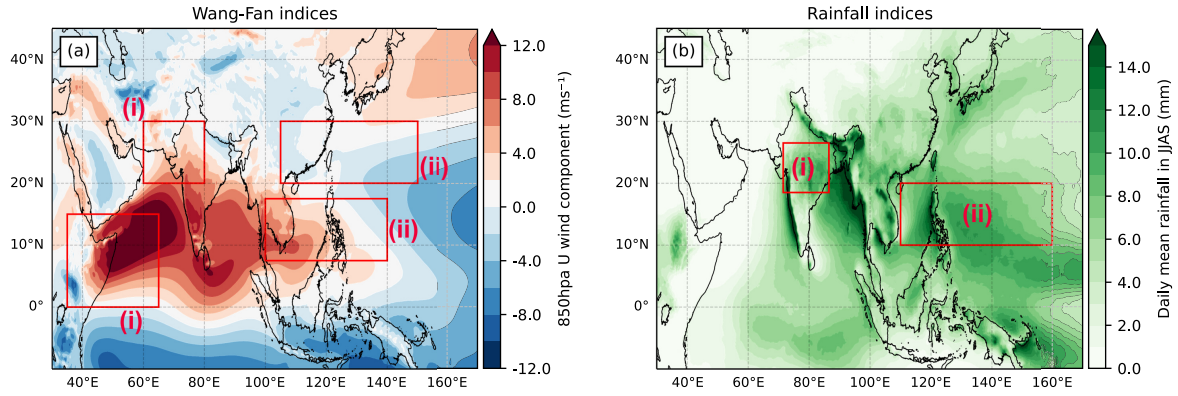

Figure 3.7: (a) ERA5 850hPa wind fields in JJAS with boxes showing regions over which area averages describe Wang-Fan indices for (i) Indian summer monsoon and (ii) Western North Pacific monsoon. (b) MSWEP daily mean rainfall in JJAS with boxes show regions over which area average rainfall describe two monsoon indices for (i) Indian summer monsoon rainfall (ISMR - 18.5–26.5°N, 71.5–86.5°E) and (ii) Western North Pacific monsoon rainfall (WNPR - 10–20°N, 110–160°E).

In the case of the regional monsoon system over the Western North Pacific (WNP), a dynamically-based index is defined as the difference between the 850hPa area averaged zonal wind in the southern (7.5°-17.5°N, 100°-140°E; westerlies) and northern (20°-30°N, 105°-150°E; easterlies - see Figure 3.7a) extents of the anomalous elongated cyclone that governs monsoon rainfall in

the region (Wang et al., 2003). This index is termed WNPi in this thesis. The two indices describe the most prominent modes of variability in the respective regions of South Asia, and better capture observed monsoon circulation variability of respective monsoon sub-system than other monsoon indices (e.g., the Webster-Yang index; Webster and Yang (1992)).

Indices of monsoon rainfall for the Indian summer monsoon and Western North Pacific monsoon are described by area averages of rainfall over respective 'core monsoon regions' shown in Figure 3.7b. Rainfall data products used in the analysis are described further in Section 3.3.3

3.3.2 Additional meteorological datasets

Variations in tropical sea surface temperature consequent of ENSO are studied using the Oceanic Niño Index (ONI), which is calculated and archived by the National Oceanic and Atmospheric Administration (NOAA) Climate Prediction Centre (CPC)[13] (Barnston, 1997; Huang et al., 2017). The ONI refers to SST anomalies in the Niño3.4 region (5°S–5°N, 120°–170°W) and is a commonly used ENSO index (Trenberth, 1997; Hanley et al., 2003; Giese and Ray, 2011). The ONI is calculated from three-month running mean temporally filtered SSTs from the Extended Reconstructed Sea Surface Temperature Version 5 (ERSSTv5; Huang et al. (2017)), defined relative to a moving 30-year climatology that is sequentially updated every five years to suppress the underlying global warming trend (Huang et al., 2017). The ONI is similar to the Niño3.4 index (the latter more frequently uses a 5-month running mean), and the two terms are used interchangeably in this thesis. However, the strict definition follows that of CPC ONI.

Two additional datasets are used to study the effects of atmospheric aerosol loading on solar PV yield. The first is the CERES (Clouds and the Earth's Radiant Energy System) SYN1deg data product, which provides direct and diffuse irradiance components for no-aerosol, no cloud, and all-sky atmospheric conditions (ERA5 lacks the no-aerosol conditions). The second is an additional reanalysis product that provides speciated atmospheric aerosol loading, specifically, the Modern-Era Retrospective analysis for Research and Applications Version 2 (MERRA-2) developed by NASA's Global Modelling and Assimilation Office (Gelaro et al., 2017). MERRA-2 has a horizontal resolution of 0.5° × 0.625°, with 72 vertical levels from the surface to 0.01 hPa and an hourly time resolution. One of the main advances of the MERRA-2 reanalysis over its predecessor (Rienecker et al., 2011) is the assimilation of multi-source observations of aerosols,

[13] https://www.cpc.ncep.noaa.gov/data/indices/

incorporating black and organic carbon, dust, sea salt and sulphates. The aerosol components of the analysis are simulated by the GOCART (Goddard Chemistry, Aerosol, Radiation and Transport) model, which represents multiple interactive processes affecting aerosol production and dispersal (Marticorena and Bergametti, 1995; Gong, 2003; Randles et al., 2017). Verification of MERRA-2 aerosol optical depth values shown a high level of agreement globally with the AERONET (Aerosol Robotic Network) (Che et al., 2019). The direct assimilation and subsequent native dynamical modelling of aerosol species marks one of the main differences between MERRA-2 and ERA5. The latter does not directly assimilate observed aerosol information and instead incorporates climatological aerosol optical depth from the Global Ozone Chemistry Aerosol Radiation and Transport (GOCART) model into its Rapid Radiative Transfer Model (RRTM) shortwave scheme.

3.3.3 Rainfall data

The physical processes responsible for precipitation over the Indian subcontinent during the ISM occur over a range of spatiotemporal scales, causing considerable variability in the duration, intensity, and spatial extent of rainfall (Goswami and Mohan, 2001). Together with a spatially and temporally incomplete observational record of past rainfall events, analysis of precipitation patterns should consider the possible effects of sampling uncertainty. Two different rainfall datasets have been considered in this thesis to gain confidence in the validity of ISM rainfall analysis.

The first is gridded dataset of daily rainfall totals derived from a national network of approximately 7000 rain gauge stations maintained by a combination of the IMD, hydro- and meteorological observatories and state governments (Pai et al., 2014). The dataset is maintained by the IMD with ongoing updates via a public data portal[14] and is considered the most comprehensive in terms of its coverage of the available historical record of rainfall gauge data.

The Multi-Source Weighted-Ensemble Precipitation (MSWEP) data set (Beck et al., 2017; Beck et al., 2019) was used as a secondary source. MSWEP is a gauge-adjusted satellite-derived rainfall product, whereby satellite infrared and microwave sensor readings are calibrated with in-situ rainfall measurements to overcome sampling issues and inaccuracy in the algorithmic derivation of rainfall estimates (Sun et al., 2018). Unlike other gauge-adjusted datasets (e.g.

[14]https://www.imdpune.gov.in/cmpg/Griddata/Rainfall_25_NetCDF.html

the Climate Hazards Group Infrared Precipitation with Stations CHIRPS, Funk et al., 2015), MSWEP provides both land and ocean rainfall data, which aids the interpretation of broader rainfall patterns within the analysis presented in this thesis. The MSWEP dataset provides 3-hourly total precipitation at 0.25° spatial resolution (Beck et al., 2017). The dataset is the only precipitation dataset to merge across a variety of observational and model inputs and has outperformed other multi-satellite or gauge-adjusted rainfall datasets in a global validation (Beck et al., 2017; Beck et al., 2019).

Figure 3.8a and b shows the long-term daily mean rainfall during the ISM season (JJAS) for the Pai et al., (2014) and MSWEP datasets (1979-2021). Figure 3.8c shows the difference between the two datasets, with the greatest discrepancy seen over the mountainous regions of the Western Ghats and portions of the Himalayan foothills. A common rainfall metric used in studies concerned with Indian climatology and variability is a weighted average of rainfall in the 'core monsoon region' (18.5–26.5°N, 71.5–86.5°E) (Rajeevan et al., 2010). This region sees the passage of low-pressure systems through the summer monsoon season and significant rainfall events. The region is of practical significance given the concentration of a large proportion of the Indian population and domestic agricultural production while also serving as an indicator of wider rainfall variability across the country. The r value of the correlation in JJAS standardised monthly mean rainfall values between the two rainfall products in the core monsoon region is 0.992. And the correlation between JJAS standardised monthly mean rainfall values and equivalent values for all-India are 0.978 and 0.984 for the Pai et al. (2014) and MSWEP dataset, respectively. So, there is considerable similarity at the monthly timescale between the two data products and much resemblance between the core region and the country as a whole.

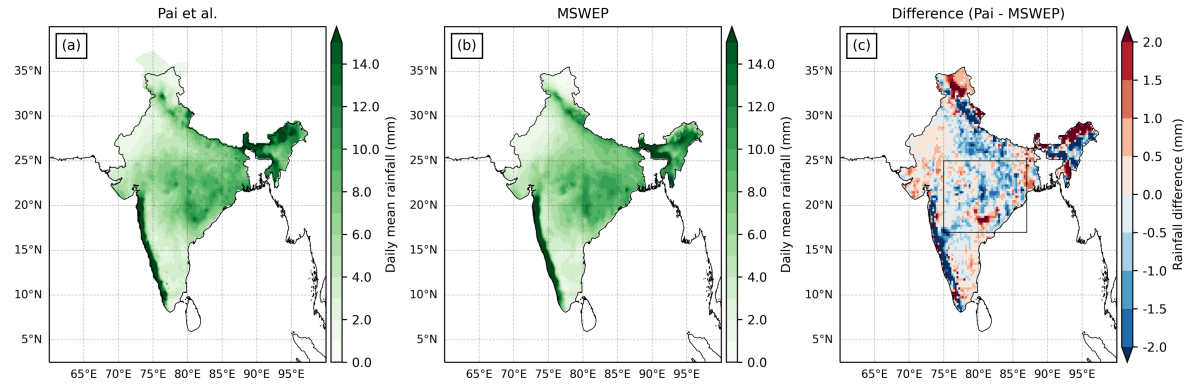

Figure 3.8: Mean daily rainfall over India with data from IMD, using Pai et al., (2014) methodology (a), and data from MSWEP (b). Difference between two rainfall data products shown in (c). Box overlaid in (c) shows core monsoon region.

3.3.4 Low pressure systems

A composite analysis of wind, irradiance, and rainfall anomalies during the occurrence of low-pressure system (LPS) events within the north Indian Ocean basin made use of a pre-existing temporal and spatial dataset[15] of historic LPS systems for the period 1979-2019, considering LPS genesis within the box 70°E-96°E, 5°N-28°N (Vishnu et al., 2020). This LPS dataset uses a feature tracking algorithm with objective thresholds of the 850hPa stream function of horizontal wind defining the LPS centroid ERA5 hourly time step.

The LPS dataset derived from the implementation of the tracking algorithm performs well when compared to subjectively analysed data sets of LPS tracks and intensities in the region, which make use of categorical definitions of LPS as defined by the IMD (Sikka, 2006; Mooley and Shukla, 1987), specifically: (i) lows with wind speed less than 8.5 ms-1 and a MLSP anomaly of at least -2hPa within radius of 3° from the low centre; (ii) Monsoon Depressions wind speeds 8.5-13.5ms-1 and MSLP anomalies -4 to 8hPa); and (iii) Cyclonic storms having wind speed more than 13.5 ms-1 and MSLP anomalies greater than -8hPa.

Other studies that make use of feature tracking algorithms (Hurley and Boos, 2015; Praveen et al., 2015; Hunt et al., 2016) either make use of older generation reanalysis data inputs, do not make resulting tracking datasets publicly available or show inferior performance to Vishnu et al. (2020). Thus, using the Vishnu et al. (2020) LPS dataset is optimal and provides internal consistency with the ERA5 reanalysis inputs.

3.3.5 Empirical Orthogonal Function (EOF) analysis

Empirical Orthogonal Function (EOF) analysis is a common statistical technique that reduces the dimensionality of large space-time datasets (See Hannachi et al. (2007) for a review and Wilks (2011); pp. 519-562 for practical implementation guide). Both simple and rotated EOF analyses are trialled to test the robustness of the resulting decomposition to possible implementation artefacts. Specifically, rotated EOF analysis relaxes the orthogonality constraint placed of modes and limits the number of variables that contribute to each EOF a priori. The widely used Python module 'xoefs' (Rieger and Levang, 2023) is used to implement both EOF analyses.

This concludes the data and methods relating to Chapter 5 that investigates candidate drivers

[15] https://zenodo.org/record/3890646

of interannual variability in wind and solar energy generation within the JJAS season.

3.4 Data and Methods for Chapter 6

Chapter 6 describes the assessment of seasonal climate forecasts of wind and solar generation. The data sources for the dynamical seasonal climate forecasts, calibration methods and verification procedures used in this assessment are described in the following sections.

3.4.1 Seasonal Forecast System data

The analysis of seasonal forecasts (SCFs) of energy generation makes use of hindcasts produced by the European Centre for Medium-Range Weather Forecasts (ECMWF) seasonal forecasting system 5 (SEAS5). The SEAS5 system is a global coupled ocean-atmosphere model and began operational use in 2017, superseding ECMWF's fourth-generation seasonal forecasting system (Johnson et al., 2019; ECMWF, 2021). The atmospheric model is the previous IFS cycle (43r1) as that used in ERA5, with a horizontal resolution of O320 (∼31km at the equator) and 91 vertical levels (ECMWF, 2021). The land, ocean, and sea ice components of SEAS5 make use of the HTESSEL land-surface model (Balsamo et al., 2009), Nucleus for European Modelling of the Ocean (NEMO) (Madec et al., 2017) and Louvain-la-Neuve Sea Ice Model (LIM2) (Fichefet and Maqueda, 1997), respectively.

ECMWF runs re-forecasts of past cases (known as hindcasts) to enable calibration and assessment of the forecast system performance. Hindcasts are initialised on the 1st of each month of the year and run for seven months, with model output variables available at a 6-hourly timestep. Hindcasts comprise 51 ensemble members, combining perturbed ocean/atmosphere initial conditions and stochastic physics perturbations. The analysis in Chapter 6 uses hindcasts initialised on the 1st of May for JJAS at a 1-month lead time (i.e., June-September inclusive), spanning the 41-years 1981-2021. SEAS5 data were obtained from the ECMWF Meteorological Archival and Retrieval System (MARS) for the following variables: 10m wind speed, surface solar radiation downwards, mean sea level pressure, sea surface temperature, total precipitation, and total cloud cover. When conducting grid scale analysis, SEAS5 data in its native resolution from MARS is interpolated to a regular lat-lon grid of 0.25 degrees to match ERA5. In several cases, statistically significant trends[16] are apparent in specific variables over the entire ERA5

[16] Assessed with a Mann-Kendal test, significant at the 95% level.

record. The ability of the SCF system to reproduce such trends will contribute to forecast skill. However, SCF skill is conventionally assessed with any clear long-term trends removed to gauge the portion of forecast skill related to seasonally persistent forcing signals. As such, observed and forecast values for 10m winds, SSRD, and SST were first detrended by removing the linear least-square regression fit. Other variables show no clear linear trends across South Asia or the tropics, so detrending was not conducted.

3.4.2 Producing seasonal energy generation forecasts

Relating seasonal predictions of meteorological variables to energy generation can follow several different data processing and forecasting methodologies (Troccoli et al., 2008). One approach is to undertake no further data processing beyond calibration of the raw forecast variables, as done by numerous operational meteorological authorities when publishing seasonal climate outlooks. In practice, the subjective interpretation of expert users then relates the forecast product to energy generation. Another approach is to apply the same transformation methods used to construct the generation synthesis directly to SCF data outputs (e.g., Lledó et al., 2019), see Section 3.2.8. However, differences between the reanalysis data product and the SCF outputs necessitate changes to the generation synthesis methodology that degrade the synthesis performance. In the case of wind, there is a lack of the 100m wind field, a lower temporal resolution (6-hourly vs. hourly), and lower horizontal and vertical resolution. For solar PV, SEAS5 data outputs have the same deficiencies in temporal and spatial resolution compared to the ERA5 reanalysis and the lack of the direct 'solar radiation at the surface' variable.

Given these deficiencies, statistical downscaling is chosen as the method for producing seasonal generation forecasts. Statistical downscaling describes post-processing procedures exploiting observed relationships between the typically coarser scale model-derived fields and an observed finer-scale variable (Von Storch et al., 1993). In the analysis presented here, several area-weighted average meteorological fields and related climate indices serve as dynamically based predictors of regional wind and solar PV generation.

The main statistical downscaling method used in Chapter 6 follows the so-called perfect-prognosis (PP) rationale (Gutiérrez et al., 2013). The PP approach first requires an adequate statistical model that describes the observed relationship between a given climate predictor and

impact variable – in this case, candidate predictor variables/indices from ERA5 and regional wind and solar generation anomalies for the JJAS season. Seasonal generation predictions are then made with the same statistical model but with predictor variables replaced with dynamical predictions from the SCF. Suitable bias and variance adjustments can be conducted before applying the statistical model to SCF predictor variables or forecast estimates following the application of the regression model (e.g., Manzanas et al., 2019). Applying the PP approach to individual ensemble members is used to yield probabilistic forecasts, with suitable calibration typically applied to the forecast ensemble (e.g., Doblas-Reyes et al., 2005). Ultimately, the performance of the PP method is dependent on both a robust predictor-predictand relationship in observations and a skilfully represented predictor in the SCF model. The PP approach has a longer history of application in the field of climate projections (Gutiérrez et al., 2013) but is increasingly used in seasonal forecasting (e.g., Manzanas et al., 2018; Baker et al., 2018; Ramon et al., 2021).

Here, the period 1979-2021 is used to establish the observed relationship between the given climate predictor and the seasonal mean capacity factors. Taking an example predictor as the ENSO3.4 index and predictand of solar PV JJAS mean generation as an example; the linear relationship is simply modelled as:

$$CF = ax + c \tag{3.6}$$

where CF is the observed generation anomalies (i.e., the validated solar PV generation synthesis), x is the observed climate predictor (i.e., the Niño3.4 index), a and c are coefficients determined through least square linear regression. Applying the regression coefficients a and c to the Niño3.4 index from the hindcast ensemble members yields the forecast capacity factor per season. The method is also applicable to multiple predictors using a multi-linear regression.

The linear regression is first calculated and applied to forecasts using all available observations and hindcast years. A forecast calibration is then undertaken by inflating ensemble variance via a method known as Climate Conserving Recalibration (CCR) (Weigel et al., 2009), and the mean bias removed. Following convention, the calibration and bias correction are undertaken in a leave-one-out set-up, whereby the year being adjusted is excluded from the calculation (i.e. each year is adjusted using information from all other years). This approach mimics an

operational setting whereby only past observations inform the empirical relationship utilised in the forecast. Following Doblas-Reyes et al. (2005), Torralba et al. (2017a) and Manzanas et al. (2019), the CCR and mean bias correction is implemented as:

$$F'_{n,t} = \rho \frac{\sigma_o}{std(\bar{F}_t)} \bar{F}_t + \sqrt{1-\rho^2} \frac{\sigma_o}{\sqrt{\langle \sigma_f^2 \rangle}} (F_{n,t} - \bar{F}_t) \tag{3.7}$$

$F_{n,t}$ and $F'_{n,t}$ denote the original and adjusted forecast for ensemble member n at year t; $\bar{F}_t$ the ensemble mean, σ_o the observed interannual standard deviation, $\langle \sigma_f^2 \rangle$ the mean intra-ensemble variance (i.e., the time mean of ensemble variance per year), and ρ the correlation between the interannual timeseries of observations and the ensemble mean. Essentially, CCR modifies the ensemble spread to achieve the same interannual variance as observations while maintaining the same interannual correlation and forecast ensemble mean (hence 'climate conserving'). Mean bias in the calibrated forecast is removed by calculating anomalies and adding the observed climatology (again in cross-validation mode). Note that the use of anomalies for climate predictors also diminishes the possible effects of time-dependant forecast errors or model drift, which may develop following forecast initialisation (Weisheimer and Palmer, 2014).

An alternative to using the observed relationship between a given climate predictor and impact variable (i.e., the PP approach) is to rely on the direct correlation between the seasonal forecast ensemble mean and observed impact variable. This approach is known as Model Output Statistics (MOS) in a numerical weather prediction context (Glahn and Lowry, 1972), though it has also been used in seasonal climate forecasting (e.g., Palin et al., 2016; Clark et al., 2017; Thornton et al., 2019). Under the assumption that the relationship between the ensemble mean predictor and predictand is linear, a probabilistic interpretation of the prediction interval of the linear regression is possible (Bett et al., 2017). Although a valid method (that is found to yield similar levels of skill and reliability as PP in Chapter 6), the focus in this thesis will be on PP. This focus on PP is because the investigation is exploratory and seeks to establish potential forecast skill and prototype applications within an energy context. As such, establishing observed relationships between climate predictors and generation predictands is essential to better understand underlying physical drivers. Ideally, SCF systems would represent observed observations accurately (as they largely do at seasonal timescales for phenomena like ENSO). However, this is not guaranteed, with bias and inaccuracy common in assessments of SCF sys-

tems in South Asia (e.g. mean or temporal bias for rainfall or a shift in the climatological Somali Jet). Consequently, relationships between SCF model outputs and generation may arise from chance or be model-specific, limiting the roll-out of SCF-derived predictors to other SCF systems. Furthermore, hindcast sets are frequently shorter than the observed period, limiting the information available to establish the statistical model between predictor(s) and predictand.

Having introduced the SEAS5 forecast system used in the investigation and method of application to produce generation forecasts, the following considers how to verify the forecast performance.

3.4.3 Verification of seasonal energy generation forecasts

Verification describes the systematic assessment of hindcast performance relative to the observed climate. Numerous measures exist for quantifying the quality or performance of hindcasts/forecasts, and each forms part of an overall assessment of forecast 'goodness' (Murphy, 1993).

These metrics cover accuracy (error relative to observations), the relative improvement of the forecast over another prediction (forecast skill, usually relative to climatology, though persistence or random chance are also used), the mean agreement between the frequency of observed events and the probability of those events indicated by the forecast (i.e. the reliability), and the forecast bias (average discrepancies between the forecasts and the observations). Both Jolliffe and Stephenson (2012) (chapters 7, 8 and 11) and Wilks (2011) (chapter 8) provide comprehensive coverage of forecast verification metrics and serve as the two resources informing the verification approach in this thesis.

The assessment of hindcast deterministic skill in Chapter 6 uses the Pearson correlation coefficient to measure the strength of the association between ensemble mean values and equivalent observations. The Pearson correlation assumes normally distributed data, and using seasonal mean anomalies helps fulfil this prerequisite. The thresholds required for statistical significance at a specified level (95% throughout this analysis) are calculated assuming a two-tailed Student's t-test.

Seasonal forecasts are typically interpreted probabilistically, whereby the likelihood of a given climate state is indicated by the number of forecast members in that state. Several aspects of the forecast can be considered when assessing performance or quality in probabilistic terms. Typically, aspects of forecast Accuracy (the magnitude of the difference between forecast and

observed probability distributions) and forecast Reliability (the mean agreement between the frequency of observed events and the probability of those events indicated by the forecast) are considered (Murphy, 1973; Murphy, 1993).

In Chapter 6, three measures of forecast accuracy are considered: the Brier score, the Ranked Probability Score (RPS), and the Continuous Ranked Probability Score (CRPS). The Brier score is the mean squared error between forecast and observed probabilities of a given event and the RPS is the multi-category version of the Brier score. Thus, the RPS measures the normalised sum of mean squared errors in cumulative probability space for a multi-category probabilistic forecast. Following convention, accuracy measures are defined using tercile forecast categories of below and above normal, which are defined relative to observed and forecast climatological frequencies (Wilks, 2011, p. 247). Therefore, Brier score and RPS are insensitive to forecast bias, as tercile categories are defined relative to the model climate. The CRPS measures a continuous variable based on the integrated squared difference between the observed and the predicted cumulative distribution functions. CPRS is sensitive to forecast bias. Skill scores for the three accuracy measures (Brier skill score (BSS), Ranked Probability Skill Score (RPSS), and Continuous Ranked Probability Skill Score (CRPSS)) are defined as the relative improvement compared to a climatological reference forecast, with values ranging between -1 and 1, where 1 indicates perfect skill.

A bootstrap resampling method is used to test whether values for the various skill scores (e.g., CRPSS) and diagnostics (e.g., the ratio of predictable components (RPC)) used in the analysis differ significantly from chance values that arise from using a finite ensemble size (n=51) and a finite number of validation cases (i.e., V = 41 hindcast years). The bootstrap approach is common within seasonal-to-decadal forest verification (Wilks, 2011; Goddard et al., 2013; Smith et al., 2013). The procedure involves generating a set of additional hindcast cases by: 1) randomly sampling V hindcast years with replacement; 2) randomly sampling N ensemble members for each sample with replacement; 3) computing the required skill score / diagnostic; and (4) repeating steps 1-3 1000 times to generate a distribution of the required skill score / diagnostic. A given null hypothesis can then be tested by calculating the confidence interval at a particular significance level based on a two-tailed t-test. For example, the null hypothesis that a given skill score is not different to zero is rejected at the 90% level when skill scores lie outside of the 5-95% confidence interval of the distribution of skill scores generated from the bootstrap

procedure. In the case of the diagnostic RPC, the null hypothesis that RPC is not different from one is rejected at the 90% level when the 5-95% confidence interval of the distribution of RPC values does not include the value 1.

Reliability is a measure of the mean squared error between the relative frequency of observed events and the probability of those events as indicated by the forecast at varying levels of likelihood (Hartmann et al., 2002). For a given event (e.g. the upper tercile category), this measure is typically depicted as a plot of increasing levels of forecast probability versus the observed relative frequency at that forecast probability level, whereby the diagonal indicates perfect reliability (i.e. the relative frequency at which a given tercile outcome occurs in the hindcast period corresponds, on average, with the probability indicated by the forecast system). Deviation above/below this diagonal represents under/overconfident forecasts. Additional attributes are usually included in this reliability diagram, including a horizontal line at the climatological frequency (e.g. 1/3 for tercile categories). A forecast that is unable to resolve events as occurring at different probabilities would lie on the horizontal line ('no-Resolution'line) at one-third, as all forecast events occur one third of the time. An additional diagonal lying halfway between the perfect forecast and horizontal is often added, with only points above this line contributing positively to the BSS (Hsu and Murphy, 1986). Forecast calibration that accounts for bias conditional on forecast probability can improve reliability.

The reliability diagram is often shown alongside a histogram of forecast categories. The property of the forecast exhibited in this histogram is termed forecast Sharpness, whereby a sharp forecast system indicates the occurrence of events distance to the mean value category (i.e. a flatter shape, with bins at the edges of the histogram well sampled) and where zero sharpness indicates a forecast system which on average reflects climatology (i.e. a clustered around the vertical line representing climatology on the Reliability diagram, also referred to as the no-Sharpness line).

Resolution (sometimes termed Discrimination) is a final aspect of forecast performance, which quantifies the extent of differentiation between observed/non-observed outcomes in the forecast and, for a given region, is depicted as the Relative Operating Characteristic (ROC) – a plot of the hit-rate against the false-alarm rate at differing probability thresholds (Mason, 1982). A forecast system with positive skill will more frequently achieve hits (correctly predicted events) over false alarms (incorrectly predicted events) and show a positive area above the diagonal. For perfect forecasts, all ensemble members will correctly predict the occurrence of an event in

all years of the verification period, and all points of hit-rate against false-alarm will fall at x=0, y=1. Thus, perfect forecast skill is indicated by an area under the ROC curve (AOC or ROC score) of 1. As no skill would be indicated by an area under the ROC curve of 0.5, a normalised skill score for ROC (ROCSS) is then defined as: ROCSS=2xAOC-1.

3.5 Data and Methods for Chapter 7

The final results chapter considers the performance of the generation synthesis under two alternative parameterisations that represent future technology scenarios. Due to data constraints on future solar PV capacity deployment, the analysis in Chapter 7 only considers wind generation. The data sources for these scenarios and the methods used are described in the following sections.

3.5.1 Repowering scenario

Two scenarios are considered to assess near-term changes in the Indian wind fleet. Firstly, a wind repowering scenario is considered whereby all turbines at wind farms in India are substituted with a single turbine model that achieves the highest annual average capacity factor. Differences in the resulting capacity factor between the existing fleet of turbines versus full replacement with state-of-the-art designs are then quantified by comparing alternative versions of the generation synthesis. A 'reference' version of the generation synthesis considers the period 2017-2021 with the existing fleet of turbines as of year-end 2021. The 'full repowering' scenario considers the same time period, with all turbines at wind farms in India substituted for the best-performing model (Suzlon S144 3.15MW). The 'full repowering' scenario considers vertical scaling of wind speeds to the greater hub height of the repowering turbine model.

The same empirically derived adjustment factors (AF) (described in earlier in Section 3.2.11) are used in both the 'reference' and 'full repowering' scenarios, such that any resulting changes in capacity factor are the result of turbine characteristics only (hub height and power curve). Progressive repowering is also considered, whereby repowering occurs step-by-step in order of wind farm age and turbine rated capacity. This analysis of progressive repowering uses the detailed wind farm data from the complied database of India wind farms (described earlier in Section Section 3.2.2).

3.5.2 Expanded scenario

The second scenario considers a near-term wind expansion in the 2025/26 timeframe. Additional wind capacity is added to the existing database of Indian wind farms that runs to 2021 using the following three sources:

1. Operational wind farms commissioned in the years 2022 and 2023 using location data from the independent research and advocacy organisation Global Energy Monitor[17], which maintains global inventories of wind installation locations (4.3GW).

2. Planned and under construction onshore wind capacity detailed in the inventory of the Central Energy Agency of India (20.1GW) (CEA, 2024).

3. Planned offshore wind capacity to the year 2026 following the Ministry of New and Renewable Energy Strategy for Offshore wind (MNRE, 2023). The strategy details plans for 37 GW in tenders by 2030 in the states of Gujarat and Tamil Nadu. The Global Wind Energy Council projects 17.3GW to be completed by 2026 (GWEC, 2023). These capacity values are split 50/50 between offshore zones in Gujarat (Gulf of Khambhat) and Tamil Nadu (Cape Comorin and Palk Strait), as designated in the MNRE strategy.

Table 3.2 provides of the capacity additions by Indian state. In total, the 'planned expansion' scenario considers an Indian wind fleet of 81.2GW, approximately double the capacity in 2021. It is assumed that all additional onshore capacity makes use of the same turbine model as in the repowering scenario. Offshore capacity makes use of a Siemens Gamesa SG11.0-200 DD 11MW 120m, which is a typical offshore model at the time of writing. The offshore segment of the 'planned expansion' scenario uses ERA5 winds with no adjustments (as no relevant observational generation data exists for such a calibration).

3.5.3 Capacity density

To assess resulting changes in energy yield consequent of the two repowering scenarios, an assumption must also be made over the capacity density of repowered or new wind installations. Capacity density describes the installed capacity of a wind or solar PV farm per unit area, typically expressed in units of MW/km2. Specified multiples of the turbine rotor diameter is a common method for defining separation distances within a wind farm, which entails a

[17]Global Energy Monitor wind tracker: https://globalenergymonitor.org/projects/global-wind-power-tracker/

State/region	Additional wind Capacity (MW)
Karnataka	10,878
Gujarat	5,789
Maharashtra	2,456
Tamil Nadu	2,098
Madhya Pradesh	1,821
Rajasthan	1,065
Andhra Pradesh	300
Gujarat offshore	8,650
Tamil Nadu offshore	8,650
Total	81,200

Table 3.2: Wind capacity additions by Indian state/region in the 'expanded scenario'.

maximum capacity density value, assuming all turbines within a farm conform to a regular layout. Figure 3.9a shows the highest density layout when spacing is defined by an ellipse of major and minor axes 8 and 4 times rotor diameter, respectively, with the major axis aligned with the direction of the prevailing wind. The rotor dimensions of the modern turbine A yields a capacity density value of 5.3MW per km in this optimal configuration.

(a) Theoretical turbine spacing

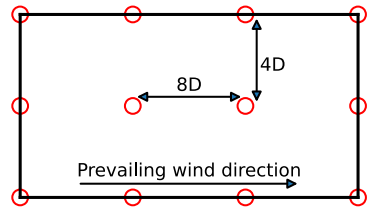

(c) Capacity density per region

Region	Mean	Min.	Max.
India	2.5	1.6	4.2
Andhra Pradesh	3.1	2.4	4.2
Karnataka	2.9	2.2	3.9
Maharashtra	2.6	1.7	3.2
Gujarat	2.4	1.6	3.3
Madhya Pradesh	2.2	1.9	2.8
Tamil Nadu	2.2	1.8	2.7
Rajasthan	2.0	1.6	2.3

(b) Capacity density existing wind farms

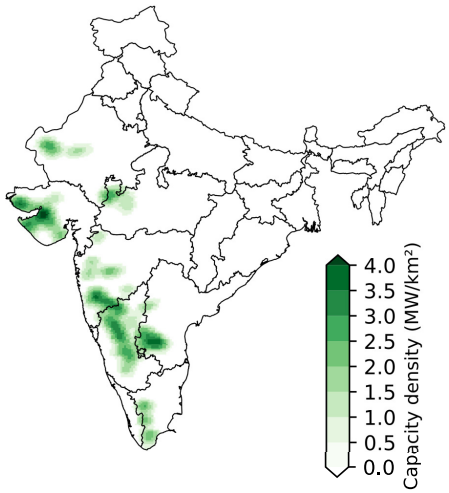

Figure 3.9: (a) Highest density theoretical turbine layout, with spacing defined by 8x4 rotor diameters (D) and major axis aligned with the direction of the prevailing wind; (b) capacity density of existing wind farms based on bounding polygons of wind turbines geolocated within OpenStreetMap data (smoothed with Gaussian kernel filter for visual clarity, as shaded bounding polygons for individual farms are illegible in whole country visualisation); and (c) summary of capacity density values of existing wind farms per state.

However, obstacles and constraints at the farm level often prevent a regular turbine siting, resulting in lower capacity density values than theoretical values under optimal layout. Fig-

ure 3.9b shows the capacity density values across existing wind farms in India, determined by calculating the area of bounding polygons around all wind farm clusters and dividing by the wind farm's total capacity. Wind farm clusters in the year 2021 are identified using exact wind turbine locations in India taken from OpenStreetMap and minimally bounding polygon areas calculated with a convex hull algorithm, a common method for defining the land footprint of wind farms (Enevoldsen and Jacobson, 2021; Harrison-Atlas et al., 2022). The OpenStreetMap data contain turbine locations only, and so a spatial join is made with the Indian Wind and Solar Database (IWSD) to yield total capacity per wind farm cluster. This method for estimating capacity density yields a median value for all-India of 2.5MW per km. This value is lower than theoretical or characteristic values used in other works (e.g., Eurek et al., 2017; Bosch et al., 2018) but in line with empirically derived values that are typically 50% or less than values derived from optimal layouts (Denholm et al., 2009; Miller and Keith, 2018). Both the 'repowering' and 'expanded' scenarios consider a continuation of the current median value of capacity density (2.5MW per km) for both onshore and offshore wind. This capacity density value for offshore wind is low by current international standards (Enevoldsen and Jacobson, 2021) but is reasonable given the geographic concentration of wind turbines in planned offshore zones for India, which necessitate greater turbine spacing to offset wake losses (Miller et al., 2015).

3.5.4 Comparison with wind generation in decarbonisation pathways

Further analysis in Chapter 7 compares wind capacity factors and energy yield in India with equivalent values in existing decarbonisation scenarios, specifically, the Working Group III database (Byers et al., 2022) of decarbonisation pathways presented in the 6th IPCC Assessment Report (Riahi, Schaeffer, et al., 2022). The majority of the 3131 pathways contained within the WGIII database are global in scope (n=2266), although a number of the pathways are from models specifically designed for country or regional analyses. Only the pathways based on a globally integrated model were evaluated for their climate response in the AR6 WGIII assessment (Riahi, Schaeffer, et al., 2022), and only 1686 scenarios passed a vetting process that disregarded pathways that deviated from historical trends or displayed unrealistic future changes. Of the 1686 pathways which passed vetting, 1202 had sufficient emissions species and projection timeframe to be considered for climate assessment with climate response emulators. Of these 1202 pathways, the 823 that included national-scale detail for India we considered in

the analysis.

The variables in AR6 pathways named 'Secondary Energy—Electricity—Wind' are used in this analysis. The 'direct equivalent' method is used for energy accounting in AR6, which counts a unit of secondary energy sourced from non-combustible sources (e.g. wind and solar PV) as a unit of primary energy. However, secondary energy is a more widely reported variable in the AR6 pathways and so is considered as the best representation of gross generation from wind and solar PV (i.e. without accounting for transmission losses). The capacity variables in AR6 pathways named 'Capacity—Electricity—Wind' are used.

This concludes the Data and Methods section of the thesis, and the four respective Results chapters now follow.

Chapter 4

Model synthesis of wind and solar PV generation in India

4.1 Rationale for investigation and research questions

The short record of observed generation from wind and solar PV technologies at the scale of Indian states (just 4-5 years) limits opportunities to appraise generation variability, particularly on interannual timescales. The objective of this chapter is to develop a model synthesis of wind and solar PV generation in India that includes geolocated farms and technology characteristics. Comparing the generation synthesis against observed values provides a basis for calibration and verification. The use of multi-decadal atmospheric reanalysis as input to the generation synthesis elucidates the climatological patterns of generation. This chapter considers the following research questions:

1. Does the transformation of raw reanalysis data fields accurately represent wind and solar generation for installations in India?
2. How effective are different calibration procedures at reducing bias in the synthetic generation time series derived from the reanalysis?
3. How similar are wind and solar PV generation profiles between regions and seasons?
4. Is the synthetic generation sensitive to the specific parametrisation of wind and solar PV technologies?

4.2 Generation synthesis

4.2.1 Wind

The synthetic wind generation time series that results from the method described in Section 3.2 is shown in Figure 4.1. This synthetic wind generation time series is for raw ERA5 wind speed data, i.e., without any bias correction. The resulting synthetic wind generation time series spans 2017-2021 and is shown in Figure 4.1 at both weekly and monthly timescales (N.B. underlying synthesis is at hourly timescale, with temporal aggregation used in Figure 4.1 for visual clarity). The actual generation time series, as reported by Regional Load Dispatch Centres (RLDCs), are displayed as black lines in Figure 4.1.

A similar seasonal generation profile is apparent for all regions, with peak generation during the Indian summer monsoon (ISM) season and a minimum in boreal winter. The smaller secondary generation peak during boreal winter is likely caused by the northeast monsoon. Higher frequency variability is smoothed in the all-India case because more uncorrelated variability in generation is cancelled out over the country-wide aggregation. The poor generation year in 2020 has been documented elsewhere within industry and governmental sources (Shekhar et al., 2021) and is evident across all regions shown in Figure 4.1.

Visual inspection of the resulting timeseries suggests a high correlation with observations, albeit with mean bias that varies between the regions. Modest, consistent underestimation of observed capacity factors is seen for the all-India case (averaging -6%). Consistent over/underestimation of a similar magnitude is apparent for the Northern and Southern regions, respectively (averaging +7%/-17%). No clear mean bias is seen in the Western region (-1.5%).

Figure 4.3 shows the same resulting synthetic generation timeseries for wind but for seven individual Indian states (those states with >200MW capacity, c.f. Figure 3.6). Of the three states that make up the Western region, only Gujarat shows modest overestimation, while both Maharashtra and Madhya Pradesh show underestimation. Underestimation of observed generation is apparent in all three states of the Southern region (Andhra Pradesh, Karnataka and Tamil Nadu). However, the underestimation is greater for the case of Tamil Nadu and less consistent through the season, with generation underestimated through summer months and overestimated in winter months.

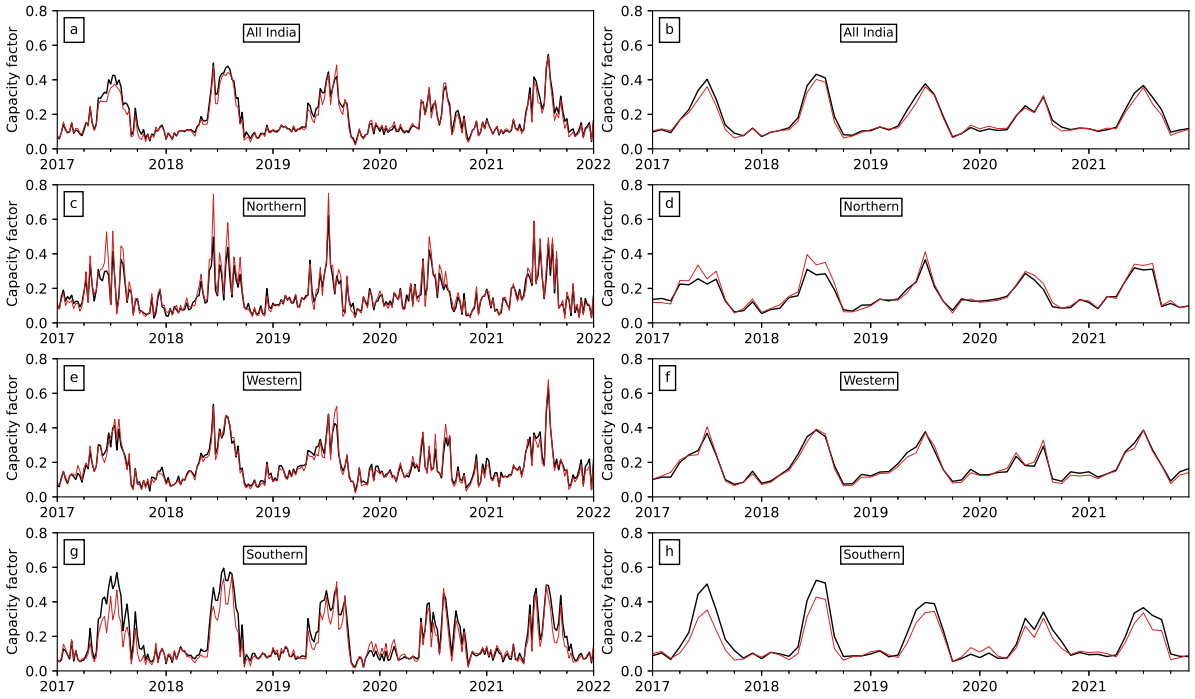

Figure 4.1: Observed (black) and synthetic (red) timeseries of wind capacity factors at a weekly (left-hand column) and monthly (right-hand column) timescales. Observed and synthesised capacity factors shown at various spatial scales: all-India (a and b), three regional grids (Northern c and d, Western e and f, Southern i and j)

The negative summer bias in Tamil Nadu likely results from misrepresentation of windspeeds in ERA5 within the four main mountain passes of the Western Ghats in Tamil Nadu (Aralvaimozhi, Shencottah, Palghat, and Cumbum). Major wind farm clusters lie immediately to the east of each pass and constitute most of the total installed wind capacity in Tamil Nadu (∼75%). The tunnelling effect of local orography within the mountain passes, and the resulting enhancement of surface wind speeds are likely only partly captured within ERA5. This effect is likely to be most active in summer when the prevailing westerly monsoon flow dominates. Outside this season, modest northeasterly winds are relatively unimpeded by topography.

For the other states showing a negative bias (Maharashtra and Madhya Pradesh in the Western Region; Karnataka and Andhra Pradesh in the Southern region), it is postulated that some of the discrepancies originate from unresolved local orographic effects in ERA5. As many installations in these states either occupy elevated or hilltop sites, it is conceivable that hill effects enhance prevailing winds (Clifton et al., 2014) at a scale below that captured by ERA5. Subranges of the Western Ghats, such as the Kalsubai Range in Maharashtra; the Vindhya range in Madhya Pradesh; ranges and outcropping across the Deccan Plateau throughout much of Karnataka and Andhra Pradesh (e.g., wind farm groupings at Chitradurga and Kadapa districts, respectively)

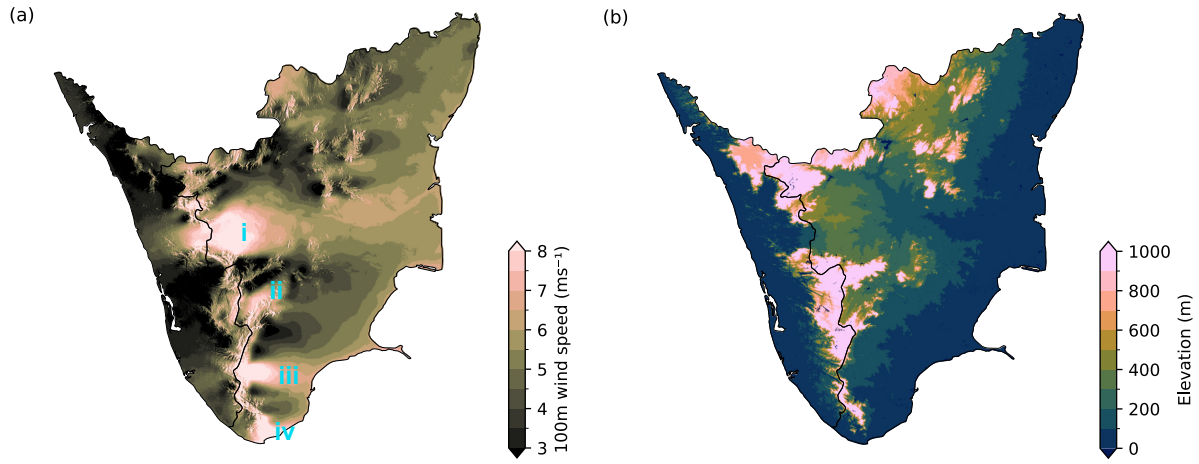

Figure 4.2: (a) 100m DTU-GWA wind speeds over southern states of Kerla and Tamil Nadu, with labelling of the four mountain passes of the Western Ghats (i) Palghat, (ii) Cumbum, (iii) Shencottah, and (iv) Aralvaimozhi. (b) elevation over southern states of Kerla and Tamil Nadu, with data from (Amatulli et al., 2018).

all host significant installations of wind capacity.

A persistent positive bias is seen in the case of Gujarat, an outcome possibly due to the coastal siting of major wind farms (e.g., within coastal regions of the Kutch and Saurashtra). The greatest positive bias is found in the Northern State of Rajasthan. Notably, the surface roughness values in ERA5 are very low within the Thar desert region of Rajasthan (<0.01, compared with values of 0.15 to 0.3 elsewhere in India), where most of the state's wind capacity is installed (>85% of the total). As the effects of surface roughness reduce the momentum of the surface wind flow (Kelly and Jørgensen, 2017), the low surface roughness values within the region potentially cause high windspeed values and explain the existence of the positive bias.

Table 4.1 summarises the performance of the generation synthesis with the three metrics described in Section 3.2.12, namely, normalised mean bias, mean absolute error (MAE) and correlation (r value). The range of normalised mean bias spans 0.94 (Northern region) to 1.22 (Tamil Nadu). MAE values decrease, and correlation increases at greater temporal aggregation levels across all regions.

4.2.2 Solar generation

The synthetic solar PV generation time series is shown in Figure 4.4 for weekly and monthly means and is produced using the raw ERA5 irradiance and temperature data, i.e., without any bias correction. The actual generation time series, as reported by Regional Load Despatch

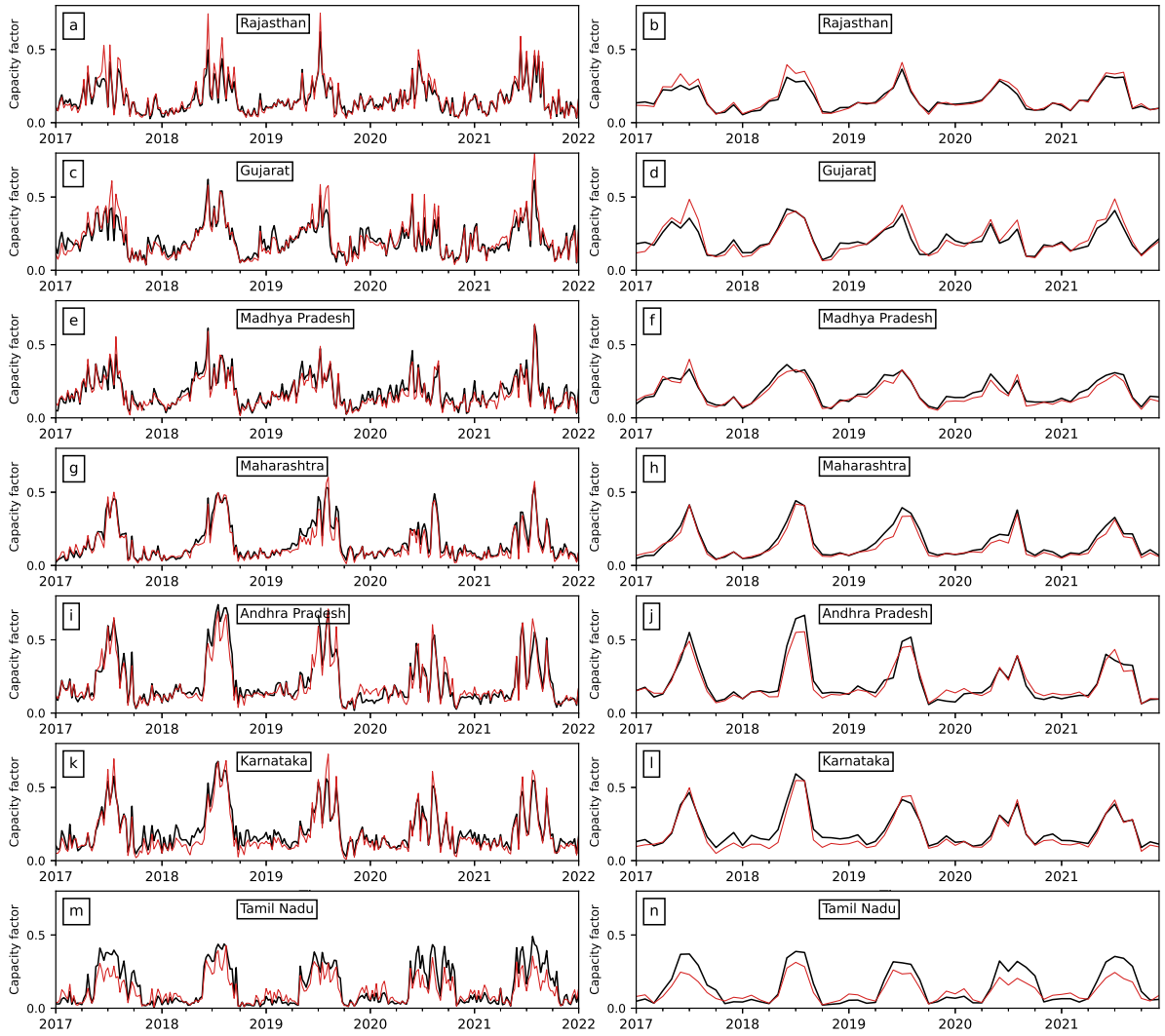

Figure 4.3: Observed (black) and synthetic (red) timeseries of wind capacity factors at a weekly (left-hand column) and monthly (right-hand column) timescales. Observed and synthesised capacity factors for seven India states

Centres (RLDCs), are displayed as black lines in Figure 4.4. The Northern RLDC lacks generation data before 2019, and monthly data is only available from 2019 onwards for the Eastern RLDC. Table 4.2 summarises the performance of the generation synthesis with the three metrics described in Section 3.2.12, namely normalised mean bias, mean absolute error (MAE) and correlation (r value).

A seasonal generation profile is common to all regions, with generation peaking during boreal spring, falling to a minimum through the summer monsoon season, and recovering through autumn and winter months. Higher frequency variability visible at the weekly averaging timescale appears slightly smoothed in the all-India case, similar to the wind case, where random uncorrelated errors cancel at the broader spatial scale. Visual inspection of the resulting timeseries

Wind					
		MAE		r value	
	Normalised mean bias	Daily	Monthly	Daily	Monthly
India	1.06	0.02	0.01	0.97	0.99
Northern	0.94	0.04	0.02	0.94	0.98
Western	1.03	0.02	0.01	0.97	0.99
Southern	1.17	0.04	0.04	0.95	0.98
Gujarat	0.97	0.04	0.03	0.93	0.95
Madhya Pradesh	1.09	0.04	0.02	0.92	0.96
Maharashtra	1.12	0.03	0.02	0.96	0.98
Andhra Pradesh	1.04	0.05	0.03	0.93	0.97
Tamil Nadu	1.22	0.05	0.05	0.90	0.95
Karnataka	1.11	0.04	0.03	0.95	0.98

Table 4.1: Key performance indicators for synthetic wind generation. Normalised mean bias refers to the ratio of observed mean capacity factor to synthetic capacity factor. Mean absolute error (MAE) in capacity factor and Pearson's correlation coefficient (r value) shown for daily, weekly, and monthly timescales.

suggests a high correlation with observations, with no clear mean positive or negative bias of significance in any of the five regions. Periods of significant positive or negative generation anomalies (such as the deficient summer season of 2020 for wind) are not apparent in the solar PV generation timeseries. When comparing surface wind speeds, the greater spatial homogeneity of solar irradiance on daily timescales results in less diversity in mean bias between the individual states of each RLDC region (not shown).

Table 4.2 summarises the performance of the solar PV generation synthesis with the three evaluation metrics. Modest underestimation of observed generation is seen in all regions, with normalised mean bias values in the range 1.02-1.07. As with the case of wind generation, MAE values decrease, and correlation increases at greater levels of temporal aggregation across all regions. Although the MAE values are lower for solar PV when compared to wind (even when normalising the MAE values by mean capacity factor), correlation values are lower than for wind across time scales, particularly for Northern and Eastern regions. This difference could, in part, be attributed to the lack of farm-specific technical details for solar PV that forces a simplified approach to the solar PV generation synthesis (fixed assumptions for orientation, array tilt, sun-tracking design, module type) and so lower fidelity in the representation of observed solar PV values. Also, inaccuracies are expected to arise from the annual resolution of commissioning dates for solar farms (see Section 3.2.3).

In the case of the Northern region, a significant proportion of total regional solar PV capacity

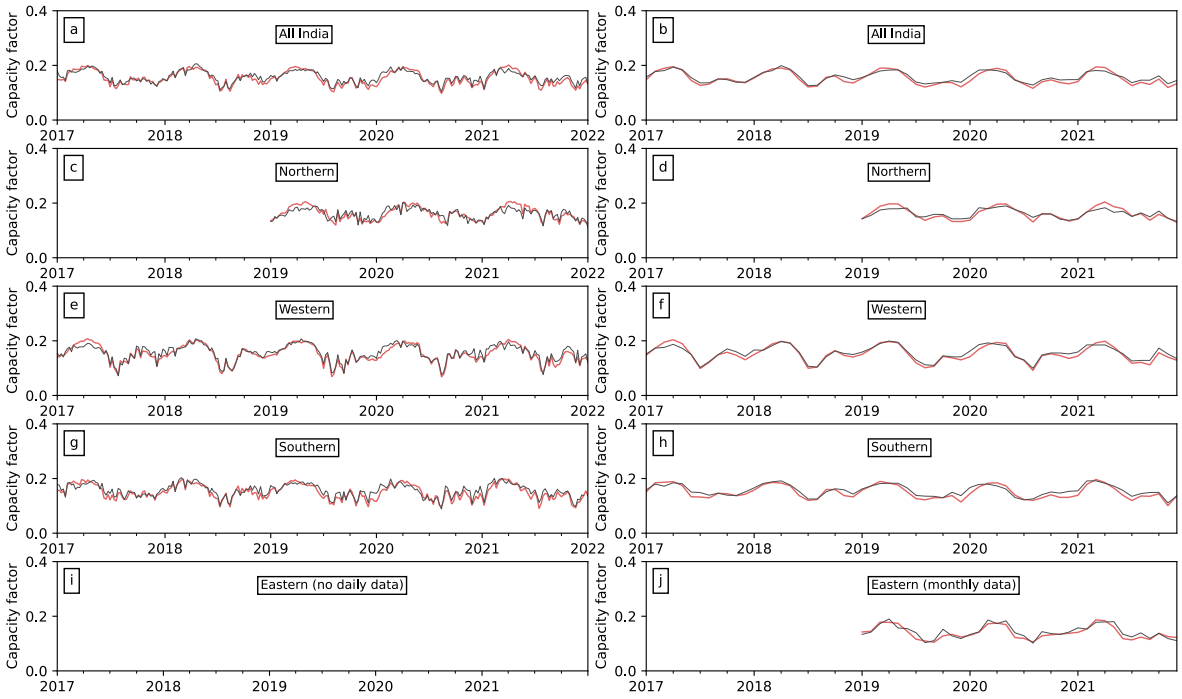

Figure 4.4: Observed (black) and synthetic (red) timeseries of solar PV capacity factors at a weekly (left-hand column) and monthly (right-hand column) timescales. Observed and synthesised capacity factors shown at various spatial scales: all-India (a and b) and four regional grids (Northern c and d, Western e and f, Southern i and j). Note, daily data was not available for the Eastern region.

is concentrated within the northwestern region of Rajasthan (including the Bhadla Solar Park, the largest solar farm in the world). This concentration implies that a relatively small number of ERA5 grid cells represent a large proportion of total capacity within the region, and so there is less possibility for the cancellation of random uncorrelated errors, which could cause an overall larger error for this region compared to regions with more spatially distributed solar PV installations. A similar effect may explain the lower correlation values found within the Eastern region, where a large fraction of the total solar PV capacity within the region is concentrated within a relatively small area.

Generally, the raw generation synthesis performs well for both wind and solar PV, particularly for regional aggregations at monthly timescales (r values >0.97 for wind and >0.9 for solar PV). The following section considers the effect of bias correction techniques on the performance of the generation synthesis.

Solar PV					
		MAE		r value	
	Normalised mean bias	Daily	Monthly	Daily	Monthly
India	1.06	0.012	0.010	0.91	0.96
Northern	1.02	0.014	0.009	0.82	0.91
Western	1.05	0.012	0.010	0.93	0.96
Southern	1.07	0.014	0.011	0.89	0.93
Eastern	1.03	-	0.010	-	0.90

Table 4.2: Key performance indicators for synthetic solar PV. Normalised mean bias refers to the ratio of observed mean capacity factor to synthetic capacity factor. Mean absolute error (MAE) in capacity factor and Pearson's correlation coefficient (r value) shown for daily, weekly, and monthly timescales.

4.2.3 Bias correction

The results presented thus far have not included any bias correction. This section considers the effects of two forms of bias correction on the generation performance. The first is a fixed mean bias correction (i.e., a constant value that applies at all timescales) using additional meteorological data sources: the DTU-GWA for wind and the GSA for solar PV. The second method applies a multiplicative factor to raw ERA5 variables such that mean bias in the period 2017-2021 is zero (see Section 3.2.11 for additional details of the bias correction techniques).

Figure 4.5 summarises the effect of these bias correction techniques on the performance of the generation time series at the daily time scale by presenting the same three performance metrics as in Table 4.1. The red markers in Figure 4.5a-g show the daily performance metrics for the wind and solar PV generation synthesis using raw ERA5 data (i.e., the same values presented in Table 4.1). The blue markers in Figure 4.5a-f show the metrics for the mean bias correction, and the green markers show the multiplicative adjustment.

By definition, the normalised mean bias is 1 for the multiplicative adjustment. The mean bias correction using DTU-GWA results in an overestimation of wind generation for all but the Northern region. Aside from the large overestimation in the southern state of Tamil Nadu, the normalised mean bias values are of similar magnitude but the opposite sign for the raw and mean bias versions of the wind generation synthesis. The mean bias correction using GSA data for the solar PV generation synthesis results in a modest overestimation in all regions. In most instances, changes in MAE and correlation between the raw ERA5 and mean bias-correction syntheses are minor for both wind and solar PV. As the difference in wind speeds between

the raw and mean bias-corrected versions are generally within the linear ramping range of the wind turbine power curve, changes in the scale-invariant r values are negligible. Also, the use of a smoothing operator on the aggregated power curve (Equation 3.1), which is calibrated to observed generation, contributes to the minimal changes to correlation following the bias correction procedure[1]. A similar effect likely explains the similar r values found for the raw and mean bias-corrected versions of the solar PV synthesis, as modest irradiance differences impact a linear ramping stage of the module response, which only becomes increasingly non-linear at very high irradiance values.

[1]Re-calibrating the aggregate power curve after the bias correction contributes no further improvement in correlation.

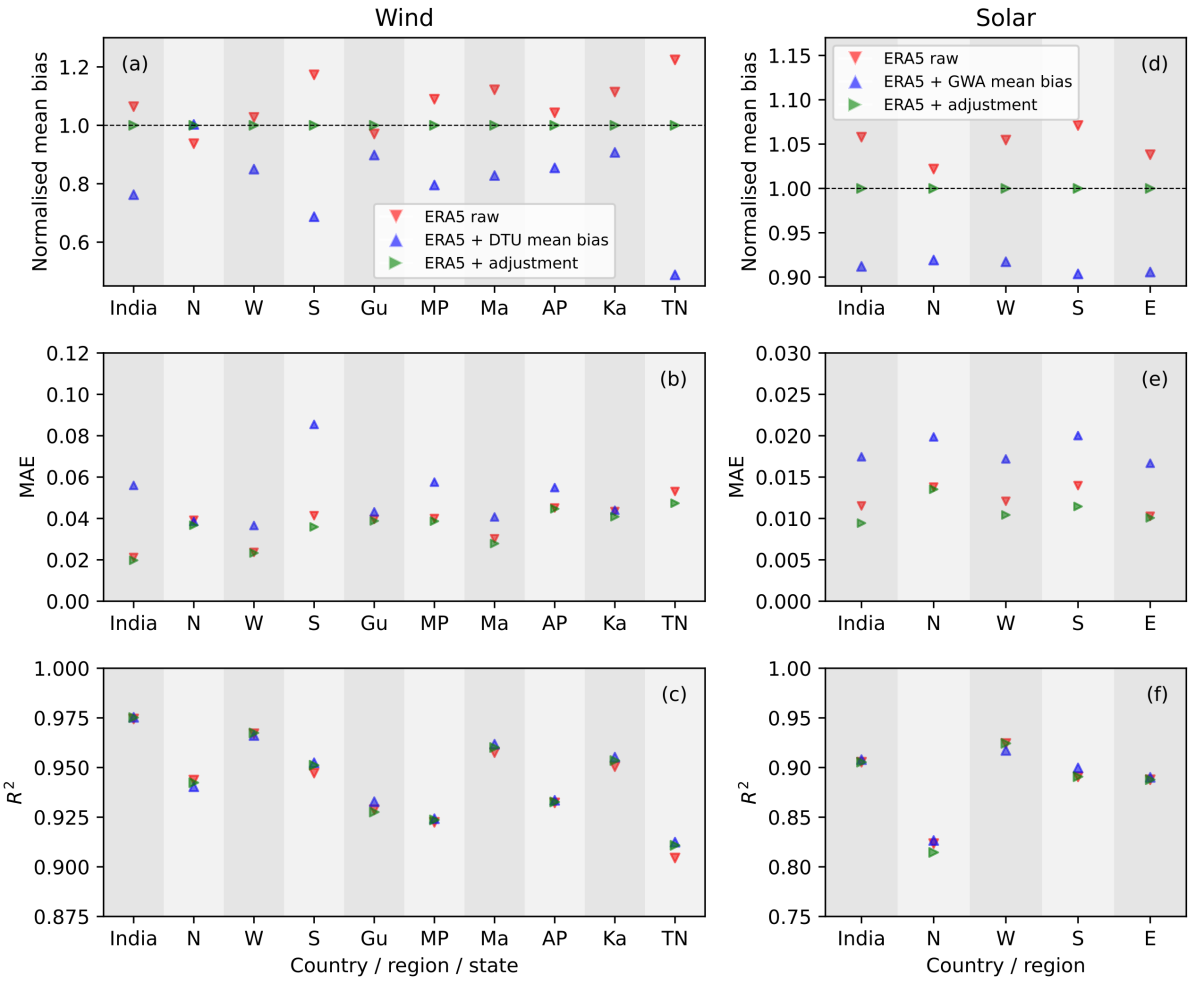

Figure 4.5: Performance metrics for wind (left-hand column) and solar PV (right-hand column) resulting from bias correction procedures. Normalised mean bias (a and d) refers to the ratio of observed mean capacity factor to synthetic capacity factor. Mean absolute error (MAE, panels b and e) and coefficient of determination (R^2, panels c and f) are calculated for daily capacity factors. Regional acronymns: N, Northern; W, Western; S, Southern; Gu, Gujarat; MP, Madhya Pradesh; Ma, Maharashtra; AP, Andhra Pradesh; Ka, Karnataka; TN, Tamil Nadu.

The generally higher 100m wind speeds in DTU-GWA compared to ERA5 have been noted within assessments of the DTU-GWA modelling chain, with the parameterisation of sub-grid orographic drag and generally higher roughness lengths in ERA5 identified as the sources of the differences (Dörenkämper et al., 2020). Furthermore, the overestimation of DTU-GWA surface wind speeds in complex terrain consequent of orographic speed-up effects has been found in Europe (Murcia et al., 2022) and was also evidenced in a verification against 16 met stations located in hilly and complex terrain in India (Ramdas et al., 2022). Peaks in the DTU-GWA >10m/s over complex mountain terrain are particularly apparent in Tamil Nadu and are the likely source of the mean positive bias in the state. Using DTU-GWA product to perform mean bias correction of reanalysis wind speeds is common in other studies (e.g., Gonzalez-Aparicio et al., 2017; Bosch et al., 2018), with a general assumption that a higher horizontal resolution enhances the fidelity of the generation synthesis (Gualtieri, 2022)). However, the results presented here suggest minimal increases in accuracy (higher r-value) resulting from the application of the bias correction with the DTU-GWA and that mean biases persist. Such findings concur with a global validation of wind generation syntheses that trailed DTU-GWA adjustments and found minor accuracy improvements and mean bias that was highly location-dependent (Gruber et al., 2022).

The ∼5% underestimation for solar PV could result from excluding sun-tracking designs within generation synthesis. However, sun-tracking designs account for only a minor share of the Indian solar fleet (13% of the total in 2022). So, the higher yield achieved by sun-tracking designs that are uncaptured in the synthesis is a likely reason for the slight underestimation.

This section on bias correction confirms the generally high performance of the generation synthesis for both wind and solar PV with raw ERA5 data (normalised mean bias is rarely more than 20%, and r values for daily generation are generally >0.9). Furthermore, using a higher resolution data product to perform a mean bias correction results in a negligible improvement to the performance of the generation synthesis (i.e., no change in r values and normalised mean bias of similar magnitude, albeit of opposite sign for wind). Finally, the second form of bias correction (applying an empirically determined multiplicative adjustment) provides the best results according to the three performance metrics considered. The values of the multiplicative adjustment per technology and state are listed in Table 4.3.

Multiplicative adjustment			
Wind		Solar PV	
Rajasthan	0.975	Rajasthan	1.025
Gujarat	0.985	Gujarat	1.07
Madhya Pradesh	1.035	Madhya Pradesh	1.065
Maharashtra	1.045	Maharashtra	1.05
Andhra Pradesh	1.015	Andhra Pradesh	1.05
Karnataka	1.45	Karnataka	1.065
Tamil Nadu	1.085	Tamil Nadu	1.065
		Eastern region	1.025

Table 4.3: Values of the multiplicative adjustment per technology and state. Adjustment applied regionally in the case of solar PV in the Eastern region.

4.2.4 Synthetic generation climatology

The multiplicative adjustments per region determined from the 2017-2021 period (Table 4.3) are applied to the ERA5 reanalysis spanning 1979-2021 to create a synthetic generation dataset spanning over four decades. The following sub-sections consider percentiles of daily generation across the full span of the reanalysis.

4.2.5 Present day wind

The daily climatology of wind generation shows a strong seasonal cycle in all regions (Figure 4.6), with generation in summer (June, July, August, September - JJAS) averaging 260% of that in winter (November, December, January, February – NDJF) for all-India. Considering the 50th percentile of generation values, 54% of total annual generation occurs in JJAS, coinciding with the Indian summer monsoon (ISM). However, it is notable that wind generation increases ahead of ISM onset, likely reflecting the formation of the summer monsoon circulation and enhanced westerly flow, consequent of tropospheric warming over Eurasia that peaks during boreal spring (Li and Yanai, 1996). The greater range of daily generation values observed in the Northern region is likely due to the concentration of most of the state's installed wind capacity (>85%) across a relatively small area centred on the northwestern city of Jaisalmer. Therefore, wind generation within the region, derived from a relatively small number of neighbouring ERA5 grid cells, results in less spatial smoothing. Across all regions, the greatest range of capacity factors coincides with the ISM season.

It is instructive to consider the seasonal pattern of both generation and demand of electrical energy as their co-variability defines requirements for grid reinforcement, storage, and comple-

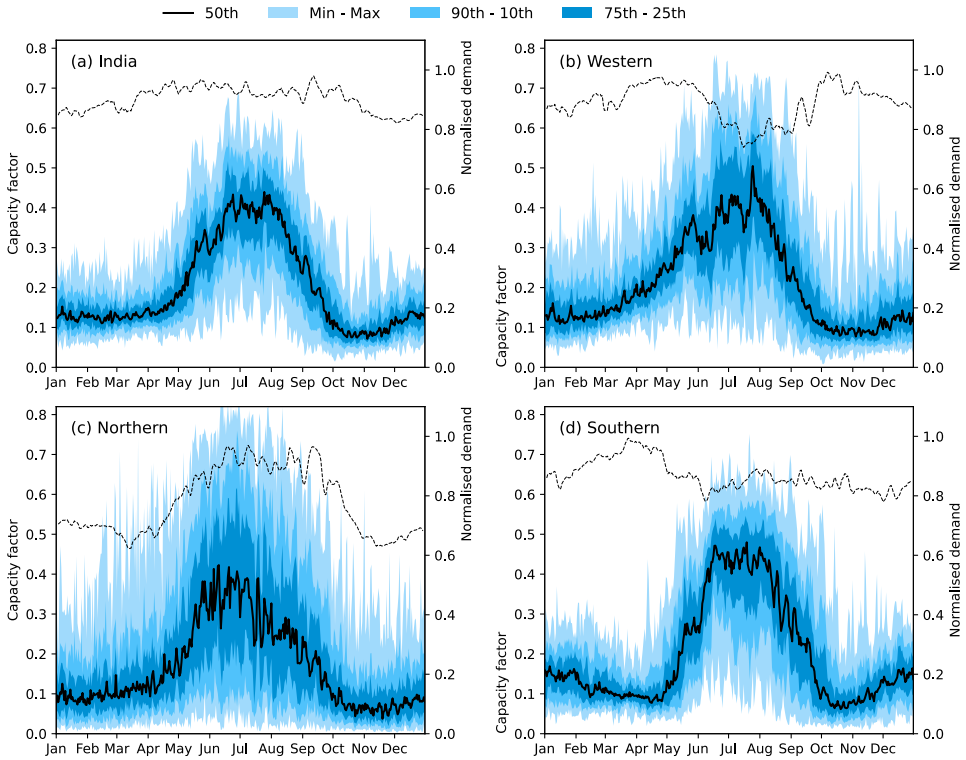

Figure 4.6: Daily climatology of synthetic wind capacity factor for all-India (a), Western (b), Northern (c) and Southern (d) regions. Synthetic wind capacity factor data is produced using the full span of the ERA5 reanalysis (1979-2021), assuming a capacity distribution as of the end of the year 2021. Black lines show the 50th percentile of daily mean capacity factor. Blue shades depict increasing percentiles of daily mean capacity factor range. Dashed black lines depict average electricity demand per region, normalised by the maximum value per region, using demand data for the period 2014-2019

mentary forms of generation (Roques et al., 2010; Bakke et al., 2016; Denholm and Mai, 2019). The normalised seasonal cycle of electricity demand overlaid in Figure 4.6 differs per region. The greatest range of electricity demand is found in the northern region, where peak values during summer fall by approximately 40% to the lowest values during winter months. Electricity demand shows a minor dip through the summer months in the western region and remains largely stable through the year in the southern region. The all-India seasonal cycle of electricity demand is also relatively muted. The seasonal pattern of electricity demand is a function of the regional economic structure (e.g., agricultural vs. service-based economy), energy end-use technologies (e.g., prevalence of electrical heating/cooling), and climate (e.g., large annual cycle in air temperature). All these factors are likely to change in future years and drive shifts in demand that could result in seasonal patterns different from the present day. However, the strong seasonal cycle in wind generation across all regions presents the possibility of seasonal mismatches between generation and demand in the future, with potential generation surplus

through the summer months and deficit during winter.

4.2.6 Present day solar PV

The daily climatology of solar PV generation also shows a seasonal cycle in all regions (Figure 4.7), albeit of lesser magnitude than wind. A clear generation slump is observed in all regions during summer (JJAS), likely corresponding with increased cloud cover and lower surface irradiance during the ISM. The western and eastern regions show the largest absolute decline during the summer months, likely due to the location of these states at the centre of the monsoon trough, with greater incidence of low-pressure systems and cloud cover. The winter months also see a period of low solar PV generation, likely a combined outcome of the annual solar cycle and the winter northeastern monsoon. Solar PV generation generally peaks in spring (March, April, and May; MAM), and declines ahead of the ISM onset, potentially linked to aeolian desert dust transport from the deserts and drylands of West Asia, the Middle East and North Africa across the Arabian Sea into peninsular India (Pease et al., 1998). Across all regions, the summer season experiences the greatest absolute and relative range of solar PV capacity factor values; however, this range is less than for wind. The greater range of capacity factors in the Southern region during winter months is likely related to the winter northeastern monsoon, which brings the majority of the total annual rainfall to southern states.

Figure 4.8 shows the seasonal cycle of the combined wind and solar PV capacity factors. The exact outcome of the combined generation of wind and solar PV depends on the installed capacity and the resulting balance between both sources. In the configuration representative of the year 2021 shown in Figure 4.8, a degree of compensation between wind and solar PV generation is found during the summer months. However, the joint minima during winter months for both wind and solar indicates a potential generation constraint should levels of installed wind and solar PV capacity increase in line with the current wind-solar PV capacity balance.

4.3 Long-term trends

4.3.1 Trends in synthetic wind generation

The annual mean synthetic wind capacity factor for all India and sub-regions shows a modest declining trend (Figure 4.9). The trends are significant at the 99% level in all regions except the

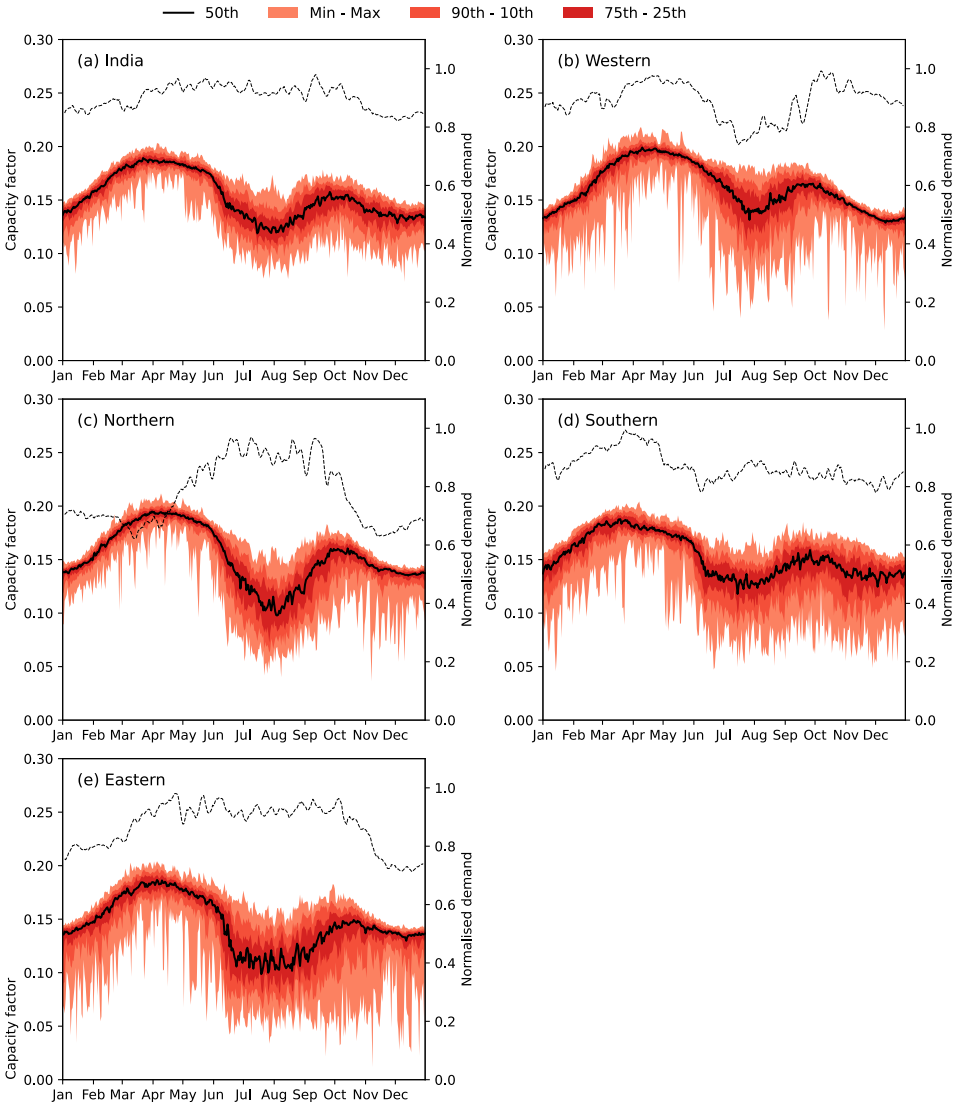

Figure 4.7: As in Figure 4.6 but for solar PV capacity factors.

Southern region, using a Mann-Kendal test. One must exercise caution in estimating long-term trends in reanalyses due to the potential for spurious effects from the time variation in the observational data used in the data assimilation process (Wohland et al., 2019). Nevertheless, a long-term negative trend in surface and lower troposphere wind speeds over India has been noted in several other studies, with the greatest absolute reductions occurring during the ISM period (Joseph and Simon, 2005; Fan et al., 2010; Jaswal and Koppar, 2013; Saha et al., 2017; Torralba et al., 2017a; Abdulla et al., 2022). Joseph and Simon (2005) found lower tropospheric zonal winds in summer have decreased by 20% in the period 1950-2002 through peninsular India, with a concomitant 30% increase in the duration of break monsoon conditions. Jaswal and Koppar (2013) found a declining trend in annual average surface winds of -0.24m/s per

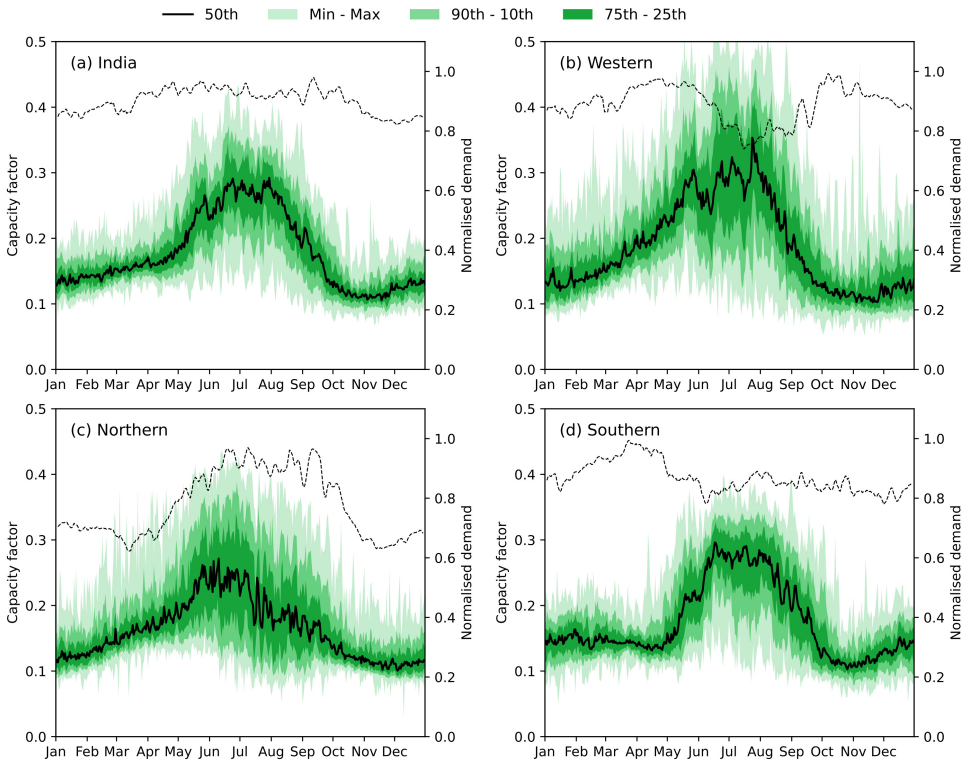

Figure 4.8: As in previous Figure but for combined wind and solar PV capacity factor.

decade in the period 1960-2008 (-11.9% of long-term average mean wind speed). Gao et al. (2018) used a reanalysis dataset to estimate wind generation in India from 1980 to 2016, finding a -3.4% per decade decline. The reductions in capacity factors observed in Figure 4.9 range between -5.2% to -2.3% per decade – i.e., in line with previous studies.

This 'stilling' phenomenon, whereby surface wind speeds over land have generally decreased since the 1970s, is widely documented elsewhere across the globe (Roderick et al., 2007; Vautard et al., 2010; McVicar et al., 2012). Several underlying causes of the declines have been proposed (Wu et al., 2018), including increased surface roughness consequent of increased in vegetation cover (Vautard et al., 2010; Zhu et al., 2016), increased surface drag consequent of urbanisation (Zhang et al., 2022), internal decadal-scale climate variability (Zeng et al., 2018; Zeng et al., 2019), or measurement errors related to instrument sensitivity, archiving errors and/or instrument position (Azorin-Molina et al., 2018). More recent studies note a slowing or reversal in the global long-term wind speed declines since the early 2010s. However, Dunn et al. (2022) suggest that these reports are attributable to data archiving errors and that underestimated wind speeds in earlier decades are possible with less sensitive, older-generation cup anemometers. The evidence of weakening surface winds since the 1970s over land is robust at

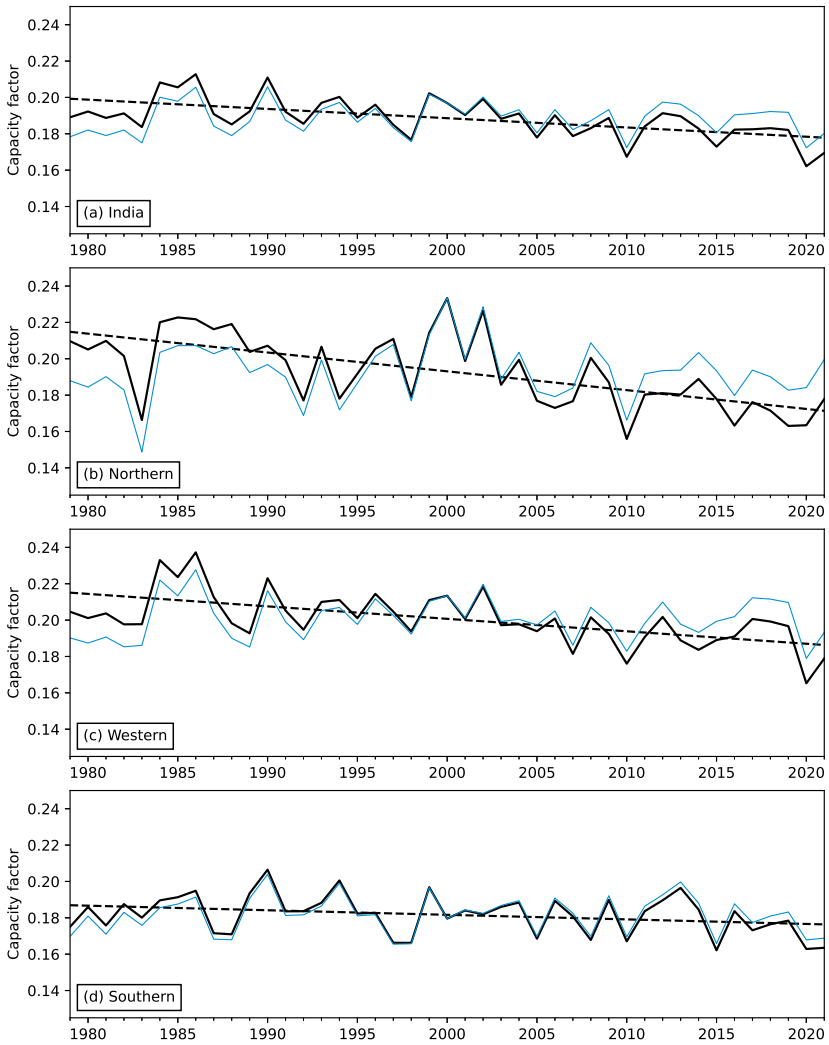

Figure 4.9: Annual mean synthetic wind capacity factor for all India (a) and three regions (b-d) for the period 1970-2021 (black line). Linear trend shown as dashed black line, and detrended timeseries shown in blue.

a global level, but with low confidence in a recovery since around 2010 and little agreement between observational datasets over India (Gulev et al., 2021). Recent evidence of a weakening of the South Asian Monsoon circulation (a candidate for possible declining trends in surface wind speeds) has mainly been attributed to increased anthropogenic aerosols (Arias et al., 2021).

An important note on these trends identified in the 43-year generation synthesis is that the decline reflects ceteris paribus conditions for the year 2021 – i.e., assuming the same types and distribution of present-day wind farms in India. In reality, changes to the Indian wind power fleet have occurred over time, with older designs of inferior performance becoming increasingly less common and improved siting and operational practice further enhancing capacity factors. This aspect of a changing wind turbine fleet is returned to in a later section that calculates the

sensitivity of the wind generation synthesis to the specified turbine model.

4.3.2 Trends in synthetic solar PV generation

The annual mean synthetic solar PV capacity factors for all-India and the sub-regions show declining trends (Figure 4.10). These trends are significant at the 99% level in all regions except the Western region, using a Mann-Kendal test. The most likely causes of these trends are changes to regional aerosol loading, cloud cover and cloud composition (Soni et al., 2012). Globally, evidence of 'global dimming' at a rate of 2-4% per decade was strongest from the 1960s to 1990s (Stanhill and Cohen, 2001; Liepert, 2002). Several regions have seen an increase in global horizontal irradiance since the 1990s, though the long-term negative trend persists across the Indian subcontinent (Wild et al., 2005; Padma Kumari et al., 2007; Ramanathan et al., 2005; Singh and Kumar, 2016) with some evidence of a slowdown in the rate of decline since the 2000s (Wild et al., 2009; Soni et al., 2016). The linear trend in Figure 4.10 is -0.9% per decade for the all-India case and between -0.5 to 1.8% per decade for the sub-regions, approximately in line with the trend in irradiance at the surface found in the studies mentioned above.

Enhanced scattering and absorption of solar irradiance have been identified as the cause of reductions in global horizontal irradiance across India, a result of increased anthropogenic aerosol loading (particularly sulphate aerosols arising from coal-power sulphur dioxide emissions (Wild et al., 2009; Yang et al., 2022)). Ahead of monsoon onset, prevailing westerly surface winds transport dust from the deserts and drylands of West Asia, the Middle East and North Africa across the Arabian Sea into peninsular India (Pease et al., 1998). This aeolian desert dust constitutes another significant aerosol source, particularly in the northern regions of India; however, trends in desert dust loading have remained stable or show a decreasing trend in recent decades (Gautam et al., 2009; Dey and Di Girolamo, 2011). Variations in the Earth's orbit and the solar output can also influence the top-of-atmosphere incident solar radiation. However, trends between minima of the 11-year solar cycle suggest minimal or insignificant trends in recent decades (Willson, 1997; Kopp, 2016) of an order of magnitude lower than changes to global horizontal irradiance at the Earth's surface, and so can be neglected. Rising air temperatures over the Indian land area could also influence solar PV generation, as solar PV module efficiency reduces with increasing ambient temperature. However, the region's annual average air temperature increase is ∼1C, implying a negligible impact on solar PV module performance and the observed capacity factors.

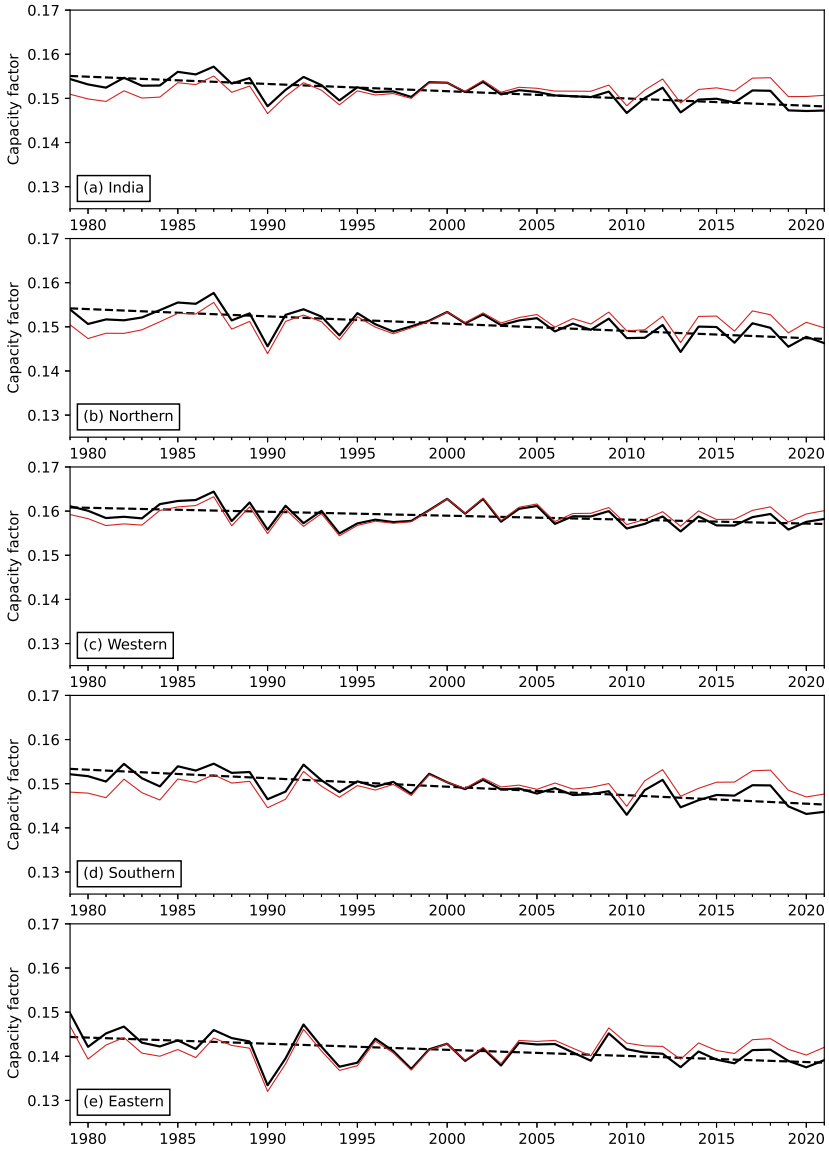

Figure 4.10: Annual mean synthetic solar PV capacity factor for all India (a) and three regions (b-d) for the period 1970-2021 (black line). Linear trend shown as dashed black line, and detrended timeseries shown in red.

As was noted for wind generation in the previous section, observed trends in actual solar PV generation will be affected by factors not considered here such as changing installed capacity over time and changes in solar PV module efficiency, which have averaged increases of ∼1% per annum globally over the past decade, with continued improvements of the same magnitude projected for the next decade (VDMA, 2022).

4.4 Generation anomalies

Figures 4.9 and 4.10 in the previous sub-section display annual capacity factor values for wind and solar PV, respectively, with linear trends overlaid. Annual and seasonal anomalies in the following sub-sections remove these long-term linear trends from the generation timeseries.

4.4.1 Annual and seasonal wind generation anomalies

The interannual variations in all-India wind capacity factors for different seasons are shown in Figure 4.11 as absolute anomalies. Interannual variability is largest in JJAS in absolute terms. Table 4.4 shows the range (max/min) and standard deviation in JJAS wind capacity factors per region in relative terms (i.e. the absolute capacity factor anomaly divided by the all-time mean value). The magnitude of interannual variability is greater for the regional subdivisions than the all-India case, in the region of +/- 20-30% of the JJAS mean. The largest negative anomaly in JJAS for all-India between 1979-2021 was the year 2020 (-29%, equivalent to a -2.9σ absolute anomaly) and the largest positive anomaly was in 1990 (+14%, equivalent to +1.8σ absolute anomaly). For comparison, an existing generation synthesis for Europe (Bloomfield and Brayshaw, 2021) shows the greatest magnitude of interannual variability for onshore wind in the DJF season, with a standard deviation in wind capacity factors ∼35% greater than the JJAS season for India. These differences are likely due to different prevailing meteorological environments within the tropics and extratropics and the different scales of spatial averaging.

	Min	Max	Std.
India	-23%	14%	8%
Northern	-30%	27%	14%
Western	-29%	18%	10%
Southern	-18%	17%	7%
Gujarat	-32%	17%	12%
Maharashtra	-26%	27%	11%
Madhya Pradesh	-26%	20%	11%
Andhra Pradesh	-22%	22%	9%
Karnataka	-18%	24%	8%
Tamil Nadu	-18%	12%	7%

Table 4.4: Range and standard deviation in relative wind generation anomaly for JJAS season per region (units are percentage of the JJAS seasonal mean capacity factor).

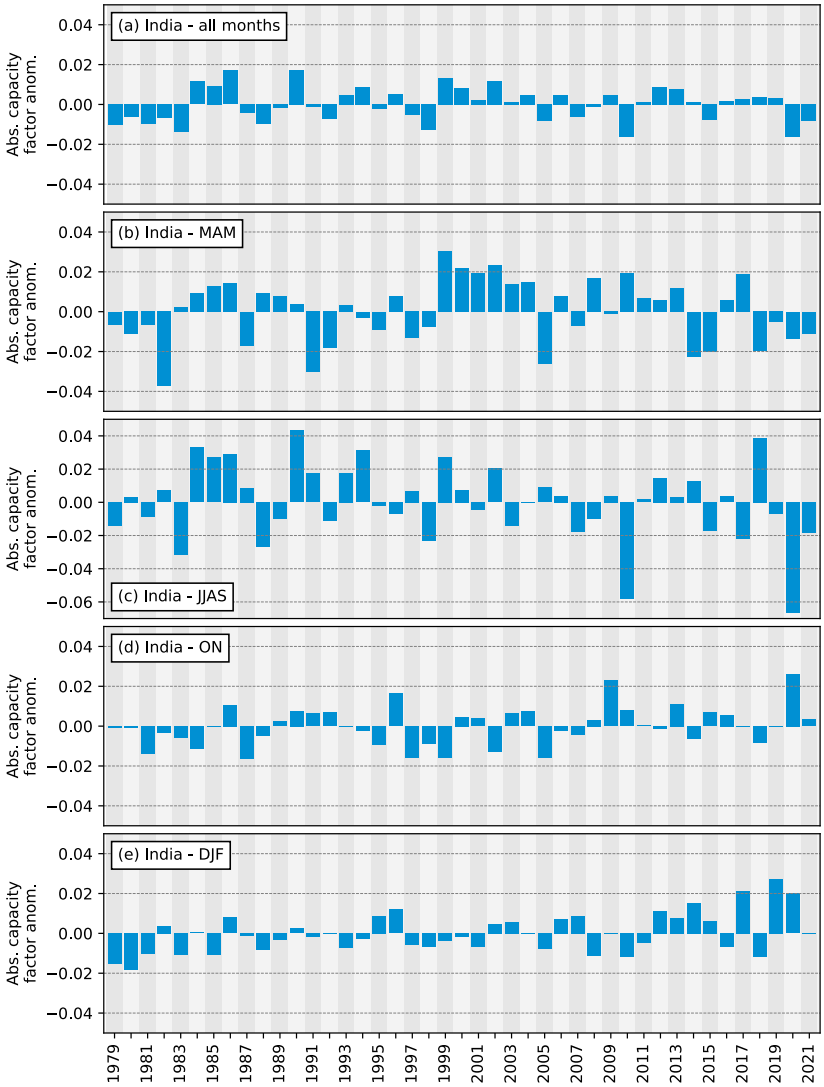

Figure 4.11: Absolute wind capacity factor anomaly for all-India for annual and seasonal averaging periods.

4.4.2 Annual and seasonal solar PV generation anomalies

The interannual variability in all-India solar PV capacity factors for different seasons is shown in Figure 4.12 as absolute anomalies. As for wind, interannual variability is largest in JJAS The greatest range in JJAS capacity factors is seen for the states Madhya Pradesh and Chhattisgarh (Table 4.5), which are both located within the monsoon trough region. The largest negative anomaly in JJAs for all-India between 1979-2021 was the year 2013 (-8%, equivalent to a -2.3σ absolute anomaly) and the largest positive anomaly was in 1987 (+9%, equivalent to a +2.5σ absolute anomaly). Using data from Bloomfield and Brayshaw (2021) for synthetic solar PV generation, the interannual standard deviation is larger in Europe for annual mean capacity fac-

tors, but comparable in magnitude for the summer season (13% of mean for European countries vs 11% across Indian states).

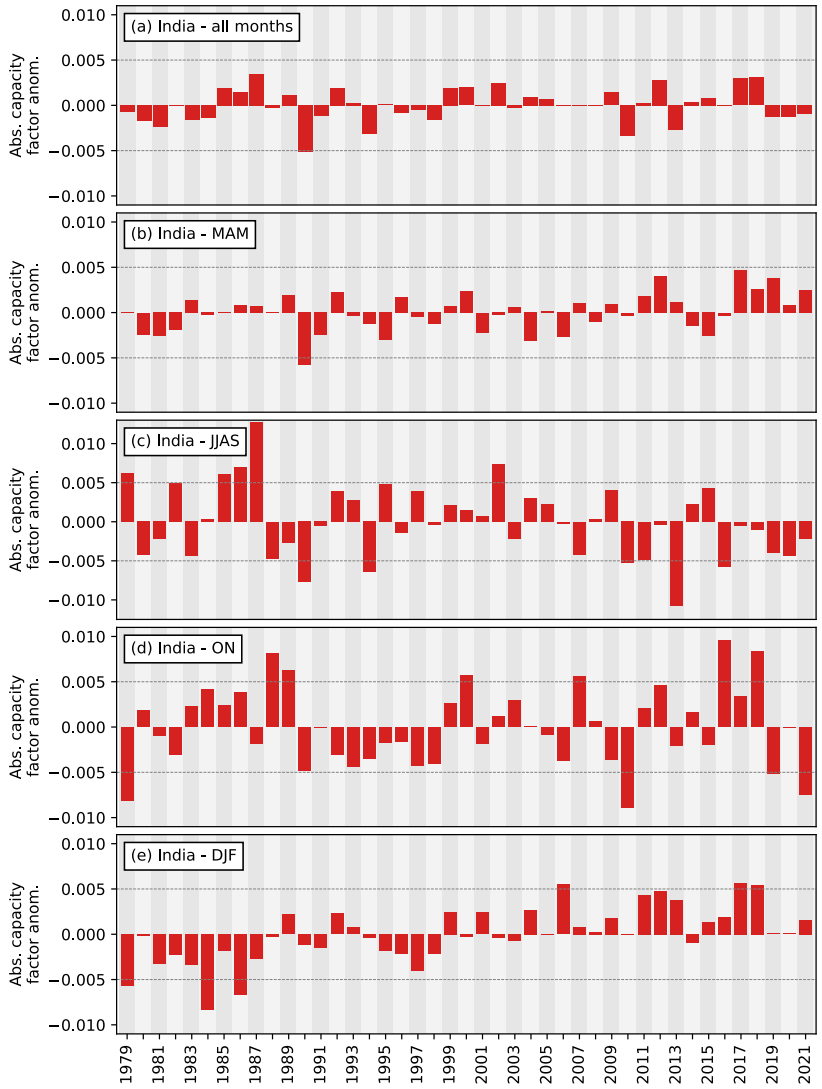

Figure 4.12: Absolute solar PV capacity factor anomaly for all-India for annual and seasonal averaging periods. Relative capacity factor anomaly refers to absolute capacity factor anomaly divided by the all-time mean capacity factor for the season.

4.4.3 Spatial patterns in seasonal generation anomalies

The following section considers the spatial covariance of generation anomalies in JJAS across India. First, the correlation in generation anomalies between regions is appraised for wind and solar PV technologies separately before considering whether anomalous years for wind and solar coincide.

	Min	Max	Std.
India	-8%	9%	3%
Northern	-10%	10%	4%
Western	-12%	14%	5%
Southern	-8%	8%	4%
Eastern	-11%	13%	5%
Rajasthan	-11%	16%	5%
Gujarat	-11%	15%	5%
Madhya Pradesh	-17%	15%	6%
Maharashtra	-14%	10%	5%
Karnataka	-8%	8%	4%
Andhra Pradesh	-7%	8%	4%
Tamil Nadu	-6%	5%	3%
Chhattisgarh	-16%	15%	6%

Table 4.5: Range and standard deviation in relative solar PV generation anomaly for JJAS season per region (units are percentage of the JJAS seasonal mean capacity factor).

4.4.4 Correlation between regions per technology

Table 4.6 shows the cross-correlation coefficients between regions for JJAS wind generation anomalies. All regions are positively correlated with all-India, with the Northern region less correlated, partly due to a lesser contribution to the all-India capacity total (∼11% in 2021 compared to ∼42% for the Western region). Neighbouring regions are positively correlated; the distant Northern and Southern regions show no significant co-variability.

	JJAS wind generation anomalies			
	India	NR	WR	SR
India	**1.0**	**0.64**	**0.94**	**0.84**
NR		**1.0**	**0.67**	0.18
WR			**1.0**	**0.63**
SR				**1.0**

Table 4.6: Cross-correlation between regions for JJAS mean wind generation anomalies, with values representing Pearson correlation coefficient. All values in bold are significant at the 95% level.

Table 4.7 shows the cross-correlation between regions for JJAS solar PV generation anomalies. All regions are positively correlated with all-India, with the Eastern region less correlated, likely due to a lesser contribution to the all-India capacity total (less than 2% in 2021) and geographically concentrated installations. The most distant Northern, Eastern and Southern regions show the weakest correlation. Potentially, the lowest cross-correlation for solar PV (Southern and Eastern regions 0.4) is related to the opposite sign rainfall anomalies typically

seen in the southern region compared to the rest of India during monsoon season with positive rainfall anomaly (Goswami and Mohan, 2001; Rajeevan et al., 2010).

	JJAS solar PV generation anomalies				
	India	NR	WR	SR	ER
India	1.0	0.81	0.91	0.92	0.65
NR		1.0	0.81	0.56	0.56
WR			1.0	0.71	0.69
SR				1.0	0.40
ER					1.0

Table 4.7: Cross correlation between regions for JJAS mean solar PV generation anomalies, with values representing Pearson correlation coefficient. All values are significant at the 95% level.

4.4.5 Correlation between technologies per region

The correlation between wind and solar PV generation anomalies in JJAS is not statistically significant (r=0.27, p=0.09; see Table 4.8). The strongest and most widespread co-variability is between wind in the Northern region and solar PV in all other regions (r=0.44-0.61; see Table 4.8). The only significant negative correlation is found between Southern region wind generation anomalies and Northern solar PV generation anomalies. The correlation between regions and sources is greater than for the all-India case, yet is still generally low and insignificant in half of the cases. This generally low co-variability between wind and solar PV suggests distinct physical drivers of generation anomalies in JJAS for the two sources, which will be investigated in Chapter 5.

		Solar			
		India	NR	WR	SR
Wind	India	0.27	0.01	0.18	**0.39**
	NR	**0.55**	**0.44**	**0.61**	**0.46**
	WR	**0.38**	0.11	0.21	**0.51**
	SR	-0.10	**-0.31**	-0.13	0.04

Table 4.8: Cross correlation between technologies and regions for JJAS mean generation anomalies, with values representing Pearson correlation coefficient. All values in bold are significant at the 95% level.

4.5 Sensitivity testing

To test the sensitivity of the results presented thus far, several aspects of the methodology are varied to determine the effects on wind and solar PV generation synthesis.

4.5.1 Wind turbine systematic assignment

As turbine models differ in hub height, rotor diameter and associated power curve, the exact turbine model used in the implementation of the generation synthesis methodology will affect the resulting capacity factors. The generation synthesis described in the above sections uses turbine-specific information (hub height and power curve) that reflects the actual turbine model per wind farm in India. Here, the generation synthesis process is repeated for the period 2017-2021 with alternative turbine models assigned to all wind farms. In total, 805 repetitions of the synthesis are considered (reflecting the number of available turbine model data). The multiplicative adjustment, defined by the actual turbine model per wind farm in India, is used in all repetitions. Therefore, differences in capacity factor between the generation syntheses reflect changes in the hub height, rotor diameter, and associated power curve only.

Figure 4.13 summarises the range of capacity factors resulting from the different turbine assignments. Taller turbines with fewer KW of rated power per unit swept area (ratio referred to as specific power) achieve the greatest capacity factors. This is because taller turbines access higher wind speeds at greater heights within the boundary layer, and as larger rotor diameters increase energy capture and generate over a wider range of wind speeds (particularly at lower wind speeds with a lower cut-in speed) (Madsen et al., 2020). Figure 4.13 highlights the highest capacity factor turbine (Suzlon S144 3.15MW, 0.35) and plots an additional point the represents the current fleet average (0.19).

The systematic assignment of different turbine models also impacts the accuracy of the generation synthesis (measured as % change in correlation for daily capacity factor values). This change in accuracy is tested by repeating the above 805 turbine assignments, but this time, implementing the same adjustment factor method to reduce mean bias relative to the observed period. As all power curves show similarities in the profile of the power response (cut-in, ramping, rated and cut-out phases), much of the observed day-to-day variability is captured by the modified versions of the generation synthesis. However, differences in the profile of the power

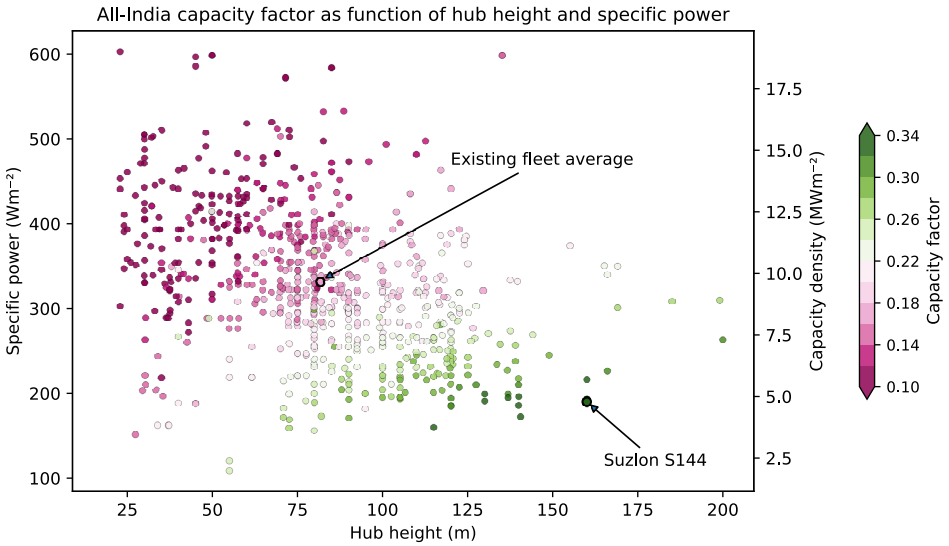

Figure 4.13: All-India capacity factor as a function of hub height and specific power, for alternative turbine model assignments (n=805, with each scatter point representing a different turbine model assigned to all wind farms in India). Arrow labels show existing Indian wind farm fleet average capacity factor and the turbine assignment with the highest capacity factor (Suzlon S144 3.15MW).

response between the assigned and accurate power curves cause a degradation in the accuracy of the generation synthesis. The 95th percentile of these changes range between -18.6 to -9.6% amongst the regions and between -8.6 to -4.9% for the 50th percentile of the changes. A common approach in comparable studies that produce wind generation syntheses is to assume a fixed turbine type nationwide. However, this sensitivity analysis suggests an appreciable degradation in synthesis accuracy under such a fixed assumption.

4.5.2 Wind spatial distribution

The wind generation synthesis presented in the main results used the best estimates of the actual farm locations. Here, the effect of a generic assignment (GA) of wind farm location is tested, whereby the synthesis is undertaken for all onshore locations (i.e., all grid cells within the boundary of mainland India), assuming a single fixed turbine model. Such an approach is common within comparable studies of wind energy generation potential and performance (e.g., Eurek et al., 2017; Bosch et al., 2018). As this sensitivity test requires all wind turbine models to be the same, comparisons are made to a reference case (RC), where the correct wind farm locations are used but with the same single fixed turbine assignment. Differences between the two results will, therefore, be associated only with the differing geographical locations of the farm locations.

Region	Mean annual capacity factor	R value	Standard deviation in daily capacity factor
India	-24.4%	-3.8%	-25.7%
Northern	-30.5%	-7.5%	-36.6%
Western	-28.8%	-6.2%	-26.5%
Southern	-17.1%	-6.9%	-24.2%
Gujarat	-38.5%	-13.6%	-38.7%
Madhya Pradesh	-37.0%	-8.4%	-36.7%
Maharashtra	-16.9%	-5.2%	-22.3%
Andhra Pradesh	-14.8%	-7.4%	-24.5%
Karnataka	-34.9%	-6.3%	-32.6%
Tamil Nadu	-10.3%	-12.7%	-18.3%

Table 4.9: Difference in annual mean wind capacity factor, correlation (r value) and stand deviation in daily mean capacity factor by region between reference case (RC) and generic assignment (GA) distribution of wind farms.

Table 4.9 summarises the main effects of the sensitivity test on the generation synthesis, showing changes in annual mean capacity factors, r value and the standard deviation in daily capacity factor per region. Average annual capacity factors are reduced in all regions, reflecting that much of India's land area is of lower wind resources than zones where wind farms are currently stationed. The correspondence of the GA daily capacity factor values to observed values is lower for all regions (reduction in r values), reflecting the heterogeneity of wind speeds between actual wind farm locations and the whole country. The standard deviation is lower in the GA case, reflecting the smoothing effect on the aggregate generation of uncorrelated generation across a greater number of generator locations.

4.5.3 Solar PV parametrisation

The parameterisation of solar PV array performance (see Equation 3.4 in Data and Methods Section 3.2.9) uses a term to approximate the effect of ambient air temperature on module temperature and consequent reductions in module efficiency. Setting this term to zero to exclude this temperature-efficiency dependence increases solar PV capacity factors by 22% for all-India (with other regions between 20-24% increases). The reduction in the correlation between the original solar PV generation timeseries and equivalent with the temperature term excluded is negligible (1-4% reductions amongst the regions). These results suggest that any inaccuracy in the specification of the temperature-efficiency term affects the mean bias of the generation synthesis but not the distribution of values.

Single-axis tracking designs are currently the global industry standard for utility-scale solar PV installations. However, as described in Data and Methods Section 3.2.3, fixed-tilt designs are common in India, making up ∼90% of total cumulative solar PV capacity. Repeating the solar PV generation synthesis with all solar installations using single-axis tracking designs increases annual average capacity factors by 33.9%. The correlation between the daily all-India solar PV generation timeseries with single-axis tracking designs and equivalent observations is ∼9.5% lower than for the fixed-tilt designs specified previously (0.87 vs 0.91). The slight reduction reflects the different diurnal generating profiles of the single-axis tracing design.

4.5.4 Solar PV spatial distribution

In the solar PV generation synthesis presented in the main results section, solar farm locations represent the actual farm location. Here, the effect of generic assignment (GA) of solar farm location is tested, whereby the synthesis is undertaken for all grid cells over the Indian land area. Such an approach is common within comparable studies of solar energy generation potential and performance. Comparisons are made to a reference case (RC), where all other technical parameters (array orientation and tilt, temperature-efficiency dependence) are the same as in the main generation synthesis. As such, differences in the solar energy generation and variability characteristics result solely from the homogeneous spatial distribution.

The effects of the GA are of the same sign as for the case of wind (lower annual mean capacity factor, r values and standard deviation in daily capacity factors), albeit of lower magnitude (Table 4.10. This outcome reflects the much greater level of homogeneity in irradiance values across the country than is the case for wind.

Region	Mean annual capacity factor	R value	Standard deviation in daily capacity factor
India	-1.5%	-4.5%	-2.7%
Northern	-1.4%	-3.7%	-5.9%
Western	-2.1%	-6.7%	-3.1%
Southern	-1.7%	-5.7%	-4.0%

Table 4.10: Annual mean solar PV capacity factor, r value and stand deviation in daily mean capacity factor by region for reference case (RC) and generic assignment (GA) distribution of solar PV farms.

4.6 Discussion

4.6.1 Summary of main findings

The implementation of the generation synthesis methodology progresses past work on the performance of wind and solar PV in India in three main areas:

1. The compilation of a database of existing installed capacity for wind and utility-scale solar PV in India.
2. The construction of a generation synthesis for wind and solar PV technologies, verified against observed daily records from Indian electricity authorities.
3. The quantification of changes to the fleet of wind and solar PV generators, particularly the effects of modernising installations to state-of-the-art tall-tower wind turbines and single-axis tracking solar PV arrays.

The key findings that accompany the analysis of these methodological advancements are as follows:

1. When using raw ERA5 variables, the generation synthesis for both wind and solar PV provides high accuracy for national and sub-national regions. The correlation between the synthesis and observed equivalents at the daily timescale for India is 0.97 for wind and 0.92 for solar PV, comparable to the levels of correspondence achieved for national aggregate generation syntheses in existing studies of other countries.
2. A mean bias is apparent in the wind generation synthesis based on raw ERA5 wind fields that varies in sign and magnitude between regions of India. A modest overestimation ($\sim$5%) of generation is apparent in the two northern most states (Rajasthan and Gujarat), whereas underestimation is apparent elsewhere (up to 20% in Tamil Nadu). Mean bias correction with the alternative wind speed product (DTU-GWA) offers no improvement in correlation, and increases the mean bias of the generation synthesis, with the generally higher wind speeds causing an overestimation of generation in all regions. A modest positive mean bias is apparent in the solar PV generation synthesis ($\sim$5%). Mean bias correction with the alternative irradiance product (GSA) reduces this mean bias, but modest overestimation persists. For both the wind and solar PV synthesis, the multiplicative bias correction method eliminated mean bias but produced a negligible effect on the

accuracy of the syntheses (correlation with observations).

3. Generation syntheses that incorporate the multiplicative bias correction method and the entire span of the reanalysis (1979-2021) enumerate the annual cycle of generation for both technologies and variability throughout the year. A strong monsoon signature is apparent for both technologies, with the summer monsoon circulation likely driving peak wind generation and summer monsoon rainfall reducing solar PV generation through the season.

4. The summer monsoon period (JJAS) shows greatest scale of interannual variability for both technologies: the interannual standard deviation represents 8% of the mean (14% for sub-regions) for wind and 3% of mean (6% for sub-regions) for solar PV.

5. Regional wind and solar PV generation anomalies in JJAS are generally significantly correlated with all-India generation anomalies, suggesting that anomalous seasons are widespread events affecting all regions simultaneously. Wind and solar PV generation anomalies in JJAS for the whole country and the sub-regions are weakly correlated, suggesting that different phenomena drive the majority of variation in JJAS between years for wind and solar PV.

6. The generation synthesis is sensitive to technical parameters, with turbine technology and single-axis tracking the most influential factors for wind and solar PV, respectively. Increases in capacity factor of up to 82% for wind and 34% for solar PV can result from changed assumptions in these technology characteristics.

The development of wind and solar PV generation syntheses for India of considerable accuracy is encouraging. The extensive generation dataset has numerous possible uses. Power system modelling studies could use generation synthesis as a plausible, verified data input rather than characteristic or idealised generation timeseries that are commonly used (e.g., Lu et al., 2020). Modifications to the generation synthesis (as was shown in the sensitivity test above) could aid economic assessments of technology upgrades (such as repowering with larger turbines or single-axis tracking arrays) or expanded roll-out of wind and solar PV technologies (e.g., into offshore regions). Generation synthesis can improve the characterisation of generation variability across timescales and help appraise design elements of power system flexibility and resilience (such as the magnitude of the joint minima in winter capacity factors shown in Figure 4.8).

This characterisation of variability could provide important insights into potential co-variability between wind and solar, which show compensatory generation on diurnal (Gangopadhyay et al., 2023) and seasonal timescales (Gulagi et al., 2022), with the phasing of the annual cycle of wind and solar PV generation particularly advantageous in the South of India (Hunt and Bloomfield, 2023).

The effects of spatial aggregation with the generation syntheses can help better understand the possible benefits of interconnection and the impact on the frequency and spatial distribution of extreme generation events. The co-variability of generation with demand for electrical energy was given cursory treatment in this chapter, highlighting potential generation surplus through the summer months and deficit during winter. Other work has noted how the anti-phasing between wind generation and air temperatures in India contributes to enhanced variability in electricity demand net of wind generation on intra-seasonal timescales (Dunning et al., 2015). Further study is required to investigate aspects of demand and variable supply co-variability, with uncertainty in future demand profiles best treated via a scenario approach (e.g., Bloomfield et al., 2021).

Finally, generation syntheses can provide a means of statistical downscaling of meteorological forecasts to provide generation predictions. Furthermore, generation syntheses can be used to elucidate the impacts of meteorological phenomena on weather-dependent supply, which can help improve generation forecasts (e.g., Brayshaw et al., 2011; Beerli et al., 2017). These final two aspects form the focus of the next two chapters.

4.6.2 Shortcomings and caveats to the analysis

Several limitations of the methodology must be taken into consideration when interpreting the results presented in this chapter. Regarding the parameterisations of wind and solar PV technologies, several simplifying assumptions and fixed parameter values are used throughout the generation synthesis. These parameter values likely vary between generators and change over time (e.g., differing wake losses between wind farms, improving solar PV module efficiency, etc.). However, the coarseness of the input data (e.g. the available data on generator location and technology characteristics) and the inherent uncertainty of the observational data (e.g., uncertainty over the inclusion of generation curtailment) limits the additional insights that further refinement of the parametrisation may yield. The availability of higher quality in-situ obser-

vation of raw meteorological variables and farm-level generation could permit a more detailed investigation of the sources of bias and enable more elaborate wind and soar PV parametrisations. Candidate reanalysis products with higher spatial resolution include ERA5-Land and the IMDAA reanalysis (Rani et al., 2021). However, both products lack the 100m wind speed variable, so they would depend more on accurate vertical extrapolation of surface winds.

The constant multiplicative adjustment factor is likely imperfect as wind generation scales non-linearly with wind speed, and biases are seasonally dependent. However, the multiplicative adjustment method improves results compared to raw ERA5 and mean bias adjusted versions and avoids over-fitting to a relatively short observational period (2017-2021). Furthermore, the accuracy of the state-level generation syntheses is comparable to national-scale wind generation syntheses in other regions (Bloomfield and Brayshaw, 2021; Gruber et al., 2022), which suggests that the findings in this study are robust when regionally aggregated. Future analyses should consider the extent to which the performance of the generation synthesis is a result of capturing diurnal and annual cycles (e.g., greater/lesser irradiance during day/night or the summer/winter season). Removing annual/diurnal cycles would reveal the extent to which the synthesis captures weather variability. Additionally, further verification of the generation synthesis performance should consider the extent to which differences between locations are captured to better quantify spatial co-variability representation (e.g. Cannon et al., 2015).

4.6.3 Link to following results chapter

The generation syntheses presented in this chapter faithfully reproduce reported generation from wind and solar PV generators across India. Expanding the generation syntheses to the 43-year reanalysis dataset allows a statistical interpretation of technically and physically plausible generation climatologies. The following chapter uses these multi-decadal generation datasets to investigate the meteorological drivers of interannual generation variability within the summer monsoon (JJAS) season. The sensitivities of the generation synthesis to technical parameters identified here may have consequences for the rapidly expanding renewable energy fleet in India. These potential impacts are addressed later in chapter 7.

Chapter 5

Drivers of interannual variability in wind and solar PV generation in India

Wind and solar PV generation in India both exhibit interannual variability (IAV), with the greatest magnitude of IAV apparent in the summer (JJAS) season for both technologies (see Section 4.4.2). IAV in wind and solar PV generation within this season is possibly tied to the Indian summer monsoon system, specifically changes in the prevailing monsoon westerlies in the case of wind and Indian summer monsoon rainfall (ISMR) in the case of solar PV. While there is extensive literature addressing drivers of subseasonal and interannual variability in the Indian summer monsoon, there is relatively little research linking this variability to wind and solar generation. Understanding the mechanisms and strength of associations between physical drivers and wind and solar generation variability can aid in the development, calibration, and verification of seasonal generation forecasts. In this chapter, the synthetic wind and solar PV generation timeseries developed in Chapter 4 are used to identify and quantify drivers of IAV in generation within the JJAS season. This assessment considers the impacts of intraseasonal variability, Pacific and Indian ocean sea surface temperature (SST) anomalies and, aerosols in the case of solar PV. Specifically, the chapter addresses the following research questions:

1. What are the main meteorological drivers of interannual variability in JJAS mean wind and solar PV generation in India?

2. What are the contributions of intraseasonal modes of variability to seasonal generation anomalies?

3. Are the strength of observed relationships between meteorological drivers of interannual variability in JJAS mean wind and solar PV generation in India consistent across regional subdivisions (i.e., Northern, Western, Southern and Eastern regions as defined in the previous chapter)?

5.1 Key drivers of variability within summer monsoon season

5.1.1 Monsoon circulation and lower-level winds

Figure 5.1a shows the JJAS 850hPa wind speed climatology and Figure 5.1b the interannual standard deviation from ERA5 during 1979-2021. The 850hPa level is chosen to represent the large-scale flow in the lower troposphere, with limited impact from surface orography over the Indian subcontinent. The Indian summer monsoon circulation pattern is prominent, with the greatest wind speeds corresponding with the position of the Somali Jet (Figure 5.1a). There is pronounced interannual variability in 850hPa winds in the region, with the standard deviation reaching ∼35% of the JJAS climatology over central India (Figure 5.1b). Figures 5.1c-f show the correlation coefficient between JJAS wind capacity factor anomalies for a specific region and 850hPa wind speeds for: c) all India, d) Western India, e) Southern India and f) Northern India. The correlation maps are broadly similar for all India, Western and Southern regions, with a positive correlation coefficient across the north Arabian sea, peninsular India and the entire downstream segment spanning the Bay of Bengal through to the South China sea. For the Northern region (Figure 5.1f), the area of positive correlation with 850hPa wind speed is less widespread.

Interestingly, a negative correlation is seen between regional Indian wind generation anomalies and wind speed in the core and southern flank of the Somali Jet, as well as across south-eastern mainland China. The dipole pattern of the correlation between the Somali Jet region and Northern/central India suggests a negative association between wind generation and ISMR, as surplus ISMR seasons are associated with an enhanced Somali Jet, increased cross equatorial flow, enhanced easterlies over Northern India, and enhanced Indian precipitation (Webster et al., 1998). Table 5.1 summarises correlation coefficients of anomalous wind generation in JJAS by region with ISMR and the dynamic index of ISM strength (following Wang and Fan (1999),

	India	NR	WR	SR
ISMR	**-0.36**	**-0.57**	**-0.41**	-0.11
W-F ISMi	**-0.45**	**-0.65**	**-0.48**	-0.16

Table 5.1: Interannual Pearson correlation coefficient between regional wind generation anomalies in JJAS and measures of summer monsoon strength, namely ISMR and ISMi. Bold values are significant at the 95% level.

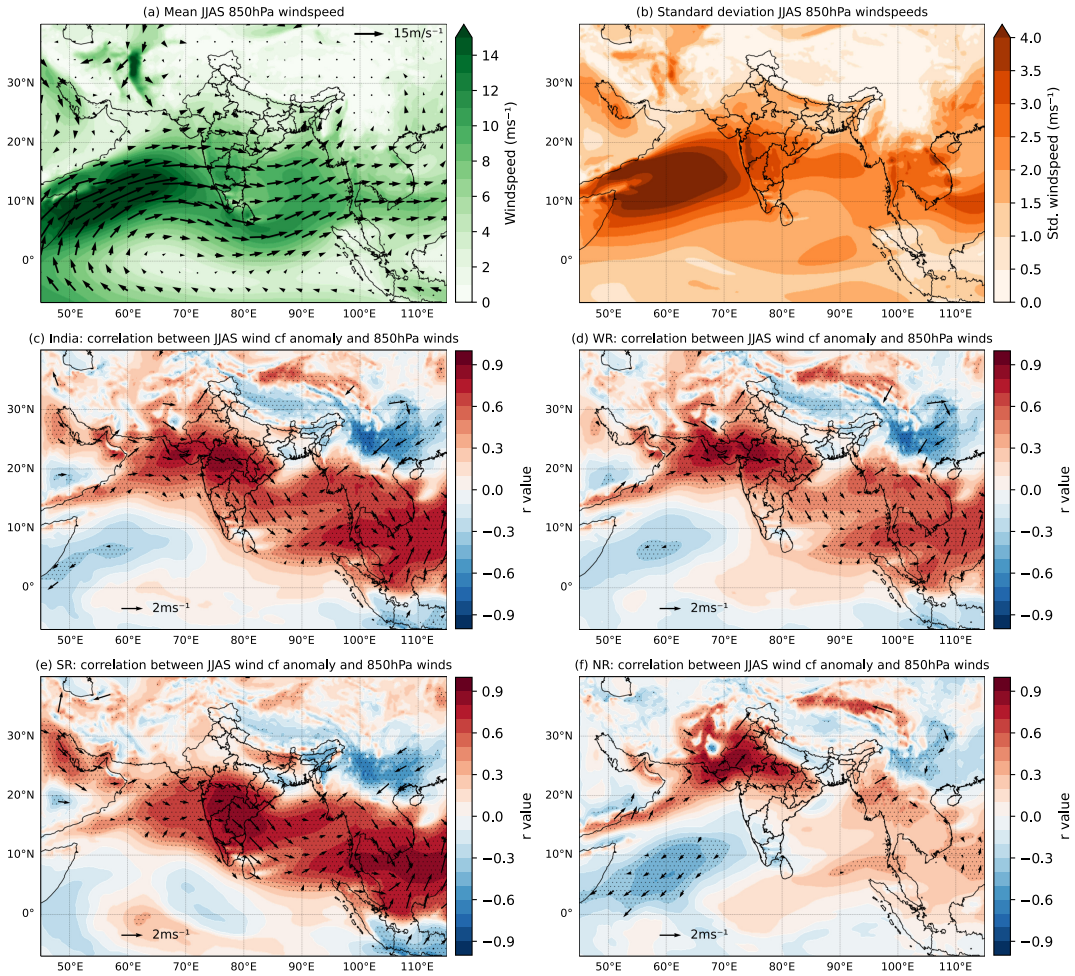

Figure 5.1: JJAS 850hPa wind speed climatology (1979-2021) (a); standard deviation in JJAS 850hPa mean wind speed (b); correlation between JJAS mean wind capacity factor anomalies and 850hPa winds for (c) all-India, (d) Western region, (e) Southern region and (f) Northern region. Stippling denotes regions significant at 95% confidence level.

termed here ISMi, see Section 3.3.1 for description). Modest negative correlations prevail, suggesting that the ISM circulation strength is not responsible for the majority of interannual wind generation variability in JJAS (N.B. Northern region represents minor share of total wind capacity in India). The following sections further investigate other drivers of sources of interannual wind generation variability in JJAS.

5.1.2 Summer monsoon rainfall and solar PV

Figure 5.2a shows climatological JJAS rainfall (technically 'total precipitation' but generally referred to here as rainfall, as is the norm in ISM literature) and Figure 5.2b interannual standard deviation for the period 1979-2021. Figures 5.2c-g show correlation coefficients between JJAS mean solar PV capacity factor anomalies per Indian sub-region and mean JJAS rainfall.

Widespread anti-correlation between rainfall and solar PV capacity factor anomalies is seen for all regions across the entire Indian subcontinent. Such a finding suggests that rain bearing convective low-pressure systems during summer months reduce incident surface solar irradiance due to the presence of optically thick deep convective clouds. Greater propensity and/or intensity of low pressure systems over India therefore cause positive rainfall anomalies and negative solar PV generation anomalies. Other work has shown a reduction in outgoing longwave radiation (a proxy for cloud height) over India during periods of positive rainfall anomalies (Annamalai and Slingo, 2001; Krishnamurthy and Shukla, 2008).

Another notable feature common to solar PV generation in all sub-regions is a region of positive correlation spanning the equatorial Indian Ocean. This positive/negative dipole between the equatorial Indian Ocean and Indian subcontinent likely reflects the movement of the Tropical Convergence Zone (TCZ) between two favoured positions in JJAS that correspond with the locations of rainfall maxima: either the equatorial Indian Ocean or the monsoon trough region, traversing the Bay of Bengal westward through the Gangetic Valley (Mohan and Goswami, 2000; Gadgil, 2003).

Table 5.2 shows the correlation coefficient between JJAS solar PV generation in the sub-regions and regionally averaged land rainfall and surface irradiance (or 'surface solar radiation downwards', SSRD, in ERA5) for the same region. It is notable that the correlation of solar PV generation anomalies with rainfall are strong, positive, and almost as high as the direct correlation with SSRD for all-India. This implies that variability in convection that drives rainfall across the regions is responsible for most of the variation in SSRD and solar PV generation. The lower correlation seen in the Eastern region likely results from the spatial mismatch between anomalous rainfall (which is greatest in the east and northeast of the Eastern region) and solar PV installations (which are concentrated in the western side of the Eastern region). Regionally averaged JJAS solar PV generation anomalies are also highly correlated with the ISMi index for monsoon intensity.

The correlations with meteorological drivers at a seasonal timescale are widespread and strong for both wind and solar PV generation anomalies. The following section considers the extent to which intraseasonal variability in these drivers causes seasonally persistent generation anomalies. This issue is relevant to the potential for skilful prediction of wind and solar generation anomalies.

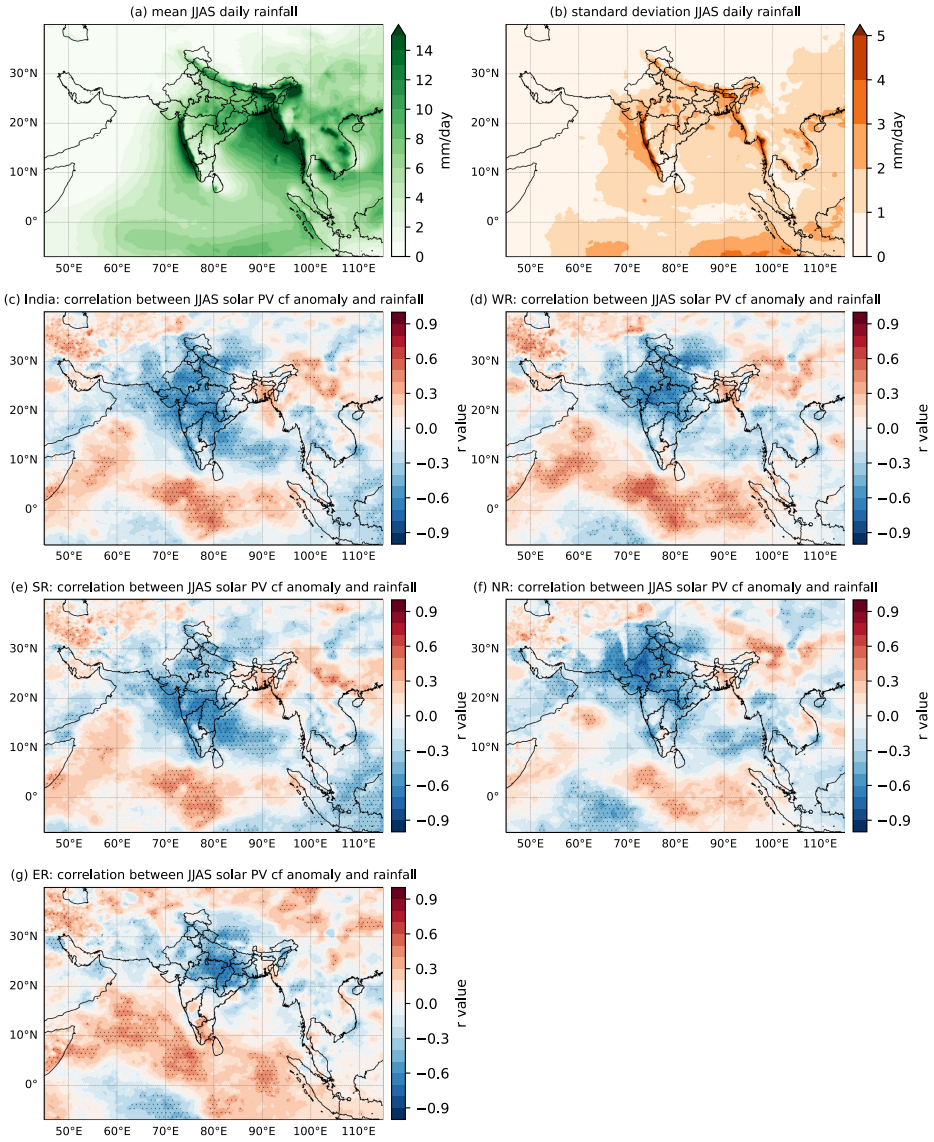

Figure 5.2: JJAS climatological rainfall (1979-2021) (a); interannual standard deviation in JJAS rainfall (b); correlation between JJAS mean solar PV capacity factor anomalies and rainfall for (c) all India, (d) Western region, (e) Southern region (f), Northern region and Eastern region (g). Stippling denotes regions significant at 95% confidence level.

5.2 Intraseasonal variability in wind and solar PV generation

Intraseasonal variability is a key feature of the Indian summer monsoon. This variability has been linked with the propensity and location of monsoonal low pressure systems, depressions, and tropical cyclones over India (Ramamurthy, 1969; Murakami, 1976; Sikka, 1980), with oscillations in the spatial and temporal coherence of low pressure systems found over two main periods: the westward propagating 10–25-day mode and northward propagating 30–60-day mode

(Moron et al., 2012). The associated changes in rainfall over India are described as alternating active and break spells (Rajeevan et al., 2010).

The extent to which intraseasonal fluctuations determine summer rainfall totals is a subject of ongoing discussion. The difficulty in conclusively determining the relative roles of intraseasonal versus interannual variability stems in large part to the similar spatial pattern of rainfall anomalies on the two timescales (Ferranti et al., 1997; Goswami and Mohan, 2001). Here, the analysis seeks to quantify the impact of intraseasonal variability on wind and solar PV generation anomalies in JJAS by conducting a composite analysis of active and break events. Active and break spells are defined as periods when the standardised index of daily rainfall anomalies for the core monsoon region is above or below one standard deviation, respectively. The core monsoon region (71.5°–86.5°E, 18.5°–26.5°N, Figure 5.3b) and standardised rainfall index is defined following Rajeevan et al. (2010). A mean value of 12.0 active and 12.1 break days per JJAS season result from the classification, considering a total 43 seasons in the period 1979-2021. The standard deviation in the number of days is 7.0 and 8.3 for active and break days, respectively. Thus, active and break days are relatively rare and vary considerably in frequency between seasons.

The zones of rainfall deficit/surplus between break and active periods are roughly symmetrical (Figures 5.3a and 5.3c), with opposite sign anomalies over central India and the Western Ghats consistent with the core monsoon region used for the analysis (Rajeevan et al., 2010). Differences in mean sea level pressure between active and break phases (Figures 5.3d and 5.3f) also show a degree of spatial symmetry. The region of anomalous low pressure during active phases coincides with the passage of low pressure systems (marked as green lines, from genesis to lysis, in Figures 5.3d and 5.3f) while the lower frequency and lack of spatial organisation of low pressure systems during break phases contributes to the positive MSLP anomaly (Krishnamurthy and Ajayamohan, 2010). The concurrent changes in 100m wind speeds show spatial conformity and

	India	NR	WR	SR	ER
Rainfall	**-0.86**	**-0.83**	**-0.82**	**-0.74**	**-0.70**
SSRD	**0.90**	**0.88**	**0.96**	**0.91**	**0.89**
W-F ISMi	**-0.73**	**-0.64**	**-0.57**	**-0.71**	-0.20

Table 5.2: Correlation between regional JJAS rainfall / SSRD anomalies / ISM-I and solar PV generation anomalies in JJAS per region. Bold values are significant at the 95% level.

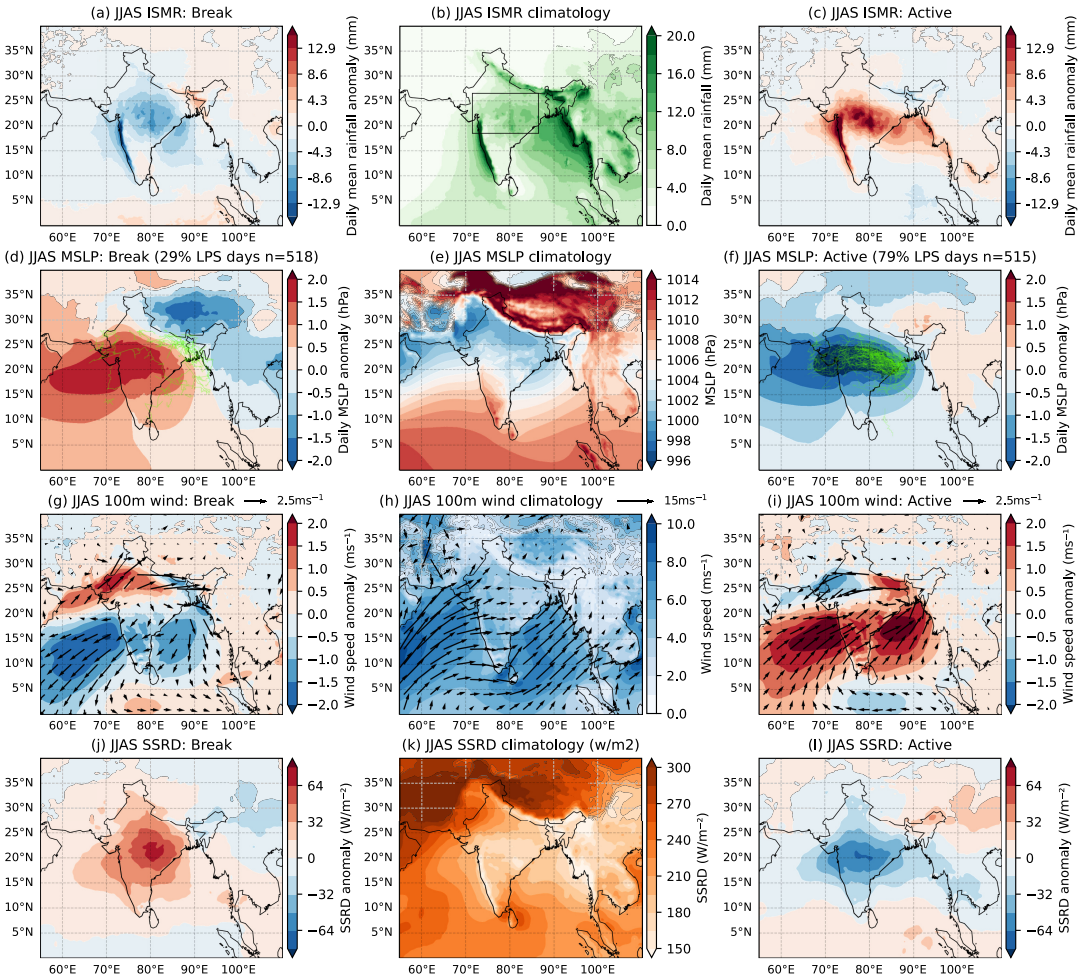

Figure 5.3: Composites of meteorological fields during active and break monsoon periods (right-hand and left-hand columns, respectively). JJAS climatology (1979-2021) shown for reference (central column). Rainfall (panels a-c); mean sea level pressure (panels d-f) with green overlaid lines in d and f signifying low pressure system tracks; 100m wind speeds (panels g-i); and SSRD (panels j-l).

comparable magnitudes of opposite sign between active and break phases (Figures 5.3g and 5.3i). Active phases coincide with enhanced westerly flow over southern and central India, as well as over the Bay of Bengal, and enhanced easterlies in the monsoon trough region, which reduces the prevailing westerlies in the northwest (Annamalai and Sperber, 2005; Goswami and Xavier, 2005; Dunning et al., 2015). Conversely, break periods correspond with a weakening of the monsoonal westerly flow over all but the north and northwest extents of the country. SSRD anomalies of similar magnitude and opposite sign between active and break events follow the core monsoon zone and align with the region of greatest storm track density (Figures 5.3j and 5.3l). Accordingly, the changes in near-surface wind speed and SSRD between active and break phases cause fluctuations in wind and solar PV generation.

		Frequency of events per season	
		Active	Break
Wind	India	-0.21	0.11
	Northern	**-0.38**	**0.34**
	Western	-0.24	0.17
	Southern	-0.01	-0.11
Solar PV	India	**-0.44**	**0.61**
	Northern	**-0.39**	**0.58**
	Western	**-0.39**	**0.62**
	Southern	**-0.39**	**0.48**
	Eastern	-0.19	**0.51**

Table 5.3: Correlation (r values) between seasonal mean JJAS wind/solar PV capacity factor anomalies and the (a) frequency of active/break events, (b) the event duration, and (c) the mean rainfall across events per season. Values significant at the 95% level in bold.

To assess the impact of intraseasonal oscillations on interannual generation anomalies, the correlation between seasonal wind and solar PV generation anomalies and event frequency is shown in Table 5.3. Correlation between wind generation anomalies and event frequency are statistically insignificant in all but the Northern region. These very weak relationships suggest interannual variability in JJAS mean wind generation is not linked to intraseasonal modes of variability over most of India (N.B. Southern and Western regions account for ∼88% of total installed wind capacity in 2021).

For solar PV, the frequency of active conditions shows a modest negative relationship with solar PV generation anomalies (r values in the range -0.31 to -0.44). For break conditions, the strength of the positive associations is marginally stronger (r values in the range 0.48 to 0.70). These associations suggest intraseasonal variability are partly responsible for interannual variability in solar PV generation in JJAS. The apparent relationship is akin to the known connection between intraseasonal and interannual ISMR variability, whereby the probability of occurrence of strong or weak monsoon years have been linked to the propensity of active and break events, respectively (Goswami and Mohan, 2001; Krishnamurthy and Ajayamohan, 2010; Webster et al., 1998; Saha et al., 2021).

Given the influence of intraseasonal variability on the ISMR, as well as the role of synoptic variability, the predictability of ISMR (and, in turn, solar PV generation) is diminished, as these fast-varying components are essentially chaotic on seasonal timescales (Palmer, 1994; Goswami and Xavier, 2005; Goswami et al., 2006; Saha et al., 2016). The magnitude of the

external component of interannual variability in ISMR (and solar PV generation) compared to internal noise will govern predictability on seasonal timescales (Charney and Shukla, 1981). Having considered the role of intraseasonal variability for seasonal anomalies, the chapter now turns to interannual climate drivers and considers the extent to which these impinge upon the ISM and wind and solar generation at seasonal timescales.

5.3 Interannual variability in JJAS mean wind generation

5.3.1 Covariance with Indian Ocean SSTs

The strength of the correlation between the Niño3.4 index and all-India wind generation anomalies in JJAS is modest, with a correlation coefficient of 0.32. However, the covariance is much stronger when considering SSTs in the India Ocean and Maritime Continent. The correlation between the standardised anomaly of SSTs in the region 7°-23°N; 60°-115°E and all-India wind generation anomalies in JJAS is -0.70.

SST anomalies in the Indian Ocean typically peak in late boreal winter or early spring, after the peak of ENSO, and can persist into the following summer, by which point the Pacific SST anomaly has dissipated (Tourre and White, 1995; Alexander et al., 2002). Figure 5.4a demonstrates such behaviour by regressing SSTs in JJAS on the November, December, January (NDJ) mean Niño3.4 index. The strong positive correlation in the Indian Ocean indicates a lagged SST response and describes the typical progression of the Indian Ocean basin mode, which is the main pattern of interannual SST variability in the region (Lau and Nath, 1996; Klein et al., 1999). The co-variability of Indian wind generation anomalies with Indian Ocean SST, which in turn is a lagged response to ENSO, motivates the investigation of concomitant climate anomalies in surface fields.

Figure 5.4b shows the correlation coefficients between JJAS MLSP and rainfall with the Niño3.4 index in the preceding winter (NDJ). The strongest correlation of MSLP is found in a region spanning the northwest Pacific, through southeast Asia into the Bay of Bengal. This MLSP correlation pattern is associated with large-scale anomalous anticyclonic circulation within the lower troposphere over the subtropical western North Pacific (WNP) following peak El Niño conditions in boreal winter (Wang et al., 2003; Yang et al., 2007). There are simultaneous increases in rainfall over the northern Indian Ocean and decreases over the WNP that are tied

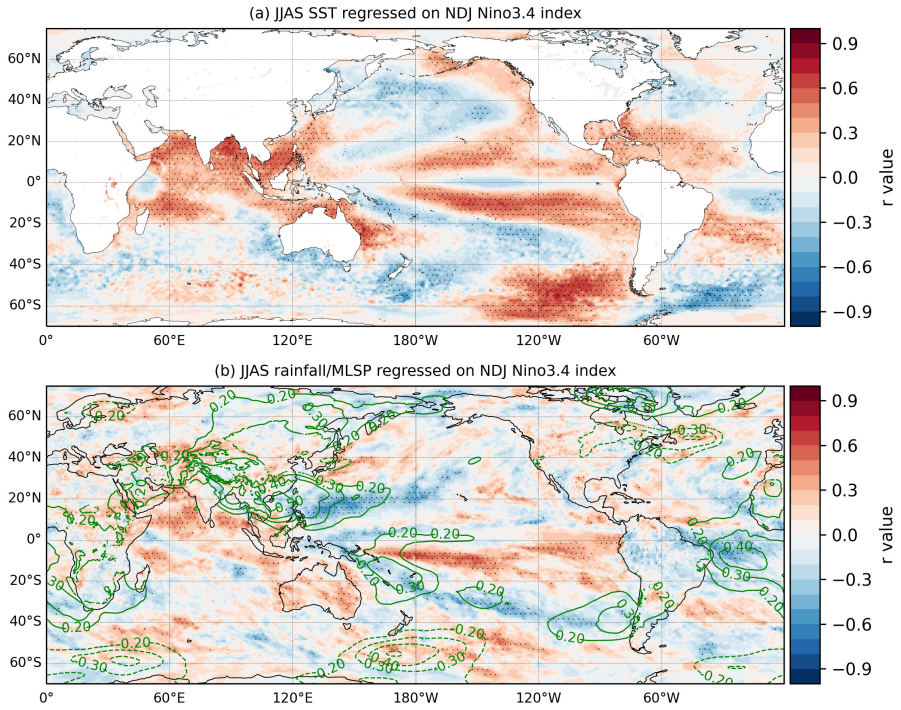

Figure 5.4: JJAS SST regressed on NDJ Niño3.4 index (a) and JJAS rainfall/MSLP regressed on NDJ Niño3.4 index (b), with green contours showing strength of correlation with MSLP.

to the anomalous large-scale circulation (Figure 5.4b). The magnitude and westward extent of the circulation in the WNP is recognised as the primary mode of interannual atmospheric variability over the South and East Asian regions in JJAS (Wang et al., 2000; Huang et al., 2012; Xie et al., 2016).

An index of the intensity of the WNP monsoon circulation, termed here WNPi (Wang and Fan, 1999), shows a strong relationship with Indian wind generation variability, particularly in Southern and Western India (Table 5.4). Furthermore, the standardised anomaly of JJAS WNP rainfall (WNPR; averaged over 110°-160°E;10°-20°N - c.f. Figure 3.7b) is highly correlated with wind generation anomalies (Table 5.4). During a weak WNP monsoon, the anomalous easterlies on the southern flank of the WNP anticyclonic anomaly oppose the climatological westerlies that originate in the region of the Somali Jet, and cross peninsula India and South East Asia, before converging with the WNP monsoon system (see Figure 5.5a) for a schematic diagram). During a strong WNP monsoon, anomalous westerlies on the southern flank of the WNP cyclonic anomaly do not impede the climatological westerly flow of the ISM (Figure 5.5b). These observed relationships between wind generation anomalies and the strength of the WNP anomaly motivate further investigation into drivers of interannual variability in summer-time circulation in the WNP region.

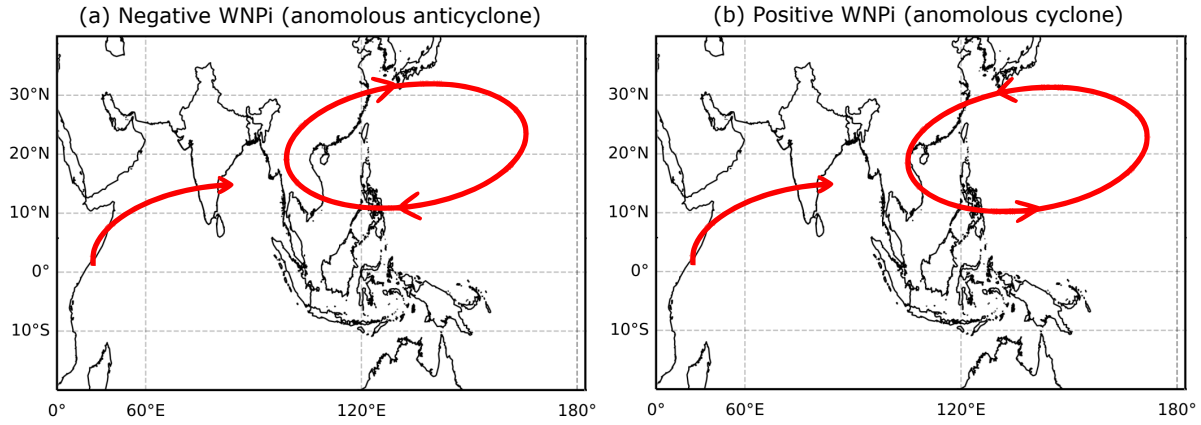

Figure 5.5: Schematic representation of westerly flow over peninsular India negative (a) and positive (b) WNPi

5.3.2 Modes of variability in the Western North Pacific (WNP)

The first and second EOFs of an EOF analysis of JJAS mean 850hPa wind anomalies over the WNP (90°E-180°E; 0°-40°N) explain 37% and 12% of the total variance, respectively. Figures 5.6a and 5.6b show EOF1 and EOF2, respectively. A dominant feature in both modes is anomalous anticyclonic circulation over the WNP, although the anomalous easterlies are more prominent in EOF1 and the centre is shifted slightly to the north in EOF2.

These two leading modes of variability capture the majority of total interannual variability in the WNP in JJAS. Both resulting principal components (PC1 and PC2) are significantly correlated with the intensity of the WNP monsoon circulation, captured by the index WNPi described previously (r = 0.60 and r = 0.73). A multiple linear regression model based on PC1 and PC2 (-0.431×PC1 -0.820×PC2) can reconstruct the observed WNPi very well, with a correlation coefficient between the observed and reconstructed WNPi of 0.93. Thus, the two EOF modes are key source of predictability. The processes underpinning the first and second modes are well documented within the literature (e.g., Yang et al., 2018) and relate to the Gill-type response mechanism to anomalous tropical heating or cooling and the Indian Ocean

	Wind generation anomalies			
	India	NR	WR	SR
WNPR	0.68	0.33	0.56	0.71
WNPi	0.75	0.34	0.63	0.79

Table 5.4: Correlation between two indices of WNP monsoon (WNPR and WNPi - c.f. Figure 3.7b) and wind generation anomalies per region in JJAS. All values significant at 95% level

capacitor mechanism, respectively.

The spatial pattern of detrended JJAS SST regressed onto PC1 is shown in Figure 5.6a and shows cold anomalies over the central Pacific and warm anomalies around the Maritime Continent, reminiscent of the equatorial dipole pattern of developing (or persisting) La Nina conditions. Rainfall and MSLP regressed on PC1 show similar patterns to canonical ENSO (not shown) and PC1 itself is highly anticorrelated with the Nino3.4 index (r value -0.81). Thus, the first mode is primarily a forced mode of ENSO. As described by Wang et al. (2013), anticyclonic anomalies over the WNP may develop as a Gill-type Rossby response to cold anomalies in the equatorial Central Pacific. Meanwhile, the warm anomalies strengthen the local meridional circulation that ascends from the Maritime Continent and descends over the WNP to enhance the anticyclonic anomaly (Sui et al., 2007; Chung et al., 2011).

The spatial pattern of detrended JJAS SST regressed onto PC2 is shown in Figure 5.6b and shows positive correlations over northern Indian Ocean and the South China, negative correlations across the eastern extent of the WNP, and positive correlations in the central and eastern tropical Pacific. Warm anomalies in the Indian Ocean are known to be induced by El Niño conditions that peak on boreal winter, and which can persist until the following summer (e.g., Klein et al., 1999; Schott et al., 2009).

The anomalously warm northern Indian Ocean generates an eastward propagating warm Kelvin wave response in the atmosphere that energises the western North Pacific anomalous anticyclone by imparting anticyclonic shear vorticity (Yang et al., 2007; Xie et al., 2009; Wu et al., 2009; Chowdary et al., 2010; Kosaka et al., 2013; Xie et al., 2016). Additionally, the anomalous easterlies to the south of the western North Pacific anomalous anticyclone counter mean south westerly monsoon flow, which reduces surface evaporation and latent heat release in the northern Indian Ocean (Du et al., 2009). Thus, EOF2 describes a coupled ocean–atmosphere mode where the western North Pacific anomalous anticyclone and northern Indian Ocean operate in a reinforcing feedback loop.

Further to the analysis of the spatial features of EOFs 1 and 2, the interannual variability in both all-India JJAS wind generation and WNP rainfall anomalies can be well described by a multiple linear regression model[1] based on PC1 and PC2, with correlation coefficients of 0.73 and 0.94, respectively (see Figures 5.6a and 5.6b). Different loadings of the first and second

[1]IMSR (-0.429×PC1 -0.823×PC2); all-India wind (-0.0155×PC1 -0.00925×PC2)

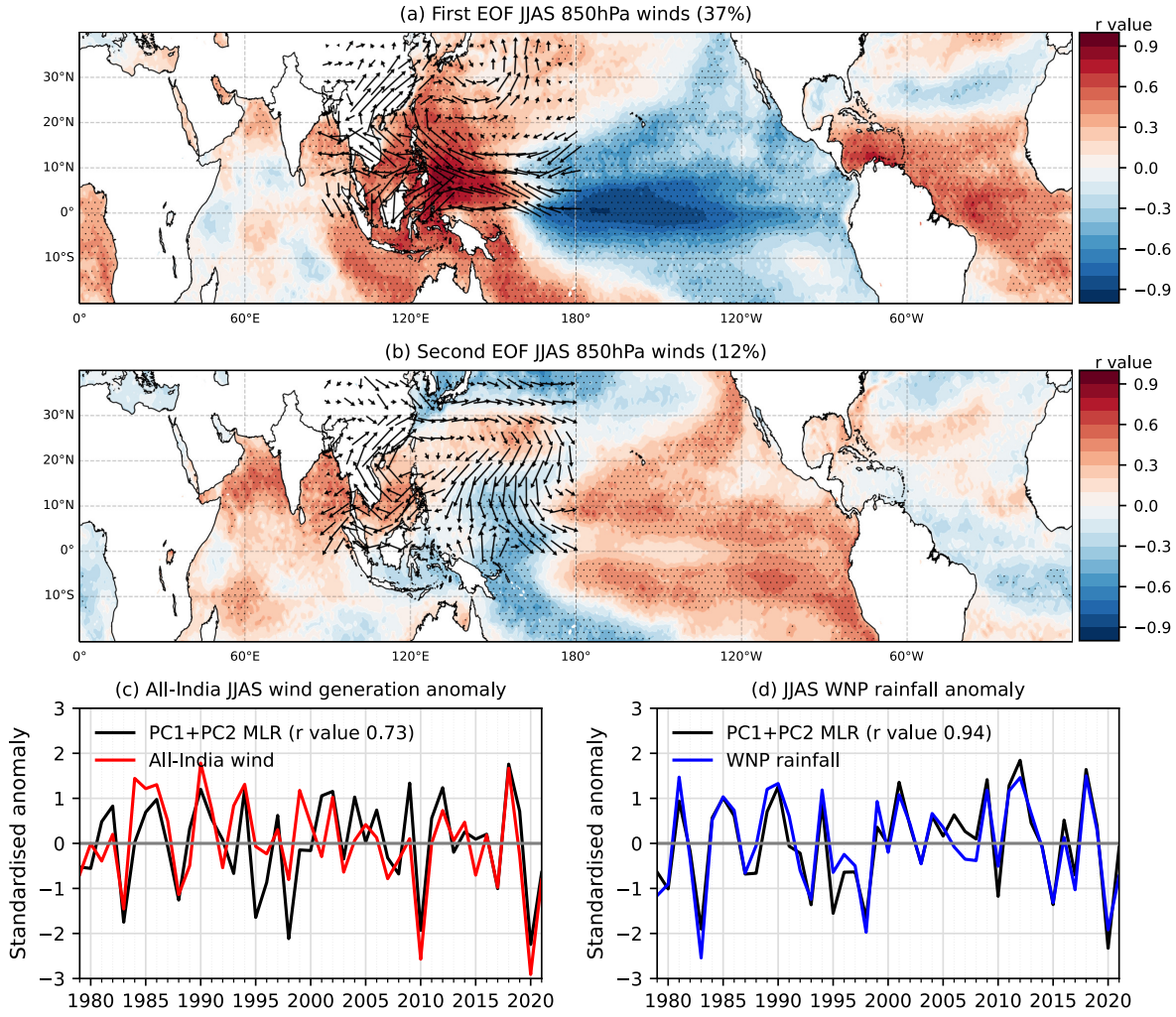

Figure 5.6: Standardised anomalies of all-India wind generation anomalies (a) and WNP rainfall (b) in JJAS (as black lines). Reconstruction of anomalies in (a) and (b) based on multi-linear regression (MLR) using PC1 and PC2 as predictor variables. First (c) and second (d) modes of EOF analysis of 850 hPa winds over the WNP (vectors) and regression pattern of resulting PC timeseries on detrended SSTs in JJAS (colour shading).

EOF modes clearly describe particular seasonal anomalies. For example, the most negative wind generation anomaly in the entire 43-year record (2020) is a combination of the third and second most negative values for PC1 and PC2, respectively. And the most negative PC2 value in the entire 43-year record is offset by the fourth most positive PC1 value, resulting in a modest negative generation anomaly in 2015. These various combinations result in the high correlation seen in the multi linear regression shown in Figure 5.6c.

5.3.3 Relevance of anomolous WNP circulation over South Asia

The previous discussion has evidenced interannual variability in the WNP as closely related to JJAS wind generation anomalies and has offered physical reasoning for such behaviour in response to anomalous SSTs in the Pacific and Indian oceans. To further evidence the impact of the WNP of wind generation over the impact of the ISM circulation, a similar EOF analysis of 850hPa winds in JJAS is conducted but with the domain constrained to South Asia. Figure 5.7a shows the correlation pattern of the first EOF mode, which explains 33% of total variance. Positive loading of this first EOF mode corresponds to a strengthening of the western North Pacific circulation and enhancement of downstream westerlies over the Indian peninsular that converge with the southern flank of the anomalous cyclonic circulation. The correlation pattern is akin to the regression of wind generation anomalies directly onto 850hPa winds (shown in Figure 5.1c-f). Accordingly, the correlation between the first principal component (PC) time series and wind generation anomalies is high (r value 0.78, see Figure 5.7c and Table 5.5).

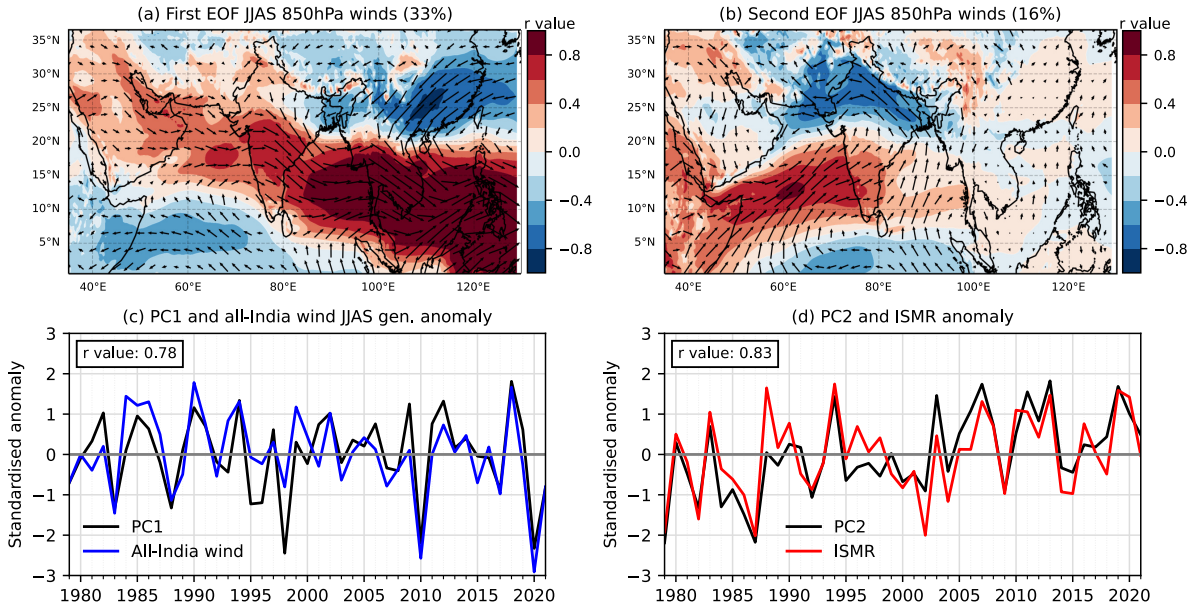

Figure 5.7: Correlation patterns for (a) first and (b) second EOF modes for JJAS 850hPa wind anomalies. Timeseries of first PC (black line in c) with JJAS wind capacity factor anomalies (blue line in c) and second PC timeseries (black line in d) with JJAS ISMR anomalies (red line in d).

The first PC timeseries is also highly correlated with regional wind generation anomalies, though to a lesser extent for the Northern region (Table 5.5). The second PC timeseries shows no significant association with regional wind generation anomalies, except for a negative association in the Northern region. This corresponds to the finding in Section 5.2 that showed an association

	EOF	India	NR	WR	SR	WR+SR
Wind	1st	**0.78**	**0.36**	**0.65**	**0.80**	**0.79**
	2nd	-0.19	**-0.50**	-0.24	0.20	-0.08
Solar PV	1st	0.16	0.10	0.09	0.29	0.27
	2nd	**-0.79**	**-0.71**	**-0.80**	**0.64**	**-0.54**

Table 5.5: Correlation between PC timeseries of first and second EOF modes and regional wind and solar PV generation anomalies in JJAS. Bold values are significant at the 95% level.

between JJAS daily wind generation anomalies in the northern region and active/break phase of the monsoon, which carry a similar north-south dipole structure to EOF2. Namely, the negative loading of EOF2 enhances prevailing westerlies through the northern region (akin to the 100m wind speed pattern during break phases, c.f. Figure 5.3). Given the strong negative association between rainfall over peninsular India and solar PV generation anomalies (c.f. Figure 5.2), the correlation found between the second PC time series and ISMR also translates to solar PV generation (Table 5.5). Correlation between the PC time series of higher EOF modes and solar PV generation anomalies is lower than 0.3 in all cases – i.e., insignificant at the 95% confidence level. The third mode of an EOF decomposition shows a pattern akin to the IOD, However, the PC time series of this mode shows no significant association with wind generation anomalies in JJAS and was not consider further. A later section discusses the relevance of IOD for solar PV generation anomalies in JJAS

In summary, the first and second PC timeseries of an EOF decomposition of 850hPa winds over South Asia describe large variance fractions of the WNP and ISM summer monsoon circulations, respectively. The first PC timeseries accounts for a large proportion of total variance in all-India and regional wind generation anomalies in JJAS. This proportion exceeds 60% for the combined generation anomaly for WR and SR, which together account for ∼88% of total installed wind capacity in India (WR+SR).

The second PC timeseries accounts for a large proportion of the total variance in all-India and regional solar PV generation anomalies in JJAS (and, additionally, wind generation in the Northern region). The following sections consider drivers of seasonally persistent anomalies of this regional monsoon system.

5.4 Interannual variability in JJAS seasonal mean solar PV generation

5.4.1 Covariance with tropical Pacific SST

ENSO is a known driver of ISM rainfall on interannual timescales and ISM rainfall is strongly related to surface solar radiation downwards (SSRD) and solar PV. Table 5.6 shows the correlation coefficients between the regional solar PV generation/ISMR anomalies and the Niño3.4 index. The well-documented anti-correlation between ENSO phase and ISM rainfall is of similar magnitude but opposite sign to the correlation between solar PV generation anomalies and Niño3.4 (r=-0.50 for ISMR-ENSO and r=0.49 for all-India solar PV-ENSO). This reflects the anti-correlation between regional solar PV generation anomalies and rainfall shown in Figure 5.2.

The nature of the ISMR/solar PV generation relationship with tropical Pacific SST anomalies is further assessed with a composite analysis based on ENSO state. Figure 5.8 elucidates this ENSO impact with anomaly composites during 14 El Niño and 14 La Niña years (14 years out of a total 43 years in the reanalysis correspond to terciles of the full sample). Rainfall and total cloud cover (TCC) anomaly composites show clear spatial conformity in anomalies of alike sign during El Niño (Figure 5.8b and 5.8e) and La Niña years (Figure 5.8c and 5.8f). This pattern is consistent with the canonical atmospheric response to ENSO phasing (see Background Literature Section 2.9.1), whereby anomalous SSTs in the eastern and central Pacific Ocean modulate the position of the Walker circulation, which, during El Niño conditions, enhances subsidence over South Asia and the maritime continent and suppresses convective activity across the region (Webster et al., 1998).

Anomaly composites of SSRD during 14 El Niño (Figure 5.8h) and 14 La Niña years (Figure 5.8i) closely follow the spatial extent of rainfall and TCC anomalies, albeit of opposite sign. Increased cloud cover during ISMR surplus seasons results in greater attenuation of incoming solar radiation through a combination of absorption and scattering. SSRD is the sum of direct and diffuse radiation components. The direct component refers to the solar radiation flux at the earth's surface without interactions with various constituents of the atmosphere. The diffuse component refers to the solar radiation flux at the earth's surface following a combination of

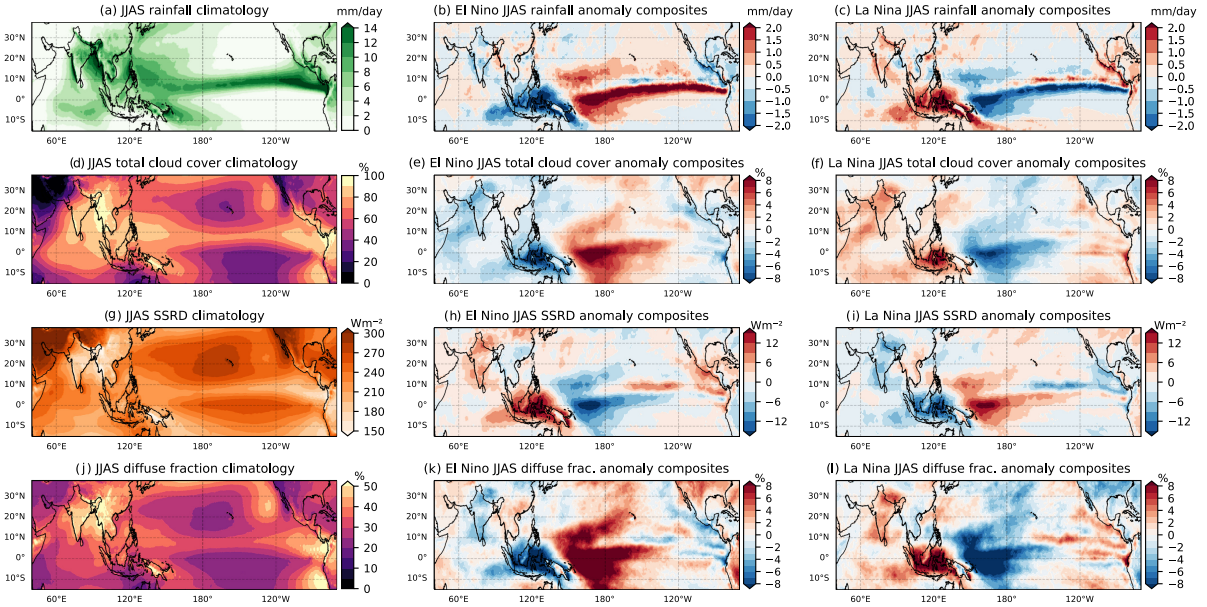

Figure 5.8: Climatological JJAS rainfall (a), SSRD (d), total cloud cover (g) and diffuse radiation fraction (j) (years 1979-2021). Anomaly composites for 14 ENSO warm/cold years (upper/lower third of Niño3.4 index in period 1979-2021) for JJAS rainfall (b,c), SSRD (e,f), total cloud cover (h,i) and diffuse radiation fraction (k,l).

scattering, reflection, and refraction. In a cloudless sky, the diffuse component represents a minor fraction of SSRD, with a small amount of Raleigh scattering resulting from interactions with molecules in the air (Kafka and Miller, 2019). In the presence of clouds and/or aerosols, the diffuse component of total incident solar irradiance increases, becoming the majority share in an entirely overcast sky. The scattering effect of cloud droplets and ice crystals is greater than the absorption of incident solar radiation in optically thick clouds of significant depth, such as those formed in convective systems (Matuszko, 2012). The scattering process directs diffuse radiation in all directions, with the increase in diffuse downward flux being less than the reduction in direct downward flux (Ban-Weiss and Collins, 2015). This effect is seen in Figure 5.8l, where both the magnitude of SSRD decreases and the diffuse fraction increases during La Niña (or SSRD increase, diffuse fraction decreases during El Niño, as in Figure 5.8k).

Solar PV module efficiency reduces at higher temperatures and warm/cool ENSO years have been shown to affect surface air temperature by up to +1/-1C in central India (Chowdary et al., 2014). However, this modest temperature change would imply a negligible effect on module efficiency between seasons of different ENSO state. Indeed, the interannual variability in surface air temperature averaged over the Indian peninsular is sufficiently modest (standard deviation of 0.6C) such that the temperature-efficiency relationship accounts for a negligible proportion

of JJAS solar PV generation variability.

5.4.2 Covariance with Indian Ocean SST (Indian Ocean Dipole)

The Indian Ocean Dipole (IOD) is one of the dominant modes of SST variability in the basin on interannual timescales and has been linked to ISMR variability (Saji et al., 1999; Ashok et al., 2004). The IOD describes a zonal dipole in the tropical Indian Ocean SSTs, with a positive phase associated with cooler SSTs in the Eastern India Ocean, off Sumatra, and warmer SSTs in the western equatorial Indian Ocean. Although not all IOD events fall within the ISM season, the tendency is for formation during the boreal summer and maturation in the following season (Schott et al., 2009), thus simultaneous interaction with ISMR and solar PV is possible.

Whether IOD is an inherent mode of variability within the Indian Ocean or a forced response to ENSO remains an active area of research, as does the relative influence of each mode of tropical SST variability on ISMR (Cherchi et al., 2021). However, evidence from the literature shows the IOD is a driver of ISMR variability on interannual timescales, via interaction with the regional Hadley circulation (Behera and Ratnam, 2018). The IOD can also modulate the effect of ENSO on ISMR when opposite phases coincide (as was the case in 1997 when a strong El Niño and positive IOD resulted in modest surplus ISMR) (Slingo and Annamalai, 2000).

Table 5.6 shows correlation coefficients between the JJAS Dipole Mode Index (DMI; the difference in SST anomalies between (90°-110°E, 10°S-0°S) and (50°-70°E, 10°S-10°N); Saji, 1999) and regional rainfall and solar PV generation anomalies. Weak positive correlations with DMI are observed across all Indian sub-regions but they are not statistically significant. The atmospheric corollary of the IOD mode, termed the Equatorial Indian Ocean Oscillation (EQUINOO), represents anomalous zonal surface flow arising from anomalous pressure gradient caused by differences in the strength of convection between eastern and western regions of the Indian Ocean (Gadgil, 2003, 2004).

EQUINOO is conventionally measured with a zonal wind index, termed EQWIN, defined as the standardised anomaly of 10m zonal winds in the equatorial box 65°E–85°E, 4.5°N–1.5°S (Gadgil et al., 2004). EQWIN shows stronger correlation with regional rainfall and solar PV generation anomalies (Table 5.6). A linear combination of Niño3.4 and EQWIN indices, defined with coefficients from a linear least-squares fit, describes a greater proportion of variability in both rainfall and solar PV generation than the individual indices themselves (Surendran et al.,

		India	NR	WR	SR	ER
ISMR	DMI	0.20	0.17	0.25	-0.04	0.22
	EQWIN	**-0.36**	-0.29	**-0.38**	-0.18	**-0.30**
	Niño3.4	**-0.50**	-0.29	**-0.38**	**-0.58**	-0.07
	EQWIN +Niño3.4	**0.76**	**0.44**	**0.68**	**0.66**	**0.34**
Solar PV generation	DMI	0.06	-0.16	-0.07	0.22	-0.10
	EQWIN	0.26	**0.33**	**0.30**	0.10	0.15
	Niño3.4	**0.49**	**0.34**	**0.32**	**0.57**	0.22
	EQWIN +Niño3.4	**0.64**	**0.53**	**0.53**	**0.61**	**0.33**

Table 5.6: Correlation between various tropical SST indices (DMI, EQWIN, Niño3.4, and linear combination of EQWIN+Niño3.4) and ISMR/solar PV generation anomalies per region. underlined values are significant at the 95% level.

2015).

Table 5.6 confirms ENSO as the largest contributor to total variance in JJAS solar PV generation anomalies. Some notable patterns are observed amongst major outliers from the co-variability observed between Niño3.4/EQWIN and solar PV generation anomalies (see Figure 5.9). Firstly, two major positive outliers occur following multi-year La Niña conditions (1985 and 1999). Second, the major negative generation anomalies in 1994 and 2013 coincide with seasons of very high occurrence of ISM active events (the 3rd and 2nd most extreme active event years, in terms of event frequency) possibly indicating a greater role of internal variability to surplus seasonal mean rainfall in these years. Furthermore, the extreme IOD event that took place in 2016 (Lu et al., 2018) caused the most negative EQWIN index value in the period considered, which would correspond with deficit ISMR and positive solar PV anomalies. However, the year 2016 also coincides with anomalously high cross-equatorial flow (the third highest in the period considered[2]), which may have contributed to increased moisture transport towards the Indian subcontinent and an offsetting of the negative IOD drying signal.

Interestingly, several occasions where rapid onset of strong La Niña follows El Niño sees the coincidence of both large negative wind and solar PV generation anomalies (namely, 2020, 2010, 1983, 1988). These years mark the top 4 most negative generation anomalies for wind and coincide with the 9th, 6th, 8th, 7th most negative solar PV generation anomalies. These four low generation years mark the lowest decile for wind generation and lowest quintile for

[2]Measured as the standardised anomalies in 850hPa winds in the box S5°-N5°; E44°-56°.

solar PV generation. In the previous chapters, weak positive association was identified between all-India wind and solar PV generation anomalies in JJAS (r=0.27). This association reduces further when excluding these five extreme low generation events from the 43 seasons considered (r=0.10).

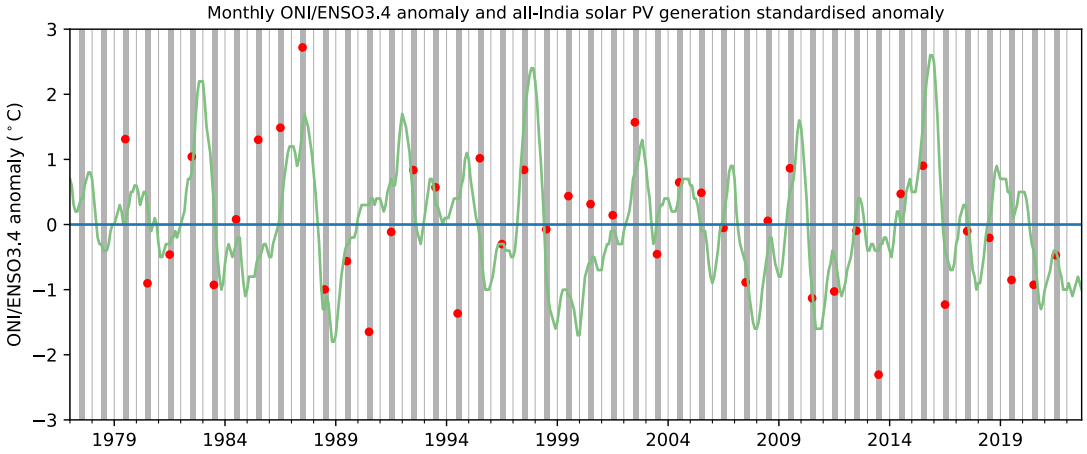

Figure 5.9: Timeseries of Niño3.4 index (in green, spanning 1979-2021) and all-India solar PV generation anomalies for JJAS (red dots, grey shading denotes JJAS season).

5.5 Possible impacts of aerosols on IMSR and solar PV generation

This subsection considers to what extent various aerosol species could affect solar PV generation and whether anomalous aerosol loading could impart a potentially predictable signal that could be exploited in seasonal generation forecasts.

Heavy aerosol loading during the summer season over the Indian peninsular results from both natural and anthropogenic emissions (Henriksson et al., 2011). The main anthropogenic sources include black carbon and sulphate aerosols, originating mainly from biomass burning and coal-fired power plants, respectively, while mineral dust from adjacent desert regions is the dominant natural source (Prasad et al., 2006). Depending on the distribution of scattering and absorbing aerosols, the combined direct negative radiative effects can both positively and negatively alter the mean monsoon circulation. For example, scattering and absorbing aerosols can cool the land surface and reduce the ocean–land thermal contrast, which serves to weaken the monsoon circulation (e.g., Ramanathan et al., 2005). On the other hand, absorbing aerosols can also enhance the wider monsoon circulation, with the 'elevated heat pump' hypothesis (e.g., Lau et al., 2006) and Tibetan Plateau snow darkening amongst the most established theories (e.g.,

Qian et al., 2011). Aerosols also impart indirect radiative effects through various interaction with clouds, and inclusion of these indirect effects within global climate model simulations have proven necessary to reproduce long-term negative rainfall trends in ISMR (e.g., Guo et al., 2015). Given the strong associated between ISMR and solar PV capacity factors, it follows that the various effects of aerosols upon ISMR could also impact upon solar PV yields.

However, even if a link between relevant aerosol parameters (e.g., aerosol optical depth) and IMSR/solar PV generation can be established, the utility of this relationship for subsequent use as a candidate predictor in a seasonal forecast of generation is limited. This is because the SEAS5 forecast system includes no dynamical means of producing an aerosol-related signal beyond prescribed climatological aerosol loading (Vitart et al., 2019). Specifically, the IFS model cycle 43r1 used in SEAS5 employs stratospheric sulphate aerosol forcings derived from CMIP5 and fixed climatological values of atmospheric composition, as well as cloud schemes that are non-interactive with various aerosol species, and no prognostic treatment of aerosols to permit dynamic, time-varying aerosol variables (Bozzo et al., 2017; Johnson et al., 2019). More recent iterations of the SEAS5 system (post 45r1, including current operational version of SEAS5) include an updated climatology of atmospheric composition (Flemming et al., 2017; Haiden et al., 2018), which has improved the performance of retrospective long-range forecasts (Bozzo et al., 2017; Flemming et al., 2022). And several studies have shown that both interactive and prognostic treatment of aerosols can improve forecast performance metrics (for ECMWF models (Morcrette et al., 2009; Benedetti and Vitart, 2018)) and for other forecasting systems (Mulcahy et al., 2014; Freire et al., 2020), albeit with additional computational expense.

The stated direction of travel for ECMWF's seamless prediction facility is to harmonise the time-varying climatology of multiple aerosol species across ERA6, SEAS6 and other Numerical weather prediction products, using the capabilities of the Copernicus Atmosphere Monitoring Service (CAMS) (ECMWF, 2023). Together with a move amongst forecasting centres towards Earth-system operational models with more detailed atmospheric chemistry modules (Buizza, 2019), it is conceivable that fully dynamic and interactive aerosols could become part of future forecast products, including seasonal timescales. Could such updates to the SEAS5 system impact upon forecast skill of ISMR and, relatedly, solar PV generation? This would depend upon the magnitude of the impact of various aerosols and related processes on solar PV yield compared to those of cloud cover, and whether SCF models can realistically reproduce relevant

aerosol sources, sinks and atmospheric interactions.

Regarding the extent to which aerosol absorption and scattering attenuates total plane-of-array irradiance, a small set of studies have quantified these direct effects of aerosols on solar PV yield in India. Using radiation data from the Clouds and the Earth's Radiant Energy System (CERES) satellite product, both Ghosh et al. (2022) and Yang et al. (2022) suggest aerosols account for a maximum of 20-30% of the total attenuation of incoming solar irradiance over India. Analysis presented in Appendix A confirms this magnitude of reduction in total irradiance at the surface over India (up to 25%, see Figure A.1a). Such reductions in total incoming solar irradiance are captured in the climatological total aerosol optical depth values used in SEAS5 (and subsequent changes in irradiance, as parameterised in the model's radiation scheme).

If an SCF were instead capable of capturing the time-varying evolution of aerosols and the attenuating effects on irradiance (as postulated in the above discussion on next-generation SCF systems), the anomalous aerosol load would determine the attenuating effect per season. However, the analysis presented in Appendix A suggests that the standard deviation in aerosol attenuating effects in JJAS is modest compared that that of clouds (standard deviation in attenuating effect of $\sim$10% versus 25% averaged over peninsular India - Figure A.1b versus A1d), so even the correct representation of aerosol anomalies in a SCF system would impart a relatively small signal on solar PV generation. Furthermore, a sizeable fraction of anomalous aerosol loading over India is anthropogenic in origin (namely, sulphate aerosols largely originating from coal-fired power plants), and so arguably not predictable on seasonal timescales (with between 40-70% of total aerosol optical depth accounted for by sulphates over India - see Appendix A Figure A.1e-f). If the in-situ attenuating effects of aerosol do not offer a major source of predictability for SCF of solar PV, could the remote effects of natural aerosols across the region instead be used? For example, mineral dust loading over the Arabian Sea and Indian peninsular reaches a maximum in early boreal summer (May-July) due to higher wind speeds from the north and east that transport large quantities of material from adjacent deserts (namely, Shamal winds transporting from the Tigris-Euphrates River basin and Levar winds over Iran (Middleton, 1986; Prospero et al., 2002)). ENSO drives anomalous rainfall during the main rainy season for these deserts regions in boreal winter and is tied to soil moisture anomalies in the subsequent spring months, which, in-turn, influences anomalous mineral dust production and aerosol loading over the Arabian sea (Banerjee and Kumar, 2016; Huang et al., 2021). This source of predictability

originating from remote mineral dust loading has been idealised modelling studies (Vinoj et al., 2014; Jin et al., 2016) and assessments of short-range retrospective forecasts with the ECMWF operational forecast model (Bozzo et al., 2017). However, the current generation of SCF systems are not capable of exploiting such climate signals.

5.6 Discussion

5.6.1 Summary of main findings

In this second results chapter, the main drivers of interannual variability in wind and solar PV generation in the JJAS season have been investigated. The analysis has progressed past work concerned with the performance of wind and solar PV in India in three main areas, each of which represent a contribution beyond that currently found in the academic or grey literature:

1. Quantified the linkages between large-scale meteorological conditions in JJAS and seasonal anomalies of wind and solar PV generation, as derived from a multi-decadal synthetic generation time series.
2. Quantified the role of intra seasonal variability in seasonal wind and solar PV generation anomalies in JJAS.
3. Demonstrated the role of anomalous monsoon circulations in the western North Pacific and Indian Ocean in modulating wind generation anomalies in JJAS.
4. Demonstrated the common associations between ISMR variability, solar PV generation and teleconnections in the tropical Pacific and Indian Oceans.

The key findings that accompany the analysis of these contributions are as follows:

1. JJAS mean wind generation anomalies are strongly correlated with lower levels winds across all regional subdivisions of India, with the associations extending upstream and downstream across broad stretches of South Asia. A negative association between wind speeds in the core Somali Jet region and wind generation anomalies is apparent across all regions and is reflected in a negative association in measures of ISMR (c.f. Table 5.1).
2. JJAS mean solar PV generation anomalies per region are strongly correlated with rainfall across corresponding regions (c.f. Figure 5.1 and Table 5.2). The strength of the associations are comparable to direct correlation with surface solar radiation downwards (SSRD),

suggesting rainfall variability is responsible for the majority of observed variability in solar PV generation.

3. Intra-seasonal variability accounts for a similar proportion of the total variation in JJAS mean solar PV generation as for ISMR (c.f. Table 5.3). No association is found between the frequency or magnitude of intra-seasonal variability and wind generation anomalies in the JJAS season (apart from a in the Northern region - c.f. Table 5.3).

4. Mean wind generation anomalies in JJAS are weakly related to tropical Pacific SST anomalies (r value of correlation with Niño3.4: 0.32), but an anomalous WNP monsoon circulation (and associated WNP monsoon indices) are strongly tied to wind generation anomalies in JJAS. Interannual variations in surface winds over peninsular India caused by anomalous western North Pacific monsoon circulation describe a greater fraction of total observed wind generation variability (¿60%) than the local ISM circulation (which is only dominant in the Northern region) (c.f. Figure 5.7 and Table 5.5)

5. The regression patterns between solar PV generation anomalies in JJAS and SST/MLSP show a clear ENSO signature, and the Niño3.4 index explains ∼25% of total variability in solar PV generation anomalies (comparable to the observed strength of the ENSO-ISMR relationship). Atmospheric variability associated with the IOD is less strongly tied to rainfall anomalies in JJAS than ENSO (less than half explanatory power of the ENSO-ISMR relationship). However, a degree of independence between ENSO and IOD variability implies that a multi-linear regression using both variables achieves a larger fraction of total variation explained in solar PV generation anomalies than each variable separately (∼40% for all-India solar PV generation anomalies - c.f. Table 5.6).

6. Although imparting a measurable effect on anomalous solar PV generation, the effects of aerosols are not considered a relevant source of predictability in SCF over India (c.f. Section 5.5).

The previous results chapter speculated that dissimilar phenomena drive wind and solar PV generation anomalies in JJAS due to weak corelation between the two sources across most regions. The analysis presented here confirms this to be the case, with WNP and ISM circulation anomalies implicated in wind and solar PV generation anomalies, respectively. This results chapter has identified several candidate predictors that describe anomalous behaviour of regional

monsoon circulations. The candidate predictors showing the strongest association are derived from lower troposphere winds for the case of wind generation and, additionally, SSTs in the case of solar PV (see Table 5.7). The prospects for developing seasonal generation forecasts are good given the high prediction skill of regional monsoon circulations in both East (e.g., Li et al., 2014; Zhang et al., 2020) and South Asia (e.g., Johnson et al., 2017; Chevuturi et al., 2021). Before evaluating these prospects in the following chapter, the various shortcomings of this chapter's analysis are considered.

Wind	Solar PV
WNPi (c.f. Table 5.4)	ISMi (c.f. Table 5.2)
1st PC 850hPa winds over South Asia (c.f. Table 5.5)	2nd PC 850hPa winds over South Asia (c.f. Table 5.5)
	EQWIN +Niño3.4 (c.f. Table 5.6)

Table 5.7: Candidate predictor variables of wind and solar PV generation anomalies in JJAS.

5.6.2 Shortcomings of the analysis and caveats

Of the various shortcomings of the analysis presented in this chapter, perhaps the greatest is the development of empirical relationships between climate predictors and generation predictands under the assumption of stationarity. Variable long-term trends in the meteorological fields considered, the presence of low frequency modes of variability, and variations in the strength of observed teleconnections all complicate the search for simple and robust statistical descriptions of generation anomalies. For instance, long term trends in monsoon rainfall over South Asia are evidenced in both observations (Bollasina et al., 2011) and future projections (Katzenberger et al., 2021). And major modes of decadal-scale variability in ocean SSTs have been implicated in the observed long-term variations of both ISM and East Asian monsoon systems. For instance, through the 20th century, available evidence suggests that the Pacific Decadal Oscillation (PDO) modulates the East Asian monsoon strength, including the monsoon circulation in the WNP (Qian and Zhou, 2014), and that the ISM is negative correlated with PDO (Krishnan and Sugi, 2003). Similar interactions between both monsoon systems and Atlantic multi-decadal oscillation (AMO) on decadal timescales have been evidenced in coupled atmosphere-ocean global general circulation model experiments (Lu et al., 2006; Luo et al., 2018). Low-frequency modes within indices of both AMO and PDO have switched sign during the 1979-2021 period

considered in the analysis, suggesting possible impacts are not accounted for in the above analysis. Additionally, the well-documented variability in the ENSO-ISMR relationship, with a weakening trend in the latter half of the 20th century (Kumar et al., 1999) and subsequent revival (Yu et al., 2021), could impact upon the relevance of the identified climate predictors through the period considered. Despite these various non stationarities, the empirical relationships between climate predicators and generation anomalies shown in this chapter also show similar strength when computed with the ERA5 back extension to 1940 (not shown), suggesting that the variance explained is robust.

A second shortcoming of the analysis that the empirical relationships between climate predictors and generation anomaly predictands explain only a fraction of the total interannual variability in generation within the JJAS season (up to ∼60% for wind and ∼40% for solar PV). Intra seasonal modes are known to limit predictability in both monsoon systems (e.g., Goswami et al., 2006; Martin et al., 2019). However, others argue that additional sources of predictability derived from slowly varying drivers increase the potential predictability of monsoon systems (e.g., Asian summer monsoon, Wang et al. (2015b); ISM, Saha et al. (2019). For example, additional candidates for ISMR predictability include aerosols (c.f. Section 5.5), Eurasian snow cover (Fasullo, 2004), and the Atlantic Niño (Kucharski et al., 2007), although the explanatory power of such variables is generally marginal compared to the effects of ENSO and IOD/IOB (Johnson et al., 2017). Possible non-linear interactions in the climate system may also enhance the explanatory power of known teleconnections (proposed relationships in this analysis all being linear by construction). For example, the North Atlantic Oscillation (NAO) has been proposed as a possible non-linear driver of Asian summer monsoon (Wu et al., 2009; Goswami et al., 2022). However, the exact physical mechanisms at play in such monsoon teleconnections, their robustness and explanatory power, as well as the fidelity of such representations in operational SCFs all remain open topics of research.

The empirical relationships defined in this chapter to explain wind and solar PV generation anomalies with observed climate predictors are based on the standing stock of wind and solar PV capacity in 2021. The relevance of these predictors as the make-up of the installed fleet changes in the coming years is not guaranteed, particularly as technology advancements and new development zones (e.g., offshore wind) could impact upon generation profiles and modify the fraction of variance explained.

Despite these noted shortcomings, in the context of probabilistic seasonal forecasts, empirical relationships that proved a partial description of total variance can still yield positive forecast value. Using such relationships to establish baselines for forecast performance are important for ongoing improvements to forecasting models and forecasting techniques. Furthermore, establishing limits to foresight and what cannot be known can also be valuable in an operational power system management setting.

5.6.3 Link to next results chapter

The drivers of interannual variability in wind and solar PV generation in JJAS identified in this chapter can serve as sources of predictability in season-ahead generation forecasts. These drivers can also aid in the development of suitable empirical models to relate meteorological anomalies to IAV in generation. Furthermore, the generation syntheses for wind and solar PV generation provide a basis upon which to verify and calibrate seasonal generation forecasts. Using the identified drivers as predictors of wind and solar PV generation, the next results chapter evaluates the performance of season-ahead generation forecasts using meteorological fields from an operational seasonal forecast system.

Chapter 6

Seasonal climate predictions of Indian wind and solar energy generation

6.1 Rationale for investigation and research questions

Chapter 5 showed that interannual variations in the regional monsoon systems in the northwest Pacific Ocean and Indian Ocean describe large fractions of the total interannual generation variance in JJAS for wind (up to ∼60%) and solar PV (up to ∼40%), respectively. The analysis further showed that the anomalous behaviour of the monsoon systems on seasonal time scales is partly driven by modes of ocean variability that exhibit predictive skill in dynamical seasonal forecast systems. In this chapter, the predictive skill of JJAS Indian wind and solar energy generation is assessed using output variables of a seasonal forecast system. Specifically, hindcasts from ECMWF System5 (SEAS5) for the JJAS summer season initialised on May 1st, spanning 1981-2021 (c.f. Section 3.4.1).

The generation forecasts rely on observed statistical relationships between climate predictor variables/indices from ERA5 and regional wind and generation for the JJAS season. Seasonal generation predictions are then derived using the same statistical model but with predictor variables replaced with dynamical predictions from the SCF. Here, the investigation first quantifies the strength of observed statistical relationships, addresses possible forecast under/over-confidence in predictor variables, quantifies skill in generation forecasts, and finally considers sensitivities of the generation forecasts to the methodological approach. This chapter addresses the following research questions:

1. Can the identified predictor variables and bias/calibration techniques yield skilful and reliable seasonal forecasts of wind and solar PV generation?

2. Are seasonal generation forecasts sensitive to the lead time and season length of the climate

predictor variable?

6.2 Using large-scale meteorological drivers to estimate generation

This section details the statistical relationships between candidate large-scale predictors and wind and solar PV energy generation that may be exploited when using the dynamical outputs of the SCF. Section 3.4.2 describes the exact implementation of this so-call perfect-prognosis approach to forecasting. The approach is favoured over any attempt to replicate the same transformation methods used to construct the generation synthesis directly to SCF data outputs, as differences between the reanalysis data product and the SCF outputs necessitate changes to the generation synthesis methodology that degrade the synthesis performance.

Chapter 5 identified five candidate predictor variables (2 for wind and 3 for solar PV), based on a physically-motivated observed relationships with large-scale climatic phenomena. To review, these predictor variables are as follows:

1. Indices of WNP relevant to wind generation: the two indices of the WNP (Western North Pacific) monsoon defined in the previous chapter are considered candidate predictors of wind generation. Namely the first principal component timeseries of 850hPa zonal wind in JJAS over the WNP region (0°-36°N; 30°-130°E) and the WNPi, which is defined as the differences between zonal 850hPa winds in JJAS averaged over southern (7.5°-17.5°N; 100°-140°E) and northern (20°-30°N; 105°-150°E) regions of the WNP.

2. Indices of ISM relevant to solar PV generation: the three indices related to the ISM (Indian summer monsoon) defined in the previous chapter are considered candidate predictors of solar PV generation. Firstly, the multi-linear regression model based on Niño3.4 and EQWIN indices; secondly, the PC2 timeseries of 850hPa horizontal winds in JJAS over the WNP region (0-36N; 30-130E); and third the ISMi, defined as the difference between horizontal 850hPa winds in JJAS averaged over northern (20°-30°N; 60°-80°E) and southern regions (0°-15°N; 35°-65°E) of the northern Indian Ocean.

Additional predictors of spatially averaged SSTs and MSLP were also considered for wind and solar PV but are strongly cross correlated with the aforementioned predictor variables, and so, for brevity, are not detailed here. Two additional meteorological fields were also investigated,

with the area-average chosen to maximise the total variance in energy generation explained, as well as considering the skill of SEAS5 for predicting the variable. These additional fields are as follows:

1. 10m wind speeds: The variable is directly related to wind generation (as shown in Figure 5.1) and high correlation values (Table 6.1) are achieved for all-India, Western and Southern regions when considering large-scale area-weighted anomalies (12°-32°N, 68°-89°E). Adjusting the exact region over which the area-averaged 10m wind speed is calculated can modestly improve correlation values for regional subdivisions (up to 20% for Northern region, <5% for Western and Southern). However, the chosen area maximises the all-India correlation.

2. Rainfall (total precipitation in SEAS5): The anticorrelation between rainfall solar PV capacity factor anomalies was shown previously in Figure 5.2. For the all-India case, the zone of strongest correlation is co-located with the region of greatest installed solar PV capacity in Rajasthan, Gujarat, Madhya Pradesh, and Maharashtra (10°-30°N, 60°-80°E), which together account for ∼50% of nation-wide solar PV capacity based on 2021 data. Modest increases in regional correlation values are achievable (<10%) tuning of the area average. The correlation between all-India solar PV generation anomalies and area-weighted rainfall in maximised using the box 10°-30°N, 60°-80°E and reaches 0.85. (N.B. total cloud cover and surface solar radiation downwards (SSRD) are alternative candidates for spatially averaged predictors. However, these achieves similar skill to rainfall and, ultimately, a lower skill than large-scale predictors, as later shown).

Table 6.1 summarises the strength of all the observed relationships considering relevant area-averaged meteorological anomaly fields and the predictor variables.

	Wind					Solar PV				
	All-India	NR	WR	SR		All-India	NR	WR	SR	ER
10m winds	0.90	0.47	0.83	0.80	ISMR	-0.82	-0.74	-0.66	-0.75	-0.40
EOF1 850 hPa winds	0.78	0.36	0.65	0.80	Niño3.4 + EQWIN	0.64	0.53	0.53	0.61	0.33
WNPi	0.74	0.33	0.62	0.78	2nd PC 850 hPa winds	-0.79	-0.71	-0.8	-0.64	-0.54
					ISMi	-0.73	-0.64	-0.57	-0.71	-0.20

Table 6.1: Correlation between wind/solar PV generation anomalies per region and candidate climate predictors. Underlined values are significant at the 95% level.

The correlations between the climatic predictors and JJAS wind generation anomalies in ERA5 show similar strengths and patterns of correlation, with the highest correlations in the Southern region and lowest in the Northern region (see Table 6.1). As all predictors describe similar large-scale variability affecting the Indian subcontinent in JJAS, and in many cases are cross-correlated, any combination of the predictors in a multi-linear regression shows little improvement in correlation values. The lower correlation values in the Northern region, particularly with the EOF1 and WNPi predictors, are because ISM circulation variability also has an influence in this region (c.f. Chapter 5, section 5.3.3), which is not entirely captured by the three predictor variables (N.B. spatially average 10m winds cover much of peninsular India, and so capture relatively larger share of WNP variability). Accordingly, measures of ISM circulation variability also show significant correlation with wind generation anomalies in the Northern region. For example, the second PC of 850hPa horizontal winds over South Asia has a higher correlation with wind generation anomalies in the Northern region than the first PC timeseries (r value of -0.50 versus 0.36). Therefore, combining predictors for wind and solar PV generation variability, which are themselves predictors of ISM circulation variability, can increase the fraction of total variance in wind generation explained in the Northern region. A multilinear regression model using the 1st and 2nd PC timeseries as predictors for the Northern region gives an r value of 0.62, which is 25% higher than any individual predictor in that region.

For JJAS solar PV generation anomalies, rainfall shows the strongest relationship, with over 67% of the total variance explained for the all-India case. Other candidate predictor variables that are less proximate than rainfall achieve moderately lower correlation values, although the second PC timeseries of 850hPa horizontal winds in JJAS over South Asia still explains over 60% of total variance in all-India solar PV generation variability for all-India. Correlation values for the Eastern region vary between predictors, likely reflecting the much lower levels of installed solar capacity in this region (∼2.5% of total installed solar PV capacity in 2021 versus roughly 30% in other regions) that are geographically concentrated compared to the other regions. Combinations of predictors offer little improvement over the best[1] predictor per region (e.g., combining ISMi and total cloud cover as predictors yields no appreciable increase in correlation compared to total cloud cover alone).

[1]Combinations of predictors were systematically tested ${}_nC_r = \frac{n!}{r(n-1)!}$. 'Best' predictor(s) refers to those which demonstrate the highest fraction of variance explained. Alternative methods could be used for the selection of the best subset of predictors, such as the Akaike Information Criterion, which retains the maximum information in the statistical relationship without necessarily keeping all the predictors (James et al., 2013).

The utility of candidate predictor variables in a seasonal forecasting context depends on both the proportion of total generation variance accounted for and the forecast skill of the predictor variables. Accordingly, a predictor variable with high explanatory power is of limited use if it is poorly predicted. The following section evaluates the performance of each candidate predictor variable in terms of the correlation between hindcast ensemble mean predictor variables and generation variability.

6.3 Assessment of deterministic generation forecast skill

Table 6.2 shows the JJAS forecast skill (i.e., the association, measured with the correlation coefficient and expressed as the r value) of the wind and solar PV predictor variables from Table 6.1 at predicting the synthetic wind and solar PV data from Chapter 4 using the one-month lead-time SEAS5 forecasts. For wind, the correlation values are similar across all combinations of predictor variables and regions. As was the case for the relationship between predictor variables and regional wind generation anomalies in ERA5, the Northern region exhibits the lowest skill and the Southern region the highest. The WNPi predictor achieves the highest skill for all-India amongst predictors of wind generation (explaining ∼40% of observed wind generation variability in JJAS)1. This high correlation reflects the large fraction of variance explained by the WNPi (Table 6.1) and the forecast skill for the WNPi (r=0.78), which is comparable to prediction skill found for other SCF systems (see Table 6.3).

Adjusting the spatial averaging for 10m winds to maximise the deterministic skill in each subregion offers marginal improvements for the Northern region (+8% in skill (0.44)), and negligible improvements to Western and Southern regions. Combining multiple predictors also offers little improvement in deterministic skill scores for wind generation over the single best performing

Wind					Solar PV					
	All-India	NR	WR	SR		All-India	NR	WR	SR	ER
10m wind	0.62	0.40	0.53	0.56	ISMR	0.33	0.20	0.18	0.39	0.11
EOF1 850 hPa winds	0.58	0.36	0.48	0.54	Niño3.4 + EQWIN	0.40	0.33	0.31	0.43	0.36
WNPi	0.64	0.45	0.56	0.56	EOF2 850 hPa winds	-0.17	-0.17	-0.25	-0.08	0.22
					ISMi	-0.47	-0.33	-0.37	-0.52	-0.40

Table 6.2: Performance of wind and solar PV generation forecasts, based on five different predictor variables each. Underlined values are significant at the 95% level.

Seasonal forecast system / hindcast set	**Correlation coefficient**	**Reference**
1) ENSEMBLES multi model ensemble (MME) JJA WNP index (1960–2005)	0.68	Li et al. (2012)
2) North American Multimodel (MME): Climate Forecast System version 2 [CFSv2], Canadian Coupled Climate Model version 3 [CanCM3] and Canadian Coupled Climate Model version 4 [CanCM4]) (1982–2010)	MME: 0.84 CFS2: 0.71 CanCM3: 0.72 Can CM4: 0.77	Nie and Guo (2019)
3) GloSea5 / BCC_CSM1.1m (1992-2011)	0.85/0.68	Wu et al. (2020)
4) GloSea5 (1993-2015)	0.84	Zhang et al. (2020)

Table 6.3: Deterministic hindcast skill for JJA and JJAS WNPi in 4 recent SCF assessments.

predictor per region. The only exception is found in the Northern region, where local 10m winds (avergae over 18°−35°N, 64°-80°E) combined with the WNPi yields a ∼12% increase in skill (r=0.50). As mentioned previously, both ISM and WNP monsoon circulation variability are implicated in JJAS wind generation anomalies in this Northern region, so the addition of the 10m winds as a predictor adds a predictable signal imparted from ISM variability, which is otherwise only partially captured in the WNPi variable.

Forecast skill for solar PV is approximately half that for wind for the all-India case, with up to ∼20% of total interannual variability in JJAS solar PV generation explained by the best performing predictor (r = 0.47 for ISMi; Table 6.2). Forecast skill is generally highest in Southern and Western regions, which coincides with the highest levels of installed capacity. The EOF2 of 850hPa winds performs particularly poorly as a predictor of solar PV generation anomalies across all regions. Because of the strong association between anomalous solar PV generation and ISM rainfall on seasonal timescales, the forecast skill is comparable to that documented for seasonal hindcast skill for ISMR. Table 6.4 summarises the deterministic forecast skill obtained in other recent assessments of ISMR at a one-month lead time.

Only the Niño3.4 + EQWIN and IMSi predictors achieve correlation values significant at the 95% level across all regions, and the latter provides the highest skill in all regions. As the Western and Southern regions constitute a greater share of the total nationwide solar PV capacity (∼67%), the marginally higher skill of the ISMi predictor in these regions translates into the highest skill for the all-India case. Combining the candidate predictor variables offers little improvement in skill for the all-India case (<2% increase for all-India when using all 4 predictors). However, larger increases in skill are achievable by combining predictors at the

Seasonal forecast system / hindcast set	**Correlation coefficient**	**Reference**
1) ENSEMBLES multi model ensemble (MME) JJAS ISMR	0.45	Rajeevan et al. (2012b)
2) GloSea5-GC2 JJA ISMR	0.41	Johnson et al. (2017)
3) North American Multimodal Ensemble (NMME) JJAS ISMR	0.47	Singh et al. (2019)
4) Climate Historical Forecast Project (CHFP) MME JJA ISMR	0.60	Jain et al. (2019)
5) SEAS5 JJA ISMR	0.33	Chevuturi et al. (2021)
6) SEAS5 JJAS ISMR	0.47	Attada et al. (2022)
7) Monsoon Mission Coupled Forecast System version 2	0.72	Jain et al. (2023))

Table 6.4: Deterministic hindcast skill for JJA and JJAS ISMR in seven recent SCF assessments.

regional level. Specifically, for the Northern and Eastern regions, increases of 20% and 8%, respectively, are attainable using the two best performing predictors (Niño3.4 + EQWIN and IMSi) in combination. Furthermore, the inclusion of either the Niño3.4 + EQWIN or ISMi predictors with best performing wind generation predictor (WNPi) increases the fraction total wind generation variance explained in the Northern region (r = 0.52; +14%).

The best performing predictors of JJAS wind and solar PV generation are summarised in Table 6.5. Across all regions for wind, the WNPi predictor provides the most skilful predictions. Predictions for the Northern region can be moderately enhanced by 12-14% by adding either 10m winds, Niño3.4+EQWIN or ISMi. As the Northern region constitutes a minor share of total installed wind capacity in India (∼15%), the all-India prediction skill is little changed using multiple predictors. For solar PV, the ISMi predictor achieves the highest forecast skill across all regions. Combining the second-best predictor for solar PV (Niño3.4+EQWIN) improves forecast skill for the Northern and Eastern regions.

6.4 Sources of skill

To confirm that skill in the best performing predictors originates from their accurate representation in the SCF model, the following demonstrates a comparison between observations and the SCF ensemble mean. As shown in Section 5.3.3 anomalous surface winds over India

and wind generation covary with anomalous circulation in the WNP sector. This covariance is demonstrated in Figure 6.1a, which shows observed JJAS SST and MSLP regressed onto all-India wind generation anomalies. The negative correlation with MSLP, which is greatest in the WNP, describes the large-scale anomalous cyclonic circulation anomaly within the lower troposphere is associated with an enhanced WNP monsoon. The SEAS5 ensemble mean captures the main features of both the MSLP and SST anomalies (Figure 6.1b), albeit with a weaker MSLP dipole between the Indian Ocean and WNP, as well as a weaker positive correlation with SST in the equatorial east Pacific. Chapter 5 showed the first and second EOFs of 850 hPa winds in the WNP region describe ENSO onset and a coupled ocean–atmosphere mode between the WNP and northern Indian Ocean, respectively (c.f. Chapter 5 Section 5.3.2). This EOF decomposition is shown for both ERA5 and the mean of SEAS5 ensemble members[2] in Figure 6.1c-f. The patterns of SST regressed onto the PCs are remarkably similar between observations and SEAS5, and the main features of the 850hPa circulation anomalies common, albeit with northeastern shift in SEAS5.

In the case of solar PV, ENSO is the largest contributor to total variance in JJAS solar PV generation anomalies (c.f. Chapter 5 Section 5.4.2). Indeed, the regression pattern between all-India JJAS mean solar PV anomalies and SST/MSLP is reminiscent of ENSO (Figure 6.2a). The pattern in SEAS5 is similar to ERA5 (Figure 6.2b), though with a slightly weaker correlation in both fields. The mechanism through which ENSO affects ISMR, total cloud cover and surface irradiance (SSRD) is discussed in the previous chapter (c.f. Section 5.4). Composites of both total cloud cover and 850hPa wind anomalies during La Nina (Figures 6.2c and d) and El Niño (Figures 6.2e and f) show comparable patterns and magnitudes in ERA5 and SEAS5, namely, enhanced zonal wind shear between the core Somali Jet region and the monsoon trough during

[2]i.e., the EOF decomposition was conducted on each ensemble member before averaging over resulting modes. Alternatively, ensemble members can be projected onto observed modes (i.e., the eigenvectors) and the resulting PCs averaged to gauge similarity in spatiotemporal variability, which is high: 0.87 and 0.76 for PC1 and 2, respectively.

Predictor(s)	Region
WNPi	Wind: India, WR, SR, ER
WNPi + ISMi	Wind: NR
ISMi	Solar PV: India, WR, SR
ISMi + Niño3.4/EQWIN	Solar PV: NR, ER

Table 6.5: Climatic predictors achieving highest deterministic skill for wind/solar PV generation in JJAS.

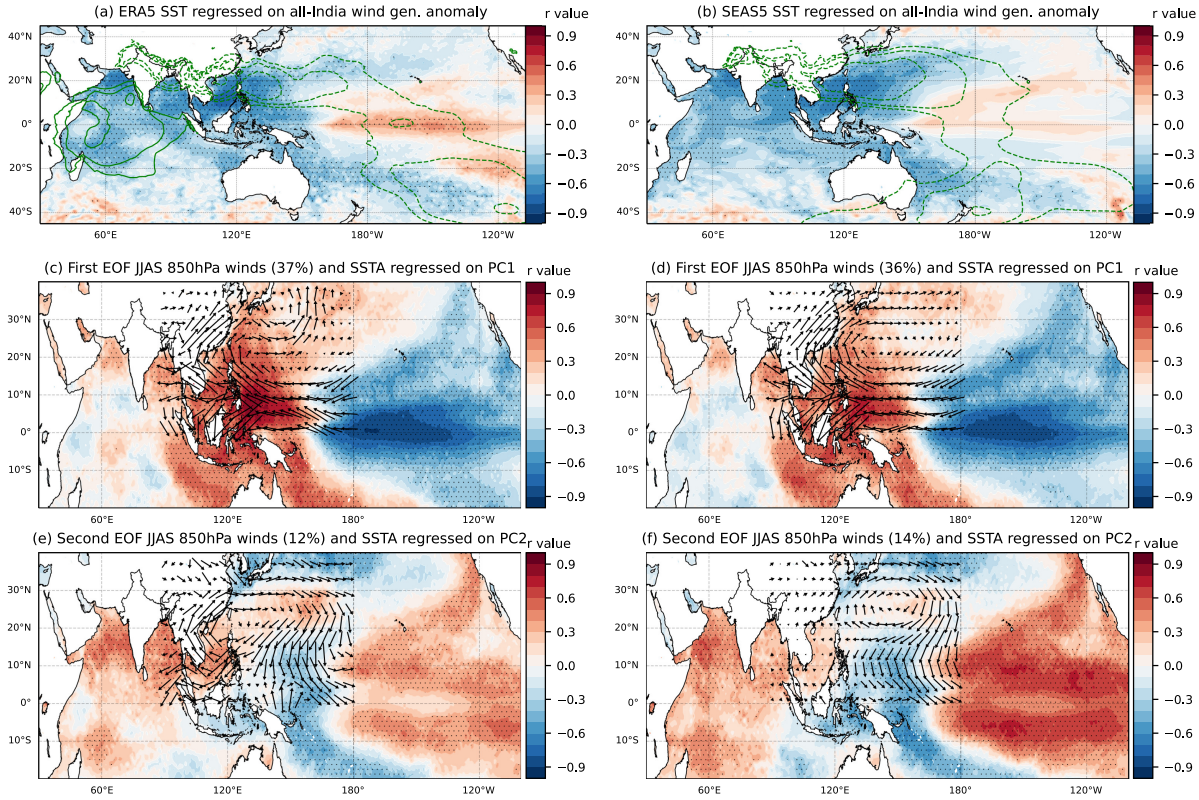

Figure 6.1: SST/MSLP regressed on all-India wind generation anomalies for ERA5 (a) and SEAS5 (b). First and second modes of EOF decomposition of 850hPa winds over Western North Pacific for ERA5 (c and e) and SEAS5 (d and f). EOF decomposition conducted on each ensemble member before averaging over all members.

La Nina, together with increased cloud cover.

6.5 Probabilistic verification of best performing model: wind generation

Using the climatic predictors detailed in Table 6.5 and their relationships to synthetic India wind capacity factors derived from ERA5 (Chapter 4), capacity factors for wind are estimated for each ensemble member of the SEAS5 hindcasts. As described in Section 3.4.2, the process of deriving and applying regression coefficients, as well as correcting ensemble spread with the Climate Conserving Recalibration (CCR), were performed using cross-validation. As such, ensemble mean correlation values are expected to be lower than the values listed in Table 6.2. As hindcasts of predictor variables were generally found to be moderately overconfident over South Asia (see Appendix B for analysis), the use of CCR is expected to inflate ensemble spread and marginally improve probabilistic measure of forecast skill and forecast reliability.

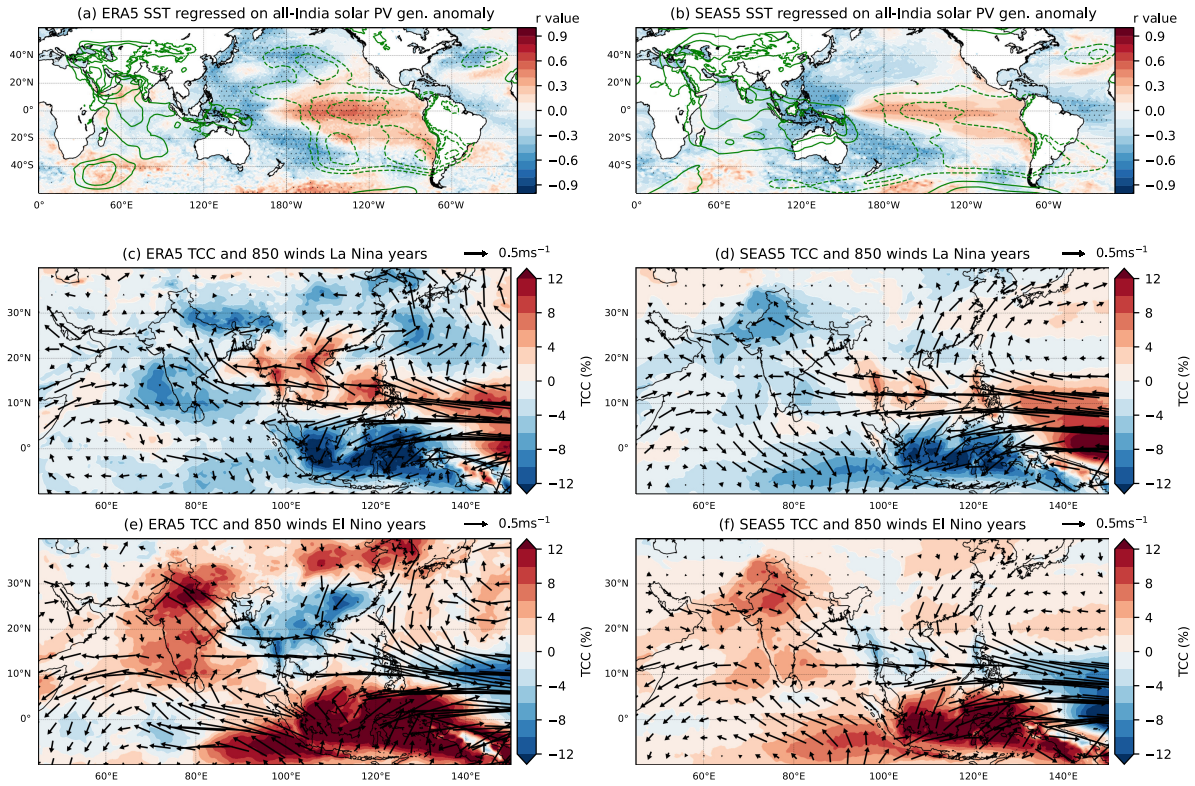

Figure 6.2: SST/MSLP regressed on all-India solar PV generation anomalies for ERA5 (a) and SEAS5 (b). Composite anomalies of total cloud cover and 850hPa winds during La Nina (n=10) and El Niño (n=9) (—JJAS Niño3.4 index—>0.5), for ERA5 (c and e) and SEAS5 (d and f).

The resulting spread in hindcasts of wind capacity factors are visualised per year in Figure 6.3 for the all-India case, with the absolute capacity factor values for each ensemble member shown as yellow points (n=51 per year). A kernel density estimate is used to aid interpretation of the spread in capacity factors given by ensemble members, with colouring of the resulting probability distribution indicating terciles of the model climatology (i.e., terciles based on all hindcast years). The percentage values show the fraction of total ensemble members in each tercile. Black points denote the observed values.

The ensemble members capture the signal of strongly negative events very well. The lowest tercile category is correctly predicted by >80% of ensemble members in four of the five lowest generation years (1983, 1988, 1998, 2010, 2020, which are also the years with the five lowest values of the predictor variable). As shown in the previous chapter, most of the large negative anomalies coincide with rapid onset of La Nina following transition from El Niño conditions.

Significant forecast skill for wind generation is found in a range of skill metrics (Table 6.6) The strength of the correlation between ensemble mean and observations remains high, despite the

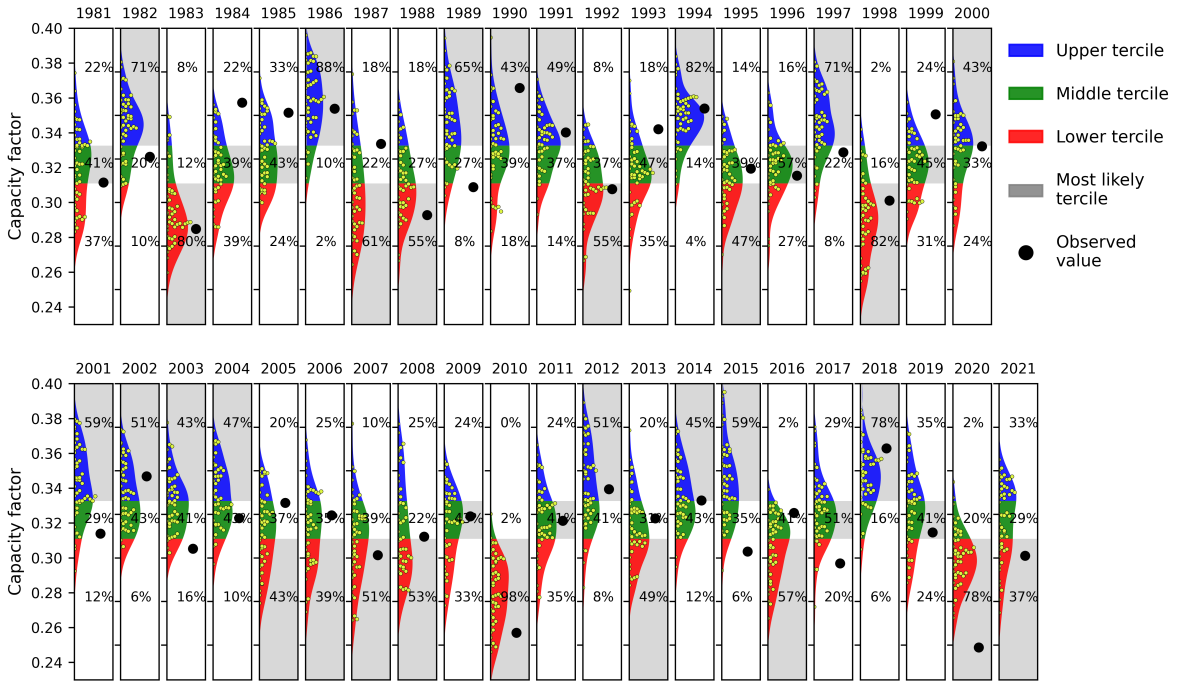

Figure 6.3: Kernel density estimate of JJAS wind capacity factors, coloured by tercile, based on SEAS5 for JJAS hindcasts in the period 1981-2021, each initialised on May 1st. Forecast probabilities per tercile category shown as overlaid text. Individual ensemble members as yellow points and observed values as black points.

use of cross-validation when applying coefficients of the observed linear regression relationships. Positive skill is generally found across forecast verification metrics considered when assessed relative to a climatological benchmark. However, insignificant skill is more often found with the discrete measures BSS and RPSS, both of which are more sensitive to ensemble size than r values and continuous measures (CRPSS) (Weigel et al., 2007). The Relative Operating Characteristic Skill Score (ROCSS) is also positive for each tercile category, indicating that the number of hits (correct predictions) is greater than the number of false alarms (incorrectly predicted non-occurrences) across a range of probability thresholds.

All skill metrics are to some extent sensitive to sample size, though this is particularly the case for assessments of forecast reliability and sharpness. In the analysis presented here, the aggregate impact variable (i.e. generation anomaly) provides just one case per hindcast year, equivalent to a sample size at least two orders of magnitude smaller than a gridpoint assessment where events could be pooled across all grid cells within a region. While acknowledging this caveat, the attributes diagram shown in Figure 6.4 is suggestive of reliable forecasts that sample a range of probabilities for at least the upper and lower tercile categories – i.e., the correct shape

Wind (JJAS) 1 month lead					
	r value	Brier (low./up./mid.)	CRPSS	RPSS	ROCSS (low./up./mid.)
India	0.61	0.27 / 0.14/ 0.10	0.38	0.42	0.56 / 0.54 / 0.42
NR	0.47	0.08 / 0.25 / 0.01	0.35	0.45	0.62 / 0.38 / -0.07
WR	0.54	0.00 / 0.22 / 0.02	0.33	0.37	0.60 / 0.38 / *0.20*
SR	0.53	0.21 / 0.00 / 0.03	0.32	0.35	0.45 / 0.56 / *0.20*

Table 6.6: Forecast quality metrics for 1-month lead JJAS wind generation. Underlined (italic) values are significant at the 95% (90%) level based on a bootstrap resampling method. All values for association (r values) significant at the 95% level using two-sided Student's t-test.

and generally with positive contributions to skill.

6.6 Probabilistic verification of best performing model: solar PV generation

Using the climatic predictors detailed in Table 6.5 and their statistical relationship with solar PV generation derived from ERA5, capacity factors for solar PV are obtained for each ensemble member of the hindcast. These are shown in Figure 6.5 using the same visualisation scheme as for the case of wind in Figure 6.4.

Positive forecast skill in the solar PV generation forecasts per region are found in many of the skill metrics (Table 6.7), although the values are lower than for wind and only marginally significant in several cases. This is particularly the case for Northern India, due to the weaker relationship between solar PV generation anomalies in the region and the ISMi predictor variable.

Solar PV (JJAS) 1-month lead					
	r value	Brier (low./up./mid.)	CRPSS	RPSS	ROCSS (low./up./mid.)
India	0.46	0.14 / 0.29 / 0.00	0.37	0.42	0.56 / *0.40* / 0.15
NR	*0.26*	0.03 / -0.02 / -0.05	0.28	0.28	0.22 / 0.22 / -0.12
WR	0.31	*0.06* / 0.17 / -0.02	0.27	0.39	0.60 / *0.30* / 0.11
SR	0.58	0.19 / 0.13 / 0.00	0.43	0.39	0.42 / 0.53 / 0.08

Table 6.7: Forecast quality metrics for 1-month lead JJAS solar PV generation. Underlined (italic) values are significant at the 95% (90%) level based on a bootstrap resampling method or in the case of correlation coefficient a two-sided Student's t-test.

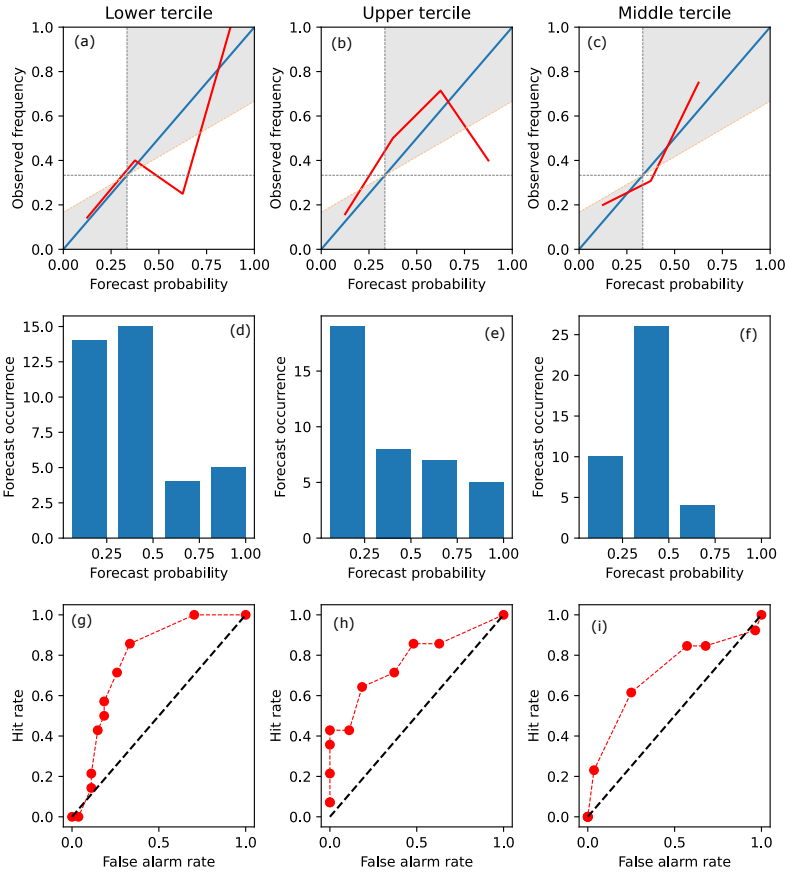

Figure 6.4: Attributes diagram for 1-month leadtime JJAS wind capacity factor forecasts based on SEAS5 for JJAS hindcasts in the period 1981-2021. (a-c) shows the reliability diagram, (d-f) shows the sharpness diagrams, and (g-i) shows the Relative Operative Characterises plots, all for lower, upper and middle tercile categories, respectively (see section 3.4.3 for further details of attributes diagram).

6.7 Sensitivity to forecast lead time and season length

6.7.1 Wind

In the literature, seasonal prediction of ISM is often assessed over a shorter JJA period, corresponding to the months of peak monsoon rainfall over the core monsoon region. It is expected that the shorter effective lead time of the forecasts (by excluding September) would marginally increase skill, while the effect of averaging across a shorter season would increase the role of noise relative to a seasonally persisting signal, thus reducing skill. Repeating the skill assessment for JJA at a 1-month lead for wind generation shows very similar levels of skill to JJAS (Table 6.8). When JJA wind generation forecasts are assessed again at a 0-month lead (i.e., forecasts initialised June 1st), skill is moderately increased across all metrics for all regions

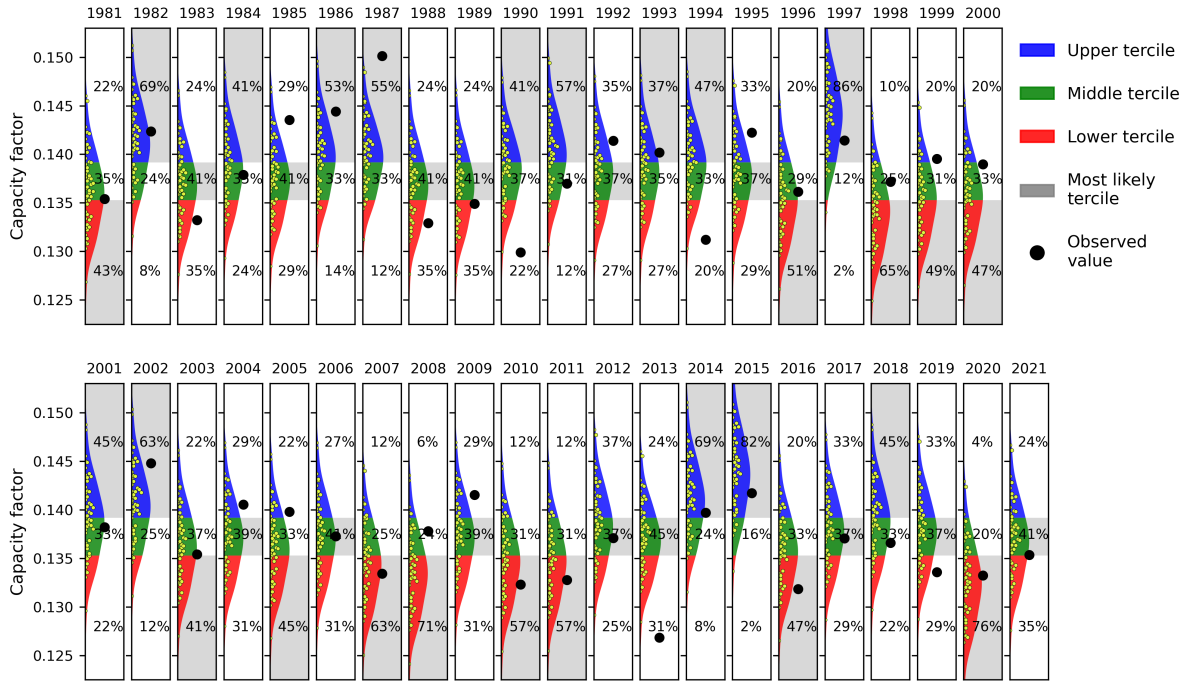

Figure 6.5: Kernel density estimate of JJAS solar PV capacity factors, coloured by tercile, based on SEAS5 hindcasts of the period 1981-2021, each initialised on May 1st. Forecast probabilities per tercile category shown as overlaid text. Individual ensemble members as yellow points and observed values as black points.

(Table 6.9). The shorter lead time has the effect of increasing the relative role of predictive signal that remains following initialisation of the SCFs over that of noise.

Wind (JJA) 1-month lead					
	r value	Brier (low./up./mid.)	CRPSS	RPSS	ROCSS (low./up./mid.)
India	0.57	0.22 / 0.16 / 0.07	0.36	0.44	0.61 / 0.51 / *0.35*
NR	0.42	0.06 / 0.22 / 0.00	0.33	0.43	0.54 / *0.38* / -0.12
WR	0.50	*0.00* / 0.20 / 0.02	0.30	0.35	0.58 / 0.25 / 0.19
SR	0.48	0.08 / 0.00 / 0.06	0.30	0.31	0.33 / *0.40* / 0.31

Table 6.8: Forecast skill metrics for 1-month lead-time JJA wind generation. Underlined (italic) values are significant at the 95% (90%) level based on a bootstrap resampling method. All correlation coefficients are significant at the 95% level using two-sided Student's t-test.

6.7.2 Solar PV

Repeating the skill assessment with the shorter JJA season at a 1-month lead for solar PV generation shows very similar levels of skill across all metrics for all regions, except in the South, where the skill reduction is greater (Table 6.10). In the case of JJA solar PV generation forecasts assessed at a 0-month lead, skill is increased across all regions except in the South,

Wind (JJA) 0-month lead					
	r value	Brier (low./up./mid.)	CRPSS	RPSS	ROCSS (low./up./mid.)
India	0.67	0.16 / 0.27 / 0.02	0.40	0.42	0.69 / 0.47 / *0.37*
NR	0.46	0.19 / 0.31 / 0.08	0.36	0.50	0.59 / 0.53 / 0.44
WR	0.62	*0.09* / 0.25 / 0.02	0.35	0.39	0.63 / *0.43* / 0.31
SR	0.50	0.05 / 0.00 / 0.06	0.29	0.32	0.32 / 0.47 / 0.27

Table 6.9: Forecast skill metrics for 0-month lead JJA wind generation. Underlined (italic) values are significant at the 95% (90%) level based on a bootstrap resampling method. All correlation coefficients are significant at the 95% level using two-sided Student's t-test.

relative to the 1-month lead JJAS forecasts (Table 6.11). The reduction in skill for the Southern region for the shorter season is likely caused by the greater contribution of September rains to seasonal mean values in this area (Mishra et al., 2012).

Solar PV (JJA) 1-month lead					
	r value	Brier (low./up./mid.)	CRPSS	RPSS	ROCSS (low./up./mid.)
India	0.33	0.09 /0.26 / 0.02	0.35	0.36	0.61 /*0.37* / 0.15
NR	*0.27*	0.02 / -0.02 / -0.03	*0.29*	0.27	0.23 / 0.23 / -0.02
WR	0.34	0.10 / 0.19 / -0.05	0.27	0.38	0.58 / 0.30 / 0.10
SR	0.35	0.10 / 0.06 / 0.02	0.36	0.39	0.23 / 0.33 / 0.03

Table 6.10: Forecast skill metrics for 1-month lead JJA solar PV generation. Underlined (italic) values are significant at the 95% (90%) level based on a bootstrap resampling method or in the case of correlation coefficients a two-sided Student's t-test.

Solar PV (JJA) 0-month lead					
	r value	Brier (low./up./mid.)	CRPSS	RPSS	ROCSS (low./up./mid.)
India	0.58	0.15 / 0.30 / 0.00	0.38	0.42	0.72 / 0.52 / 0.10
NR	0.36	0.01 /0.05 / 0.00	0.36	0.31	0.35 / 0.15 /-0.02
WR	0.55	*0.18* / 0.33 / 0.01	0.36	0.43	0.70 / *0.50* / 0.20
SR	0.50	0.15 / 0.15 / 0.04	0.40	0.41	0.46 / 0.42 / 0.20

Table 6.11: Forecast skill metrics for 0-month lead JJA solar PV generation. Underlined (italic) values are significant at the 95% (90%) level based on a bootstrap resampling method or in the case of correlation coefficients a two-sided Student's t-test.

6.8 Multi model forecasts

Generally, multi-model predictions improve forecast skill through a combination of error compensation and a greater signal-to-noise ratio (i.e., more ensemble members, Hagedorn et al. (2005) and DelSole et al. (2014). Table 6.12 details seven additional SCF systems considered here as part of a cursory assessment of multi-model predictions. Hindcasts for additional models

System name	Centre/country	Hindcast ensemble size	References
GloSea-6 (MetO-S602)	Met Office, UK	28	https://www.metoffice.gov.uk
Meteo-France System 8	Meteo-France, France	25	https://www.umr-cnrm.fr
CMCC SPSv3.5	Italy	40	Gualdi et al. (2020)
DWD-GCFS2.1	Offenbach, Germany	30	Fröhlich et al. (2021)
CFS2 NCEP	NOAA, USA	24	Saha et al. (2014)
JMA-MRI-CPS3	MRI-JMA, Japan	10	Hirahara et al. (2023)
GEM5-NEMO (ECCC-S3)	Canada	10	Lin et al. (2020)

Table 6.12: Seven SCF systems in C3S used for assessment of MME forecasts.

		All-India wind		All-India solar PV	
#	System name	r value	CRPSS	r value	CRPSS
1	ECMWF System5	0.54	0.32	0.46	0.30
2	GloSea-6 (MetO-S602)	0.43	0.23	0.36	0.22
3	Meteo-France System 8	0.39	0.25	0.32	0.23
4	CMCC SPSv3.5	0.54	0.26	0.45	0.21
5	DWD-GCFS2.1	0.37	0.27	0.33	0.25
6	CFS2 NCEP	0.42	0.21	0.34	0.20
7	JMA-MRI-CPS3	0.21	0.19	0.19	0.16
8	GEM5-NEMO (ECCC-S3)	0.49	0.28	0.35	0.21
	MME: 1+2+3+4+5+6+7+8	0.51	0.30	0.42	0.28
	MME: 1+4+6+8	0.57	0.33	0.47	0.31

Table 6.13: Deterministic (r value) and probabilistic (CRPSS) verification measures for all-India wind and solar PV generation forecasts constructed using individual and combined C3S models.

come from the Copernicus Climate Data Store (C3S) and span the common period 1993-2016. All models show positive skill in forecasting wind and solar PV generation, though none outperform SEAS5 (Table 6.13). The deterministic skill of the 51-member SEAS5 over this period is 0.54 and 0.46 for all-India wind and solar PV capacity factors, respectively. Adding in hindcasts from the additional 7 SCF systems (167 ensemble members) yields deterministic skill of 0.51 and 0.42 for all-India wind and solar PV capacity factors, respectively. A combination of the four best-performing models to make multi-model generation wind and solar PV forecasts offers modest improvements in measures of deterministic and probabilistic skill (∼5% increase, Table 6.13).

Several factors likely contribute to this modest change in forecast performance. Firstly, deterministic forecast skill asymptotes with relatively few ensemble members (shown in Appendix B) and suggests modest increases in the signal-to-noise ratio for candidate predictors with an

increased ensemble size through multi-model combination. Second, the SEA5 hindcasts are only marginally overconfident (quantified in Appendix B) and so limited change to ensemble spread would result from adding models (Weigel et al., 2009). Furthermore, the Climate Conserving Recalibration (CCR) calibration technique used to produce the generation forecasts adjusts ensemble spread and improves probabilistic measures of forecast skill. The probability space is likely already well-sampled and is relatively free of systematic and conditional bias with the CCR-adjusted 51-member System5 model.

6.9 Predictability of extreme generation daily frequency

Periods of extreme high or low generation can be problematic for the electricity network. Where wind or solar PV generation (plus other energy sources) exceeds either demand or the local network capacity, there is a risk of curtailment – i.e., unused generation that can entail costly compensation of farm operators. When wind or solar PV generation falls short of anticipated output, other sources/sinks of energy must be called into action to cover the short fall, typically entailing extra costs. Therefore, any indication ahead of time as to the expected frequency of extreme high or low generation events may hold value for the planning and management of the electricity system.

Here, the upper and lower 10th percentiles of daily generation during JJAS over all sample years are used to define extreme generation days. Figure 6.6 shows a correlation between the number of high generation days in JJAS and the JJAS mean generation anomaly for both technologies (r=0.60 for wind and r=0.75 for solar PV). Similarly, the number of low generation days is anticorrelated with the JJAS seasonal mean anomaly (r=-0.76 for wind and r=-0.85 for solar PV). The relationships hold over a range of percentile thresholds (Table 6.14) and suggest that the skilful prediction of the seasonal mean generation anomalies shown in the previous section could be translated into skill in the frequency of extreme generation anomalies within the season.

Table 6.15 shows the correlation between the frequency of high and low generation days per season and both the ERA5 and SEAS5 derived JJAS values calculated using the optimum climatic predictor variables described in Section 6.3. The correlations are stronger for the low generation events than for the high generation events, with approximately one third of interannual variability in low generation days captured by SEAS5 for both wind and solar.

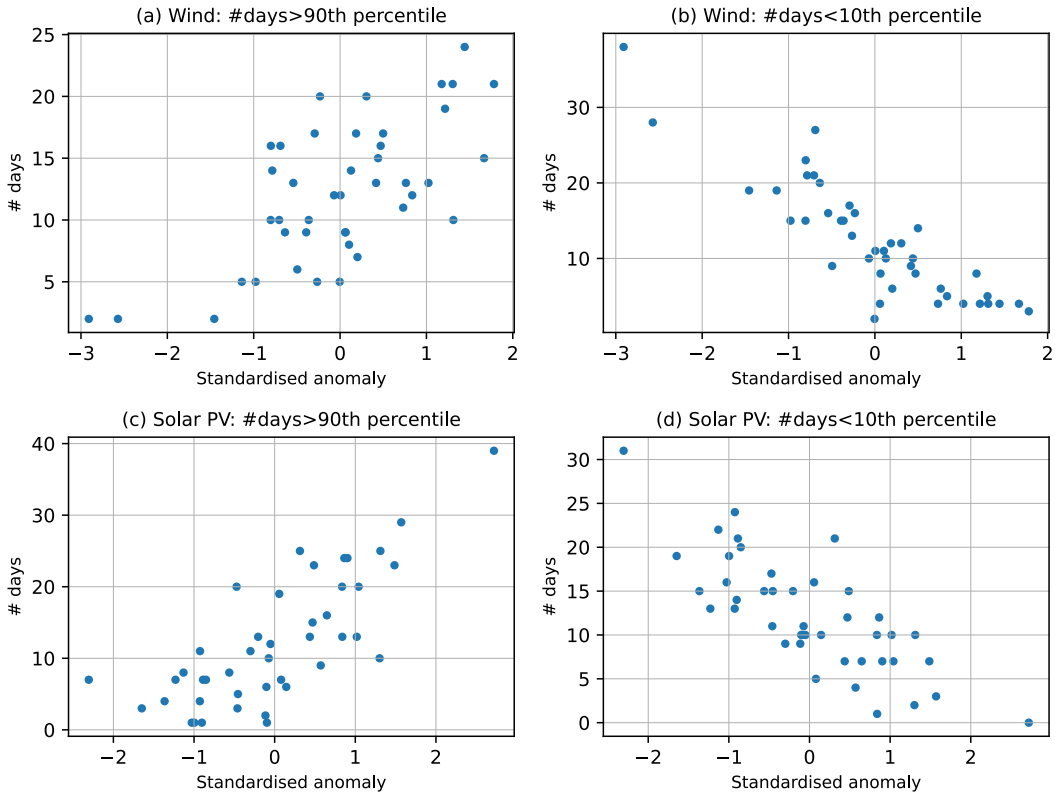

Figure 6.6: Relationship between standardised anomalies of JJAS mean generation for wind (upper panels) and solar (lower panels) and number of extreme generation days in JJAS (<10th percentile or >90th percentile).

Wind				Solar PV			
Less than		Greater than		Less than		Greater than	
0.05	-0.68	0.95	0.49	0.05	-0.72	0.95	0.67
0.10	-0.85	0.90	0.60	0.10	-0.76	0.90	0.75
0.15	-0.85	0.85	0.76	0.15	-0.82	0.85	0.86
0.20	-0.89	0.80	0.80	0.20	-0.89	0.80	0.90
0.25	-0.91	0.75	0.86	0.25	-0.92	0.75	0.94

Table 6.14: Observed relationship between JJAS mean generation anomalies and number of days equalling or exceeding percentiles of daily generation in JJAS for wind and solar PV. Strength of association assessed with Spearman rank correlation coefficient.

The skill of seasonal predictions for extreme generation days is further evidenced with contingency tables for predicting above the median number of extreme days per season, for both wind (Table 6.16) and solar PV (Table 6.17). The rate of hits and correct rejections exceed misses and false alarms by more than double for both wind and solar PV (hit rate: 74% and 70% wind and solar PV, respectively; false alarm rate: 32% and 29% wind and solar PV, respectively). The skill of the discrete day count forecast assessed with the Heidke skill score are positive at significant at the 90% level (0.42 for wind and 0.41 for solar PV), considering a random sampling

	>=90th percentile		<=10th percentile	
	Obs. JJAS mean generation anomaly	Ensemble mean JJAS mean generation anomaly	Obs. JJAS mean generation anomaly	Ensemble mean JJAS mean generation anomaly
Wind	0.47	0.30	-0.60	-0.55
Solar PV	0.57	0.17	-0.72	-0.59

Table 6.15: Relationship between observed and forecast predictor variables (as described in Section 6.3) for JJAS mean generation anomalies and number of days equalling or exceeding percentiles of daily generation in JJAS for wind and solar PV. Values represent Spearman rank correlation coefficient.

and replacement strategy repeated 1000 times.

		Observed	
		Yes	No
Forecast	Yes	14 (hits)	7 (false alarm)
	No	5 (misses)	15 (correct rejection)

Table 6.16: Contingency table for number of days equalling or below lower 10th percentile of daily wind generation for all-India per JJAS season, using 1-month lead System5 forecasts.

		Observed	
		Yes	No
Forecast	Yes	14 (hits)	6 (false alarm)
	No	6 (misses)	15 (correct rejection)

Table 6.17: Contingency table for number of days equalling or below lower 10th percentile of daily solar PV generation for all-India per JJAS season, using 1-month lead System5 forecasts.

6.10 Discussion

6.10.1 Summary of main findings

This chapter has investigated the performance of the ECMWF System5 seasonal climate forecasts for yielding wind and solar PV capacity factor predictions for the summer season in India.

The investigation presented in this chapter progresses past energy-meteorology work in India in two main areas, each of which represents a contribution beyond that currently found in the academic or grey literature:

1. Demonstrated the use of a generation syntheses for wind and solar PV in India and regional subdivisions to calibrate seasonal climate forecasts of wind and solar PV generation based

on large-scale climate predictor variables.

2. Demonstrated significant skill for seasonal climate forecasts of wind and solar PV capacity factors in India and regional subdivisions.

The key findings that accompany these advances are:

1. The approximately linear relationships between candidate predictor variables and observed generation offer opportunities for the statistical downscaling of forecasts. The ensemble mean skill was similar across three predictor variables trialled for wind (40% of interannual variability explained), with the WNPi showing the highest skill. Modest improvements in the Northern India region were achieved when using either local 10m winds or ISM predictor indices (e.g. Niño3.4+EQWIN) as additional predictors. Deterministic skill was marginally better amongst the regional-scale predictor variables trialled for solar PV (Niño3.4+EQWIN and ISMi) when compared to spatially averaged rainfall (also for total cloud cover and SSRD – not shown), with up to 20% of interannual variability explained.

2. The source of predictive skill in SEAS5 stems from the representation of the main modes of variability over South Asia. Namely, the intensity of the anticyclonic system in the WNP and its relationship with both tropical Pacific and Indian Ocean SST anomalies, which is relevant to wind generation. Additionally, the accurate representation of ENSO and associated changes in rainfall and cloud cover over peninsular India, which is relevant to solar PV. Measures of skill are positive and significant for both wind and solar PV, though marginal and rarely significant for the regional Indian subdivisions for solar PV.

3. Forecast performance for 1-month lead time predictions of JJA capacity factors is similar to JJAS for wind and marginally lower for solar PV (due to lower skill in the Southern region). The skill of 0-month lead-time predictions of JJA capacity factors are notably higher than JJAS wind predictions, though only marginally so for solar PV (again due to lower skill in the Southern region, where September rains likely contribute to forecast skill).

4. Seven additional SCF systems were considered in a cursory assessment of multi-model generation predictions. All models show positive skill in forecasting wind and solar PV generation, though none outperform SEAS5. A combination of the four best-performing models to make multi-model generation wind and solar PV forecasts offers modest im-

provements in measures of deterministic and probabilistic skill.

5. The association between seasonal mean capacity factor anomalies and the frequency of extreme daily anomalies within the season can be used as a source of skilful prediction for extreme day counts on seasonal timescales.

In summary, the verification of seasonal generation forecasts for wind and solar PV presented in this chapter shows positive and significant skill. This skill is particularly apparent for wind, where the forecasts for all-India wind capacity factors at one-month lead significantly outperform climatological forecasts, with the ensemble mean explaining over 40% of interannual variability. This level of deterministic skill is comparable to other 1-month lead predictions of energy sector impact variables, including boreal winter winds/NAO in Europe (Clark et al., 2017); boreal winter gas demand in the United Kingdom (Thornton et al., 2019), boreal summer electricity demand in Italy (De Felice et al., 2015); and wind speeds over high wind resource zones of China (Bett et al., 2017; Lockwood et al., 2019). By contrast, the forecast performance for solar PV capacity factors is modest, although all-India deterministic skill at one-month lead is comparable to ISMR prediction skill (c.f. Table 6.4).

6.10.2 Shortcomings of the analysis and possible extensions

Several limitations of the methodology are highlighted here, which should be considered when interpreting the chapter results. Firstly, the verification is performed with the ERA5 based generation synthesis, which only approximates actual observed generation. Despite the overall good performance of the generation synthesis shown in Chapter 4, further refinement of the dataset (e.g., additional calibration as more historical generation data becomes available) and further robustness testing (e.g., use of different reanalysis datasets) would add to the overall confidence in the verification and prediction quality.

Second, the verification is conditioned on the 41-year hindcast period considered. Non-stationarities in the climate system may influence the strength of teleconnections relevant to the prediction skill shown here. For example, the variable strength of the ENSO-ISMR relationship is well-documented (discussed in Chapter 5), with a weakening since the 1980s and subsequent revival in the past decade. Non-stationarity in seasonal forecast skill has been shown in other studies. For example, deterministic skill for JJAS ISMR in the ENSEMBLEs project was 0.09 for 1989–2005 and 0.63 for 1960 to 1988 (Wang et al., 2015b), 2015). Splitting the hindcast period

into early (1981-2001) and late (2002-2021) periods suggests higher skill in the late period for both wind (wind full: 0.61, early: 0.48, late: 0.67) and solar PV (solar full: 0.46, early: 0.33; late: 0.56). For wind, interdecadal changes in the strength of the teleconnection with ENSO are a recognised feature of the East Asian monsoon (and WNP anticyclone, (Wang et al., 2008)), with the increased frequency of central Pacific ENSO since the early 1990s stimulating larger and north-westward shifted anomalous cyclonic circulation over the WNP during central Pacific El Niño, and vice versa for La Niña (WU and Wang, 2019). The increase in forecast skill for wind in the later hindcast period appears to come from a stronger predictor-predictand relationship (i.e., relationship between WNPi and wind generation), as the strength of the SEAS5 and observed WNPi predictors (i.e., predicted and observed WNPi) remains similar. In the case of solar PV, the greater forecast skill in the later period could be related to the observed recovery in the relationship between ENSO–ISMR around the year 2000 (Yu et al., 2021; Yang and Huang, 2021). Enhanced ISMR prediction skill for the post-2000 period has been evidenced elsewhere (Pillai et al., 2022), with a suggestion of a greater signal from tropical Atlantic SST anomalies that act independently of ENSO after 2000 (Kucharski et al., 2009).

Further sub-setting of the hindcast based on climate state may elucidate sensitivities and contingencies affecting predictability. Numerous so-called 'windows of opportunity', within which forecast skill is enhanced, have been demonstrated on S2S timescales (Mariotti et al., 2020). For example, the deterministic forecast skill of the WNP circulation in boreal summer has shown a phase-dependency with ENSO, with notably poor skill during La Niña decaying phases (Li et al., 2014).

The analysis in this chapter identified extreme low generation seasons for wind following rapid transitions between ENSO phases, specifically in the four seasons where JJAS wind capacity factors fall below one at least standard deviation (2020, 2010, 1983, 1988). The physical reasoning for the large negative anomalies following peak boreal winter El Niño conditions transitioning to La Nina by the following summer is described in Chapter 5. Namely, a large anticyclonic anomaly that counters the WNP climatological monsoon circulation and downstream climatological westerlies over India. These seasonal anomalies in the low-level winds are well-captured in SEAS5. Analysis of the ERA5 back-extension for 1940-1978 showed that the relationship between anomalous WNP monsoon circulation and synthetic wind generation anomalies in JJAS also exists over this period (r=0.50). Although formal assessment of skill over a small subset

of ENSO transition events would not be statistically robust, these three lines of evidence (i.e., 1. theoretical reasoning, 2. SCF system representation, and 3. observational record) build confidence in the forecasted negative anomalies. Similar reasoning is used by Dunstone et al. (2023) to argue that the pronounced summer La Niña in 2022 opened a window of opportunity to forecast extreme rainfall over Pakistan with enhanced confidence.

The analysis presented in this chapter uses simple linear or multi-linear regression relationships between predictands and predictors to downscale seasonal forecasts. Section 3.4.2 alluded to another downscaling methodology, namely, the direct association between forecast ensemble mean and impact variables (Bett et al., 2022). However, applying this method of direct relationship between SCF model output and generation anomalies gives virtually identical verification results (not shown). A range of other statistical downscaling techniques is also relevant to seasonal forecasting, e.g., circulation analogues (Lorenz, 1969; Zorita and Von Storch, 1999) weather generators (Wilby and Wigley, 1997), and various machine learning methods (e.g., Vandal et al. (2017) and Sachindra et al. (2018). The non-linear and asymmetric behaviour of WNP to ENSO states may favour non-linear empirical models. However, such an approach risks overfitting across a short hindcast period. Furthermore, different bias correction/calibration methods exist for seasonal forecasts (e.g., quantile mapping, ratio of predictable components). Although verification measures across these various bias correction/calibration methods have shown only marginal differences in other regions of South Asia (e.g., Manzanas et al. (2019).

Following convention, the validation in this chapter uses a climatological benchmark forecast. Further assessment against persistence and statistical forecasts would provide further insights into the value added from dynamical forecasts. Although the statistical-empirical forecasts of ISMR issued by the Indian Meteorological Department have been shown to provide poor forecast skill at one-month lead times ($\sim$0.34, Madolli et al. (2022)), numerous other statistical models of ISMR demonstrate enhanced forecast skill based on precursor climate conditions (e.g., Wang et al. (2015a) and Di Capua et al. (2019). Robust statistical relationships may help identify relevant candidate predictors in improved statistical-dynamical forecasts. Of relevance to the case of wind, Wang et al. (2013) used physically motivated predictors across three ocean basins to describe the anomalous WNP monsoon circulation and associated tropical cyclone activity.

Despite the promising indications of forecast skill demonstrated in this chapter, a substantial fraction of interannual variability remains unexplained for both wind and solar PV. The

potential utility of seasonal forecasts by practitioners therefore needs to consider the specific forecast application and, of relevance to the energy industry, the economic costs/benefits of forecast-contingent decisions and outcomes. Where such an enumeration is possible, forecast value depends on the relative balance between the costs of taking pre-emptive action to mitigate a weather event versus the potential un-mitigated loss should the event occur. The simplest and most used version of this 'application-specific' verification is the 'static cost-loss' decision-analytic model (Murphy, 1977; Richardson, 2000). However, such an idealised model is typically difficult to apply to real-world decision contexts, where numerous contextual factors may become equally relevant and shape the relative pros and cons of forecast-influence contingencies (e.g. prior experience, the level of comprehension of the forecast information and the availability of contingency measures, etc.). In such a practical situation, granular contextual knowledge of the forecast user and decision setting may offer more instructive insights into forecast value, such as the ability to 'hedge' or revisit forecast-influenced decisions.

6.10.3 Link to next results chapter

So far, the research in this thesis has been based on a generation climatology representing the standing stock of wind and solar PV installed capacity in India in 2021. However, a significant increase in the scale of wind and solar PV capacity is required to meet India's interim national climate targets, including a four-fold increase in wind energy generation and a seven-fold increase in solar PV energy generation over current levels by 2032 (PIB, 2023a). Numerous decarbonisation pathway studies identify even greater capacity levels necessary to meet lower-end global temperature targets (e.g. the UNFCCC 1.5C Paris Agreement target).

These levels of capacity increase will entail a different geographical configuration of wind and solar PV fleets from today. Furthermore, changes in wind turbine and PV array technologies are also relevant on these timescales. The flowing chapter (7) considers the sensitivity of generation climatology to plausible technology changes for the coming decades. Specifically, changes to the location, capacity volume, and technology characteristics of a larger wind and solar PV fleet.

Chapter 7

Repowered and expanded scenario analysis

7.1 Rationale for investigation and research questions

So far, the investigation has considered meteorological drivers of JJAS anomalies in synthetic generation timeseries for wind and solar PV generation and prospects for seasonal prediction. However, these generation syntheses represent the existing wind and solar PV installations at the end of 2021. Substantial increases in wind and solar PV installed capacity are expected in the coming decades for India to achieve its national climate targets to reach net zero carbon emissions by 2070. Achieving the ambitious renewable energy targets for India will require significant expansion of greenfield wind and solar farms. However, there is also a role for upgrading the technical characteristics of turbines at existing farms which has received less attention. This final results chapter investigates the plausible changes to capacity factors and energy yield consequent of alternative wind fleet parametrisations and demonstrates the associated changes in the variability characteristic of generation.

Due to data availability[1], the analysis in this chapter focuses on wind technologies. This focus is particularly relevant to India's ambitious net-zero climate goals, which include plans for a four-fold increase in current levels of wind energy generation by the early 2030s. Meeting these targets will be challenging as many of the best sites already host wind farms (MNRE, 2022c), which generally comprise older, technically obsolete turbine designs that attain low capacity factors[2] by international standards (Das, Binit, 2023). Although India holds significant wind potential in absolute terms (official government estimate of 695GW[3]), the resources are modest compared with many other regions globally, with 98% of 100m wind speeds over land rated

[1]Database of solar farms lacks detailed plant-level technical characteristics and commissioning dates. And location-specific data on planned solar PV expansion is limited (36% of 2030 target versus 73% for wind).

[2]Averaged over the last five years, wind capacity factors across India rank lowest out of countries with more than 1GW installed capacity, considering onshore wind capacity and generation data (IRENA, 2023a) for 36 countries with >1GW capacity.

[3]Capacity potential estimate evaluated at 120m hub height (NWEI, 2019).

below class III[4] (<7.5m/s annual mean). Making optimal use of available wind resources is of critical importance for India's climate goals.

Motivated by this context, the chapter considers the following research questions:

1. How would a changing wind fleet in India affect *capacity factors* from the respective technologies?
2. How would a changing wind fleet in India affect *generation* from the respective technologies?
3. How would a changing wind and solar PV fleet in India affect the variability characteristics of generation for the respective technologies?

7.2 Scenarios for plausible changes in wind fleet

As described in Section 3.5, two scenarios are considered to assess changes in the Indian wind fleet. The first is a wind repowering scenario that substitutes all turbines at wind farms in India with a single turbine model that achieves the highest annual average capacity factor. Section 4.5.1 in chapter 4 identified this turbine model by systematically rerunning the generation synthesis with a large database of turbine models (and associated power curves and hub heights). The Suzlon S144 3.15MW 160m turbine was the highest-yielding model, with a capacity factor of 0.35. This turbine saw commercial application in India in the autumn of 2023 when 16 S144 turbines were purchased for a project in Gujarat (Suzlon, 2023). As a point of comparison, Figure 7.1 provides a breakdown of the current wind fleet in India based on the data compiled in the database of Indian wind farms (Section 3.2.2). Peak installation rates in the mid-2010s mainly comprised turbines less than 2MW rated capacity. By 2021, ∼80% of the wind fleet comprised turbines with less than 2MW rated capacity, with a capacity-weighted hub height across the whole fleet less than 80m. Therefore, the Suzlon S144 would represent a considerable upgrade in fleet average hub height and rated capacity. This upgrade is denoted the 'repowering' scenario.

In real-world settings, the choice of turbine model is specific to the wind climate of a candidate site, with energy yield and financial performance as the decisive optimisation variables, subject to additional planning and logistical constraints (González et al., 2014). Here, the aim is

[4]Based on area of Indian mainland (excluding Himalayan range), data from www.globalwindatlas.info

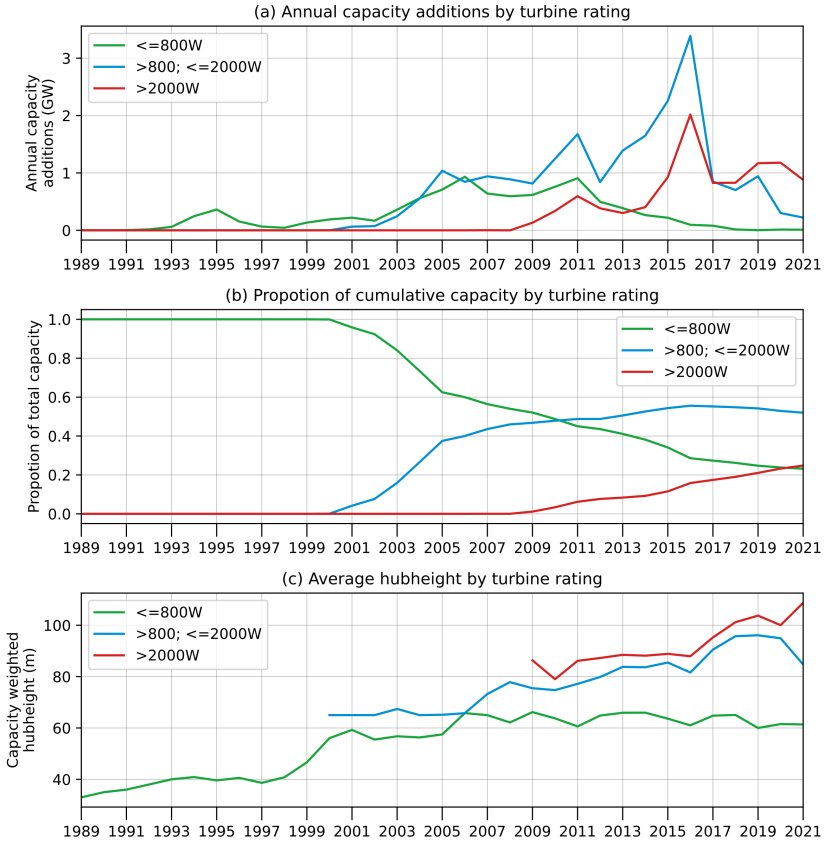

Figure 7.1: (a) Historical wind installations per year within three brackets of turbine rating; (b) proportion of total cumulative capacity within each bracket of turbine rating; (c) average (capacity weighted) hub height within each bracket of turbine rating, per year.

to demonstrate the relative energy performance between existing turbines and a characteristic state-of-the-art turbine rather than perform any such optimisation. However, the chosen re-powering turbine is representative of a modern onshore wind turbine suitable for class III winds (annual mean wind speeds of 7.5 to 8.5m/s, i.e., the wind climate of India) and is indicative of wider industry trends towards lower specific power turbines with taller towers (specific power refers to KW of rated power per unit swept area). Figure 7.2 charts specific power as a function of hub height, with shading denoting the first year of market availability. As indicated in Figure 7.2, the Suzlon 3.15MW 160m turbine fits the wider trend.

The second scenario considered in the chapter is a near-term expansion scenario for wind. As described in Section 3.5, the additional 41.4GW wind generation considers capacity installed in the years 2022 and 2023, as well as planned and under construction listed in official government data, due for completion by 2025/26. The expansion scenario comprises 24.4GW onshore and 17.3GW offshore capacity, which makes for a total all-India wind capacity of 80.9GW. Figure 7.3 signifies the geographical locations of the existing wind installations and new installations

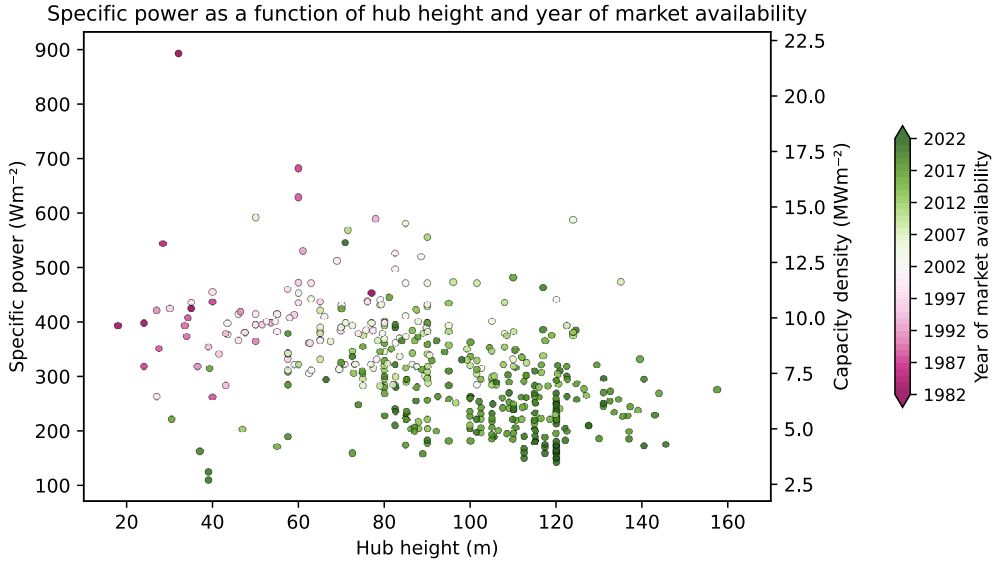

Figure 7.2: Specific power as a function of hub height, shaded by year of market availability of the turbine model (considering 805 turbine models). Theoretical capacity density as secondary y-axis, assuming regular 8Dx4D turbine spacing. Data source: wind turbine technical characteristic database from 'thewindpower.net'.

envisaged in the 'planned expansion' scenario.

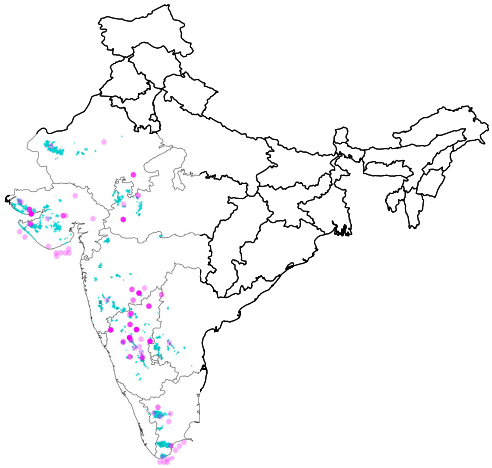

Figure 7.3: Location of existing wind farms in 2021 (40GW, blue points) and additional wind farms considered in the 'expanded scenario' (42GW, purple points). Points display spatial information only, with size differentiation for visual clarity.

7.3 Plausible changes in wind capacity factors

Compared to the reference generation synthesis that represents the locations and turbine models of Indian wind farms at the end of 2021, assigning the best-performing turbine (Suzlon S144 3.15MW, 160m hub height) to all wind farms (i.e., 'full repowering') achieves an 82% increase

in capacity factors for all-India (Table 7.1). The greatest regional increase in capacity factors is in Maharashtra (+94%) and Tamil Nadu (+96%). These states have the oldest average age wind turbines, with ∼50% of total wind capacity installed before the year 2010.

The 'planned expansion' scenario achieves a 111% increase in capacity factors for all-India (Table 7.1). Considering just the onshore segment of the 'planned expansion' scenario, the increase in capacity factors for all-India is 82% - i.e., the same as under repowering. The higher average windspeeds in the offshore development zones contribute to a higher capacity factor of the combined fleet (onshore + offshore). At the same time, additional onshore wind farms appear to occupy regions with comparable wind resources, at least when aggregated at the state level. Prospects for the performance of a large Indian offshore wind fleet warrant further detailed study[5], though the capacity factors estimated here for the ∼17GW in planned offshore wind expansion zones (0.47-0.60) is within the region found in other studies (Nagababu et al., 2017; FOWIND, 2018; Patel et al., 2022).

	Annual mean capacity factor				
Region	Reference	Full repowering	Planned expansion	Fractional change full repowering	Fractional change planned expansion
All-India (onshore)	0.19	0.35	0.35	0.82	0.82
Northern region	0.18	0.35	0.33	0.92	0.83
Western region	0.21	0.37	0.37	0.76	0.76
Southern region	0.17	0.31	0.33	0.83	0.94
Gujarat	0.26	0.43	0.39	0.67	0.5
Madhya Pradesh	0.18	0.33	0.33	0.86	0.83
Maharashtra	0.15	0.29	0.34	0.94	1.27
Andhra Pradesh	0.21	0.35	0.35	0.66	0.67
Tamil Nadu	0.14	0.27	0.28	0.96	1
Karnataka	0.2	0.37	0.37	0.84	0.85
Gujarat offshore	n.a.	n.a.	0.47	n.a.	n.a.
Tamil Nadu offshore	n.a.	n.a.	0.6	n.a.	n.a.
All-India (onshore + offshore)	n.a.	n.a.	0.4	n.a.	1.11

Table 7.1: Annual mean wind capacity factor by region for wind farm locations and turbine models at the end of 2021 (reference) and highest capacity factor turbine assigned to all farms (full repowering).

7.4 Plausible changes in wind generation

As described in Section 3.5.3, attaining greater levels of wind generation with repowered or expanded wind farms depends not only on the use of state-of-the-art technologies (i.e., turbines

[5]With no offshore capacity currently in operation in India, no relevant historical generation data is available for verification/calibration.

that achieve the greatest capacity factor) but also on the density at which new wind turbines can be installed. The empirical assessment of capacity density for existing farms in India yielded 2.5MW/km^2. The assumption that existing values of capacity density will persist under repowering and expansion implies that increases in generation scale one-to-one with increases in capacity factor.

Using the information on commissioning year and turbine rated power contained within the database of Indian wind farms, it is possible to calculate generation increases with a progressively repowered wind fleet. Figures 7.4a and 7.4b show capacity factors and relative changes in wind generation, respectively, when progressively repowering in order of wind turbine vintage year (i.e. repowering the oldest turbines first). By comparison, Figures 7.4c and 7.4d show capacity factors and relative changes in wind generation, respectively, when progressively repowering in order of turbine rating (i.e., repowering the smallest turbines first). By the year 2032, 43% of the entire fleet would be of retirement age (>20 years), entailing a 45% increase in generation from repowering of this outmoded segment of total capacity (Figure 7.4b). Early retirement and repowering of existing farms is an option to gain further generation increases and would result in a ∼65% rise for all-India when replacing turbines under 2MW, the threshold considered in India's current repowering policy (Figure 7.4d).

The maximum increases in generation attainable under repowering (i.e., full replacement of the existing fleet) are detailed in Table 7.2, rendering the 82% increase for the ∼40GW all-India onshore capacity. Table 7.2 also details the levels of generation that result from the 'planned expansion' scenario – i.e., a more than four-fold increase to 282TWh/year for the 80.9GW all-India on and offshore capacity. This large increase in generation is a combination of the doubling of capacity factors and the doubling of installed capacity compared to the wind fleet in 2021.

7.4.1 Implications for decarbonisation

7.4.2 The National Electricity Plan of India

The previous sections have shown that both scenarios significantly increase capacity factors and generation. Comparisons with national renewables targets and capacity levels from decarbonisation scenarios demonstrate the significance of these increases. The National Electricity Plan of India (NEP) proposes 121GW of wind capacity and 258TWh/year generation by 2032

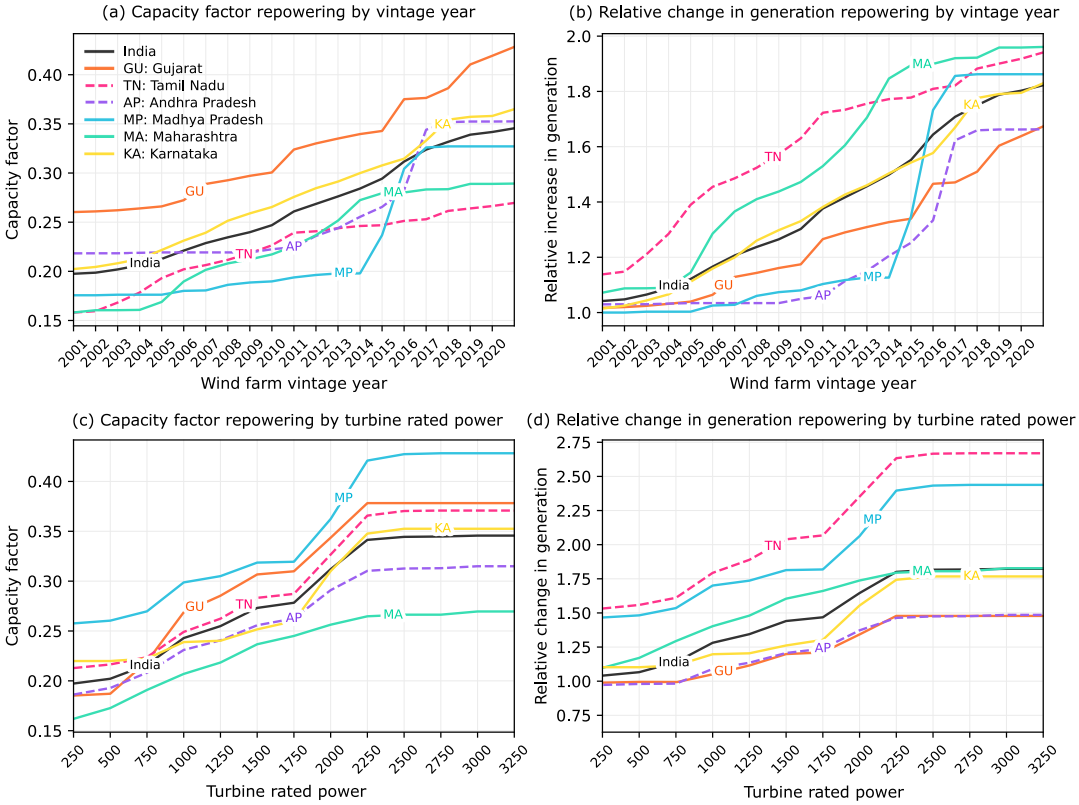

Figure 7.4: Capacity factor (a, c) and relative change in generation (b, d) per region considering repowering by wind farm vintage year (a,b) and turbine rated power (c,d) (i.e., repowering all wind farms that comprise turbines of a given vintage year / turbine rated capacity). Relative change in generation refers to the ratio of repowered generation and generation resulting from existing wind farm distribution in the year 2021.

(Table 7.3). The implicit capacity factors for these NEP figures are 0.24 fleetwide and 0.27 for additional capacity, assuming present-day installations remain operational. The 'repowering'

	Annual mean generation (TWh)		
Region	Reference	Full repowering	Planned expansion
All-India (onshore)	64	117	194
Northern region	7	14	16
Western region	31	53	87
Southern region	27	51	93
Gujarat	21	30	51
Madhya Pradesh	4	8	13
Maharashtra	7	15	23
Andhra Pradesh	8	13	14
Tamil Nadu	11	22	28
Karnataka	9	17	53
Gujarat offshore	n.a.	n.a.	35
Tamil Nadu offshore	n.a.	n.a.	46
All-India (onshore + offshore)	n.a.	n.a.	282

Table 7.2: Wind generation per year attained under two scenarios considered.

scenario significantly exceeds these implicit capacity factors (∼0.35). A fully repowered fleet achieves 45% of the 2032 NEP generation target (comparing generation values in Tables 7.2 and 7.3). The capacity factors in the 'expanded' scenario are higher still (∼0.40) and fulfil 109% of the 2032 NEP wind generation requirement when coupled with the greater installed capacity (80.9GW).

On the one hand, this magnitude of generation increase for wind is ambitious, as it requires total renovation of the existing wind fleet. However, Figure 7.4 shows that most of the increase in capacity factors from repowering is attained by replacing turbines under 2MW rated power, which is the threshold considered in India's current repowering policy. Thus, an Indian wind fleet that tracks planned expansion and implements the current repowering policy by the year 2025/26 can feasibly exceed the 2032 generation targets.

	Capacity (GW)	Generation (TWh)	Capacity factor
2021	40	63	0.18
2032	121	258	0.24
Additional	82	195	0.27

Table 7.3: National wind capacity, generation and fleetwide capacity factors in 2032 as envisaged in Indian NEP (PIB, 2023), for all wind capacity and additional wind capacity installed since 2021 (assuming present day installations remain operational).

7.4.3 IPCC AR6 decarbonisation pathways

The wind capacity and generation volumes detailed in India's NEP offer just one estimate of the levels of expansion required from the wind sector that are consistent with wider net-zero ambitions. Other works provide numerous estimates of wind capacity and generation volumes in India for the coming decades. The national-scale decarbonisation pathways considered by Working Group III (WGIII) of the Intergovernmental Panel on Climate Change (IPCC) Sixth Assessment Report (AR6) offer a large number of technology pathways for wind in India (n=823, see Figure 7.5a), which form part of a globally integrated evaluation of end-of-century global warming outcomes.

All 388 of the IPCC decarbonisation pathways for India that are consistent with end-of-21st-century warming outcomes of less than 2°C envisage a massive scale-up of wind energy. The median value of wind generation from this subset (n=388) of IPCC scenarios is 512TWh/year (see dashed horizontal line 'IPCC' in Figure 7.5b), with 334 of these pathways exceeding the

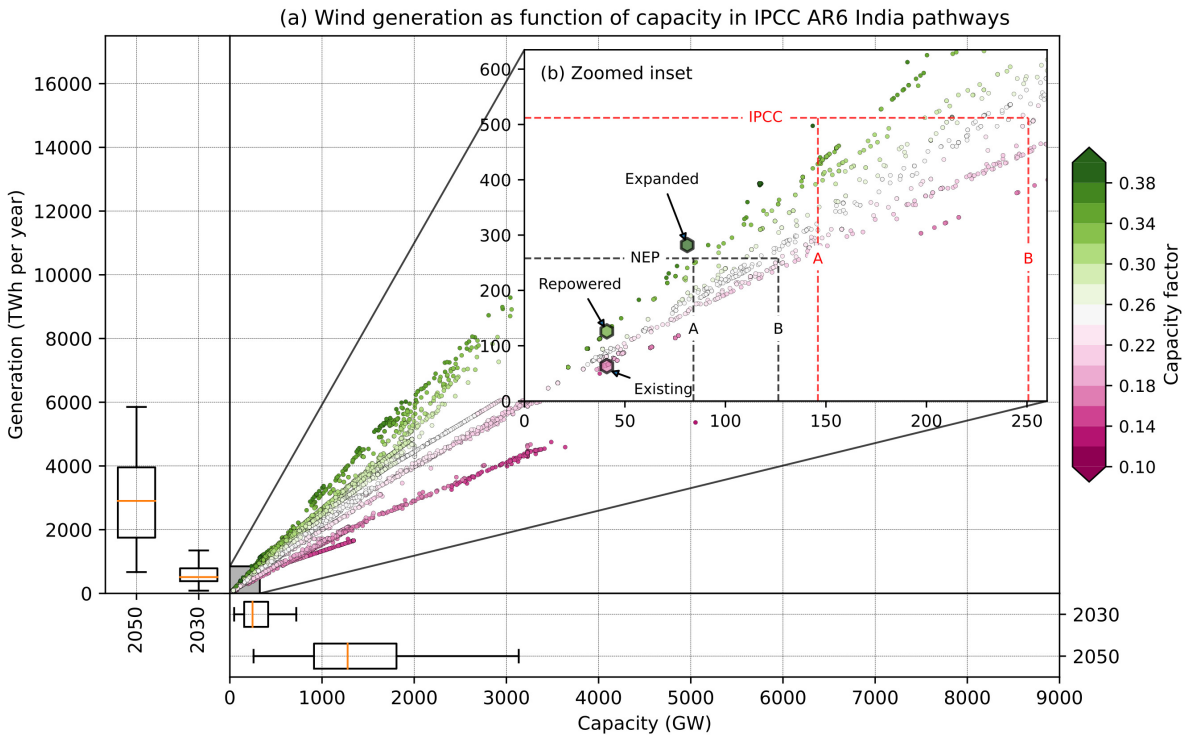

Figure 7.5: (a) Generation versus capacity for India decarbonisation pathways from IPCC AR6 (n=823) in the 2030 to 2100 timeframe, with shading denoting implied capacity factor (ratio of secondary wind energy per year and wind capacity x365.25x24). Box-and-whisker plots denote 10/25/50/75/90th percentiles of capacity and generation in 2030 and 2050 for India decarbonisation pathways that achieve an end of 21st-century warming outcome of less than 2°C with ∼50% likelihood (n=149). (b) inset axes show lower range of capacity/generation values. Guidelines in (b) depict generation/capacity requirements for NEP2032 targets (258GWh/year; 84.1GW 'NEP-A' and 126.3GW 'NEP-B') and median wind generation value for IPCC AR6 India decarbonisation pathways in 2030 that achieve less than a 2°C end-of-century global warming outcome (512GWh/year - 167GW 'IPPC-A' and 251GW 'IPCC-B'). Guidelines A and B denote capacity requirements resulting from capacity factor values for full repowering and the median of capacity factors implicit within IPCC AR6 India decarbonisation pathways, respectively.

generation levels considered within the Indian NEP by 2030 (258TWh/year, see horizontal dashed line 'NEP' in Figure 7.5b). The capacity factors implicit within these IPCC pathways span a wide range (0.14-0.38; see colour shading in Figures 7.5a and 7.5b), with a median value of 0.23 in 2030. This range in implicit capacity factors reflects differing assumptions and parameterisations of wind energy within the different Integrated Assessment Model frameworks.

The effect of different capacity factors on wind capacity requirements for a particular generation outcome is highlighted in Figure 7.5b with additional dashed vertical guidelines. 'NEP-A' in Figure 7.5b shows the capacity requirement (84.1GW) at the repowered capacity factor of 0.35. 'NEP-B' in Figure 7.5b shows the capacity requirement (126.3GW) at the median of capacity factors in 2030 implicit within the subset of IPCC AR6 (n=338, 0.23). A similar assessment

of necessary capacity can be made for the median value of wind generation from the subset (n=338) of IPCC scenarios (512TWh/year). A capacity factor value of 0.4 (i.e., that attained expanded scenario) requires 167GW (IPCC-A), while a capacity factor value of 0.23 requires 251GW (IPCC-B).

This analysis highlights the large impact of capacity factors on the magnitude of wind capacity scale-up, with net-zero compliant levels of generation achievable with less installed capacity when higher capacity factor values are upheld.

7.5 Implications for variability in generation

The results presented so far are for annual averages. However, patterns of generation on other timescales and how these change under the two scenarios are important considerations for electricity system operations and planning. Here, changes in the generation patterns across timescales are quantified for the all-India case with generation syntheses for the two future scenarios based on meteorological variability in the 43-year timespan of the ERA5 reanalysis (1979-2021).

7.5.1 Changes in variability profile: repowering scenario

Full repowering increases the absolute magnitude of variability in generation across a range of timescales. The changes to temporal variation reflect the steeper ramping segment of lower specific power turbines (Swisher et al., 2022) and the increased magnitude of wind speeds at greater hub height. The maximum magnitude and relative frequency of rapid positive or negative changes in capacity factor (termed ramps) are greater for the repowered case (Figure 7.6a). For example, capacity factor ramp events of $\sim \pm 10\%$ within a 6-hour period occur four times more frequently in the repowered case ($\sim$20% of hours each year precede such events in the repowered case versus $\sim$5% for current installations).

Regarding the average generation profile across a single day, a strong diurnal cycle is apparent for both the existing and repowered cases (Figure 7.6b), consistent with insolation-driven sensible heating over land that creates gradients in surface pressure with adjacent oceans and enhanced downward turbulent mixing of momentum (Dai and Deser, 1999). However, the absolute magnitude of the diurnal cycle in generation increases by 270% in the repowered case (absolute range of 0.07 and 0.19 for existing and repowered cases, respectively). The modest

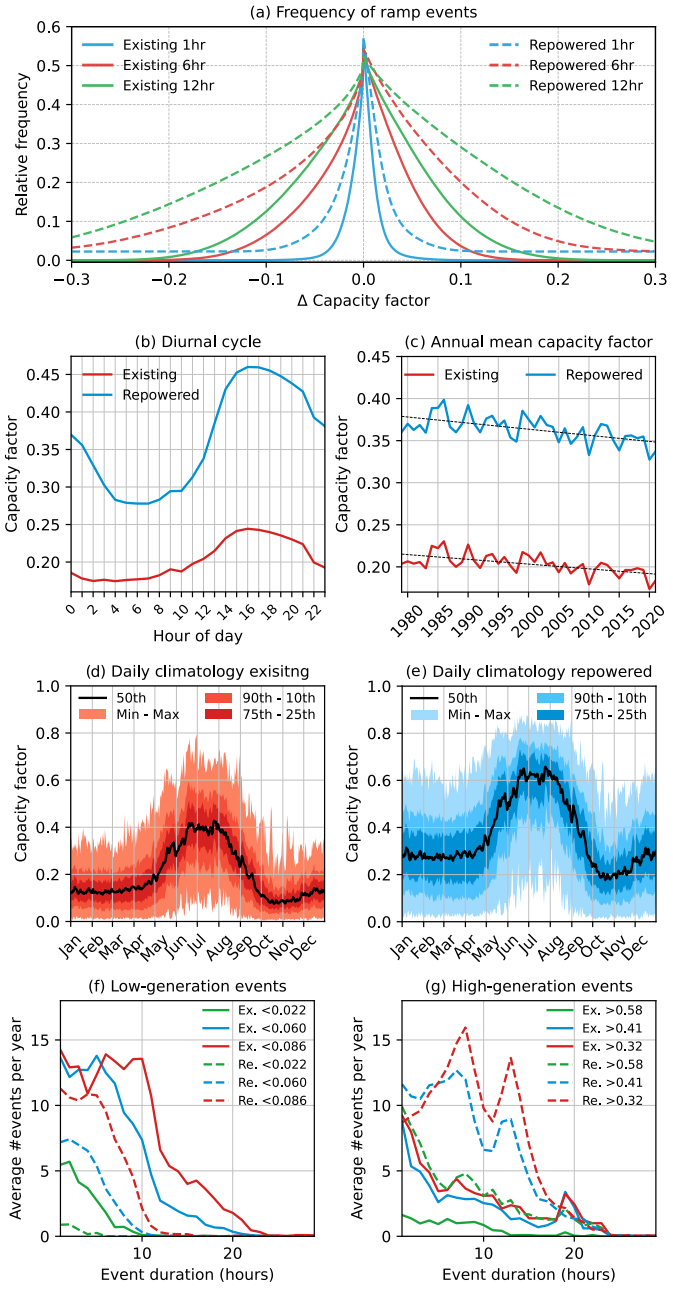

Figure 7.6: Temporal analysis of generation synthesis for existing and repower wind fleets for the period 1979-2021, showing (a) average proportion of hours per year preceding ramps in all-India capacity factor within 1-hour, 6-hour and 12-hour periods; (b) annual average diurnal cycle of all-India capacity factor (hour of day in Indian Standard Time); (c) annual mean capacity factor for all-India, with linear trends overlaid, significant at the 99% level using a Mann-Kendal test; (d and e) daily climatology for existing and repowered wind farms, respectively, with shading signifying percentiles of generation climatology; (f and g) frequency of low/high generation events, respectively, by duration for three absolute thresholds of capacity factor (corresponding to the 1st, 10th and 20th / 99th, 90th and 80th percentiles of capacity factors under the existing wind fleet) for all-India in existing ('Ex.') and 'repowered scenario' ('Re.').

negative trends in the annual mean values of the generation syntheses (Figure 7.6c) possibly reflect a 'stilling' phenomenon, which has been documented elsewhere across the globe (McVicar

et al., 2012) and is noted in other studies of near-surface winds in India (Joseph and Simon, 2005; Jaswal and Koppar, 2013). Removing these long-term trends, the range in annual mean generation increases by 25.3% and the standard deviation by 33.2% for all-India in the repowered case. The relative magnitude of interannual variability remains virtually the same under repowering, with max/min years amounting to ∼9% of the mean for all-India and ∼ ±15% for individual states.

The daily climatology of generation (Figures 7.6d and 7.6e) remains qualitatively similar in both cases, with 54% and 48% of total annual generation falling within the period June to September for existing and repowered cases, respectively. However, the absolute range of daily capacity factors increases in the repowered case, with the greatest increases observed outside of the summer monsoon season. This is likely due to steep linear response of the power curve in the ∼0.25-0.75 interval, which conveys the effect of the diurnal cycle in wind speeds in the repowered case but not for the existing deployment (for which average capacity factors are <0.25 outside of the summer monsoon period). Despite increases in the absolute magnitude of variability across timescales, the shift in the distribution of generation values upwards under repowering implies less frequent low-generation and more frequent high-generation events (Figures 7.6f and 7.6g), a consequence of the increased responsiveness of the power curve at lower wind speeds and the greater magnitude of wind speeds at taller hub heights. For example, incidences of capacity factors falling below the 10th percentile for at least 10 continuous hours average five cases per year for the existing wind farm fleet but disappear almost entirely in the repowered case.

7.5.2 Changes in variability profile: expansion scenario

The characteristics of temporal variability for all-India generation in the 'planned expansion' scenario are comparable to those under the 'repowering' scenario. It might be expected that the magnitude and relative frequency of ramp events are less in the 'planned expansion' scenario due to greater geographical smoothing effects (greater diversity of onshore farm locations, plus two large offshore locations) and generally less variable wind speeds at offshore locations (Pryor and Barthelmie, 2011). However, Figure 7.7a is qualitatively indistinguishable from the equivalent plot for the repowered case (Figure 7.6a) and likely results from the large concentration of capacity over relatively small areas in the two offshore development zones and the relatively modest contribution of offshore wind to overall capacity (∼20%).

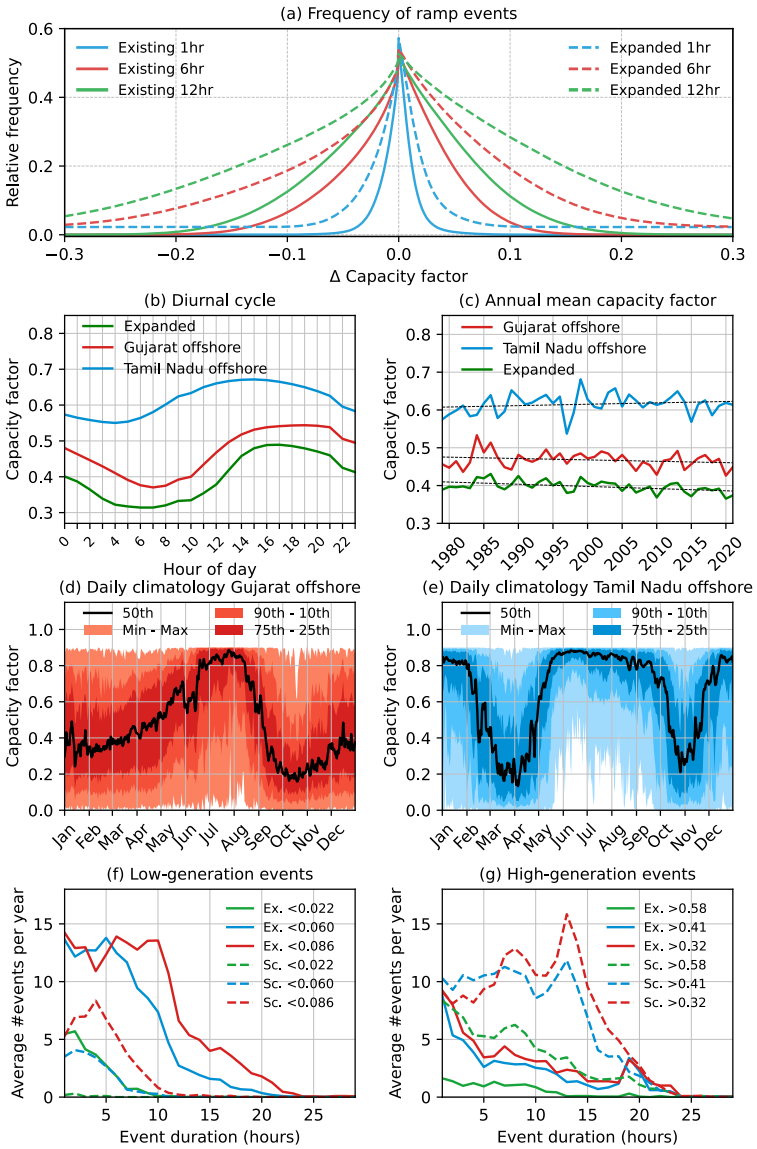

Figure 7.7: Temporal analysis of generation synthesis for 'expanded' scenario for the period 1979-2021, showing (a) average proportion of hours per year preceding ramps in 'expanded scenario' all-India capacity factor within 1-hour, 6-hour and 12-hour periods; (b) annual average diurnal cycle of 'expanded scenario' all-India capacity factor and offshore segments (hour of day in Indian Standard Time); (c) annual mean capacity factor for all-India and offshore segments, with linear trends overlaid (d and e) daily climatology for offshore segment for Gujarat and Tamil Nadu, respectively, with shading signifying percentiles of generation climatology; (f and g) frequency of low/high generation events, respectively, by duration for three absolute thresholds of capacity factor (corresponding to the 1st, 10th and 20th / 99th, 90th and 80th percentiles of capacity factors under the existing wind fleet), for all-India in existing ('Ex.') and 'expanded scenario' ('Sc.').

Figure 7.6b shows that the average diurnal cycles for the two offshore zones follow similar patterns to the 'expanded' and 'repowered' profiles, although the absolute range in capacity factor is less in both instances. Generally, the greater thermal capacity of water compared to land results in less surface heating and vertical thermal mixing of near-surface winds and

a smaller diurnal range in windspeeds than over land (Barthelmie et al., 1996). Figure 7.6c shows the timeseries of annual mean capacity factors for the two offshore zones, both of which show non-significant linear trends. The absolute range in all-India annual mean capacity factors is 4% higher in the 'planned expansion' scenario compared to 'repowering', and the standard deviation 10% greater. However, the greater average capacity factors in the 'planned expansion' scenario imply that the relative magnitude of interannual variability is around 10-15% less than in the 'repowering' scenario.

In the 'planned expansion' scenario, the daily climatology of all-India capacity factors over the year is similar to the 'repowered' case (not shown), albeit with a higher average output and a slight increase through boreal winter months. To elucidate the likely drivers of these differences, Figures 7.7d and 7.7e show the daily climatology of capacity factors over the year for the aggregated output of the two offshore zones in the 'planned expansion' scenario. Both zones show higher capacity factors close to rated output (minus losses) for several summer months.

The offshore zone in Tamil Nadu also shows strong winter season peaks that likely correspond with the North-eastern winter monsoon. This winter monsoon season brings enhanced north easterly winds that reach a maximum along the eastern and south-eastern shore of peninsular India and are consistent with the low pressure located over the southwestern Bay of Bengal and the accompanying cyclonic circulation (Rajeevan et al., 2010; Sengupta and Nigam, 2019). Finally, the even greater shift in the distribution of capacity factors upwards under the 'planned expansion' scenario implies even less frequent low-generation and more frequent high-generation events (Figures 7.7f and 7.7g). For example, 10-hour long periods below the 90th percentile of all-India capacity factors number seven events per year for the existing wind fleet but disappear entirely in the 'expanded scenario'.

7.5.3 Changes in associations with meteorological drivers

This section considers whether the statistical relationships between the climatic predictor variables for wind generation identified in Chapters 5 and 6 hold for the two scenarios considered here. Table 7.4 shows the correlation coefficients for the existing fleet (i.e., the same as in Table 6.1, Chapter 6) and for the 'repowered' and 'planned expansion' scenarios. The correlation values are very similar across all regions under both scenarios, with very modest increases in

the Northern and Western regions. These increases could be due to slightly steeper ramping and/or constant rated power sections of the turbine power curve considered in the repowered and expanded scenarios. Also, a greater degree of spatial smoothing occurs in the 'planned expansion' scenario, likely causing very slight increases in correlation values. JJAS capacity factor anomalies for individual offshore zones are slightly less than the regional aggregates, likely due to the large concentration of capacity (∼8.5GW) over relatively small areas. However, the generally high correlation values show that generation anomalies averaged over the summer season for near-term wind development in India remain well-described by the previously identified predictor variables.

Predictor	All-India	NR	WR	SR	Gujarat Offshore	Tamil Nadu Offshore
10m winds	0.90/**0.90**/0.92	0.47/**0.52**/0.55	0.83/**0.85**/0.85	0.80/**0.79**/0.78	0.82	0.43
EOF1 850 hPa winds	0.78/**0.79**/0.79	0.36/**0.38**/0.39	0.65/**0.66**/0.66	0.80/**0.79**/0.77	0.61	0.37
W-F WNPi	0.74/**0.76**/0.77	0.33/**0.36**/0.37	0.62/**0.64**/0.66	0.78/**0.76**/0.75	0.61	0.35

Table 7.4: Correlation between JJAS mean wind capacity factor anomalies per region and candidate predictors described in Chapter 6, Section 6.2. Values in regular font are for existing wind capacity, bold font for the 'Repowered' scenario, and underlined values for the 'Planned expansion' scenario.

7.6 A note on solar PV

Due to data availability, near-term capacity development scenarios were not considered for solar PV. However, ambitious plans for the rapid expansion of solar PV capacity in India suggest that analyses based on generation syntheses representative of existing should be regularly updated and consider plausible future changes in the solar fleet. The National Electricity Plan of India (NEP) proposes 365GW of solar PV capacity and 657.7TWh per year by 2032 (Table 7.5). The implicit capacity factors for these NEP figures are 0.205 fleetwide and 0.215 for additional capacity, assuming present-day installations remain operational.

For solar PV, the change in present-day fleetwide capacity factors of +43% is greater than in the sensitivity test conducted in Chapter 4 that considered single-axis tracking designs (+33.9%). However, ongoing improvement in conversion efficiency of 1% per annum is anticipated for the next decade (VDMA, 2022). Therefore, the + ∼43% increases are attainable when accounting for combined improvements from the single-axis tracking designs and ongoing efficiency improvements of ∼7% above state-of-the-art technologies (e.g., 1.339 x 1.07=1.43).

	Capacity (GW)	Generation (TWh)	Capacity factor
2021	48.0	63.0	0.150
2032	364.5	657.7	0.205
Additional	316.5	594.7	0.215

Table 7.5: National solar PV capacity, generation and fleetwide capacity factors in 2032 as envisaged in Indian NEP (PIB, 2023), for all solar PV capacity and additional solar PV capacity installed since 2021 (assuming present day installations remain operational).

Whether these levels of generation could be achieved for future periods depends on the availability of suitable sites of comparable resource quality and the density at which state-of-the-art wind and solar PV technologies can be installed. Candidate sites for new solar PV installations are likely widespread throughout India as solar irradiance resources are relatively homogenous across the country. Although single-axis tracking installations require greater spacing to limit between-row shading (implying a lower capacity density), the greater capacity factors achieved would more than compensate such that the generation- or yield-density of installations is greater than existing solar farms (i.e., state-of-the-art solar PV installations requiring no more land footprint per unit generation than existing fleet).

As was the case for wind, all 368 of the IPCC decarbonisation pathways for India that are consistent with end-of-21st-century climate warming outcomes of less than 2°C envisage a massive scale-up of solar PV energy. The median value of solar PV generation from this subset (n=368) of IPCC scenarios is 696 TWh/year in 2030 (see vertical box-plot in Figure 7.8), which is comparable to the generation levels considered within the Indian NEP by 2032 (658TWh/year). The capacity factors implicit within these IPCC pathways span a wide range (0.07-0.38; see colour shading in Figure 7.8), with a median value of 0.185 in 2030. The implicit capacity factors within the Indian NEP and achievable capacity factors with single-tracking parameterisation and ongoing efficiency improvements of ∼0.20-0.22 are above the 80th percentile of capacity factor implicit within IPCC scenarios. Utility-scale solar PV installations in the southeastern region of the United States (a region of comparable solar resource to India) that use single tracking technologies have averaged capacity factors of 0.23 over the last five years (Bolinger et al., 2023). Thus, the ∼0.20-0.22 values for India are consistent with international experience and suggest that net-zero compliant levels of generation are achievable with less installed capacity when higher capacity factor values are upheld.

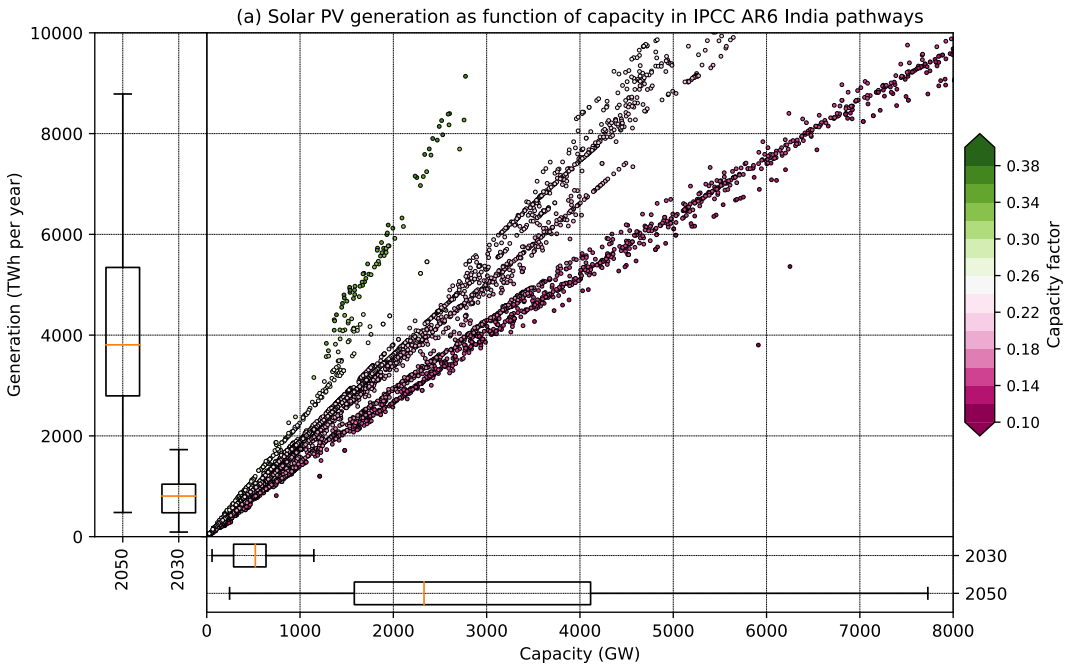

Figure 7.8: Generation versus capacity for India decarbonisation pathways from IPCC AR6 (n=778) in the 2030 to 2100 timeframe, with shading denoting implied capacity factor (ratio of secondary solar PV energy per year and wind capacity x365.25x24). Box-and-whisker plots denote 10/25/50/75/90th percentiles of capacity and generation in 2030 and 2050 for India decarbonisation pathways that achieve an end of 21st-cenurty warming outcome of less than 2°C with ∼50% likelihood (n=149).

7.7 Discussion

7.7.1 Summary of main findings

This analysis presented in this Chapter progresses past work on the performance of wind energy in India by using a generation synthesis approach to assess differences in energy yield between the existing fleet of turbines versus two near-term future scenarios. The key findings are as follows:

1. Fully repowering India's wind turbine fleet using a characteristic modern turbine, with a taller tower and lower specific power, could boost capacity factors from the existing wind fleet by 82% nationwide (0.35), with the greatest regional increase in Tamil Nadu state (+96%).

2. The planned expansion of India's wind fleet in the 2025/26 timeframe (+40GW) results in a nationwide wind capacity factor of 0.40 when using the same modern turbine design, or +111% over the existing fleet. Planned expansion onshore shows similar capacity factors

to the repowered case, while the higher capacity factors (0.47-0.60) of planned offshore expansion drive the increase in the fleetwide average.

3. The capacity factors achieved under 'repowering' and 'planned expansion' scenarios exceed equivalent estimates within the National Electricity Plan of India (0.27 fleetwide) and national decarbonisation pathways compiled by the Intergovernmental Panel on Climate Change (median value of 0.23), suggesting less total installed capacity is required to achieve specific generation outcomes than previously estimated.

4. Both 'repowering' and 'planned expansion' scenarios modify the variability characteristics of generation in a similar way, namely, increasing the absolute magnitude of changes across timescales, reflecting the steeper ramping segment of lower specific power turbines and the increased magnitude of wind speeds at greater hub height.

5. The strength of the relationships between predictor variables for wind generation anomalies in JJAS that were identified in Chapter 6 Section 6.2 hold for both the 'repowering' and 'planned expansion' scenarios. Thus, the prediction skill for summer season wind generation anomalies demonstrated in Chapter 6 would apply under plausible near-term developments of wind sector in India.

6. Capacity factors implicit within the Indian NEP (0.205) are consistent with values achievable with single-axis tracking designs at current solar farm locations in India and a greater than ∼80% of capacity factors assumed in national decarbonisation pathways complied in AR4 of the IPCC.

Repowering will become increasingly common within the unfolding energy transition, as a greater proportion of existing wind capacity reaches its design lifetime (Kitzing et al., 2020). The importance of repowering for India's energy transition has been recognised in government energy policy (MoEFCC, 2022; MNRE, 2022a) and this chapter highlights significant role of fleetwide turbine upgrades. Although renewal of all turbines in India may proceed progressively rather than all at once, the analysis has shown that repowering wind turbines under 2MW rated capacity (the threshold considered in India's national repowering policy) could increase fleetwide capacity factors to ∼0.3[6], some 25% greater than the capacity factors implicit within the current National Electricity Plan of India. Whether these increased capacity factors could

[6]For comparison, turbines installed onshore in 2022 in Europe achieved capacity factors in the range 0.30-0.45, while the European onshore fleet average capacity factor is 0.24.

translate into higher energy generation depends on the relative capacity density at which new turbines are installed. However, the conservative assumption used in this analysis that the capacity densities of existing wind farms across India will persist under repowering suggests generation gains from repowering are at least proportionate to capacity factor increases.

The assessment of 'planned expansion' has shown even greater capacity factors are achievable due to the contribution of higher yielding offshore development and similar capacity factors at new onshore farms, compared to existing sites. The achievable capacity factors at even greater levels of wind expansion will require further study and would need to consider the possible saturation of the best wind resources sites. However, the 'planned expansion' scenario shows capacity factors at the top-end (>90th percentile) of values found across decarbonisation pathways for India compiled by IPCC AR6 WGIII and indicates that the very ambitious levels of wind generation consistent with low end of 21st-cenurty warming outcomes are achievable with appreciably less installed capacity. Similar conclusions could also be made for solar PV.

Despite the promise of higher capacity factors demonstrated here, the greater level of absolute generation variability underlines the increasing need for power system flexibility within a decarbonised energy system, implying greater levels of energy storage, responsive demand, grid reinforcement/interconnection, and complementary forms of generation (Denholm and Mai, 2019; Strbac et al., 2020; Bistline et al., 2021). Without such flexibility, electricity network constraints would heighten the risk of curtailment of the increased generation from repowering. Improved characterisation of generation variability across timescales using generation syntheses can help appraise design elements of power system flexibility, particularly the likelihood of extreme low generation events (e.g., Cannon et al., 2015), which although less frequent under full repowering, are not eliminated.

7.7.2 Shortcomings and caveats to the analysis

The assessment of energy yield improvements using modern wind turbine (and single-axis tracking in the case of solar PV) is necessarily high-level and detailed site-specific study of repowering options could differ from the aggregated state and country-level findings. In the case of wind, the full repowering scenario is hypothetical and subject to multiple practical challenges. However, in pure performance terms, the capacity factors attained under full-repowering are comparable in magnitude to those found in farm-level repowering studies in India (e.g., Boopathi et al.,

2021) and international repowering experience (e.g., Villena-Ruiz et al., 2018), and so likely reflect realistic performance values rather than artifacts of the synthesis methodology.

In practice, the economic case for repowering must balance forgone revenue from the decommissioned farm versus enhanced income after the upgrade, and such assessments require high-resolution, site-specific investment-grade information (Shafiullah et al., 2013). However, the appreciable accuracy of the generation synthesis for regional aggregates suggests using it a basis for future investigations into the economic case for early-retirement and subsequent repowering would be suitable at the aggregate level.

The assessment of changes in capacity factors and generation in this Chapter consider various regional aggregates without any technical and practical constraints of a real-world electricity system. However, the existing conditions on the Indian electricity grid include network constraints, limited interstate or international interconnection, limited storage, and inflexible "must-run" capacity. Such conditions might constrain the increased generation of repowered and expanded wind farms and increase the risk of curtailment. Nevertheless, numerous initiatives in India seek to address power system flexibility/reinforcement constraints. Namely, the second phase of the Green Energy Corridors project (+700km transmission lines), the National Energy Storage Mission (40GW storage by 2025), and an updated Indian Electricity Grid Code for 2023 that formalises storage and demand response within ancillary services (NREL, 2023).

Chapter 8

Discussion and Conclusions

Despite the importance of wind and solar PV energy sources in the planned expansion of the Indian electricity system, existing works offer few insights into the characteristic performance of these two energy sources. This blind spot is partly due to the limited data available for historical generation and plant-level technological information. Furthermore, past studies have relied on simplified methodological approaches, like typical meteorological years, characteristic time slices, or idealised technological parameterisations. Possibly due to the lack of long generation time series that faithfully capture actual energy yields, few investigations offer descriptions of the relationships between meteorological drivers and wind and solar PV generation variability in India. This absence is particularly apparent for interannual timescales. And despite the considerable legacy of seasonal climate forecasting (SCF) in South Asia, with much attention devoted to Indian summer monsoon rainfall, little work considers SCF applications to energy generation in India.

This thesis offers a step forward by developing a validated model synthesis of wind and solar PV generation in India based on 43 years of input data from an atmospheric reanalysis and a detailed description of existing plants. Using these generation syntheses, statistical relationships with meteorological drivers were investigated, focussing on interannual variability in the summer monsoon season. These same statistical relationships were also used as the basis for hybrid dynamical-statistical predictions of wind and solar PV capacity factors, made at one-month lead times using output fields from the operational ECMWF System5. Further testing quantified changes to the generation syntheses and associations with meteorological drivers under scenarios of future technological development.

The remainder of this chapter summarises the key findings from this thesis and comprises the following sections:

1. A summary of the main results in each of the four results chapters.

2. A critical reflection on the thesis findings and discussion on the wider relevance to the energy situation in India.

3. Suggestions for future research.

4. A conclusion and outlook.

8.1 Summary of main findings

8.1.1 Summary of First Results Chapter

The first result chapter presented generation syntheses for wind and solar PV at the national and sub-national scale. Using a simple multiplicative bias correction approach to eliminate mean biases, the generation syntheses replicated observed generation with appreciable accuracy. Compared to observed generation values for all-India at the daily timescale, an r value of 0.98 and MAPE value 8% was achieved for wind and an r value of 0.92 and MAPE value 9% for solar PV. This accuracy is comparable to the levels of correspondence achieved for national aggregate generation syntheses in existing studies of other countries (e.g., Gruber et al., 2019; Bloomfield et al., 2020). Although numerous studies have produced generation syntheses using reanalysis data inputs for other countries (e.g., Kubik et al., 2013; Staffell and Pfenninger, 2016; Ren et al., 2019), this work presents the first validated version for all wind farms in India.

The summer monsoon period (JJAS) shows greatest scale of interannual variability for both technologies, with a standard deviation of 8% of the mean (14% for sub-regions) for wind and 3% of the mean (6% for sub-regions) for solar PV. For comparison, an existing generation synthesis for Europe (Bloomfield and Brayshaw, 2021) shows the greatest magnitude of interannual variability in DJF season, with a standard deviation in wind capacity factors approximately 35-40% greater than the JJAS season for India. These differences are likely due to different prevailing meteorological environments within the tropics and extratropics and the different scales of spatial averaging. For solar PV, the interannual standard deviation is larger in Europe for annual mean capacity factors, but comparable in magnitude for the summer season.

The accuracy of the generation syntheses at the scale of regional aggregations results from the cancelling out of a greater number of random uncorrelated variations at the larger spatial aggregation (Holttinen, 2005). This regional-scale accuracy motivates many possible analyses, not least the effects of technology modernisation. Furthermore, regional wind and solar PV

generation anomalies in JJAS are generally highly correlated with all-India generation anomalies, suggesting that anomalous seasons are widespread events affecting all regions simultaneously. While wind and solar PV generation anomalies in JJAS for the whole country and the sub-regions are weakly correlated, suggesting that different phenomena drive the majority of variation in JJAS between years for wind and solar PV.

8.1.2 Summary of Second Results Chapter

The second results chapter (5) sought to identify candidate drivers of generation variability in JJAS and describe strength and mechanisms of observed associations. The chapter constitutes the first use of a multi-decadal synthetic generation time series in such an investigation. The investigation first considered intra seasonal variability, with alternating active and break spells a key feature of the Indian summer monsoon, describing periods of enhanced or suppressed rainfall, respectively (Rajeevan et al., 2010). The frequency or magnitude of active and break spells accounts for a similar proportion of the total variation in JJAS mean solar PV generation as for ISMR ($\sim$20%). No such association is found in the case of wind generation anomalies in the JJAS season (apart from a modest association in the Northern region, up to $\sim$15%). Interannual variations in surface winds over peninsular India caused by anomalous western north Pacific (WNP) monsoon circulation describe a greater fraction of total observed wind generation variability (>60%) than the local Indian summer monsoon circulation (which is only dominant in the Northern region). Two measures of anomalous WNP monsoon were identified that each describes comparable levels of variance in wind generation anomalies in JJAS:

1. The WNPi (index based on original definition in Wang and Fang, 1999), defined as the differences between zonal 850hPa winds in JJAS averaged over southern and northern regions of the WNP.

2. The first principal component timeseries of 850hPa zonal winds in JJAS over the South Asia region.

In the case of solar PV, three measures of an anomalous Indian summer monsoon circulation were identified and co-vary with JJAS solar PV generation anomalies with a similar correlation to that of ISMR:

1. The ISMi (index based on original definition in Wang and Fan (1999)), defined as the difference between the 850-hPa zonal winds in a southern region located over the clima-

tological position of the Somali Jet (westerlies) and a northern region co-located with the monsoon trough (easterlies). The ISMi captures the strength of monsoon westerlies and is indicative of anomalous lower-tropospheric vorticity that causes the monsoon trough (Wang et al., 2001).

2. The second principal component timeseries of 850hPa zonal winds in JJAS over the South Asia region.

3. Given the close association between ISMR and solar PV generation anomalies, the two greatest sources of seasonal predictability in ISMR (ENSO and IOD) also served as predictors for solar PV generation anomalies in JJAS (specifically, the ENSO3.4 and EQWIN indices).

Aerosols were not considered a relevant source of predictability as the SEAS5 forecast system includes no dynamical means of producing an aerosol-related signal beyond prescribed climatological aerosol loading (Vitart et al., 2019). However, an additional analysis of irradiance fields derived from satellite measurements showed that aerosols impart a measurable effect on anomalous solar PV generation in JJAS. Further experiments found in the literature suggest that remote mineral dust loading from originating Middle Eastern deserts can drive anomalous ISMR. The suggestion being that aerosols could be exploited as an additional source of predictability on seasonal timescales where SCF systems include suitable assimilation and dynamical treatment of aerosols and associated attenuating effects.

The suitability of the identified candidate drivers of generation variability were tested using the ERA5 back-extension to 1940 and using an alternative reanalysis data input (NCEP/NCAR Reanalysis). The strength of the relationships was found as comparable in both test cases, further evidencing the identified drivers of generation anomalies as robust.

8.1.3 Summary of Third Results Chapter

The third results chapter (6) used the observed relationships between meteorological drivers of generation anomalies in JJAS as a basis for producing generation forecasts with the output variables from a hindcast set produced by ECMWF System5. Modest overconfidence in the hindcast ensemble was found across candidate forecast variables, as is typically found for seasonal forecasts in the tropics (e.g. Weisheimer et al. (2011) and Jain et al. (2019)).

Predictor variables trailed for wind all explained up to 40% of interannual variability in generation anomalies in JJAS, with the WF-WNPi showing the highest skill. For solar PV, deterministic skill was best for regional-scale predictor variables (ENSO3.4+EQWIN and W-F ISMi) when compared to area averages of proximate variables (rainfall, SSRD, and TCC), with up to 20% of interannual variability in JJAS explained. In the case of wind, modest improvements to deterministic forecast skill in the Northern region were attained when using ISM indices (e.g. ENSO3.4+EQWIN) as additional predictors, consequent of the joint role of WNP and ISM circulations in producing regional generation anomalies. Measures of probabilistic forecast skill and discrimination were positive and significant for all-India wind, as well as regional subdivisions. For solar PV, measures of probabilistic skill are positive and significant for all-India, though are marginal and rarely significant at the regional subdivisions.

A strong association was found between seasonal mean capacity factor anomalies and the frequency of extreme day counts (days where generation is above/below percentile thresholds of the daily generation distribution, r value $\sim$0.5-0.7). This association also translated into reasonable skill in forecasting the frequency of extreme generation days in JJAS, particularly for day counts below the lower 10th percentile (r value $>$0.55 for wind and solar PV). The deterministic forecast skill for the WNP circulation in JJAS is comparable to that reported in comparable studies (e.g., Zhang et al., 2020) and the skill for all-India wind generation anomalies in JJAS comparable to 1-month lead predictions of energy sector impact variables found in other regions (e.g., Thornton et al., 2019). In the case of solar PV capacity factors, the forecast skill was found to be modest, although all-India deterministic skill at one-month lead is comparable to ISMR prediction skill (r value $>$0.40).

8.1.4 Summary of Fourth Results Chapter

The fourth results chapter tested the relevance of the generation syntheses to planned capacity increases. Due to data availability, the analysis focussed on wind energy only. The analysis quantified plausible changes to generation and associated variability characteristics under two scenarios: a 'repowering scenario' in which all turbines in India are substituted with the highest-yielding model and a near-term 'expansion scenario' that included an additional 41.4GW (80.9GW fleet total) of recently built and pipeline wind capacity.

The analysis demonstrated that fully repowering India's fleet using modern turbine designs

with taller towers and lower specific power boosts capacity factors from the existing wind fleet by 82% nationwide. The planned expansion of India's wind fleet in the 2025/26 timeframe (+40GW) results in a nationwide wind capacity factor of 0.40, or +111% over the existing fleet. Repowering wind turbines under 2MW rated capacity (the threshold considered in India's national repowering policy) increases fleetwide capacity factors to ∼0.3, some 25% greater than the capacity factors implicit within the current National Electricity Plan of India (PIB, 2023a). Whether these increased capacity factors could translate into higher energy generation depends on the relative capacity density at which new turbines are installed. Though, the capacity densities of existing wind farms across India are approximately half the value resulting from modern turbines spaced at regular multiples of rotor diameter (∼2.5MW/km^2 versus ∼5MW/km^2), suggesting generation gains from repowering are at least proportionate to capacity factor increases. Furthermore, the plausible capacity factors achievable under these alternative parameterisations are at the upper end (>90th percentile for wind and >80th for solar PV) of values found across decarbonisation pathways for India compiled by WGIII of the IPCC in AR6.

Chapter 7 also demonstrated how modern wind turbine designs modify the variability characteristics of generation, namely, increasing the absolute scale of changes across timescales. This result is a consequence of the steeper ramping segment of lower specific power turbines and the increased magnitude of wind speeds at greater hub height. This result underlines the increasing need for power system flexibility within a decarbonised energy system (Strbac et al., 2020), implying greater levels of energy storage, responsive demand, grid reinforcement/interconnection, and complementary forms of generation (Denholm and Mai, 2019; Bistline et al., 2021). Without such flexibility, electricity network constraints would heighten the risk of curtailment of the increased generation from repowering. Improved characterisation of generation variability across timescales can help appraise design elements of power system flexibility, particularly the likelihood of extreme low generation events (e.g., Cannon et al., 2015), which although less frequent under full repowering, are not eliminated. Finally, Chapter 7 showed that the same statistical relationships between predictor variables for wind generation anomalies in JJAS previously identified in Chapter 6 also hold for both the 'repowering' and 'planned expansion' scenarios. Thus, the prediction skill for summer season wind generation anomalies demonstrated in Chapter 6 would remain stable for the plausible near-term development of wind sector in India.

8.2 Critical reflection and wider relevance

The investigation in this thesis has considered existing wind and solar PV installations in India and near-term capacity expansion. However, India's ambitious net-zero climate goals include plans for a four-fold increase in current levels of wind energy generation and a six-fold increase in solar PV by the year 2032 (PIB, 2023a). The National Electricity Plan of India estimates the capacity required to achieve these generation targets, with wind and solar PV constituting 54% of 900GW of total power capacity (64% with existing and planned hydroelectric power). Such a vast scale of increase requires further study of large expansion scenarios. Furthermore, the investigation was somewhat hypothetical and was conducted independently of any well-defined practical applications.

Despite the limited treatment of these two aspects, the following sections review what conclusions can be drawn from the investigation. And with reference to additional sector and country-specific context, the wider relevance of the investigation findings to large-scale wind and solar deployment is discussed. The flowing sections are split into three distinct issues: (1) strategic planning of capacity expansion, (2) short and long-duration energy storage, and (3) operational decision-making.

8.2.1 Strategic planning of capacity expansion

The generation syntheses offered a means of selectively altering technology parameterisations to gauge consequent effects on energy yield. Versions of the generation syntheses that used parameterisations of current best-available-technologies (modern wind turbines and single-axis tracking) achieved capacity factors at the top-end (>90th percentile for wind and >80th for solar PV) of values found across decarbonisation pathways for India compiled by WGIII of the IPCC in AR6 (c.f. Chapter 7), suggesting less installed capacity is required to achieve a certain generation outcome.

Most nations[1] have announced or are deliberating net-zero emissions targets and use such decarbonisation pathway studies to guide strategic decisions on technology choices and inform energy policy. Although decarbonisation pathways are not necessarily calibrated to observed performances, accurate characterisation of the energy yield from an expanded wind and so-

[1] 131 countries, equivalent to 78% of total global emissions annually, with net-zero polices in-law, announced or in deliberation (ECIU, 2022).

lar PV fleet is necessary to inform the strategic design of renewably powered energy systems. Ground-truthing the performance of specific technologies within decarbonisation pathways or complementing such information with calibrated generation syntheses is, therefore, an important exercise to gauge implications for policymaking. Analysing AR6 decarbonisation pathways for other countries and regions to determine the range of implicit capacity factors is an important task, with implications for the strategic planning of land-use, network infrastructure and electricity markets that can accommodate terawatt-scale capacity increases.

Ongoing technological progress, leading to increased turbine dimensions and solar array efficiency, will drive capacity factors beyond the levels estimated here, which could further add to the generation benefits of repowering and technology upgrades. Specific to wind, low specific power turbines and increases in hub heights are becoming the industry standard (IEA, 2022a; Beiter et al., 2022) and ultra-low wind turbines could open previous unviable sites or provide improved variability characteristics[2]. Taller, longer-bladed turbines imply higher capacity factors but also potentially lower 'generation-density' and land-use footprint of wind power. This is an important consideration for land-scarce countries like India, where land rights are contested and the procurement of land for renewable projects is challenging (Mohan, 2017; Kiesecker et al., 2019). Further detailed study of relevant technical, social, and commercial factors is required to appraise wind expansion and land requirements at a scale consistent with the order-of-magnitude capacity scaleup envisaged in net-zero pathways (e.g., trade-offs between capacity density and wake losses (Miller and Kleidon, 2016; Badger and Volker, 2017); visual and physical disturbance to local residents (Kitzing et al., 2020; Shafiullah et al., 2013); and the multi-owner structure of existing wind farms (Das, Binit, 2023).

Repowering will become increasingly common within the unfolding energy transition, as a greater proportion of existing wind capacity reaches its design lifetime (Kitzing et al., 2020). Despite the recognised importance of repowering for India's energy transition (MNRE, 2022a), existing studies lack country-wide assessment of changes in wind energy generation resulting from turbine technology upgrades. Repowering offers several economic and logistical advantages over developing greenfield sites for wind farms, including the potential reuse of existing feasibility studies and planning appraisals, existing road access, and transmission connections. These factors offer a possible route to expediting the delivery of ambitious renewables targets

[2]The theoretical ultra-low specific power turbine presented in Swisher et al. (2022) achieves 0.44 capacity factor for all-India onshore wind when implemented with the repowering methodology.

and boosting the currently underutilised domestic turbine manufacturing industry (IRENA, 2023b). A growing wind energy sector may also generate employment that can compensate for job losses in a constrained fossil-power sector. However, the exact distributional effects require further study. Additionally, the development of a generation synthesis provides a basis for future investigations into the economic case for early retirement of ageing wind farms and subsequent repowering.

8.2.2 Dimensioning and designing energy storage

Existing studies that use detailed energy system model representations of the Indian electricity network to study the expanded use of wind and solar PV highlight the need for various forms of energy storage to enable a stable and reliable electricity supply (e.g., Sepulveda et al., 2021; Levin et al., 2023). Battery storage technologies are frequently highlighted as key to providing short-term storage (1-4 hours) at high capacity (GW) and low energy volume (GWh) to cope with diurnal mismatches between supply and demand. Namely, oversupply from solar PV during daylight hours (charging), followed by pronounced ramping of net load into the evening hours (sunset and evening peak demand), and sustained lower demand through the night (discharging). This strategy will be of particular importance during boreal summer in India, when peak demand and ramping of demand net of wind and solar PV generation is greatest, driven in large part by cooling and lighting loads in northern and central regions and the greater absolute diurnal range in solar PV generation (MoP, 2021).

However, the dependability of such a strategy relies on consistent wind+solar surpluses or other forms of readily dispatchable generation. Chapter 6 showed a considerable range in the number of extreme generation days for wind and solar PV in JJAS between years. For example, solar PV generation falling below the 10th percentile of daily generation during JJAS (capacity factor of 0.12, ∼20% below median) numbered 0-31 days, while for wind, the day counts numbered 1-38 days (capacity factor of 0.11, ∼60% below median). Dimensioning of battery storage and additional rapidly dispatchable generation will require further consideration of the joint distributions of sub-daily wind and solar PV generation. Such joint distributions may experience a degree of favourable phasing during both active and break phases of the summer monsoon. As defined in Chapter 5, active phases correspond with positive (negative) wind speed (surface irradiance) anomalies through central and southern India. However, the extent of any aggregate compensatory effect of moving between phases would dependent upon the exact location and

volume of installed capacity of each technology.

Existing studies also identify long-duration energy storage (LDS) as economically beneficial and/or necessary in future electricity systems with high variable renewable energy (VRE) shares (>∼60-80% of annual electrical energy) or stringent emissions reductions (e.g., Blanco and Faaij, 2018). Exact definitions vary, though LDS typically involves high energy-to-power capacity ratios with multi-hour to multi-day energy volumes (Dowling et al., 2020). At lower VRE shares, conventional thermal or hydroelectric capacity is typically considered economically more viable than LDS, even when operating at far lower load factors (i.e., running much less frequently than at present- (e.g., De Sisternes et al., 2016; IEA, 2022b). Wind and solar PV constitute ∼35% of annual electricity energy supply in 2032 under the National Electricity Plan (NEP) of India projections (rising to ∼49% under the repowering assumptions discussed in Chapter 7). Thus long-duration energy storage may not be required within this timeframe. Indeed, the Indian NEP does not consider the technology's use. However, other India-specific studies of high VRE-share power systems, typically with more stringent emission reductions, do indicate a need for long-duration storage in the 2030-2040 timeframe (e.g., Gulagi et al., 2022; Lu et al., 2020; Barbar et al., 2023). Furthermore, this requirement increases under wind-heavy deployments due to the greater seasonal disparity in capacity factors between boreal summer and winter (Jain et al., 2021).

In certain regional contexts, hydropower and pumped storage could offer a long-duration storage solution. Though despite the considerable hydropower capacity in India (∼42GW), and planned expansion of pumped storage to 2032 (+22GW), the energy value of these technologies would remain marginal under current plans - in the region of 48GWh by 2032 (NEP, 2023). An alternative to long-duration storage is considerable overbuild of VRE (Tong et al., 2021), though curtailment rates (i.e., unused surplus generation) would likely be prohibitively high in the strongly seasonal Indian climate. Regional interconnection could offer another alternative to provide greater geographical smoothing of generation (Shaner et al., 2018). Although widespread generation anomalies across India were identified in Chapter 4, reducing the possibilities of in-country regional balancing, at least in the JJAS season. Few market-ready utility-scale long-duration storage technologies exist, although numerous candidate technologies are at the early stages of commercialisation at-scale, including compressed air energy storage, thermal energy storage, flow batteries, and power-to-gas-to-power solutions, involving production, storage,

and oxidation or combustion of hydrogen or synthetic methane (Hunter et al., 2021).

Studies that consider the use of LDS in Europe (e.g., Jafari et al., 2020; Ruhnau and Qvist, 2022) and the United States (e.g., Dowling et al., 2020) highlight the benefits of multi-day storage using such technologies in filling prolonged deficits during boreal summer when wind output is lower. As energy system optimisations are sensitive to interannual variability (Pfenninger, 2017, Collins et al., 2018), multi-year studies that include LDS note how storage requirements vary depending on the time frame considered. For example, Dowling et al. (2020) found that the use of different weather years in their optimisation of a decarbonised electricity system in the United States produced storage capacities that differed by 213%. The effects of different weather years would likely affect similar assessments for India. For example, based on the generation syntheses for all-India, energy yield for wind and solar PV at the capacity levels considered in the 2032 NEP drops in JJAS by 15% of the median in 2020 (the largest negative anomaly) and increase to 9% of the median in 1986 (the largest positive anomaly). Interannual variability in generation would also impact aspects of electricity market design, such as the dimensioning and valuation of capacity markets (i.e., how much to pay controllable capacity to wait in standby to cover unexpected generation shortfalls), and price support mechanisms for renewables (e.g., incorrectly priced support when using unrepresentative capacity factors) (Coker et al., 2020).

8.2.3 Forecast value in operational decision-making

Various weather and forecast information are used by decision-makers within the electricity sector to help manage the impacts of weather and climate variability. In the Indian context, wind and solar PV farm operators are required to share daily generation forecasts for their assets for the subsequent 24 hours with the electricity system operator, while state and regional load dispatch centres consider generation forecasts out to a week (Joshi et al., 2022). In other world regions, SCFs are used in addition to weather forecasts to help grid operators assess the sufficiency of available generation to meet anticipated demand at a specified level of confidence (termed resource adequacy) and to guide efficient pricing of power contracts in wholesale electricity markets (Troccoli et al., 2018). However, no such use of forecast information is documented in India beyond the 1-day and 1-week time horizons (Mitra et al., 2022).

A key premise of the investigation in this thesis is that forecasts for the season ahead can prove valuable to the electricity sector by enabling timely operational decision-making and in-

terventions. This premise is inherent to many applied research initiatives and studies that link forecast skill on seasonal timescales to potential forecast value within an applied setting (e.g. Bett et al., 2017; Torralba et al., 2017). Analyses beyond quantification of forecast skill and reliability also seek to explicitly quantify various measures of forecast value, often using decision-analytic frameworks. Simplified models include 'expected utility' (Von Neumann, 1944; Thompson and Brier, 1955) and 'static cost/loss' frameworks (Murphy, 1977), while more elaborate, sector-specific decision-analytic models allow for refined decisions, such as hedging options or concurrent, repeat interventions (e.g., Maza et al., 2008; Brayshaw et al., 2020). However, such models invariably require significant abstraction of the decision-making context and process—specifically, choices between well-defined actions and discrete resulting consequences.

Furthermore, numerous examples from a range of different sectors, spanning timescales of weather to multidecadal climate, have shown how the production and availability of forecast information does not necessarily ensure forecast value or beneficial use (Changnon et al., 1995; Rayner et al., 2005; Dilling et al., 2011). Evidence suggests a wide range of additional factors affect the uptake of weather and climate forecasts amongst decision-makers, including the availability of alternative courses of action (Lemos et al., 2002), more pressing organisational priorities (Measham et al., 2011), the form and channels of forecast communication (Hansen, 2002), and other contextual elements of the decision-making space. This apparent gap between the generation and application of scientific information is also found in other areas of environmental decision-making (McNie, 2007) and feeds into broader discussions on the role of scientific input to policymaking (Sarewitz et al., 2007). Conventionally, where the impact of scientific information is found lacking, the policy response has sought to increase the information supply, often funding additional research to meet the supposed demand for knowledge (Sarewitz et al., 2007; Meyer, 2011). However, it is argued that a focus on increasing the volume of science-based information, frequently developed in isolation for the intended user, risks misalignment with the particular information needs of decision-makers (Cash et al., 2006; Feldman et al., 2009).

This thesis could be considered as an extension of such a reductive, 'science-first' approach, and further demonstration of actual or potential forecast value within the Indian electricity system context will require deeper consideration of operational procedures (Hanlon et al., 2018) and direct collaboration with practitioners (Kirchhoff, 2013). An application-specific evaluation of forecast value could aid prospective SCF users in gauging potential benefits before undertaking

necessary investments in procurement, training, etc. (Bruno Soares et al., 2018; Perrels et al., 2020), while forecast providers could better understand and tailor climate information and services to specific user needs (Vaughan and Dessai, 2014; Goodess et al., 2022).

Numerous features of the Indian electricity system in its current form would likely shape the opportunity space for SCF applications. Chief among these defining features is the limited interconnection between Indian states and the high level of autonomy amongst state load dispatch centres (the authorities responsible for network operations and balancing) (MoP, 2021). Even where interstate interconnection permits a degree of balancing, a lack of centralised data collection and dissemination on generator availability precludes interregional coordination and balancing (RMI, 2023). Furthermore, contract trading in nascent wholesale power, imbalance, and ancillary service markets beyond the day-ahead is limited (Mitra et al., 2022). In addition to these structural aspects of the existing electricity system, the partial evidence that does exist on the use of forecast information in electricity system management in India suggests limited expertise amongst state load dispatch centres in developing generation forecasts (NITI Aayog, 2015), and limited trust of generation forecasts provided by Renewable Energy Management Centres (REMCs) (Joshi and Inskeep, 2023). A total of 13 REMCs are currently operational nationwide and provide week-ahead forecasting, monitoring, and situational awareness of renewable energy assets. Additionally, the degree of centralisation versus autonomy in the production and provision of generation forecasts is an ongoing source of tension in the current setup of electricity market (Joshi and Inskeep, 2023).

The present situation in India with the use of short-term forecasts parallels with learnings from other regions that have implemented SCF into energy sector decision-making. In Europe, the electricity sector was among the early adopters of SCF information (Dessai et al., 2013; White et al., 2017, Cortekar et al., 2020), although numerous barriers to use had to be navigated and uptake is yet to reach maturity (Bruno Soares et al., 2018). Common issues include a lack of fit between available forecast products and user requirements, difficulty interpreting SCF products, a perception amongst users of variable or unverified levels of forecast quality, and a lack of proof-of-concept demonstration of the value of SCFs (Buontempo et al., 2014; Bruno Soares et al., 2015, 2016; Goodess et al., 2019; Suhari et al., 2022). Where SCF information is poorly suited to the organisational contexts and operational remit of specific decision-makers within the energy sector (or worse yet, is misunderstood), there is a risk that potential cost-savings and

profit increases will not be realised, consumers will suffer higher energy prices, electricity system reliability will decrease and, ultimately, the deployment of the most promising of low-carbon energy technologies will be delayed.

Leveraging SCF information in an Indian electricity system context would require a more detailed understanding of industry decision-makers' information needs, operational contexts, and demonstration of SCF value in proof-of-concept or prototype applications. Fortunately, the existing literature on climate service development provides an entry point for future research and guidance over best practices in climate information applications (e.g., Lemos et al. (2012)). Of paramount importance is ensuring the correct information fit amongst users – i.e., whether the information is considered accurate, credible, salient and timely (Stern et al., 1999; Cash et al., 2003). Also, the relationship between new and established knowledge – e.g., whether conventional operational practices permit the use of novel information (e.g. Rayner et al., 2005). Additionally, the degree and quality of collaboration between scientists and practitioners in developing information are essential (Kirchoff et al., 2013). The importance of boundary organisations and their role in brokering between knowledge producers and practitioners has been emphasised in the literature (Buizer et al., 2016), as has the need to communicate uncertainties effectively (Meyer, 2011; Taylor et al., 2015). Beyond user-reported barriers and enablers of climate information, examples of prototype SCF products and services for the energy sector have brought additional learning, including the need for highly detailed specifications for users' operational procedures (Hanlon et al., 2018, Hewit at al., 2021), the importance local social and economic setting in shaping the decision context and scope of service design (Golding et al., 2017) and the potential for design study methods in bridging usability gaps (Christel et al., 2018).

8.3 Future research

The investigation marks a starting point for future research into weather and climate impacts on energy systems, both in India and further afield. The following discusses a selection of the most promising avenues for further study.

8.3.1 Generation synthesis

1. Further improvements in the accuracy of the wind and solar PV generation synthesis for India, including additional observational data to improve calibration, seasonally varying adjustment factors to enhance accuracy, and extra plant-level detail, particularly for solar PV (e.g., information on single-axis tracking or fixed tilt, inverter load ratio, rooftop or ground mounted, etc.).

2. The input data and rationale behind the generation synthesis methodology are adaptable to other weather-dependent energy sources, notably hydroelectric power. Hydropower is particularly relevant to the northern region of India, where it forms ∼20% of total installed capacity across all sources and >90% in four northern states (CEA, 2022). Numerous methodologies based on physical and statistical models exist for relating meteorological input data to hydropower (e.g., De Felice et al., 2018; Ho et al., 2020). Daily plant-level hydro generation output data is available for verification purposes from the Indian National Power Portal[3]. Generation syntheses from the main renewable sources (wind, solar PV and hydropower) would then allow for further analysis of generation co-variability and complementarity.

3. The co-variability of power demand with generation is an important consideration for power system functioning and informs requirements for grid reinforcement, storage, and complementary forms of generation. Multidecadal electricity demand syntheses for India are absent from the literature. But relevant statistical methods exist for relating meteorological drivers and historical patterns to power demand (e.g., Thornton et al., 2016) and could be extended to the Indian case. In the Indian context, air conditioning is an important emerging weather-sensitive driver of electrical power demand (Barbar et al., 2021). And other work has noted how the anti-phasing between wind generation and air temperatures in India contributes to enhanced variability in electricity demand net of wind generation on intra-seasonal timescales (Dunning et al., 2017). Weather-dependent co-variability and impacts of net electricity load will be important questions for future research.

4. The generation synthesis methodology is readably adaptable to other world regions. Although numerous examples exist for various countries (e.g., Kubick, 2013; Ren et al., 2019;

[3]https://npp.gov.in/dgrReports

Bloomfield et al., 2021; Gruber et al., 2022), many studies lack detailed characterisation of existing or future technology characteristics (typically fixed assumptions of power curves and non-geolocated plant data). Furthermore, validation of generation estimates against observed generation to correct known biases in meteorological input data is not common (Staffell and Pfenninger, 2016; Gruber et al., 2019). An increasing number of open data initiatives enable technology and location specific syntheses[4], which are verifiable against observed power output[5].

5. The generation synthesis methodology is adaptable to incorporate other model input data, such as climate model data (e.g., Hdidouan et al., 2017; Bloomfield et al., 2021), higher temporal frequency outputs from SCF systems (e.g., Lledo et al., 2019), climate model control runs, or large hindcast sets to quantify the risk of extreme events for the power system (e.g., extreme low generation events – Kay et al., 2023) and low-frequency variability (Wohland et al., 2020). Furthermore, forcing scenarios could be used to further investigate trends that affect renewable resources (e.g., the declining trends identified for wind and solar PV in Chapter 4).

8.3.2 Meteorological drivers of generation anomalies

6. A cursory treatment of intraseasonal variability within the Indian summer monsoon season was presented in Chapter 5. However, intra seasonal oscillations are also prevalent within the western north Pacific monsoon system (e.g., Wang et al., 2020) and share a common spatial mode to the seasonally persistent variability pattern (i.e., an anomalous low-level anticyclone). As this internal variability explains up to half of total monthly internal variance in low-level zonal winds over the region, an assessment of associated impacts on wind generation anomalies is desirable.

7. Alternative methodological approaches for assessing weather impacts on generation should be applied to the Indian case. For example, weather regimes that classify meteorological variations (usually large-scale circulations) into consistent patterns have been used to elucidate impacts on renewable power generation and electricity demand (Brayshaw et al., 2011; Grams et al 2017, Thornton et al 2017, van der Wiel et al., 2019; Wohland et

[4]E.g., Openly available database of global plant-level power infrastructure: Global Energy Monitor: https://globalenergymonitor.org/

[5]E.g., Crowdsourced global database of realtime power data: Electricity Maps: https://github.com/electricitymaps/electricitymaps-contrib/blob/master/DATA_SOURCES.md

al., 2021). Weather regimes have been applied in the context of rainfall patterns in India, with seven broadscale circulation categories found suitable to describe year-round rainfall variability (Neal et al., 2020). Sector-specific impacts (including the energy sector) are yet to be investigated.

8. The co-variability and co-occurrence of particular generation events warrants further detailed study. The investigation identified generally weak correlation between wind and solar PV generation anomalies in JJAS, though the very largest negative wind generation anomalies in JJAS (>1std., n=4) did co-occur with negative solar PV generation anomalies that ranked in the lower 20th percentile of seasonal anomalies. A degree of complementarity was also shown in the seasonal generation profile of wind and solar PV, though the extent of possible balancing is dependent on the relative share between the two technologies. Further investigation of event co-occurrence ought to consider extreme events over various timescales, such as the simultaneous high/low generation days across multi energy sources (e.g., Otero et al., 2022; Richardson et al., 2023). Suitable compound event metrics will be required to assess both spatial and temporal aspects of compounding (Bloomfield et al., 2024). And impacts beyond the power supply may prove relevant in multi-sector impact framework, notably the water sector in an Indian context, where droughts and flooding present multiple energy sector impacts (Joshi et al., 2022).

8.3.3 Generation forecasting

9. A natural extension of the verification of seasonal generation forecasts presented here is to consider other seasons and energy sources. A comprehensive verification could consider other observational datasets (including generation syntheses based on other reanalysis data) and baseline forecasts other than climatology (e.g., statistical-empirical predictions).

10. Model diversity in multi model assessment has been identified as contributing to pooled skill (e.g., Alessandri et al., 2018). And so, a worthwhile extension of the verification would consider other SCF systems, such as operational models from other Global Producing Centres, the Asian-Pacific Economic Cooperation Climate Centre, or the modified version of CFS2 maintained by the Indian Institute of Tropical Meteorology. Furthermore, the assessment of multi model skill in this thesis considered all ensemble members equally. An extended analysis could consider the numerous options for preferential weighting or

selection of ensemble members, e.g., based on past skill (Robertson et al., 2004; Tebaldi, and Knutti, 2007), machine learning techniques (e.g., Cohen et al., 2019; Gonzalez et al., 2021), or real-time observations (Brajard et al., 2023).

8.3.4 Scenario analysis

11. The 'planned expansion' scenario considered in Chapter 7 represents near-term development of wind capacity in India (+40GW). However, significant expansion beyond these levels of wind capacity is envisaged in national development plans and across multiple assessments of decarbonisation pathways for India. Typically, an order of magnitude scale-up over present-day levels of wind and solar PV capacity is required in the 2030 timeframe, up to two orders of magnitude by 2050. Such drastic pace and scale of change should prompt investigation of additional 'large expansion' scenarios and the consequent effects on generation. Exploring such scenarios with the generation syntheses methods developed in this thesis will require spatially explicit deployment scenarios. Such scenarios would also aid an integrated, cross-sectoral assessment of renewables expansion, such as the requirements for grid and road infrastructure, land-use planning, and wider socio-economic and distributional effects.

12. The assessment of generation variability in this thesis was conducted at the scale of regional and country-level aggregations and was unconstrained by the technical limitations of a real-world power system. Numerous spatial and temporal constraints would modulate generation variability in a real power system, including network constraints, inflexible 'must-run' capacity, the demand profile, etc. Coupling generation syntheses with power system models that can capture a wider range of electricity system behaviour could elucidate contemporaneous, interactive, and non-linear impacts of different wind and solar PV configurations. Although power system models have generally improved the representation of meteorological variability in recent years (e.g., Ringkjøb et al., 2018), few power system models and modelling initiatives fully exploit all the possible benefits of using generation syntheses, i.e., long timeseries at high temporal resolution, with flexible spatial aggregation and technology parameterisations (e.g., Hilbers et al., 2020).

8.3.5 Applications

13. Despite the practical relevance of this thesis to power system planning and operations in India, the investigation was conducted independently of any well-defined practical applications. Much remains to be learned about the decision contexts and climate information needs of various actors in the electricity system of India. Future work should determine the nature of decision contexts facing organisations involved in the operation of wind, solar PV and associated energy infrastructures, current approaches to decision processes, existing information inputs, and contingencies made possible by new forecast information. Determining necessary levels of skill to enable use and whether SCF can attain such levels for a given region and variable are key factors affecting usability (Crochemore et al., 2021). Studying weather-dependent decision processes would be of use beyond just SCF for wind and solar PV and could help identify potential knowledge-value gaps between other climate information products and energy sector components across other timescales (White et al., 2022). Key agencies in India to be considered in future cooperation include national[6] and regional load dispatch centres (for the five electricity zones), Renewable Energy Management Centres (REMCs) and the Indian Meteorological Department (IMD). The IMD is the WMO-designated Regional Climate Centre and has considerable experience and input to the South Asia Seasonal Climate Outlook Forum (SASCOF).

14. The importance of involving practitioners within research efforts extends beyond the development of meteorological forecasts for operational decisions. The generation synthesis methodologies presented in this thesis have relevance to strategic design, planning, and policy development of an expanded renewables fleet in India and beyond. There exists considerable appetite amongst national governments for policy-relevant information to guide national climate strategies (Weber et al. 2018; Krabbe et al. 2015; Kriegler et al., 2019) and an emerging literature around participatory modelling and 'climate-scenario services' (Auer et al., 2022) provides a blueprint for operationalising the principles of knowledge co-production (Norstrom et al., 2020). Collaboration with relevant power sector decision makers[7] could provide an opportunity to demonstrate possible applications of generation syntheses, co-produce new capacity expansion scenarios and accompanying generation syntheses, and reverse-engineer optimised scenarios (e.g., using practitioner

[6]The "National Grid Controller of India Ltd", formerly Power System Operation Corporation Ltd (POSOCO)
[7]Particularly, the Ministry of Power and Central Electricity Agency (CEA) in India.

knowledge to identify particularly unfavourable supply conditions and working backwards to produce generation syntheses that avoid or are resilient to such conditions). Beyond their utility in quantifying existing and emerging energy performances and weather-related risks, generation syntheses could also serve as devices for communicating and translation between scientists and stakeholders. The established literature on the use of scenarios as 'boundary objects' to support collaboration, reflection, and mediation between diverse groups of expertise provides an entry point for future research (e.g., Star and Griesemer, 1989; Taylor et al., 2014).

8.4 Conclusion and outlook

This thesis has shown several encouraging results that advance the state of knowledge of energy meteorology in India. Firstly, accurate generation syntheses provide a means of studying the statistical properties of key renewable technologies over a range of timescales. Maintaining and updating generation syntheses, improving data inputs, and expanding their coverage to other technologies and regions are all important future research tasks. Propagating the methods and resulting data of generations syntheses can enable numerous applications, such as power system modelling, economic appraisal and future climate impact assessment.

Second, the links between large-scale meteorological phenomena and generation anomalies in summer provide a basis for seasonal prediction. Future generation forecasting initiatives should go beyond the proof-of-concept exposition in this thesis and look to operational seasonal generation forecasts that can be shared and refined with relevant decision-makers. Regional seasonal generation outlooks could provide situational awareness for electricity system operators and facilitate coordination at a broader scale.

Thirdly, plausible modifications to wind and solar PV technologies in the coming years impart meaningful changes to India's energy yield and generation variability. These sensitivity tests have real-world implications, greatly affecting estimates of future capacity requirements in technology pathway studies consistent with net-zero climate ambitions. It is hoped that ground truthing and sensitivity testing of future technology pathway studies with generation synthesis methodologies will become standard practice. Such approaches apply to all world regions and would help decision-makers appraise the strategic and operational requirements of future electricity systems.

Appendix A

Appendix Chapter 5

A.1 Attenuating effect of aerosols on irradiance

To quantify the direct effects of aerosols on total in-plane irradiance (TI, i.e., the sum of direct and diffuse irradiance components as received by the solar PV array), irradiance fields from the CERES (Clouds and the Earth's Radiant Energy System) SYN1deg data product for the period 2000 to 2022 are run through the celestial geometry equations described in Data and Methods section 3.2.9. The reason for using the CERES product rather than ERA5 is because the CERES product includes direct and diffuse irradiance components for no-aerosol (TI_{na}), no cloud (TI_{nc}), and all-sky atmospheric conditions (ERA5 lacks the no-aerosol conditions). With this additional field, the relative reduction in TI caused by aerosols was determined by (TI_{na}-TI_{as})/TI_{as} and the relative reduction in TI caused by clouds by (TI_{nc}-TI_{as})/TI_{as}. Although the CERES and ERA5 products derive irradiance values with different methods, the differences in alike irradiance fields in JJAS over India are negligible between the two data products, and a version of the solar PV generation synthesis constructed with CERES data product shows comparable accuracy to the ERA5 version (r value of 0.93 for all-India monthly generation from CERES in the verification period 2017-2021, compared to 0.95 for ERA5).

Figure A.1 shows the mean relative reduction in TI caused by aerosols in JJAS, reaching a maximum of 25% in the north west of India. Figure A.1c shows the relative mean reduction in TI caused by clouds in JJAS, reaching a maximum of 92% in central India (and lowest values of ∼16% in the north west of India – N.B. the different colour scale between Figure A.1a and A.1c). The standard deviation across the 23 years times series of the relative reduction in TI caused by aerosols and that caused by clouds are shown in Figure A.1b and A.1d, respectively. The standard deviation value for the relative reduction in TI caused by clouds is approximately double that caused by aerosol across peninsular India.

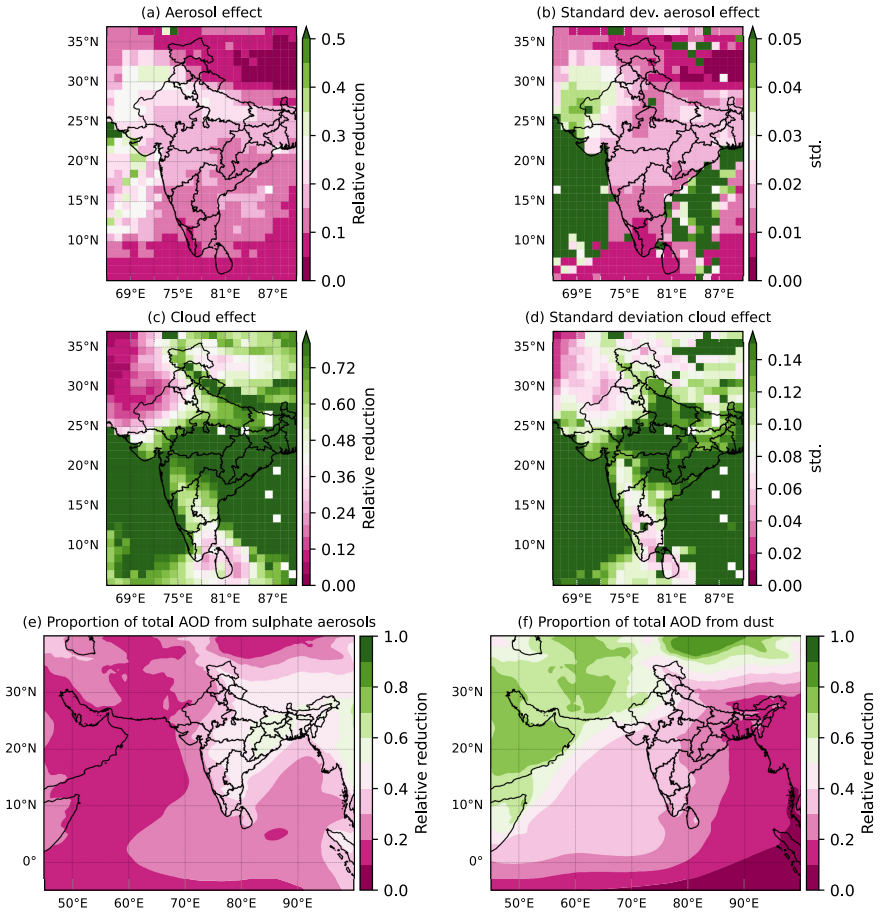

Figure A.1: mean relative reduction in TI caused by aerosols (a) and clouds (c) in JJAS, standard deviation in the relative reduction in TI caused by aerosols (b) and clouds (d), and proportion of total AOD from sulphate aerosols (e) and mineral dust (f).

Figure A.1e shows the proportion of total AOD from sulphate aerosols and Figure A.1f the proportion from mineral dust. These two figures make use of the speciated AOD fields available in MERRA2, considering averages over the period 1980-2022. Sulphate aerosols dominate in central and eastern peninsular India, whereas mineral dust is the dominant share of total AOD over desert regions of the Middle east and a small region confined to the north west of India.

Appendix B

Appendix Chapter 6

B.1 Over/underconfidence and the ratio of predictable components

Systematic differences in the variability characteristics of a forecast ensemble compared to observations will degrade measures of forecast quality (Wilks, 2011). For a perfect model, the relative strength of signal and noise in the model (i.e., the fraction of total variability that is predictable) would equal that of observations (Eade et al., 2014). The signal apparent in the observed climate (i.e., the predictable component) is routinely estimated as the fraction of observed variance explained by model ensemble mean hindcasts (Wang et al., 2006; Eade et al., 2014). The signal-to-noise ratio in the model, can be defined by the ratio of the variance of the ensemble mean to the mean variance of each ensemble member (Kumar, 2009). The Ratio of Predictable Components (RPC) was introduced by Eade et al. (2014) to estimate the signal-to-noise ratio in climate forecasts. Because the numerator of this metric includes the correlation coefficient of the ensemble mean with observations, the measure is only meaningful when there is forecast skill. For a perfect forecast, the RPC should be 1. An RPC value greater than unity indicates underconfidence and an over-dispersive forecast, where the ensemble mean agrees well with observations, but less well with each ensemble member, thus underestimating the predictability of the real world. Conversely, where the noise of the SCF system is less than the equivalent observed estimate, the ensemble members will be too close to the ensemble mean, suggesting that the true forecast uncertainty is underestimated (Weigel et al., 2009). This situation is indicative of overconfident or under-dispersive forecasts, with a falsely inflated sharpness, which are likely unreliable (Chevuturi et al., 2021).

Figure B.1 shows the RPC values for the variables relevant to the predictors discussed in Chapter 7. RPC values slightly below unity within the tropics suggest moderate overconfidence within

this region, which is a feature commonly found in seasonal forecasts (Weisheimer et al., 2011) and mirrors a similar finding with MSLP in boreal wintertime with the ECMWF System 4 model (Baker et al., 2018). Conversely, regions with RPC>1 are less widespread with an exception over South Asia, where RPC>1 for MSLP (Figure B.2d). This appears to coincide with the ISM trough; a zone experiencing much variability due to the passage of low-pressure system during the summer monsoon period.

An RPC value greater than unity indicates underconfidence and an over-dispersive forecast, where the ensemble mean agrees well with observations but less well with each ensemble member, thus underestimating the predictability of the real world.

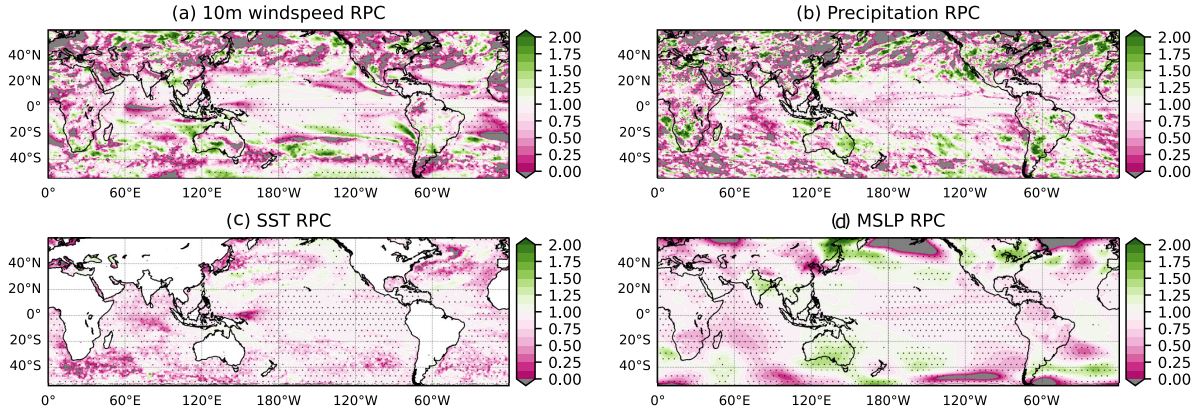

Figure B.1: Ratio of predictable components for JJAS 1-month lead hindcasts of 4 variables. Stippling signifies where RPC is significantly different unity at the 90% level, based on a bootstrap resampling method (N.B., the null hypothesis that RPC is not different from 1 is rejected at the 90% level when the 5-95% confidence interval of the distribution of RPC values does not include the value 1). Regions in grey are where ensemble mean correlation with observations is negative.

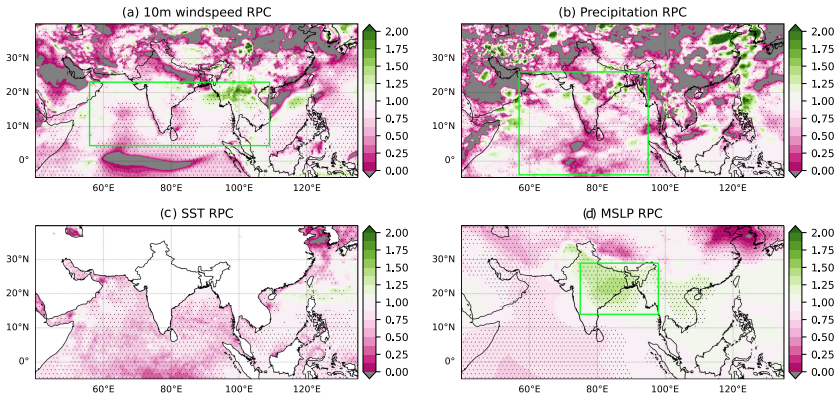

Figure B.2: As for Figure B.1 but zoomed to South Asian region. Green boxes indicate regions over which area-averaged hindcast skill is evaluated.

Regions where RPC>1, imply a larger ensemble size is required to achieve forecast skill (Scaife

and Smith, 2018). This is demonstrated in Figure B.3a by plotting the correlation between the ensemble mean and observations as a function of ensemble size for MSLP averaged over the green box in Figure B.3d. The correlation values begin to asymptote at approximately 12 ensemble members. This contrasts with a levelling-off in ensemble mean correlation with ensemble size at approximately 4-5 members for the slightly overconfident forecasts of 10m wind speeds and total cloud cover (Figure B.3b and B.3c, respectively, corresponding with area averages of green boxes in Figure B.2a and B.2b, respectively). Underconfidence can be tested by computing the skill of the ensemble mean when predicting individual ensemble members, the so-called perfect model test (red lines in Figure B.3). The MSLP case consistently shows higher skill for the model predicting observations than predicting itself, while both the 10m wind speed and total cloud cover cases show better skill for predicting single ensemble members than the real world, as expected. This so-called signal-to-noise paradox has been widely identified in the extratropics (e.g. Eade et al. (2014), Kumar et al. (2014), Scaife et al. (2014), and Scaife and Smith (2018)), though overestimates of the predictability of tropical rainfall have also been documented in East Africa (Walker et al., 2019).

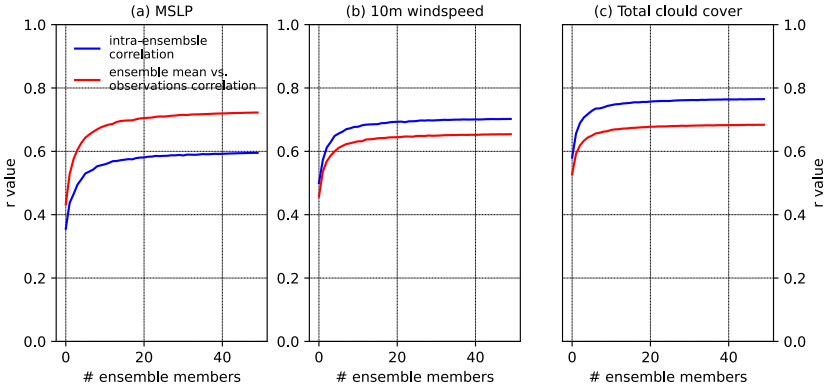

Figure B.3: Correlation between the ensemble mean MSLP (a)/10m wind speeds (b)/total cloud cover (c) with equivalent observations as a function of ensemble size (red line). Average correlation between the ensemble mean MSLP (a)/10m wind speeds (b)/total cloud cover (c) with individual ensemble members.

As overconfidence (RPC<1) prevails in almost all regions of the tropics for these candidate predictor variables (see Table B.1), the conventional methods of forecast calibration described in Section 3.4.2, namely Climate Conserving Recalibration, is justified as a means of inflating ensemble variance to improve the reliability of forecasts.

	Wind		Solar PV
10m wind	**0.92**	TCC	**0.82**
EOF1 850hPa u-winds	0.97	Niño3.4 + EQWIN	0.91
WNPi	0.94	EOF2 850hPa winds	0.90
		ISMi	**0.80**

Table B.1: Table A1: RPC values for candidate predictors of JJAS wind and solar PV generation anomalies. Values in bold are significantly different from 1 at the 90% level, using a bootstrap resampling method. The null hypothesis that RPC is not different from one is rejected at the 90% level when the 5-95% confidence interval of the distribution of RPC values does not include the value 1.

References

Abdulla, Cheriyeri Poyil, Valliyil Mohammed Aboobacker, Puthuveetil Razak Shanas, Vijayakumaran Vijith, Raveendran Sajeev, and Ponnumony Vethamony (2022). "Climatology and variability of wind speeds along the southwest coast of India derived from Climate Forecast System Reanalysis winds". In: *International Journal of Climatology* 42.16, pp. 8738–8754.

Alexander, Michael A, Ileana Bladé, Matthew Newman, John R Lanzante, Ngar-Cheung Lau, and James D Scott (2002). "The atmospheric bridge: The influence of ENSO teleconnections on air–sea interaction over the global oceans". In: *Journal of Climate* 15.16, pp. 2205–2231.

Amatulli, Giuseppe, Sami Domisch, Mao-Ning Tuanmu, Benoit Parmentier, Ajay Ranipeta, Jeremy Malczyk, and Walter Jetz (2018). "A suite of global, cross-scale topographic variables for environmental and biodiversity modeling". In: *Scientific data* 5.1, pp. 1–15.

Annamalai, H and JM Slingo (2001). "Active/break cycles: Diagnosis of the intraseasonal variability of the Asian summer monsoon". In: *Climate Dynamics* 18, pp. 85–102.

Annamalai, H and KR Sperber (2005). "Regional heat sources and the active and break phases of boreal summer intraseasonal (30–50 day) variability". In: *Journal of the Atmospheric Sciences* 62.8, pp. 2726–2748.

Archer, Cristina L and Mark Z Jacobson (2007). "Supplying baseload power and reducing transmission requirements by interconnecting wind farms". In: *Journal of applied meteorology and Climatology* 46.11, pp. 1701–1717.

Arctech (2022). *Arctech Launches New Video Documenting 1.7GW Milestone Project in Rajasthan, India.* Online. Available at: http://www.arctechsolar.us/news/329. Accessed: 3rd January 2023.

Arias, Paola A, Nicolas Bellouin, Erika Coppola, Richard G Jones, Gerhard Krinner, Jochem Marotzke, Vaishali Naik, Matthew D Palmer, Gian-Kasper Plattner, Joeri Rogelj, et al. (2021). "Technical summary". In: *Climate Change 2021 – The Physical Science Basis*. Cambridge University Press, pp. 35–144.

Arwade, Sanjay R, Matthew A Lackner, and Mircea D Grigoriu (2011). "Probabilistic models for wind turbine and wind farm performance". In: *Journal of Solar Energy Engineering* 133.4.

Ashok, Karumuri, Zhaoyong Guan, NH Saji, and Toshio Yamagata (2004). "Individual and combined influences of ENSO and the Indian Ocean dipole on the Indian summer monsoon". In: *Journal of Climate* 17.16, pp. 3141–3155.

Ashok, Karumuri, Zhaoyong Guan, and Toshio Yamagata (2001). "Impact of the Indian Ocean dipole on the relationship between the Indian monsoon rainfall and ENSO". In: *Geophysical Research Letters* 28.23, pp. 4499–4502.

ASPI (2022). *India Climate Action Brief, Asia Society Policy Institute (ASPI).* Online. Available at: https://asiasociety.org/sites/default/files/2022-05/ASPI_ClimateActionBrief_India.pdf Accessed: 11th January 2023.

Attada, Raju, Muhammad Azhar Ehsan, and Prasanth A Pillai (2022). "Evaluation of potential predictability of Indian summer monsoon rainfall in ECMWF's fifth-generation seasonal forecast system (SEAS5)". In: *Pure and Applied Geophysics* 179.12, pp. 4639–4655.

Azorin-Molina, Cesar, Jesus Asin, Tim R McVicar, Lorenzo Minola, Juan I Lopez-Moreno, Sergio M Vicente-Serrano, and Deliang Chen (2018). "Evaluating anemometer drift: A statistical approach to correct biases in wind speed measurement". In: *Atmospheric research* 203, pp. 175–188.

Badger, Jake, Neil Davis, Andrea N Hahmann, Bjarke Tobias Olsen, Xiaoli Guo Larsén, Mark C Kelly, Patrick Volker, Merete Badger, Tobias Torben Ahsbahs, Niels Gylling Mortensen, et al. (2015). "The new worldwide microscale wind resource assessment data on IRENA's global atlas. the EUDP Global Wind Atlas". In: *EWEA Technology Workshop: Resource Assessment 2015.*

Badger, Jake and Patrick JH Volker (2017). "Efficient large-scale wind turbine deployment can meet global electricity generation needs". In: *Proceedings of the National Academy of Sciences* 114.43, E8945–E8945.

Baker, LH, LC Shaffrey, and Adam A Scaife (2018). "Improved seasonal prediction of UK regional precipitation using atmospheric circulation". In: *International Journal of Climatology* 38, e437–e453.

Bakke, Ida, Stein-Erik Fleten, Lars Ivar Hagfors, Verena Hagspiel, Beate Norheim, and Sonja Wogrin (2016). "Investment in electric energy storage under uncertainty: a real options approach". In: *Computational Management Science* 13, pp. 483–500.

Balsamo, Gianpaolo, Anton Beljaars, Klaus Scipal, Pedro Viterbo, Bart van den Hurk, Martin Hirschi, and Alan K Betts (2009). "A revised hydrology for the ECMWF model: Verification from field site to terrestrial water storage and impact in the Integrated Forecast System". In: *Journal of Hydrometeorology* 10.3, pp. 623–643.

Ban-Weiss, G.A. and W.D. Collins (2015). "AEROSOLS — Role in Radiative Transfer". In: *Encyclopedia of Atmospheric Sciences (Second Edition)*. Ed. by Gerald R. North, John Pyle, and Fuqing Zhang. Second Edition. Oxford: Academic Press, pp. 66–75.

Banerjee, Priyanka and S Prasanna Kumar (2016). "ENSO modulation of interannual variability of dust aerosols over the northwest Indian Ocean". In: *Journal of Climate* 29.4, pp. 1287–1303.

Barbar, Marc, Dharik S Mallapragada, and Robert J Stoner (2023). "Impact of demand growth on decarbonizing India's electricity sector and the role for energy storage". In: *Energy and Climate Change* 4, p. 100098.

Barnston, Anthony G (1997). "Documentation of a highly ENSO-related SST region in the equatorial Pacific". In: *Atmosphere-ocean* 35, pp. 367–383.

Barthelmie, Rebecca J, Kurt S Hansen, and Sara C Pryor (2012). "Meteorological controls on wind turbine wakes". In: *Proceedings of the IEEE* 101.4, pp. 1010–1019.

Barthelmie, Rebecca Jane and LE Jensen (2010). "Evaluation of wind farm efficiency and wind turbine wakes at the Nysted offshore wind farm". In: *Wind Energy* 13.6, pp. 573–586.

Barthelmie, RJ, B Grisogono, and SC Pryor (1996). "Observations and simulations of diurnal cycles of near-surface wind speeds over land and sea". In: *Journal of Geophysical Research: Atmospheres* 101.D16, pp. 21327–21337.

Beck, Hylke E, Albert IJM Van Dijk, Vincenzo Levizzani, Jaap Schellekens, Diego G Miralles, Brecht Martens, and Ad De Roo (2017). "MSWEP: 3-hourly 0.25 global gridded precipitation (1979–2015) by merging gauge, satellite, and reanalysis data". In: *Hydrology and Earth System Sciences* 21.1, pp. 589–615.

Beck, Hylke E, Eric F Wood, Ming Pan, Colby K Fisher, Diego G Miralles, Albert IJM Van Dijk, Tim R McVicar, and Robert F Adler (2019). "MSWEP V2 global 3-hourly 0.1 precipitation: methodology and quantitative assessment". In: *Bulletin of the American Meteorological Society* 100.3, pp. 473–500.

Beck and Martin Mahony (2018). "The IPCC and the new map of science and politics". In: *Wiley Interdisciplinary Reviews: Climate Change* 9.6, e547.

Beerli, Remo, Heini Wernli, and Christian M Grams (2017). "Does the lower stratosphere provide predictability for month-ahead wind electricity generation in Europe?" In: *Quarterly Journal of the Royal Meteorological Society* 143.709, pp. 3025–3036.

Behera, Swadhin K and JV Ratnam (2018). "Quasi-asymmetric response of the Indian summer monsoon rainfall to opposite phases of the IOD". In: *Scientific Reports* 8.1, p. 123.

Beiter, Philipp, Joseph T Rand, Joachim Seel, Eric Lantz, Patrick Gilman, and Ryan Wiser (2022). "Expert perspectives on the wind plant of the future". In: *Wind Energy* 25.8, pp. 1363–1378.

Bell, Bill, Hans Hersbach, Adrian Simmons, Paul Berrisford, Per Dahlgren, András Horányi, Joaquín Muñoz-Sabater, Julien Nicolas, Raluca Radu, Dinand Schepers, et al. (2021). "The ERA5 global reanalysis: Preliminary extension to 1950". In: *Quarterly Journal of the Royal Meteorological Society* 147.741, pp. 4186–4227.

Belmonte Rivas, Maria and Ad Stoffelen (2019). "Characterizing ERA-Interim and ERA5 surface wind biases using ASCAT". In: *Ocean Science* 15.3, pp. 831–852.

Benedetti, Angela and Frédéric Vitart (2018). "Can the direct effect of aerosols improve subseasonal predictability?" In: *Monthly Weather Review* 146.10, pp. 3481–3498.

Bergen, Arthur R (2009). *Power systems analysis*. Pearson Education India.

Bett, Philip and Hazel Thornton (2016). "The climatological relationships between wind and solar energy supply in Britain". In: *Renewable Energy* 87, pp. 96–110.

Bett, Philip E, Hazel E Thornton, Julia F Lockwood, Adam A Scaife, Nicola Golding, Chris Hewitt, Rong Zhu, Peiqun Zhang, and Chaofan Li (2017). "Skill and reliability of seasonal forecasts for the Chinese energy sector". In: *Journal of Applied Meteorology and Climatology* 56.11, pp. 3099–3114.

Bett, Philip E, Hazel E Thornton, Alberto Troccoli, Matteo De Felice, Emma Suckling, Laurent Dubus, Yves-Marie Saint-Drenan, and David J Brayshaw (2022). "A simplified seasonal forecasting strategy, applied to wind and solar power in Europe". In: *Climate services* 27, p. 100318.

Bhattacharya, Subhadip, Rangan Banerjee, Ariel Liebman, and Roger Dargaville (2022). "Analysing the impact of lockdown due to the COVID-19 pandemic on the Indian electricity sector". In: *International Journal of Electrical Power & Energy Systems* 141, p. 108097.

Bhattacharya, Subhadip, Rangan Banerjee, Venkatasailanathan Ramadesigan, Ariel Liebman, and Roger Dargaville (2024). "Bending the emission curve—The role of renewables and nuclear power in achieving a net-zero power system in India". In: *Renewable and Sustainable Energy Reviews* 189, p. 113954.

Bianchi, Emilio, Tomás Guozden, and Roberto Kozulj (2022). "Assessing low frequency variations in solar and wind power and their climatic teleconnections". In: *Renewable Energy* 190, pp. 560–571.

Bistline, John (2021). "Variability in deeply decarbonized electricity systems". In: *Environmental Science & Technology* 55.9, pp. 5629–5635.

Bistline, John, Geoffrey Blanford, Trieu Mai, and James Merrick (2021). "Modeling variable renewable energy and storage in the power sector". In: *Energy Policy* 156, p. 112424.

Bjerknes, Jakob (1969). "Atmospheric teleconnections from the equatorial Pacific". In: *Monthly Weather Review* 97.3, pp. 163–172.

Blanco, Herib and André Faaij (2018). "A review at the role of storage in energy systems with a focus on Power to Gas and long-term storage". In: *Renewable and Sustainable Energy Reviews* 81, pp. 1049–1086.

Blandford, HF (1886). "Rainfall of India, mem". In: *India Meteorological Department* 2, pp. 217–448.

Blanford, Henry Francis (1884). "II. On the connexion of the Himalaya snowfall with dry winds and seasons of drought in India". In: *Proceedings of the Royal Society of London* 37.232-234, pp. 3–22.

Bloomfield, Hannah and David Brayshaw (2021). *ERA5 derived time series of European aggregated surface weather variables, wind power, and solar power capacity factors: hourly data from 1950-2020*. University of Reading.

Bloomfield, Hannah C, David J Brayshaw, and Andrew J Charlton-Perez (2020). "Characterizing the winter meteorological drivers of the European electricity system using targeted circulation types". In: *Meteorological Applications* 27.1, e1858.

Bloomfield, Hannah C, Caroline M Wainwright, and Nick Mitchell (2022). "Characterizing the variability and meteorological drivers of wind power and solar power generation over Africa". In: *Meteorological Applications* 29.5, e2093.

Bloomfield, HC, DJ Brayshaw, Alberto Troccoli, CM Goodess, Matteo De Felice, Laurent Dubus, PE Bett, and Y-M Saint-Drenan (2021). "Quantifying the sensitivity of eEropean power systems to energy scenarios and climate change projections". In: *Renewable Energy* 164, pp. 1062–1075.

Bojovic, Dragana, Andria Nicodemou, Asun Lera St. Clair, Isadora Christel, and Francisco J Doblas-Reyes (2022). "Exploring the landscape of seasonal forecast provision by Global Producing Centres". In: *Climatic Change* 172.1, p. 8.

Bollasina, Massimo A, Yi Ming, and V Ramaswamy (2011). "Anthropogenic aerosols and the weakening of the South Asian summer monsoon". In: *Science* 334.6055, pp. 502–505.

Boopathi, K, S Ramaswamy, V Kirubakaran, K Uma, G Saravanan, S Thyagaraj, and K Balaraman (2021). "Economic investigation of repowering of the existing wind farms with hybrid wind and solar power plants: a case study". In: *International Journal of Energy and Environmental Engineering* 12, pp. 855–871.

Bosch, Jonathan, Iain Staffell, and Adam D Hawkes (2018). "Temporally explicit and spatially resolved global offshore wind energy potentials". In: *Energy* 163, pp. 766–781.

Bozzo, A, S Remy, Angela Benedetti, J Flemming, P Bechtold, MJ Rodwell, and Jean-Jacques Morcrette (2017). *Implementation of a CAMS-based aerosol climatology in the IFS*. Vol. 801. European Centre for Medium-Range Weather Forecasts Reading, UK.

Brayshaw, David James, Alberto Troccoli, Rachael Fordham, and John Methven (2011). "The impact of large scale atmospheric circulation patterns on wind power generation and its potential predictability: A case study over the UK". In: *Renewable Energy* 36.8, pp. 2087–2096.

BridgetoIndia (2022). *India Solar Rooftop Map December 2021*. Online. Available at: `https://bridgetoindia.com/backend/wp-content/uploads/2022/04/BRIDGE-TO-INDIA-India-Solar-Rooftop-Map-December-2021.pdf` Accessed: 22nd November 2022.

Brown Weiss, Edith (1982). "The value of seasonal climate forecasts in managing energy resources". In: *Journal of Applied Meteorology and Climatology* 21.4, pp. 510–517.

Buizza, Roberto (2019). "Introduction to the special issue on "25 years of ensemble forecasting"". In: *Quarterly Journal of the Royal Meteorological Society* 145, pp. 1–11.

Buontempo, Carlo, Samantha N Burgess, Dick Dee, Bernard Pinty, Jean-Noël Thépaut, Michel Rixen, Samuel Almond, David Armstrong, Anca Brookshaw, Angel Lopez Alos, et al. (2022). "The Copernicus Climate Change Service: Climate Science in Action". In: *Bulletin of the American Meteorological Society* 103.12, E2669–E2687.

Byers, Edward et al. (2022). *AR6 Scenarios Database*. International Institute for Applied Systems Analysis.

Camargo, Luis Ramirez and Johannes Schmidt (2020). "Simulation of multi-annual time series of solar photovoltaic power: Is the ERA5-land reanalysis the next big step?" In: *Sustainable Energy Technologies and Assessments* 42, p. 100829.

Canadell, Josep G, Pedro MS Monteiro, Marcos H Costa, Leticia Cotrim Da Cunha, Peter M Cox, Alexey V Eliseev, Stephanie Henson, Masao Ishii, Samuel Jaccard, Charles Koven, et al. (2021). "Global carbon and other biogeochemical cycles and feedbacks". In: *Climate Change 2021 – The Physical Science Basis*. Cambridge University Press, pp. 673–815.

Cane, Mark A, Stephen E Zebiak, and Sean C Dolan (1986). "Experimental forecasts of EL Nino". In: *Nature* 321.6073, pp. 827–832.

Cannon, Dirk J, David J Brayshaw, John Methven, Phil J Coker, and D Lenaghan (2015). "Using reanalysis data to quantify extreme wind power generation statistics: A 33 year case study in Great Britain". In: *Renewable Energy* 75, pp. 767–778.

CarbonBrief (2015). *The Carbon Brief Interview: Dr Hoesung Lee*. Online. Available at: `https://www.carbonbrief.org/the-carbon-brief-interview-dr-hoesung-lee/` Accessed: 11th September 2021.

Carroll, James, Alasdair McDonald, Iain Dinwoodie, David McMillan, Matthew Revie, and Iraklis Lazakis (2017). "Availability, operation and maintenance costs of offshore wind turbines with different drive train configurations". In: *Wind Energy* 20.2, pp. 361–378.

Carta, José A, Sergio Velázquez, and Pedro Cabrera (2013). "A review of measure-correlate-predict (MCP) methods used to estimate long-term wind characteristics at a target site". In: *Renewable and Sustainable Energy Reviews* 27, pp. 362–400.

CEA (2022). *Central Energy Authority: Renewable Project Monitoring Division*. Online. Available at: `https://cea.nic.in/renewable-project-monitoring/?lang=en` Accessed: 22nd November 2022.

– (2023). *Report on Optimal Generation Capacity Mix For 2029-30*. New Delhi, India: Central Electricity Agency.

– (2024). *Report on under construction Renewable Energy Projects*. Online. Available at: `https://cea.nic.in/quarterly-report/?lang=en` Accessed: 20th January 2024.

CECL (2020). *Consolidated Energy Consultants Limited. Directory of Indian Windpower 2020*.

– (2022). *Consolidated Energy Consultants Limited. Directory of Indian Windpower 2022*.

Changnon, David and Stanley A Changnon (2010). "Major growth in some business-related uses of climate information". In: *Journal of Applied Meteorology and Climatology* 49.3, pp. 325–331.

Changnon, Stanley A, Joyce M Changnon, and David Changnon (1995). "Uses and applications of climate forecasts for power utilities". In: *Bulletin of the American Meteorological Society* 76.5, pp. 711–720.

Charney, Jg G and J Shukla (1981). "Predictability of monsoons". In: *Monsoon dynamics*, pp. 99–110.

Charney, Jule G (1969). "A further note on large-scale motions in the tropics". In: *Journal of Atmospheric Sciences* 26.1, pp. 182–185.

Che, Huizheng, Ke Gui, Xiangao Xia, Yaqiang Wang, Brent N Holben, Philippe Goloub, Emilio Cuevas-Agulló, Hong Wang, Yu Zheng, Hujia Zhao, et al. (2019). "Large contribution of meteorological factors to inter-decadal changes in regional aerosol optical depth". In: *Atmospheric Chemistry and Physics* 19.16, pp. 10497–10523.

Cherchi, Annalisa, Pascal Terray, Satyaban B Ratna, Syam Sankar, KP Sooraj, and Swadhin Behera (2021). "Indian Ocean Dipole influence on Indian summer monsoon and ENSO: A review". In: *Indian summer monsoon variability*, pp. 157–182.

Chevuturi, Amulya, Andrew G Turner, Stephanie Johnson, Antje Weisheimer, Jonathan KP Shonk, Timothy N Stockdale, and Retish Senan (2021). "Forecast skill of the Indian monsoon and its onset in the ECMWF seasonal forecasting system 5 (SEAS5)". In: *Climate Dynamics* 56, pp. 2941–2957.

Chiacchio, Marc and Martin Wild (2010). "Influence of NAO and clouds on long-term seasonal variations of surface solar radiation in Europe". In: *Journal of Geophysical Research: Atmospheres* 115.D10.

Chowdary, JS, Nisha John, and C Gnanaseelan (2014). "Interannual variability of surface air-temperature over India: impact of ENSO and Indian Ocean Sea surface temperature". In: *International Journal of Climatology* 34.2, pp. 416–429.

Chowdary, JS, Shang-Ping Xie, June-Yi Lee, Yu Kosaka, and Bin Wang (2010). "Predictability of summer northwest Pacific climate in 11 coupled model hindcasts: Local and remote forcing". In: *Journal of Geophysical Research: Atmospheres* 115.D22.

Chu, Cheng-Ta and Adam D Hawkes (2020). "A geographic information system-based global variable renewable potential assessment using spatially resolved simulation". In: *Energy* 193, p. 116630.

Chung, Pei-Hsuan, Chung-Hsiung Sui, and Tim Li (2011). "Interannual relationships between the tropical sea surface temperature and summertime subtropical anticyclone over the western North Pacific". In: *Journal of Geophysical Research: Atmospheres* 116.D13.

Cionni, Irene, Jaume Ramon, Llorenc Lledo, Harilaos Loukos, and Thomas Noel (2017). *Validation of observational dataset and recommendations to the energy users. Deliverable D3.1.* Tech. rep. European Commission.

Clark, Robin T, Philip E Bett, Hazel E Thornton, and Adam A Scaife (2017). "Skilful seasonal predictions for the European energy industry". In: *Environmental Research Letters* 12.2, p. 024002.

Clarke, L et al. (2014). "Chapter 6 - Assessing Transformation Pathways". In: *Climate Change 2014: Mitigation of Climate Change. Contribution of Working Group III to the Fifth Assessment Report of the Intergovernmental Panel on Climate Change*. Cambridge University Press.

Clarke, Leon, Yi-Ming Wei, Angel de la Vega Navarro, Amit Garg, Andrea N Hahmann, Smail Khennas, Inês ML Azevedo, Andreas Löschel, Ajay Kumar Singh, Linda Steg, et al. (2022). "Energy Systems". In: *Climate Change 2022: Mitigation of Climate Change. Contribution of Working Group III to the Sixth Assessment Report of the Intergovernmental Panel on Climate Change*. Cambridge University Press.

Clift, Peter D and R Alan Plumb (2008). *The Asian monsoon: causes, history and effects.* Vol. 288. Cambridge University Press Cambridge.

Clifton, A, MH Daniels, and M Lehning (2014). "Effect of winds in a mountain pass on turbine performance". In: *Wind Energy* 17.10, pp. 1543–1562.

Colantuono, Giuseppe, Yimin Wang, Edward Hanna, and Robert Erdélyi (2014). "Signature of the North Atlantic Oscillation on British solar radiation availability and PV potential: The winter zonal seesaw". In: *Solar Energy* 107, pp. 210–219.

Commin, Andrew N, Andrew S French, Matteo Marasco, Jennifer Loxton, Stuart W Gibb, and John McClatchey (2017). "The influence of the North Atlantic Oscillation on diverse renewable generation in Scotland". In: *Applied Energy* 205, pp. 855–867.

Cradden, Lucy C, Frank McDermott, Laura Zubiate, Conor Sweeney, and Mark O'Malley (2017). "A 34-year simulation of wind generation potential for Ireland and the impact of large-scale atmospheric pressure patterns". In: *Renewable Energy* 106, pp. 165–176.

CSTEP (2016). *Re-assessment of India's On-shore Wind Power Potential*. Online. Available at: `https://cstep.in/drupal/sites/default/files/2019-01/CSTEP_RR_Re-assessment_of_India's_On-shore_Wind_Power_Potential_2016.pdf` Accessed: 11th September 2021.

Curtis, John, Muireann Á Lynch, and Laura Zubiate (2016). "The impact of the North Atlantic Oscillation on electricity markets: A case study on Ireland". In: *Energy Economics* 58, pp. 186–198.

Dai, Aiguo and Clara Deser (1999). "Diurnal and semidiurnal variations in global surface wind and divergence fields". In: *Journal of Geophysical Research: Atmospheres* 104.D24, pp. 31109–31125.

Das, Aheli and Somnath Baidya Roy (2021). "Evaluation of subseasonal to seasonal forecasts over India for renewable energy applications". In: *Advances in Geosciences* 56, pp. 89–96.

Das, Binit (2023). *Repowering Wind Farms: Maximizing energy yield from existing site layouts*. New Delhi, India: Centre for Science and Environment.

Davidson, Michael R and Dev Millstein (2022). "Limitations of reanalysis data for wind power applications". In: *Wind Energy* 25.9, pp. 1646–1653.

Davy, Robert J and Alberto Troccoli (2012). "Interannual variability of solar energy generation in Australia". In: *Solar Energy* 86.12, pp. 3554–3560.

De Felice, Matteo, Andrea Alessandri, and Franco Catalano (2015). "Seasonal climate forecasts for medium-term electricity demand forecasting". In: *Applied Energy* 137, pp. 435–444.

De Felice, Matteo, Marta Bruno Soares, Andrea Alessandri, and Alberto Troccoli (2019). "Scoping the potential usefulness of seasonal climate forecasts for solar power management". In: *Renewable Energy* 142, pp. 215–223.

De Sisternes, Fernando J, Jesse D Jenkins, and Audun Botterud (2016). "The value of energy storage in decarbonizing the electricity sector". In: *Applied Energy* 175, pp. 368–379.

Decker, Mark, Michael A. Brunke, Zhuo Wang, Koichi Sakaguchi, Xubin Zeng, and Michael G. Bosilovich (2012). "Evaluation of the Reanalysis Products from GSFC, NCEP, and ECMWF Using Flux Tower Observations". In: *Journal of Climate* 25 (6), pp. 1916–1944.

DelSole, Timothy, Jyothi Nattala, and Michael K Tippett (2014). "Skill improvement from increased ensemble size and model diversity". In: *Geophysical Research Letters* 41.20, pp. 7331–7342.

Denholm, Paul, Maureen Hand, Maddalena Jackson, and Sean Ong (2009). *Land use requirements of modern wind power plants in the United States*. Tech. rep. National Renewable Energy Lab.(NREL), Golden, CO (United States).

Denholm, Paul and Trieu Mai (2019). "Timescales of energy storage needed for reducing renewable energy curtailment". In: *Renewable Energy* 130, pp. 388–399.

UN-DESA (2023). *UN DESA Policy Brief No. 153: India overtakes China as the world's most populous country.* Online. Available at: `https://www.un.org/development/desa/dpad/wp-content/uploads/sites/45/PB153.pdf` Accessed: 15th May 2023.

Deshmukh, Ranjit, Grace C Wu, Duncan S Callaway, and Amol Phadke (2019). "Geospatial and techno-economic analysis of wind and solar resources in India". In: *Renewable Energy* 134, pp. 947–960.

Dey, Sagnik and Larry Di Girolamo (2011). "A decade of change in aerosol properties over the Indian subcontinent". In: *Geophysical Research Letters* 38.14.

Di Capua, Giorgia, M Kretschmer, J Runge, A Alessandri, RV Donner, B van Den Hurk, R Vellore, R Krishnan, and D Coumou (2019). "Long-lead statistical forecasts of the Indian summer monsoon rainfall based on causal precursors". In: *Weather and Forecasting* 34.5, pp. 1377–1394.

Doblas-Reyes, FJ, R Hagedorn, TN Palmer, and J-J Morcrette (2006). "Impact of increasing greenhouse gas concentrations in seasonal ensemble forecasts". In: *Geophysical Research Letters* 33.7.

Doblas-Reyes, Francisco J, Javier García-Serrano, Fabian Lienert, Aida Pintó Biescas, and Luis RL Rodrigues (2013). "Seasonal climate predictability and forecasting: status and prospects". In: *Wiley Interdisciplinary Reviews: Climate Change* 4.4, pp. 245–268.

Doblas-Reyes, Francisco J, Renate Hagedorn, and TN Palmer (2005). "The rationale behind the success of multi-model ensembles in seasonal forecasting—II. Calibration and combination". In: *Tellus A: Dynamic Meteorology and Oceanography* 57.3, pp. 234–252.

Dörenkämper, Martin, Bjarke T Olsen, Björn Witha, Andrea N Hahmann, Neil N Davis, Jordi Barcons, Yasemin Ezber, Elena García-Bustamante, J Fidel González-Rouco, Jorge Navarro,

et al. (2020). “The making of the new European wind atlas–part 2: Production and evaluation”. In: *Geoscientific Model Development* 13.10, pp. 5079–5102.

Dowling, Jacqueline A, Katherine Z Rinaldi, Tyler H Ruggles, Steven J Davis, Mengyao Yuan, Fan Tong, Nathan S Lewis, and Ken Caldeira (2020). “Role of long-duration energy storage in variable renewable electricity systems”. In: *Joule* 4.9, pp. 1907–1928.

Drew, Daniel R, Dirk J Cannon, David J Brayshaw, Janet F Barlow, and Phil J Coker (2015). “The impact of future offshore wind farms on wind power generation in Great Britain”. In: *Resources* 4.1, pp. 155–171.

Du, Yan, Shang-Ping Xie, Gang Huang, and Kaiming Hu (2009). “Role of air–sea interaction in the long persistence of El Niño–induced north Indian Ocean warming”. In: *Journal of Climate* 22.8, pp. 2023–2038.

Dubus, Laurent, Shylesh Muralidharan, and Alberto Troccoli (2018). “What does the energy industry require from meteorology?” In: *Weather & Climate Services for the Energy Industry*, pp. 41–63.

Dunn, Robert JH, Cesar Azorin-Molina, Matthew J Menne, Zhenzhong Zeng, Nancy W Casey, and Cheng Shen (2022). “Reduction in reversal of global stilling arising from correction to encoding of calm periods”. In: *Environmental Research Communications* 4.6, p. 061003.

Dunnett, Sebastian, Alessandro Sorichetta, Gail Taylor, and Felix Eigenbrod (2020). “Harmonised global datasets of wind and solar farm locations and power”. In: *Scientific Data* 7.1, pp. 1–12.

Dunning, CM, AG Turner, and DJ Brayshaw (2015). “The impact of monsoon intraseasonal variability on renewable power generation in India”. In: *Environmental Research Letters* 10.6, p. 064002.

Dunstone, Nick, Doug Smith, Adam Scaife, Leon Hermanson, Rosie Eade, Niall Robinson, Martin Andrews, and Jeff Knight (2016). “Skilful predictions of the winter North Atlantic Oscillation one year ahead”. In: *Nature Geoscience* 9.11, pp. 809–814.

Dunstone, Nick, Doug M Smith, Steven C Hardiman, Paul Davies, Sarah Ineson, Shipra Jain, Chris Kent, Gill Martin, and Adam A Scaife (2023). “Windows of opportunity for predicting seasonal climate extremes highlighted by the Pakistan floods of 2022”. In: *Nature Communications* 14.1, p. 6544.

Eade, Rosie, Doug Smith, Adam Scaife, Emily Wallace, Nick Dunstone, Leon Hermanson, and Niall Robinson (2014). "Do seasonal-to-decadal climate predictions underestimate the predictability of the real world?" In: *Geophysical Research Letters* 41.15, pp. 5620–5628.

Earl, Nick, Steve Dorling, Richard Hewston, and Roland Von Glasow (2013). "1980–2010 variability in UK surface wind climate". In: *Journal of Climate* 26.4, pp. 1172–1191.

ECIU (2022). *Net Zero Tracker*. Online. Available at: https://eciu.net/netzerotracker Accessed: 3rd April 2023.

ECMWF (2015). *Radiation Quantities in the ECMWF model and MARS*. Online. `https://www.ecmwf.int/sites/default/files/elibrary/2015/18490-radiation-quantities-ecmwf-model-and-mars.pdf` Accessed: 12th September 2022.

– (2019). *Global reanalysis: goodbye ERA-Interim, hello ERA5*. Online. `https://www.ecmwf.int/en/newsletter/159/meteorology/global-reanalysis-goodbye-era-interim-hello-era5` Accessed: 18th September 2022.

– (2021). *SEAS5 user guide Version 1.2*. European Centre for Medium-Range Weather Forecasts. Online. `https://www.ecmwf.int/sites/default/files/elibrary/2021/81237-seas5-user-guide_1.pdf` Accessed: 18th September 2022.

EIA (2021). *Electric Power Monthly - Table 6.2.B. Net Summer Capacity Using Primarily Renewable Energy Sources and by State*. Online. Available at: `www.eia.gov/electricity/monthly/epm_table_grapher.php?t=epmt_6_02_b`. Accessed: 17th December 2021.

Elliston, Ben, Mark Diesendorf, and Iain MacGill (2012). "Simulations of scenarios with 100% renewable electricity in the Australian National Electricity Market". In: *Energy Policy* 45, pp. 606–613.

Ely, Caroline R, David J Brayshaw, John Methven, James Cox, and Oliver Pearce (2013). "Implications of the North Atlantic Oscillation for a UK–Norway renewable power system". In: *Energy Policy* 62, pp. 1420–1427.

Emeis, Stefan (2018). *Wind energy meteorology: atmospheric physics for wind power generation*. Springer.

Enevoldsen, Peter and Mark Z Jacobson (2021). "Data investigation of installed and output power densities of onshore and offshore wind turbines worldwide". In: *Energy for Sustainable Development* 60, pp. 40–51.

Engeland, Kolbjørn, Marco Borga, Jean-Dominique Creutin, Baptiste François, Maria-Helena Ramos, and Jean-Philippe Vidal (2017). "Space-time variability of climate variables and in-

termittent renewable electricity production–A review". In: *Renewable and Sustainable Energy Reviews* 79, pp. 600–617.

Eurek, Kelly, Patrick Sullivan, Michael Gleason, Dylan Hettinger, Donna Heimiller, and Anthony Lopez (2017). "An improved global wind resource estimate for integrated assessment models". In: *Energy Economics* 64, pp. 552–567.

Fan, Fangxing, Michael E Mann, Sukyoung Lee, and Jenni L Evans (2010). "Observed and modeled changes in the South Asian summer monsoon over the historical period". In: *Journal of Climate* 23.19, pp. 5193–5205.

Fant, Charles, Bhaskar Gunturu, and Adam Schlosser (2016). "Characterizing wind power resource reliability in southern Africa". In: *Applied Energy* 161, pp. 565–573.

Fasullo, John (2004). "A stratified diagnosis of the Indian monsoon—Eurasian snow cover relationship". In: *Journal of Climate* 17.5, pp. 1110–1122.

Fattori, Fabrizio, Norma Anglani, Iain Staffell, and Stefan Pfenninger (2017). "High solar photovoltaic penetration in the absence of substantial wind capacity: storage requirements and effects on capacity adequacy". In: *Energy* 137, pp. 193–208.

Faulstich, Stefan, Berthold Hahn, and Peter J Tavner (2011). "Wind turbine downtime and its importance for offshore deployment". In: *Wind Energy* 14.3, pp. 327–337.

Ferranti, L, JM Slingo, TN Palmer, and BJ Hoskins (1997). "Relations between interannual and intraseasonal monsoon variability as diagnosed from AMIP integrations". In: *Quarterly Journal of the Royal Meteorological Society* 123.541, pp. 1323–1357.

Fichefet, Thierry and MA Morales Maqueda (1997). "Sensitivity of a global sea ice model to the treatment of ice thermodynamics and dynamics". In: *Journal of Geophysical Research: Oceans* 102.C6, pp. 12609–12646.

Findlater, J (1969). "A major low-level air current near the Indian Ocean during the northern summer". In: *Quarterly Journal of the Royal Meteorological Society* 95.404, pp. 362–380.

Flemming, Johannes, Angela Benedetti, Antje Inness, Richard J Engelen, Luke Jones, Vincent Huijnen, Samuel Remy, Mark Parrington, Martin Suttie, Alessio Bozzo, et al. (2017). "The CAMS interim reanalysis of carbon monoxide, ozone and aerosol for 2003–2015". In: *Atmospheric Chemistry and Physics* 17.3, pp. 1945–1983.

Flemming, Johannes, Samuel Remy, Robin Hogan, Vincent Huijnen, Thomas Haiden, Zak Kipling, Mark Parrington, Antje Inness, and Sebastien Garrigues (2022). "The impact of

CAMS prognostic aerosols on temperature forecast with the ECMWF weather forecast model". In: *EGU General Assembly Conference Abstracts*, EGU22–12175.

Foley, Aoife M, Paul G Leahy, Antonino Marvuglia, and Eamon J McKeogh (2012). "Current methods and advances in forecasting of wind power generation". In: *Renewable Energy* 37.1, pp. 1–8.

FOWIND (2018). *Feasibility Study for Offshore Wind Farm Development In Tamil Nadu*. Tech. rep. FOWIND.

François, B (2016). "Influence of winter North-Atlantic oscillation on climate-related-energy penetration in Europe". In: *Renewable Energy* 99, pp. 602–613.

Frank, Christopher, Stephanie Fiedler, and Susanne Crewell (2021). "Balancing potential of natural variability and extremes in photovoltaic and wind energy production for European countries". In: *Renewable Energy* 163, pp. 674–684.

Frank, Christopher, Sabrina Wahl, Jan D Keller, Bernhard Pospichal, Andreas Hense, and Susanne Crewell (2018). "Bias correction of a novel European reanalysis data set for solar energy applications". In: *Solar Energy* 164, pp. 12–24.

Freire, Julliana LM, Karla M Longo, Saulo R Freitas, Caio AS Coelho, Andrea M Molod, Jelena Marshak, Arlindo da Silva, and Bruno Z Ribeiro (2020). "To what extent biomass burning aerosols impact South America seasonal climate predictions?" In: *Geophysical Research Letters* 47.16, e2020GL088096.

Funk, Chris, Pete Peterson, Martin Landsfeld, Diego Pedreros, James Verdin, Shraddhanand Shukla, Gregory Husak, James Rowland, Laura Harrison, Andrew Hoell, et al. (2015). "The climate hazards infrared precipitation with stations—a new environmental record for monitoring extremes". In: *Scientific data* 2.1, pp. 1–21.

Gadgil, Sulochana (2003). "The Indian monsoon and its variability". In: *Annual Review of Earth and Planetary Sciences* 31.1, pp. 429–467.

Gadgil, Sulochana, PN Vinayachandran, PA Francis, and Siddhartha Gadgil (2004). "Extremes of the Indian summer monsoon rainfall, ENSO and equatorial Indian Ocean oscillation". In: *Geophysical Research Letters* 31.12.

Gangopadhyay, Anasuya, Ashwin K Seshadri, and Ralf Toumi (2023). "Beneficial role of diurnal smoothing for grid integration of wind power". In: *Environmental Research Letters* 18.1, p. 014022.

Gao, Meng, Yihui Ding, Shaojie Song, Xiao Lu, Xinyu Chen, and Michael B McElroy (2018). "Secular decrease of wind power potential in India associated with warming in the Indian Ocean". In: *Science Advances* 4.12, eaat5256.

García-Morales, Marta Benito and Laurent Dubus (2007). "Forecasting precipitation for hydroelectric power management: how to exploit GCM's seasonal ensemble forecasts". In: *International Journal of Climatology* 27.12, pp. 1691–1705.

Gautam, Ritesh, NC Hsu, K-M Lau, S-C Tsay, and Menas Kafatos (2009). "Enhanced premonsoon warming over the Himalayan-Gangetic region from 1979 to 2007". In: *Geophysical Research Letters* 36.7.

Gelaro, Ronald, Will McCarty, Max J Suárez, Ricardo Todling, Andrea Molod, Lawrence Takacs, Cynthia A Randles, Anton Darmenov, Michael G Bosilovich, Rolf Reichle, et al. (2017). "The modern-era retrospective analysis for research and applications, version 2 (MERRA-2)". In: *Journal of Climate* 30.14, pp. 5419–5454.

Ghosh, Sushovan, Sagnik Dey, Dilip Ganguly, Somnath Baidya Roy, and Kunal Bali (2022). "Cleaner air would enhance India's annual solar energy production by 6–28 TWh". In: *Environmental Research Letters* 17.5, p. 054007.

Giese, Benjamin S and Sulagna Ray (2011). "El Niño variability in simple ocean data assimilation (SODA), 1871–2008". In: *Journal of Geophysical Research: Oceans* 116.C2.

Gillett, Nathan P, Vivek K Arora, Damon Matthews, and Myles R Allen (2013). "Constraining the ratio of global warming to cumulative CO2 emissions using CMIP5 simulations". In: *Journal of Climate* 26.18, pp. 6844–6858.

Glahn, Harry R and Dale A Lowry (1972). "The use of model output statistics (MOS) in objective weather forecasting". In: *Journal of Applied Meteorology and Climatology* 11.8, pp. 1203–1211.

Goddard, Lisa, A Kumar, A Solomon, D Smith, G Boer, P Gonzalez, V Kharin, W Merryfield, Clara Deser, Simon J Mason, et al. (2013). "A verification framework for interannual-to-decadal predictions experiments". In: *Climate Dynamics* 40, pp. 245–272.

Goddard, Lisa, Simon J Mason, Stephen E Zebiak, Chester F Ropelewski, Reid Basher, and Mark A Cane (2001). "Current approaches to seasonal to interannual climate predictions". In: *International Journal of Climatology* 21.9, pp. 1111–1152.

Gong, SL (2003). "A parameterization of sea-salt aerosol source function for sub-and super-micron particles". In: *Global Biogeochemical Cycles* 17.4.

González, Javier Serrano, Manuel Burgos Payán, Jesús Manuel Riquelme Santos, and Francisco González-Longatt (2014). "A review and recent developments in the optimal wind-turbine micro-siting problem". In: *Renewable and Sustainable Energy Reviews* 30, pp. 133–144.

Gonzalez-Aparicio, Iratxe, Fabio Monforti, Patrick Volker, Andreas Zucker, Francesco Careri, Thomas Huld, and Jake Badger (2017). "Simulating European wind power generation applying statistical downscaling to reanalysis data". In: *Applied Energy* 199, pp. 155–168.

Goswami, Bhupendra Nath and RS Ajaya Mohan (2001). "Intraseasonal oscillations and interannual variability of the Indian summer monsoon". In: *Journal of Climate* 14.6, pp. 1180–1198.

Goswami, Bhupendra Nath, Guoxiong Wu, and T Yasunari (2006). "The annual cycle, intraseasonal oscillations, and roadblock to seasonal predictability of the Asian summer monsoon". In: *Journal of Climate* 19.20, pp. 5078–5099.

Goswami, Bhupendra Nath and Prince K Xavier (2005). "Dynamics of "internal" interannual variability of the Indian summer monsoon in a GCM". In: *Journal of Geophysical Research: Atmospheres* 110.D24.

Goswami, BN, Deepayan Chakraborty, PV Rajesh, and Adway Mitra (2022). "Predictability of South-Asian monsoon rainfall beyond the legacy of Tropical Ocean Global Atmosphere program (TOGA)". In: *npj Climate and Atmospheric Science* 5.1, p. 58.

Grams, Christian M, Remo Beerli, Stefan Pfenninger, Iain Staffell, and Heini Wernli (2017). "Balancing Europe's wind-power output through spatial deployment informed by weather regimes". In: *Nature Climate Change* 7.8, pp. 557–562.

Gruber, Katharina, Claude Klöckl, Peter Regner, Johann Baumgartner, and Johannes Schmidt (2019). "Assessing the Global Wind Atlas and local measurements for bias correction of wind power generation simulated from MERRA-2 in Brazil". In: *Energy* 189, p. 116212.

Gruber, Katharina, Peter Regner, Sebastian Wehrle, Marianne Zeyringer, and Johannes Schmidt (2022). "Towards global validation of wind power simulations: A multi-country assessment of wind power simulation from MERRA-2 and ERA-5 reanalyses bias-corrected with the global wind atlas". In: *Energy* 238, p. 121520.

Gualtieri, G (2022). "Analysing the uncertainties of reanalysis data used for wind resource assessment: A critical review". In: *Renewable and Sustainable Energy Reviews* 167, p. 112741.

Gulagi, Ashish, Manish Ram, Dmitrii Bogdanov, Sandeep Sarin, Theophilus Nii Odai Mensah, and Christian Breyer (2022). "The role of renewables for rapid transitioning of the power sector across states in India". In: *Nature Communications* 13.1, p. 5499.

Gulagi, Ashish, Manish Ram, and Christian Breyer (2020). "Role of the transmission grid and solar wind complementarity in mitigating the monsoon effect in a fully sustainable electricity system for India". In: *IET Renewable Power Generation* 14.2, pp. 254–262.

Gulev, Sergey K, Peter W Thorne, Jinho Ahn, Frank J Dentener, Catia M Domingues, Sebastian Gerland, Daoyi Gong, Darrell S Kaufman, Hyacinth C Nnamchi, Johannes Quaas, et al. (2021). "Changing state of the climate system". In: *Climate Change 2021 – The Physical Science Basis*. Cambridge University Press, pp. 287–422.

Guo, Liang, Andrew G Turner, and Eleanor J Highwood (2015). "Impacts of 20th century aerosol emissions on the South Asian monsoon in the CMIP5 models". In: *Atmospheric Chemistry and Physics* 15.11, pp. 6367–6378.

Gutiérrez, José M, Daniel San-Martín, Swen Brands, R Manzanas, and S Herrera (2013). "Reassessing statistical downscaling techniques for their robust application under climate change conditions". In: *Journal of Climate* 26.1, pp. 171–188.

Gütschow, Johannes, M Louise Jeffery, Annika Günther, and Malte Meinshausen (2021). "Country-resolved combined emission and socio-economic pathways based on the Representative Concentration Pathway (RCP) and Shared Socio-Economic Pathway (SSP) scenarios". In: *Earth System Science Data* 13.3, pp. 1005–1040.

GWEC (2023). *India Wind Energy Market Outlook 2023-2027*. Online. Available at: `https://gwec.net/wp-content/uploads/2023/08/GWEC-India-Outlook-Aug-2023-1.pdf` Accessed: 20th January 2024.

Hadley, George (1735). "VI. Concerning the cause of the general trade-winds". In: *Philosophical Transactions of the Royal Society of London* 39.437, pp. 58–62.

Hagedorn, Renate, Francisco J Doblas-Reyes, and Tim N Palmer (2005). "The rationale behind the success of multi-model ensembles in seasonal forecasting—I. Basic concept". In: *Tellus A: Dynamic Meteorology and Oceanography* 57.3, pp. 219–233.

Hahn, Douglas G and J Shukla (1976). "An apparent relationship between Eurasian snow cover and Indian monsoon rainfall". In: *Journal of the Atmospheric Sciences* 33.12, pp. 2461–2462.

Haiden, T., Martin Janousek, Jean-Raymond Bidlot, R. Buizza, L. Ferranti, F. Prates, and Frédéric Vitart (2018). "Evaluation of ECMWF forecasts, including the 2018 upgrade". In: *ECMWF Technical Memoranda* 831.

Halley, Edmond (1753). "An historical account of the trade winds, and monsoons, observable in the seas between and near the Tropicks, with an attempt to assign the physical cause of the said winds". In: *Philosophical Transactions of the Royal Society of London* 16.183, pp. 153–168.

Hamlington, BD, PE Hamlington, SG Collins, SR Alexander, and K-Y Kim (2015). "Effects of climate oscillations on wind resource variability in the United States". In: *Geophysical Research Letters* 42.1, pp. 145–152.

Hanley, Deborah E, Mark A Bourassa, James J O'Brien, Shawn R Smith, and Elizabeth R Spade (2003). "A quantitative evaluation of ENSO indices". In: *Journal of Climate* 16.8, pp. 1249–1258.

Hannachi, Abdel, Ian T Jolliffe, and David B Stephenson (2007). "Empirical orthogonal functions and related techniques in atmospheric science: A review". In: *International Journal of Climatology: A Journal of the Royal Meteorological Society* 27.9, pp. 1119–1152.

Hansen, Kenneth, Christian Breyer, and Henrik Lund (2019). "Status and perspectives on 100% renewable energy systems". In: *Energy* 175, pp. 471–480.

Harrison-Atlas, Dylan, Anthony Lopez, and Eric Lantz (2022). "Dynamic land use implications of rapidly expanding and evolving wind power deployment". In: *Environmental Research Letters* 17.4, p. 044064.

Hartmann, Holly C, Thomas C Pagano, Soroosh Sorooshian, and Roger Bales (2002). "Confidence builders: Evaluating seasonal climate forecasts from user perspectives". In: *Bulletin of the American Meteorological Society* 83.5, pp. 683–698.

Hastenrath, Stefan and Leonard Druyan (1993). "Circulation anomaly mechanisms in the tropical Atlantic sector during the Northeast Brazil rainy season: Results from the GISS General Circulation model". In: *Journal of Geophysical Research: Atmospheres* 98.D8, pp. 14917–14923.

Hawkins, S, D Eager, and GP Harrison (2011). "Characterising the reliability of production from future British offshore wind fleets". In: *IET Conference on Renewable Power Generation*.

He, Yanyi, Kaicun Wang, and Fei Feng (2021). "Improvement of ERA5 over ERA-Interim in simulating surface incident solar radiation throughout China". In: *Journal of Climate* 34.10, pp. 3853–3867.

Henao, Felipe, Juan P Viteri, Yeny Rodríguez, Juan Gómez, and Isaac Dyner (2020). "Annual and interannual complementarities of renewable energy sources in Colombia". In: *Renewable and Sustainable Energy Reviews* 134, p. 110318.

Henriksson, SV, A Laaksonen, V-M Kerminen, P Räisänen, H Järvinen, A-M Sundström, and G De Leeuw (2011). "Spatial distributions and seasonal cycles of aerosols in India and China seen in global climate-aerosol model". In: *Atmospheric Chemistry and Physics* 11.15, pp. 7975–7990.

Hersbach, Hans, Bill Bell, Paul Berrisford, Shoji Hirahara, András Horányi, Joaquín Muñoz-Sabater, Julien Nicolas, Carole Peubey, Raluca Radu, Dinand Schepers, et al. (2020). "The ERA5 global reanalysis". In: *Quarterly Journal of the Royal Meteorological Society* 146.730, pp. 1999–2049.

Hill, Cody A, Matthew Clayton Such, Dongmei Chen, Juan Gonzalez, and W Mack Grady (2012). "Battery energy storage for enabling integration of distributed solar power generation". In: *IEEE Transactions on smart grid* 3.2, pp. 850–857.

Hoffmann, Lars, Gebhard Günther, Dan Li, Olaf Stein, Xue Wu, Sabine Griessbach, Yi Heng, Paul Konopka, Rolf Müller, Bärbel Vogel, et al. (2019). "From ERA-Interim to ERA5: the considerable impact of ECMWF's next-generation reanalysis on Lagrangian transport simulations". In: *Atmospheric Chemistry and Physics* 19.5, pp. 3097–3124.

Holmgren, William F, Clifford W Hansen, and Mark A Mikofski (2018). "pvlib python: A python package for modeling solar energy systems". In: *Journal of Open Source Software* 3.29, p. 884.

Holttinen, Hannele (2005). "Impact of hourly wind power variations on the system operation in the Nordic countries". In: *Wind Energy: An International Journal for Progress and Applications in Wind Power Conversion Technology* 8.2, pp. 197–218.

Holttinen, Hannele, J Kiviluoma, N Helistö, T Levy, N Menemenlis, J Liu, et al. (2021). "Design and operation of energy systems with large amounts of variable generation". In: *Final Summary Report, IEA Wind TCP Task 25, VTT Technology* 396.

Holttinen, Hannele, Peter Meibom, Antje Orths, Bernhard Lange, Mark O'Malley, John Olav Tande, Ana Estanqueiro, Emilio Gomez, Lennart Söder, Goran Strbac, et al. (2011). "Impacts

of large amounts of wind power on design and operation of power systems, results of IEA collaboration". In: *Wind Energy* 14.2, pp. 179–192.

Hoogwijk, M (2004). "On the Global and Regional Potential of Renewable Energy Sources." PhD thesis.

Hossain, J and K Raghavan (2021). *Potential for windfarms in India. V.V.N. Kishore (Ed.), Renewable Energy utilization: Scope, Economics and perspectives, 81-85419-01-9.*

Hossain, Jami, Vinay Sinha, and VVN Kishore (2011). "A GIS based assessment of potential for windfarms in India". In: *Renewable Energy* 36.12, pp. 3257–3267.

Hoyos, Carlos D and Peter J Webster (2007). "The role of intraseasonal variability in the nature of Asian monsoon precipitation". In: *Journal of Climate* 20.17, pp. 4402–4424.

Hsu, Wu-ron and Allan H Murphy (1986). "The attributes diagram A geometrical framework for assessing the quality of probability forecasts". In: *International Journal of Forecasting* 2.3, pp. 285–293.

Huang, Boyin, Peter W Thorne, Viva F Banzon, Tim Boyer, Gennady Chepurin, Jay H Lawrimore, Matthew J Menne, Thomas M Smith, Russell S Vose, and Huai-Min Zhang (2017). "Extended reconstructed sea surface temperature, version 5 (ERSSTv5): upgrades, validations, and intercomparisons". In: *Journal of Climate* 30.20, pp. 8179–8205.

Huang, Ronghui, Jilong Chen, Lin Wang, and Zhongda Lin (2012). "Characteristics, processes, and causes of the spatio-temporal variabilities of the East Asian monsoon system". In: *Advances in Atmospheric Sciences* 29, pp. 910–942.

Huang, Yuhong, Xiaodong Liu, Zhi-Yong Yin, and Zhisheng An (2021). "Global impact of ENSO on dust activities with emphasis on the key region from the Arabian Peninsula to Central Asia". In: *Journal of Geophysical Research: Atmospheres* 126.9, e2020JD034068.

Huber, Matthias, Desislava Dimkova, and Thomas Hamacher (2014). "Integration of wind and solar power in Europe: Assessment of flexibility requirements". In: *Energy* 69, pp. 236–246.

Huld, Thomas, Gabi Friesen, Artur Skoczek, Robert P Kenny, Tony Sample, Michael Field, and Ewan D Dunlop (2011). "A power-rating model for crystalline silicon PV modules". In: *Solar Energy Materials and Solar Cells* 95.12, pp. 3359–3369.

Huld, Thomas and Ana M Gracia Amillo (2015). "Estimating PV module performance over large geographical regions: The role of irradiance, air temperature, wind speed and solar spectrum". In: *Energies* 8.6, pp. 5159–5181.

Huld, Thomas, Richard Müller, and Attilio Gambardella (2012). "A new solar radiation database for estimating PV performance in Europe and Africa". In: *Solar Energy* 86.6, pp. 1803–1815.

Huld, Thomas, Marcel Šúri, and Ewan D. Dunlop (2008). "Geographical variation of the conversion efficiency of crystalline silicon photovoltaic modules in Europe". In: *Progress in Photovoltaics: Research and Applications* 16 (7), pp. 595–607.

Hunt, Kieran and Hannah Bloomfield (2023). *Quantifying renewable energy potential and realised capacity in India: opportunities and challenges.* Pre-print. DOI: {10.13140/RG.2.2.18752.20489}.

Hunt, Kieran MR, Andrew G Turner, Peter M Inness, David E Parker, and Richard C Levine (2016). "On the structure and dynamics of Indian monsoon depressions". In: *Monthly Weather Review* 144.9, pp. 3391–3416.

Hurley, John V and William R Boos (2015). "A global climatology of monsoon low-pressure systems". In: *Quarterly Journal of the Royal Meteorological Society* 141.689, pp. 1049–1064.

IEA (2020). *Power systems in transition Challenges and opportunities ahead for electricity security.* Paris, France: IEA.

– (2021). *International Energy Agency Photovoltaic Power Systems Programme (IEA PVPS) Trends in Photovoltaic Applications 2021.* Online. Available at: https://iea-pvps.org/wp-content/uploads/2022/01/IEA-PVPS-Trends-report-2021-4.pdf. Accessed: 22nd November 2022.

– (2022a). *International Energy Agency World Energy Outlook 2022.* Paris, France: IEA.

– (2022b). *Managing Seasonal and Interannual Variability of Renewables.* Paris, France: IEA.

– (2023). *International Energy Agency Renewables 2023, Analysis and forecasts to 2028.* Paris, France: IEA.

– (2024). *Annual variable renewable energy share and corresponding system integration phase in selected countries/regions, 2022.* Online. Available at: https://www.iea.org/data-and-statistics/charts/annual-variable-renewable-energy-share-and-corresponding-system-integration-phase-in-selected-countries-regions-2022 Accessed: 2nd December 2023.

IEEFA (2021). *Viability Assessment of New. Domestic Solar Module Manufacturing Units.* Online. https://ieefa.org/wp-content/uploads/2021/01/Viability-Assessment_New-Domestic-Solar-Module-Manufacturing-Units_January-2021.pdf Accessed: 6th January 2023.

IGES (2022). *Institute for Global Environmental Strategies (IGES) CDM database.* Online. Available at: www.iges.or.jp/en/pub/iges-cdm-project-database/en Accessed: 22nd November 2022.

IMF (2020). *International Monetary Fund World Economic Outlook Database.* Online. Available at: https://www.imf.org/en/Publications/WEO/weo-database/2023/April Accessed: 15th May 2023.

Ineson, S and AA Scaife (2009). "The role of the stratosphere in the European climate response to El Niño". In: *Nature Geoscience* 2.1, pp. 32–36.

Inman, Rich H, Hugo TC Pedro, and Carlos FM Coimbra (2013). "Solar forecasting methods for renewable energy integration". In: *Progress in energy and combustion science* 39.6, pp. 535–576.

IPCC (2022). *Keynote address by the IPCC Chair Hoesung Lee at the opening of the First Technical Dialogue of the Global Stocktake.* Online. Available at: https://www.ipcc.ch/2022/06/10/keynote-address-hoesung-lee-technical-dialogue-global-stocktake/ Accessed: 11th September 2021.

IRENA (2022). *Renewable Power Generation Costs in 2021.* Abu Dhabi: International Renewable Energy Agency.

– (2023a). *Renewable electricity capacity and generation statistics, International Renewable Energy Agency (IRENA).* Online. Available at: https://www.irena.org/Data/Downloads/Tools Accessed: 15th May 2023.

– (2023b). *Renewable Energy and jobs: Annual review 2023.* Abu Dhabi.: International Renewable Energy Agency.

Jain, Deepeshkumar, Suryachandra Rao, Ramu Dandi, Prasanth Pillai, Ankur Srivastava, and Maheshwar Pradhan (2023). "Monsoon Mission Coupled Forecast System Version 2.0: Model Description and Indian Monsoon Simulations". In: *Geoscientific Model Development Discussions* 2023, pp. 1–29.

Jain, Shipra, Adam A Scaife, and Ashis K Mitra (2019). "Skill of Indian summer monsoon rainfall prediction in multiple seasonal prediction systems". In: *Climate Dynamics* 52, pp. 5291–5301.

Jain, Sourabh, Nikunj Kumar Jain, Piyush Choudhary, and William Vaughn (2021). "Designing terawatt scale renewable electricity system: A dynamic analysis for India". In: *Energy Strategy Reviews* 38, p. 100753.

James, Gareth, Daniela Witten, Trevor Hastie, Robert Tibshirani, et al. (2013). *An introduction to statistical learning*. Vol. 112. Springer.

Jaswal, AK and AL Koppar (2013). "Climatology and trends in near-surface wind speed over India during 1961-2008". In: *Mausam* 64.3, pp. 417–436.

Jerez, Sonia, David Barriopedro, Alejandro García-López, Raquel Lorente-Plazas, Andrés M Somoza, Marco Turco, Judit Carrillo, and Ricardo M Trigo (2023). "An Action-Oriented Approach to Make the Most of the Wind and Solar Power Complementarity". In: *Earth's Future* 11.6, e2022EF003332.

Jerez, Sonia, Françoise Thais, Isabelle Tobin, Martin Wild, Augustin Colette, Pascal Yiou, and Robert Vautard (2015). "The CLIMIX model: a tool to create and evaluate spatially-resolved scenarios of photovoltaic and wind power development". In: *Renewable and Sustainable Energy Reviews* 42, pp. 1–15.

Jerez, Sonia and Ricardo M Trigo (2013). "Time-scale and extent at which large-scale circulation modes determine the wind and solar potential in the Iberian Peninsula". In: *Environmental Research Letters* 8.4, p. 044035.

Jin, Qinjian, Zong-Liang Yang, and Jiangfeng Wei (2016). "Seasonal responses of Indian summer monsoon to dust aerosols in the Middle East, India, and China". In: *Journal of Climate* 29.17, pp. 6329–6349.

Johnson, Stephanie J, Timothy N Stockdale, Laura Ferranti, Magdalena A Balmaseda, Franco Molteni, Linus Magnusson, Steffen Tietsche, Damien Decremer, Antje Weisheimer, Gianpaolo Balsamo, et al. (2019). "SEAS5: the new ECMWF seasonal forecast system". In: *Geoscientific Model Development* 12.3, pp. 1087–1117.

Johnson, Stephanie J, Andrew Turner, Steven Woolnough, Gill Martin, and Craig MacLachlan (2017). "An assessment of Indian monsoon seasonal forecasts and mechanisms underlying monsoon interannual variability in the Met Office GloSea5-GC2 system". In: *Climate Dynamics* 48, pp. 1447–1465.

Jolliffe, Ian T and David B Stephenson (2012). *Forecast verification: a practitioner's guide in atmospheric science*. John Wiley & Sons.

Joseph, PV and Anu Simon (2005). "Weakening trend of the southwest monsoon current through peninsular India from 1950 to the present". In: *Current Science*, pp. 687–694.

Joshi, Mohit and Sarah Inskeep (2023). *Institutional Framework of Variable Renewable Energy Forecasting in India*.

Joshi, Mohit, David Palchak, Thushara De Silva, and Gord Stephen (2022). *Reliability and Resiliency in South Asia's Power Sector-Pathways for Research, Modeling, and Implementation.* Tech. rep. National Renewable Energy Lab.(NREL), Golden, CO (United States).

Joskow, Paul L (2011). "Comparing the costs of intermittent and dispatchable electricity generating technologies". In: *American Economic Review* 101.3, pp. 238–241.

Juruš, Pavel, Kryštof Eben, Jaroslav Resler, Pavel Krč, Ivan Kasanickỳ, Emil Pelikán, Marek Brabec, and Jiří Hošek (2013). "Estimating climatological variability of solar energy production". In: *Solar Energy* 98, pp. 255–264.

Kafka, Jennifer L and Mark A Miller (2019). "A climatology of solar irradiance and its controls across the United States: Implications for solar panel orientation". In: *Renewable Energy* 135, pp. 897–907.

Katzenberger, Anja, Jacob Schewe, Julia Pongratz, and Anders Levermann (2021). "Robust increase of Indian monsoon rainfall and its variability under future warming in CMIP6 models". In: *Earth System Dynamics* 12.2, pp. 367–386.

Keellings, David, Johanna Engström, and Peter Waylen (2015). "The sunshine state: investigating external drivers of sky conditions". In: *Physical Geography* 36.2, pp. 113–126.

Kelly, Mark and Hans E Jørgensen (2017). "Statistical characterization of roughness uncertainty and impact on wind resource estimation". In: *Wind Energy Science* 2.1, pp. 189–209.

Kempton, Willett, Felipe M Pimenta, Dana E Veron, and Brian A Colle (2010). "Electric power from offshore wind via synoptic-scale interconnection". In: *Proceedings of the National Academy of Sciences* 107.16, pp. 7240–7245.

Kies, Alexander, Bruno U Schyska, Mariia Bilousova, Omar El Sayed, Jakub Jurasz, and Horst Stoecker (2021). "Critical review of renewable generation datasets and their implications for European power system models". In: *Renewable and Sustainable Energy Reviews* 152, p. 111614.

Kiesecker, Joseph, Sharon Baruch-Mordo, Mike Heiner, Dhaval Negandhi, James Oakleaf, Christina Kennedy, and Pareexit Chauhan (2019). "Renewable Energy and land use in India: a vision to facilitate sustainable development". In: *Sustainability* 12.1, p. 281.

Kiss, Péter, László Varga, and Imre M Jánosi (2009). "Comparison of wind power estimates from the ECMWF reanalyses with direct turbine measurements". In: *Journal of Renewable and Sustainable Energy* 1.3.

Kitzing, Lena, Morten Kofoed Jensen, Thomas Telsnig, and Eric Lantz (2020). "Multifaceted drivers for onshore wind energy repowering and their implications for energy transition". In: *Nature Energy* 5.12, pp. 1012–1021.

Klein, Stephen A, Brian J Soden, and Ngar-Cheung Lau (1999). "Remote sea surface temperature variations during ENSO: Evidence for a tropical atmospheric bridge". In: *Journal of Climate* 12.4, pp. 917–932.

Klink, Katherine (2007). "Atmospheric circulation effects on wind speed variability at turbine height". In: *Journal of applied meteorology and climatology* 46.4, pp. 445–456.

Knox, JB, H Moses, and MC MacCracken (1985). "Summary report of the workshop on the interactions of climate and energy". In: *Bulletin of the American Meteorological Society* 66.2, pp. 174–184.

Kopp, Greg (2016). "Magnitudes and timescales of total solar irradiance variability". In: *Journal of space weather and space climate* 6, A30.

Kosaka, Yu, Shang-Ping Xie, Ngar-Cheung Lau, and Gabriel A Vecchi (2013). "Origin of seasonal predictability for summer climate over the Northwestern Pacific". In: *Proceedings of the National Academy of Sciences* 110.19, pp. 7574–7579.

Krishna Kumar, K, Martin Hoerling, and Balaji Rajagopalan (2005). "Advancing dynamical prediction of Indian monsoon rainfall". In: *Geophysical Research Letters* 32.8.

Krishnamurthy, V and RS Ajayamohan (2010). "Composite structure of monsoon low pressure systems and its relation to Indian rainfall". In: *Journal of Climate* 23.16, pp. 4285–4305.

Krishnamurthy, V and J Shukla (2007). "Intraseasonal and seasonally persisting patterns of Indian monsoon rainfall". In: *Journal of Climate* 20.1, pp. 3–20.

Krishnamurthy, V and Jagadish Shukla (2000). "Intraseasonal and interannual variability of rainfall over India". In: *Journal of Climate* 13.24, pp. 4366–4377.

Krishnamurthy, V and JJCD Shukla (2008). "Seasonal persistence and propagation of intraseasonal patterns over the Indian monsoon region". In: *Climate Dynamics* 30, pp. 353–369.

Krishnamurti, Tiruvalam Natarajan and HN Bhalme (1976). "Oscillations of a monsoon system. Part I. Observational aspects". In: *Journal of Atmospheric Sciences* 33.10, pp. 1937–1954.

Krishnan, R and M Sugi (2003). "Pacific decadal oscillation and variability of the Indian summer monsoon rainfall". In: *Climate Dynamics* 21, pp. 233–242.

Kubik, ML, David J Brayshaw, Phil J Coker, and Janet F Barlow (2013). "Exploring the role of reanalysis data in simulating regional wind generation variability over Northern Ireland". In: *Renewable Energy* 57, pp. 558–561.

Kucharski, F, A Bracco, JH Yoo, AM Tompkins, L Feudale, P Ruti, and A Dell'Aquila (2009). "A Gill–Matsuno-type mechanism explains the tropical Atlantic influence on African and Indian monsoon rainfall". In: *Quarterly Journal of the Royal Meteorological Society* 135.640, pp. 569–579.

Kucharski, Fred, A Bracco, JH Yoo, and F Molteni (2007). "Low-frequency variability of the Indian monsoon–ENSO relationship and the tropical Atlantic: The "weakening" of the 1980s and 1990s". In: *Journal of Climate* 20.16, pp. 4255–4266.

Kulkarni, Ashwini, K Koteswara Rao, Manish K Joshi, Archana Rai, and P Darshana (2021). "ENSO–Indian summer monsoon teleconnections". In: *Indian Summer Monsoon Variability*. Elsevier, pp. 51–68.

Kulkarni, Sumeet, MC Deo, and Subimal Ghosh (2018). "Impact of active and break wind spells on the demand–supply balance in wind energy in India". In: *Meteorology and Atmospheric Physics* 130, pp. 81–97.

Kumar, Arun (2009). "Finite samples and uncertainty estimates for skill measures for seasonal prediction". In: *Monthly Weather Review* 137.8, pp. 2622–2631.

Kumar, Arun, Peitao Peng, and Mingyue Chen (2014). "Is there a relationship between potential and actual skill?" In: *Monthly Weather Review* 142.6, pp. 2220–2227.

Kumar, K Krishna, Balaji Rajagopalan, and Mark A Cane (1999). "On the weakening relationship between the Indian monsoon and ENSO". In: *Science* 284.5423, pp. 2156–2159.

Lau, KM, MK Kim, and KM Kim (2006). "Asian summer monsoon anomalies induced by aerosol direct forcing: the role of the Tibetan Plateau". In: *Climate Dynamics* 26, pp. 855–864.

Lau, Ka-Ming and PH Chan (1986). "Aspects of the 40–50 day oscillation during the northern summer as inferred from outgoing longwave radiation". In: *Monthly Weather Review* 114.7, pp. 1354–1367.

Lau, Ngar-Cheung and Mary Jo Nath (1996). "The role of the "atmospheric bridge" in linking tropical Pacific ENSO events to extratropical SST anomalies". In: *Journal of Climate* 9.9, pp. 2036–2057.

Lau, William K-M, Duane E Waliser, William KM Lau, Duane E Waliser, and BN Goswami (2012). "South Asian monsoon". In: *Intraseasonal variability in the atmosphere-ocean climate system*, pp. 21–72.

Levin, Todd, John Bistline, Ramteen Sioshansi, Wesley J Cole, Jonghwan Kwon, Scott P Burger, George W Crabtree, Jesse D Jenkins, Rebecca O'Neil, Magnus Korpås, et al. (2023). "Energy storage solutions to decarbonize electricity through enhanced capacity expansion modelling". In: *Nature Energy* 8.11, pp. 1199–1208.

Li, Chaofan, Riyu Lu, and Buwen Dong (2012). "Predictability of the western North Pacific summer climate demonstrated by the coupled models of ENSEMBLES". In: *Climate Dynamics* 39, pp. 329–346.

– (2014). "Predictability of the western North Pacific summer climate associated with different ENSO phases by ENSEMBLES multi-model seasonal forecasts". In: *Climate Dynamics* 43, pp. 1829–1845.

Li, Chengfeng and Michio Yanai (1996). "The onset and interannual variability of the Asian summer monsoon in relation to land–sea thermal contrast". In: *Journal of Climate* 9.2, pp. 358–375.

Li, Xiuping, Shiyuan Zhong, Xindi Bian, Warren Heilman, Yong Luo, and Wenjie Dong (2010). "Hydroclimate and variability in the Great Lakes region as derived from the North American Regional Reanalysis". In: *Journal of Geophysical Research: Atmospheres* 115.D12.

Liepert, Beate G (2002). "Observed reductions of surface solar radiation at sites in the United States and worldwide from 1961 to 1990". In: *Geophysical Research Letters* 29.10, pp. 61–1.

Livezey, Robert E (1990). "Variability of skill of long-range forecasts and implications for their use and value". In: *Bulletin of the American Meteorological Society* 71.3, pp. 300–309.

Lledó, Ll, Verónica Torralba, Albert Soret, Jaume Ramon, and Francisco J Doblas-Reyes (2019). "Seasonal forecasts of wind power generation". In: *Renewable Energy* 143, pp. 91–100.

Lledó, Llorenç, Jaume Ramon, Albert Soret, and Francisco-Javier Doblas-Reyes (2022). "Seasonal prediction of renewable energy generation in Europe based on four teleconnection indices". In: *Renewable Energy* 186, pp. 420–430.

Lockwood, Julia F, Hazel E Thornton, Nick Dunstone, Adam A Scaife, Philip E Bett, Chaofan Li, and Hong-Li Ren (2019). "Skilful seasonal prediction of winter wind speeds in China". In: *Climate Dynamics* 53, pp. 3937–3955.

Lorenz, Edward N (1969). "Atmospheric predictability as revealed by naturally occurring analogues". In: *Journal of Atmospheric Sciences* 26.4, pp. 636–646.

Loutzenhiser, PG, H Manz, C Felsmann, PA Strachan, TH Frank, and GM Maxwell (2007). "Empirical validation of models to compute solar irradiance on inclined surfaces for building energy simulation". In: *Solar Energy* 81.2, pp. 254–267.

Lu, Bo, Hong-Li Ren, Adam A Scaife, Jie Wu, Nick Dunstone, Doug Smith, Jianghua Wan, Rosie Eade, Craig MacLachlan, and Margaret Gordon (2018). "An extreme negative Indian Ocean Dipole event in 2016: dynamics and predictability". In: *Climate Dynamics* 51, pp. 89–100.

Lu, Riyu, Buwen Dong, and Hui Ding (2006). "Impact of the Atlantic Multidecadal Oscillation on the Asian summer monsoon". In: *Geophysical Research Letters* 33.24.

Lu, Tianguang, Peter Sherman, Xinyu Chen, Shi Chen, Xi Lu, and Michael McElroy (2020). "India's potential for integrating solar and on-and offshore wind power into its energy system". In: *Nature communications* 11.1, p. 4750.

Lu, Xi, M. B. McElroy, and Juha Kiviluoma (2009). "Global potential for wind-generated electricity". In: *Proceedings of the National Academy of Sciences* 106 (27), pp. 10933–10938.

Luderer, Gunnar, Silvia Madeddu, Leon Merfort, Falko Ueckerdt, Michaja Pehl, Robert Pietzcker, Marianna Rottoli, Felix Schreyer, Nico Bauer, Lavinia Baumstark, et al. (2022). "Impact of declining renewable energy costs on electrification in low-emission scenarios". In: *Nature Energy* 7.1, pp. 32–42.

Lumbreras, S and A Ramos (2013). "Offshore wind farm electrical design: a review". In: *Wind Energy* 16.3, pp. 459–473.

Luo, Feifei, Shuanglin Li, Yongqi Gao, Lea Svendsen, Tore Furevik, and Noel Keenlyside (2018). "The connection between the Atlantic Multidecadal Oscillation and the Indian Summer Monsoon since the Industrial Revolution is intrinsic to the climate system". In: *Environmental Research Letters* 13.9, p. 094020.

Lydia, M, S Suresh Kumar, A Immanuel Selvakumar, and G Edwin Prem Kumar (2014). "A comprehensive review on wind turbine power curve modeling techniques". In: *Renewable and Sustainable Energy Reviews* 30, pp. 452–460.

Lynch, Kieran J, David J Brayshaw, and Andrew Charlton-Perez (2014). "Verification of European subseasonal wind speed forecasts". In: *Monthly Weather Review* 142.8, pp. 2978–2990.

Madec, Gurvan, Romain Bourdallé-Badie, Pierre-Antoine Bouttier, Clement Bricaud, Diego Bruciaferri, Daley Calvert, Jérôme Chanut, Emanuela Clementi, Andrew Coward, Damiano Delrosso, et al. (2017). *NEMO ocean engine*. Tech. rep. Notes du Pôle de modélisation de l'Institut Pierre-Simon Laplace (IPSL): (27). ISSN 1288-1619.

Madolli, Mallappa J, Sushil K Himanshu, Epari Ritesh Patro, and Carlo De Michele (2022). "Past, present and future perspectives of seasonal prediction of Indian summer monsoon rainfall: A review". In: *Asia-Pacific Journal of Atmospheric Sciences* 58.4, pp. 591–615.

Madsen, H Aa, F Zahle, F Meng, T Barlas, F Rasmussen, and RT Rudolf (2020). "Initial performance and load analysis of the LowWind turbine in comparison with a conventional turbine". In: *Journal of Physics: Conference Series*. Vol. 1618. 3. IOP Publishing, p. 032011.

Mahrt, Larry (1999). "Stratified atmospheric boundary layers". In: *Boundary-Layer Meteorology* 90, pp. 375–396.

Mahtta, Richa, Pawan Kumar Joshi, and Alok Kumar Jindal (2014). "Solar power potential mapping in India using remote sensing inputs and environmental parameters". In: *Renewable Energy* 71, pp. 255–262.

Manzanas, R, A Lucero, A Weisheimer, and José M Gutiérrez (2018). "Can bias correction and statistical downscaling methods improve the skill of seasonal precipitation forecasts?" In: *Climate Dynamics* 50, pp. 1161–1176.

Manzanas, Rodrigo, José Manuel Gutiérrez, Jonas Bhend, Stephan Hemri, Francisco J Doblas-Reyes, V Torralba, E Penabad, and Anca Brookshaw (2019). "Bias adjustment and ensemble recalibration methods for seasonal forecasting: a comprehensive intercomparison using the C3S dataset". In: *Climate Dynamics* 53, pp. 1287–1305.

Mariotti, Annarita, Cory Baggett, Elizabeth A Barnes, Emily Becker, Amy Butler, Dan C Collins, Paul A Dirmeyer, Laura Ferranti, Nathaniel C Johnson, Jeanine Jones, et al. (2020). "Windows of opportunity for skillful forecasts subseasonal to seasonal and beyond". In: *Bulletin of the American Meteorological Society* 101.5, E608–E625.

Marquis, Melinda, Jim Wilczak, Mark Ahlstrom, Justin Sharp, Andrew Stern, J Charles Smith, and Stan Calvert (2011). "Forecasting the wind to reach significant penetration levels of wind energy". In: *Bulletin of the American Meteorological Society* 92.9, pp. 1159–1171.

Marticorena, Beatrice and Gilles Bergametti (1995). "Modeling the atmospheric dust cycle: 1. Design of a soil-derived dust emission scheme". In: *Journal of Geophysical Research: atmospheres* 100.D8, pp. 16415–16430.

Martin, Gill M, Amulya Chevuturi, Ruth E Comer, Nick J Dunstone, Adam A Scaife, and Daquan Zhang (2019). "Predictability of South China Sea summer monsoon onset". In: *Advances in Atmospheric Sciences* 36, pp. 253–260.

Mason, Ian (1982). "A model for assessment of weather forecasts". In: *Aust. Meteor. Mag* 30.4, pp. 291–303.

Matuszko, Dorota (2012). "Influence of the extent and genera of cloud cover on solar radiation intensity". In: *International Journal of Climatology* 32.15, pp. 2403–2414.

McKenna, Russell, Stefan Pfenninger, Heidi Heinrichs, Johannes Schmidt, Iain Staffell, Christian Bauer, Katharina Gruber, Andrea N Hahmann, Malte Jansen, Michael Klingler, et al. (2022). "High-resolution large-scale onshore wind energy assessments: A review of potential definitions, methodologies and future research needs". In: *Renewable Energy* 182, pp. 659–684.

McPhaden, Michael J, Stephen E Zebiak, and Michael H Glantz (2006). "ENSO as an integrating concept in earth science". In: *Science* 314.5806, pp. 1740–1745.

McVicar, Tim R, Michael L Roderick, Randall J Donohue, Ling Tao Li, Thomas G Van Niel, Axel Thomas, Jürgen Grieser, Deepak Jhajharia, Youcef Himri, Natalie M Mahowald, et al. (2012). "Global review and synthesis of trends in observed terrestrial near-surface wind speeds: Implications for evaporation". In: *Journal of Hydrology* 416, pp. 182–205.

Middleton, NJ (1986). "A geography of dust storms in South-west Asia". In: *Journal of Climatology* 6.2, pp. 183–196.

Miller, Lee M, Nathaniel A Brunsell, David B Mechem, Fabian Gans, Andrew J Monaghan, Robert Vautard, David W Keith, and Axel Kleidon (2015). "Two methods for estimating limits to large-scale wind power generation". In: *Proceedings of the National Academy of Sciences* 112.36, pp. 11169–11174.

Miller, Lee M and David W Keith (2018). "Observation-based solar and wind power capacity factors and power densities". In: *Environmental Research Letters* 13.10, p. 104008.

Miller, Lee M and Axel Kleidon (2016). "Wind speed reductions by large-scale wind turbine deployments lower turbine efficiencies and set low generation limits". In: *Proceedings of the National Academy of Sciences* 113.48, pp. 13570–13575.

Milligan, Michael, Bethany Frew, Ella Zhou, and Douglas J Arent (2015). *Advancing system flexibility for high penetration renewable integration (Chinese translation)*. Tech. rep. National Renewable Energy Lab.(NREL), Golden, CO (United States).

Mills, Andrew (2010). *Implications of wide-area geographic diversity for short-term variability of solar power*. Tech. rep. Lawrence Berkeley National Laboratory.

Mishra, Vimal, Brian V Smoliak, Dennis P Lettenmaier, and John M Wallace (2012). "A prominent pattern of year-to-year variability in Indian Summer Monsoon Rainfall". In: *Proceedings of the National Academy of Sciences* 109.19, pp. 7213–7217.

MNRE (2022a). *National Repowering Policy for Wind Projects 2022*. New Delhi, India: Ministry of New and Renewable Energy (MNRE), Government of India.

– (2022b). *State-wise installed capacity of Renewable Power*. Online. Available at: `https://mnre.gov.in/img/documents/uploads/file_s-1681211407657.pdf`. Accessed 4th April 2023.

– (2022c). *Twenty-Seventh Report Standing Committee On Energy - Evaluation of Wind Energy in India*. New Delhi, India: Ministry of New and Renewable Energy.

– (2023). *Strategy for Establishment of Offshore Wind Energy Projects*. Online. Available at: `https://mnre.gov.in/document/strategy-paper-for-establishment-of-offshore-wind-energy-projects/` Accessed: 20th January 2024.

Modi, Vijay, Susan McDade, Dominique Lallement, Jamal Saghir, et al. (2005). *Energy Services for the Millennium Development Goals*. World Bank.

MoEFCC (2022). *India's long-term low-carbon development strategy*. Ministry of Environment, Forest and Climate Change, Government of India.

Mohan, Aniruddh (2017). "Whose land is it anyway? Energy futures & land use in India". In: *Energy Policy* 110, pp. 257–262.

Mohan, RS Ajaya and BN Goswami (2000). "A common spatial mode for intra-seasonal and inter-annual variation and predictability of the Indian summer monsoon". In: *Current Science*, pp. 1106–1111.

Molina, María O, Claudia Gutiérrez, and Enrique Sánchez (2021). "Comparison of ERA5 surface wind speed climatologies over Europe with observations from the HadISD dataset". In: *International Journal of Climatology* 41.10, pp. 4864–4878.

Mooley, DA and B Parthasarathy (1983). "Variability of the Indian summer monsoon and tropical circulation features". In: *Monthly Weather Review* 111.5, pp. 967–978.

Mooley, DA and J Shukla (1987). *Characteristics of the westward-moving summer monsoon low pressure systems over the Indian region and their relationship with the monsoon rainfall*. University of Maryland, Department of Meteorology, Center for Ocean-Land.

MoP (2021). *Development of Power Market in India, Phase 1: Implementation of Market-Based Economic Dispatch (MBED)*.

Morcrette, J-J, O Boucher, L Jones, D Salmond, P Bechtold, A Beljaars, A Benedetti, A Bonet, JW Kaiser, M Razinger, et al. (2009). "Aerosol analysis and forecast in the European Centre for medium-range weather forecasts integrated forecast system: Forward modeling". In: *Journal of Geophysical Research: Atmospheres* 114.D6.

Moron, Vincent, Andrew W Robertson, and Michael Ghil (2012). "Impact of the modulated annual cycle and intraseasonal oscillation on daily-to-interannual rainfall variability across monsoonal India". In: *Climate Dynamics* 38, pp. 2409–2435.

MOSPI (2021). *Energy Statistics India 2021*. Ministry of Statistics and Programme Implementation Government of India.

Mulcahy, JP, DN Walters, Nicolas Bellouin, and SF Milton (2014). "Impacts of increasing the aerosol complexity in the Met Office global numerical weather prediction model". In: *Atmospheric Chemistry and Physics* 14.9, pp. 4749–4778.

Murakami, Masato (1976). "Analysis of summer monsoon fluctuations over India". In: *Journal of the Meteorological Society of Japan. Ser. II* 54.1, pp. 15–31.

Murcia, Juan Pablo, Matti Juhani Koivisto, Graziela Luzia, Bjarke T Olsen, Andrea N Hahmann, Poul Ejnar Sørensen, and Magnus Als (2022). "Validation of European-scale simulated wind speed and wind generation time series". In: *Applied Energy* 305, p. 117794.

Murphy, Allan H (1973). "A new vector partition of the probability score". In: *Journal of Applied Meteorology and Climatology* 12.4, pp. 595–600.

– (1977). "The value of climatological, categorical and probabilistic forecasts in the cost-loss ratio situation". In: *Monthly Weather Review* 105.7, pp. 803–816.

– (1993). "What is a good forecast? An essay on the nature of goodness in weather forecasting". In: *Weather and forecasting* 8.2, pp. 281–293.

Nagababu, Garlapati, Surendra Singh Kachhwaha, Natansh K Naidu, and Vimal Savsani (2017). "Application of reanalysis data to estimate offshore wind potential in EEZ of India based on marine ecosystem considerations". In: *Energy* 118, pp. 622–631.

Nie, Huiwen and Yan Guo (2019). "An evaluation of East Asian summer monsoon forecast with the North American Multimodel Ensemble hindcast data". In: *International Journal of Climatology* 39.12, pp. 4838–4852.

NITI Aayog (2022). *Geospatial Energy Map of India*. Online. Available at: `https://www.niti.gov.in/energy-swaraj-geospatial-energy-map-india-presents-immense-potential-and-opportunities`. Accessed: 22nd November 2022.

Norgaard, Per and Hannele Holttinen (2004). "A multi-turbine power curve approach". In: *Nordic wind power conference*. Vol. 1. Chalmers, pp. 1–2.

NREL (2023). *India's Action Plan for Power Sector Decarbonisation*. Golden, Colorado.: National Renewable Energy Laboratory (NREL).

Okumus, Inci and Ali Dinler (2016). "Current status of wind energy forecasting and a hybrid method for hourly predictions". In: *Energy Conversion and Management* 123, pp. 362–371.

Olauson, Jon (2018). "ERA5: The new champion of wind power modelling?" In: *Renewable Energy* 126, pp. 322–331.

Olauson, Jon, Mohd Nasir Ayob, Mikael Bergkvist, Nicole Carpman, Valeria Castellucci, Anders Goude, David Lingfors, Rafael Waters, and Joakim Widén (2016). "Net load variability in Nordic countries with a highly or fully renewable power system". In: *Nature Energy* 1.12, pp. 1–8.

Olauson, Jon and Mikael Bergkvist (2015). "Modelling the Swedish wind power production using MERRA reanalysis data". In: *Renewable Energy* 76, pp. 717–725.

Olauson, Jon, Per Edström, and Jesper Rydén (2017). "Wind turbine performance decline in Sweden". In: *Wind Energy* 20.12, pp. 2049–2053.

Orlov, Anton, Jana Sillmann, and Ilaria Vigo (2020). "Better seasonal forecasts for the renewable energy industry". In: *Nature Energy* 5.2, pp. 108–110.

Padma Kumari, B, Anil L Londhe, Samuel Daniel, and Dattatray B Jadhav (2007). "Observational evidence of solar dimming: Offsetting surface warming over India". In: *Geophysical Research Letters* 34.21.

Pai, DS and M Rajeevan (2006). "Empirical prediction of Indian summer monsoon rainfall with different lead periods based on global SST anomalies". In: *Meteorology and Atmospheric Physics* 92.1, pp. 33–43.

Pai, DS, M Rajeevan, OP Sreejith, B Mukhopadhyay, and NS Satbha (2014). "Development of a new high spatial resolution (0.25× 0.25) long period (1901-2010) daily gridded rainfall data set over India and its comparison with existing data sets over the region". In: *Mausam* 65.1, pp. 1–18.

Palchak, David, Jaquelin Cochran, Ranjit Deshmukh, Ali Ehlen, R Soonee, S Narasimhan, Mohit Joshi, Brendan McBennett, Michael Milligan, Priya Sreedharan, et al. (2017). *GREENING THE GRID: pathways to integrate 175 gigawatts of renewable energy into India's electric grid, vol. I—national study*. National Renewable Energy Laboratory (NREL).

Palin, Erika J, Adam A Scaife, Emily Wallace, Edward CD Pope, Alberto Arribas, and Anca Brookshaw (2016). "Skillful seasonal forecasts of winter disruption to the UK transport system". In: *Journal of Applied Meteorology and Climatology* 55.2, pp. 325–344.

Palmer, Tim N (2000). "Predicting uncertainty in forecasts of weather and climate". In: *Reports on progress in Physics* 63.2, p. 71.

Palmer, TN (1994). "Chaos and predictability in forecasting the monsoon". In: *Proc. Indian Nat. Sci. Acad.* Vol. 60, pp. 57–66.

Pan, J, F Zhang, and J Guo (2021). *New energy technology research: Opportunities and challenges*. Tech. rep. Springer Nature Limited.

Pant, GB and Shri B Parthasarathy (1981). "Some aspects of an association between the southern oscillation and Indian summer monsoon". In: *Archives for Meteorology, Geophysics, and Bioclimatology Series B* 29.3, pp. 245–252.

Patel, Ravi P, Garlapati Nagababu, Surendra Singh Kachhwaha, and VV Arun Kumar Surisetty (2022). "A revised offshore wind resource assessment and site selection along the Indian coast using ERA5 near-hub-height wind products". In: *Ocean Engineering* 254, p. 111341.

Pease, Patrick P, Vatche P Tchakerian, and Neil W Tindale (1998). "Aerosols over the Arabian Sea: geochemistry and source areas for aeolian desert dust". In: *Journal of Arid Environments* 39.3, pp. 477–496.

Pfenninger, Stefan, Joseph DeCarolis, Lion Hirth, Sylvain Quoilin, and Iain Staffell (2017). "The importance of open data and software: Is energy research lagging behind?" In: *Energy Policy* 101, pp. 211–215.

Pfenninger, Stefan, Adam Hawkes, and James Keirstead (2014). "Energy systems modeling for twenty-first century energy challenges". In: *Renewable and Sustainable Energy Reviews* 33, pp. 74–86.

Pfenninger, Stefan and Iain Staffell (2016). "Long-term patterns of European PV output using 30 years of validated hourly reanalysis and satellite data". In: *Energy* 114, pp. 1251–1265.

Phadke, Amol, Ranjit Bharvirkar, and Jagmeet Khangura (2012). *Reassessing wind potential estimates for India: economic and policy implications*. Lawrence Berkeley National Laboratory.

PIB (2023a). *Central Electricity Authority notifies the National Electricity Plan for the period of 2022-32*. Online. Available at: `https://pib.gov.in/PressReleaseIframePage.aspx?PRID=1928750` Accessed: 11th January 2023.

– (2023b). *India's National Climate Research agenda released at International Climate Research Conclave*. Online. Available at: https://pib.gov.in/PressReleaseIframePage.aspx?PRID=1927516. Accessed: 2nd December 2023.

Pillai, Prasanth A, Suryachandra A Rao, Kiran V. Gangadharan, Maheswar Pradhan, Ankur Srivastava, and Deepesh K Jain (2022). "Impact of reduced ENSO variability and amplitude on ISMR prediction in the long-lead forecasts of monsoon mission CFS". In: *International Journal of Climatology* 42.16, pp. 9166–9181.

Poletti, Stephen and Iain Staffell (2021). "Understanding New Zealand's wind resources as a route to 100% renewable electricity". In: *Renewable Energy* 170, pp. 449–461.

Pozo-Vázquez, D, J Tovar-Pescador, SR Gámiz-Fortis, MJ Esteban-Parra, and Y Castro-Díez (2004). "NAO and solar radiation variability in the European North Atlantic region". In: *Geophysical Research Letters* 31.5.

Prasad, Anup K, Ramesh P Singh, and Menas Kafatos (2006). "Influence of coal based thermal power plants on aerosol optical properties in the Indo-Gangetic basin". In: *Geophysical Research Letters* 33.5.

Praveen, V, S Sandeep, and RS Ajayamohan (2015). "On the relationship between mean monsoon precipitation and low pressure systems in climate model simulations". In: *Journal of Climate* 28.13, pp. 5305–5324.

Preethi, B, RH Kripalani, and K Krishna Kumar (2010). "Indian summer monsoon rainfall variability in global coupled ocean-atmospheric models". In: *Climate Dynamics* 35, pp. 1521–1539.

Prospero, Joseph M, Paul Ginoux, Omar Torres, Sharon E Nicholson, and Thomas E Gill (2002). "Environmental characterization of global sources of atmospheric soil dust identified with the Nimbus 7 Total Ozone Mapping Spectrometer (TOMS) absorbing aerosol product". In: *Reviews of geophysics* 40.1, pp. 2–1.

Pryor, SC and RJ Barthelmie (2011). "Assessing climate change impacts on the near-term stability of the wind energy resource over the United States". In: *Proceedings of the National Academy of Sciences* 108.20, pp. 8167–8171.

Qian, Cheng and Tianjun Zhou (2014). "Multidecadal variability of North China aridity and its relationship to PDO during 1900–2010". In: *Journal of Climate* 27.3, pp. 1210–1222.

Qian, Yun, MG Flanner, LR Leung, and Weiguo Wang (2011). "Sensitivity studies on the impacts of Tibetan Plateau snowpack pollution on the Asian hydrological cycle and monsoon climate". In: *Atmospheric Chemistry and Physics* 11.5, pp. 1929–1948.

Rajeevan, M and PA Francis (2007). "Monsoon variability: Links to major oscillations over the equatorial Pacific and Indian oceans". In: *Current Science* 93.2, pp. 182–194.

Rajeevan, M, Sulochana Gadgil, and Jyoti Bhate (2010). "Active and break spells of the Indian summer monsoon". In: *Journal of earth system science* 119, pp. 229–247.

Rajeevan, M, CK Unnikrishnan, Jyoti Bhate, K Niranjan Kumar, and PP Sreekala (2012a). "Northeast monsoon over India: variability and prediction". In: *Meteorological Applications* 19.2, pp. 226–236.

Rajeevan, M, CK Unnikrishnan, and B Preethi (2012b). "Evaluation of the ENSEMBLES multi-model seasonal forecasts of Indian summer monsoon variability". In: *Climate Dynamics* 38, pp. 2257–2274.

Ramachandra, TV, Rishabh Jain, and Gautham Krishnadas (2011). "Hotspots of solar potential in India". In: *Renewable and sustainable energy reviews* 15.6, pp. 3178–3186.

Ramamurthy, K (1969). *Monsoon of India: some aspects of the 'break' in the Indian southwest monsoon during July and August*. India Meteorological Department New Delhi, pp. 1–57.

Ramanathan, Veerabhadran, Christine Chung, Dongchul Kim, T Bettge, L Buja, Jeffrey T Kiehl, Warren M Washington, Qiang Fu, Devraj R Sikka, and Martin Wild (2005). "Atmospheric brown clouds: Impacts on South Asian climate and hydrological cycle". In: *Proceedings of the National Academy of Sciences* 102.15, pp. 5326–5333.

Ramdas, Bhukya, J Bastin, B Krishnan, T Suresh Kumar, JC David Solomon, and K Balaraman (2022). "Validation of Global Wind Atlas for India". In: *2022 IEEE International Power and Renewable Energy Conference (IPRECON)*. IEEE, pp. 1–6.

Ramon, Jaume, Llorenç Lledó, Pierre-Antoine Bretonnière, Margarida Samsó, and Francisco J Doblas-Reyes (2021). "A perfect prognosis downscaling methodology for seasonal prediction of local-scale wind speeds". In: *Environmental Research Letters* 16.5, p. 054010.

Randles, CA, AM Da Silva, V Buchard, PR Colarco, A Darmenov, R Govindaraju, A Smirnov, B Holben, R Ferrare, J Hair, et al. (2017). "The MERRA-2 aerosol reanalysis, 1980 onward. Part I: System description and data assimilation evaluation". In: *Journal of Climate* 30.17, pp. 6823–6850.

Rani, S Indira, T Arulalan, John P George, EN Rajagopal, Richard Renshaw, Adam Maycock, Dale M Barker, and M Rajeevan (2021). "IMDAA: High-resolution satellite-era reanalysis for the Indian monsoon region". In: *Journal of Climate* 34.12, pp. 5109–5133.

Rasmusson, Eugene M and Thomas H Carpenter (1982). "Variations in tropical sea surface temperature and surface wind fields associated with the Southern Oscillation/El Niño". In: *Monthly Weather Review* 110.5, pp. 354–384.

– (1983). "The relationship between eastern equatorial Pacific sea surface temperatures and rainfall over India and Sri Lanka". In: *Monthly Weather Review* 111.3, pp. 517–528.

Ren, Guorui, Jie Wan, Jinfu Liu, and Daren Yu (2019). "Characterization of wind resource in China from a new perspective". In: *Energy* 167, pp. 994–1010.

Rhodes, Brandon Craig (2011). "PyEphem: astronomical ephemeris for Python". In: *Astrophysics Source Code Library*, ascl–1112.

Riahi, Keywan, Roberto Schaeffer, et al. (2022). "Mitigation Pathways Compatible with Long-Term Goals". In: *Climate Change 2022: Mitigation of Climate Change. Contribution of Working Group III to the Sixth Assessment Report of the Intergovernmental Panel on Climate Change*. Cambridge University Press, UK.

Richardson, David S (2000). "Skill and relative economic value of the ECMWF ensemble prediction system". In: *Quarterly Journal of the Royal Meteorological Society* 126.563, pp. 649–667.

Rieger, N. and S. J. Levang (2023). *xeofs: Comprehensive EOF analysis in Python with xarray: A versatile, multidimensional, and scalable tool for advanced climate data analysis*. Version x.y.z. Available at `https://github.com/nicrie/xeofs`.

Rienecker, Michele M, Max J Suarez, Ronald Gelaro, Ricardo Todling, Julio Bacmeister, Emily Liu, Michael G Bosilovich, Siegfried D Schubert, Lawrence Takacs, Gi-Kong Kim, et al. (2011). "MERRA: NASA's modern-era retrospective analysis for research and applications". In: *Journal of Climate* 24.14, pp. 3624–3648.

Ringkjøb, Hans-Kristian, Peter M Haugan, and Ida Marie Solbrekke (2018). "A review of modelling tools for energy and electricity systems with large shares of variable renewables". In: *Renewable and Sustainable Energy Reviews* 96, pp. 440–459.

Roderick, Michael L, Leon D Rotstayn, Graham D Farquhar, and Michael T Hobbins (2007). "On the attribution of changing pan evaporation". In: *Geophysical Research Letters* 34.17.

Rogelj, Joeri, Gunnar Luderer, Robert C Pietzcker, Elmar Kriegler, Michiel Schaeffer, Volker Krey, and Keywan Riahi (2015). "Energy system transformations for limiting end-of-century warming to below 1.5 C". In: *Nature Climate Change* 5.6, pp. 519–527.

Roques, Fabien, Céline Hiroux, and Marcelo Saguan (2010). "Optimal wind power deployment in Europe—A portfolio approach". In: *Energy Policy* 38.7, pp. 3245–3256.

Rose, Amy, Ilya Chernyakhovskiy, Joseph Palchak, Samuel Koebrich, and Mohit Joshi (2020). *Least-Cost Pathways for India's Electric Power Sector*. Tech. rep. National Renewable Energy Lab.(NREL), Golden, CO (United States).

Rose, Stephen and Jay Apt (2015a). "What can reanalysis data tell us about wind power?" In: *Renewable Energy* 83, pp. 963–969.

– (2015b). "What can reanalysis data tell us about wind power?" In: *Renewable Energy* 83, pp. 963–969.

Ryberg, David Severin, Dilara Gulcin Caglayan, Sabrina Schmitt, Jochen Linßen, Detlef Stolten, and Martin Robinius (2019). "The future of European onshore wind energy potential: Detailed distribution and simulation of advanced turbine designs". In: *Energy* 182, pp. 1222–1238.

Sachindra, DA, Khandakar Ahmed, Md Mamunur Rashid, S Shahid, and BJC Perera (2018). "Statistical downscaling of precipitation using machine learning techniques". In: *Atmospheric research* 212, pp. 240–258.

Saha, Subodh Kumar, Anupam Hazra, Samir Pokhrel, Hemantkumar S Chaudhari, K Sujith, Archana Rai, Hasibur Rahaman, and BN Goswami (2019). "Unraveling the mystery of Indian summer monsoon prediction: Improved estimate of predictability limit". In: *Journal of Geophysical Research: Atmospheres* 124.4, pp. 1962–1974.

Saha, Subodh Kumar, Mahen Konwar, Samir Pokhrel, Anupam Hazra, Hemantkumar S Chaudhari, and Archana Rai (2021). "Interplay between subseasonal rainfall and global predictors in modulating interannual to multidecadal predictability of the ISMR". In: *Geophysical Research Letters* 48.1, e2020GL091458.

Saha, Subodh Kumar, Samir Pokhrel, Kiran Salunke, Ashish Dhakate, Hemantkumar S Chaudhari, Hasibur Rahaman, K Sujith, Anupam Hazra, and DR Sikka (2016). "Potential predictability of I ndian summer monsoon rainfall in NCEP CFSv2". In: *Journal of Advances in Modeling Earth Systems* 8.1, pp. 96–120.

Saha, Suranjana, Shrinivas Moorthi, Xingren Wu, Jiande Wang, Sudhir Nadiga, Patrick Tripp, David Behringer, Yu-Tai Hou, Hui-ya Chuang, Mark Iredell, et al. (2014). "The NCEP climate forecast system version 2". In: *Journal of Climate* 27.6, pp. 2185–2208.

Saha, Upal, Rohit Chakraborty, Animesh Maitra, and AK Singh (2017). "East-west coastal asymmetry in the summertime near surface wind speed and its projected change in future climate over the Indian region". In: *Global and Planetary Change* 152, pp. 76–87.

Saint-Drenan, Yves-Marie, Lucien Wald, Thierry Ranchin, Laurent Dubus, and Alberto Troccoli (2018). "An approach for the estimation of the aggregated photovoltaic power generated in several European countries from meteorological data". In: *Advances in Science and Research* 15, pp. 51–62.

Saji, NH, Bhupendra Nath Goswami, PN Vinayachandran, and Toshio Yamagata (1999). "A dipole mode in the tropical Indian Ocean". In: *Nature* 401.6751, pp. 360–363.

Santos-Alamillos, Francisco J, David J Brayshaw, John Methven, Nikolaos S Thomaidis, José A Ruiz-Arias, and David Pozo-Vázquez (2017). "Exploring the meteorological potential for planning a high performance European electricity super-grid: optimal power capacity distribution among countries". In: *Environmental Research Letters* 12.11, p. 114030.

Satyanarayana, G Ch, RH Lucy Supriya, and DV Bhaskar Rao (2019). "Wind energy assessment over the Andhra Pradesh and Telangana regions". In: *Meteorological Applications* 26.1, pp. 14–29.

Satyanarayana Gubbala, China, Venkata Bhaskar Rao Dodla, and Srinivas Desamsetti (2021). "Assessment of wind energy potential over India using high-resolution global reanalysis data". In: *Journal of Earth System Science* 130, pp. 1–19.

Scaife, AA, A Arribas, E Blockley, A Brookshaw, RT Clark, N Dunstone, R Eade, D Fereday, CK Folland, M Gordon, et al. (2014). "Skillful long-range prediction of European and North American winters". In: *Geophysical Research Letters* 41.7, pp. 2514–2519.

Scaife, Adam A and Doug Smith (2018). "A signal-to-noise paradox in climate science". In: *npj Climate and Atmospheric Science* 1.1, p. 28.

Schallenberg-Rodriguez, Julieta (2013). "A methodological review to estimate techno-economical wind energy production". In: *Renewable and Sustainable Energy Reviews* 21, pp. 272–287.

Schott, Friedrich A, Shang-Ping Xie, and Julian P McCreary Jr (2009). "Indian Ocean circulation and climate variability". In: *Reviews of Geophysics* 47.1.

Sengupta, Agniv and Sumant Nigam (2019). "The northeast winter monsoon over the Indian subcontinent and Southeast Asia: Evolution, interannual variability, and model simulations". In: *Journal of Climate* 32.1, pp. 231–249.

Sepulveda, Nestor A, Jesse D Jenkins, Aurora Edington, Dharik S Mallapragada, and Richard K Lester (2021). "The design space for long-duration energy storage in decarbonized power systems". In: *Nature Energy* 6.5, pp. 506–516.

Shafiullah, GM, Amanullah MT Oo, ABM Shawkat Ali, and Peter Wolfs (2013). "Potential challenges of integrating large-scale wind energy into the power grid–A review". In: *Renewable and sustainable energy reviews* 20, pp. 306–321.

Shaner, Matthew R, Steven J Davis, Nathan S Lewis, and Ken Caldeira (2018). "Geophysical constraints on the reliability of solar and wind power in the United States". In: *Energy & Environmental Science* 11.4, pp. 914–925.

Shekhar, Jai, Selna Saji, Disha Agarwal, Asim Ahmed, and Tarun Joseph (2021). *Assessing and Planning for Variability in India's Wind Resource*. Tech. rep. Council on Energy, Environment and Water (CEEW) and REConnect Energy Solutions.

Sherman, Peter, Xinyu Chen, and Michael B McElroy (2017). "Wind-generated electricity in China: Decreasing potential, inter-annual variability and association with changing climate". In: *Scientific reports* 7.1, p. 16294.

Shukla, J (1987). "Interannual variability of monsoons". In: *Monsoons* 14, pp. 399–464.

Sikka, DR (1980). "Some aspects of the large scale fluctuations of summer monsoon rainfall over India in relation to fluctuations in the planetary and regional scale circulation parameters". In: *Proceedings of the Indian Academy of Sciences-Earth and Planetary Sciences* 89, pp. 179–195.

– (2006). *A study on the monsoon low pressure systems over the Indian region and their relationship with drought and excess monsoon seasonal rainfall*. Center for Ocean-Land-Atmosphere Studies, Center for the Application of Research on the Environment.

Sikka, DR and Sulochana Gadgil (1978). "Large-scale rainfall over India during the summer monsoon and its relation to the lower and upper tropospheric vorticity". In: *Mausam* 29.1, pp. 219–231.

– (1980). "On the maximum cloud zone and the ITCZ over Indian longitudes during the south-west monsoon". In: *Monthly Weather Review* 108.11, pp. 1840–1853.

Sims, Ralph et al. (2011). "Integration of Renewable Energy into Present and Future Energy Systems". English. In: *IPCC Special Report on Renewable Energy Sources and Climate Change Mitigation*. Ed. by Ottmar Edenhofer et al. United Kingdom: Cambridge University Press.

Sinden, Graham (2007). "Characteristics of the UK wind resource: Long-term patterns and relationship to electricity demand". In: *Energy Policy* 35.1, pp. 112–127.

Singh, Bohar, Ben Cash, and James L Kinter III (2019). "Indian summer monsoon variability forecasts in the North American multimodel ensemble". In: *Climate Dynamics* 53, pp. 7321–7334.

Singh, Jyotsna and Manoj Kumar (2016). "Solar radiation over four cities of India: Trend analysis using Mann-Kendall test". In: *International Journal of Renewable Energy Research* 6.4, pp. 1385–95.

Slingo, JM and H Annamalai (2000). "1997: The El Niño of the century and the response of the Indian summer monsoon". In: *Monthly Weather Review* 128.6, pp. 1778–1797.

Slingo, Julia and Tim Palmer (2011). "Uncertainty in weather and climate prediction". In: *Philosophical Transactions of the Royal Society A: Mathematical, Physical and Engineering Sciences* 369.1956, pp. 4751–4767.

Slingo, Julia, Hilary Spencer, Brian Hoskins, Paul Berrisford, and Emily Black (2005). "The meteorology of the Western Indian Ocean, and the influence of the East African Highlands". In: *Philosophical Transactions of the Royal Society A: Mathematical, Physical and Engineering Sciences* 363.1826, pp. 25–42.

Smith, Doug M, Rosie Eade, and Holger Pohlmann (2013). "A comparison of full-field and anomaly initialization for seasonal to decadal climate prediction". In: *Climate Dynamics* 41, pp. 3325–3338.

Smith, Doug M, Adam A Scaife, Rosie Eade, and Jeff R Knight (2016). "Seasonal to decadal prediction of the winter North Atlantic Oscillation: Emerging capability and future prospects". In: *Quarterly Journal of the Royal Meteorological Society* 142.695, pp. 611–617.

Soares, Marta Bruno and Suraje Dessai (2015). "Exploring the use of seasonal climate forecasts in Europe through expert elicitation". In: *Climate Risk Management* 10, pp. 8–16.

Soni, VK, G Pandithurai, and DS Pai (2012). "Evaluation of long-term changes of solar radiation in India". In: *International Journal of Climatology* 32.4, pp. 540–551.

– (2016). "Is there a transition of solar radiation from dimming to brightening over India?" In: *Atmospheric research* 169, pp. 209–224.

Staffell, Iain and Richard Green (2014). "How does wind farm performance decline with age?" In: *Renewable Energy* 66, pp. 775–786.

Staffell, Iain and Stefan Pfenninger (2016). "Using bias-corrected reanalysis to simulate current and future wind power output". In: *Energy* 114, pp. 1224–1239.

– (2018). "The increasing impact of weather on electricity supply and demand". In: *Energy* 145, pp. 65–78.

Stanhill, Gerald and Shabtai Cohen (2001). "Global dimming: a review of the evidence for a widespread and significant reduction in global radiation with discussion of its probable causes and possible agricultural consequences". In: *Agricultural and forest meteorology* 107.4, pp. 255–278.

Strbac, Goran, Danny Pudjianto, Marko Aunedi, Predrag Djapic, Fei Teng, Xi Zhang, Hossein Ameli, Roberto Moreira, and Nigel Brandon (2020). "Role and value of flexibility in facilitating cost-effective energy system decarbonisation". In: *Progress in Energy* 2.4, p. 042001.

Sui, Chung-Hsiung, Pei-Hsuan Chung, and Tim Li (2007). "Interannual and interdecadal variability of the summertime western North Pacific subtropical high". In: *Geophysical Research Letters* 34.11.

Sun, Qiaohong, Chiyuan Miao, Qingyun Duan, Hamed Ashouri, Soroosh Sorooshian, and Kuo-Lin Hsu (2018). "A review of global precipitation data sets: Data sources, estimation, and intercomparisons". In: *Reviews of Geophysics* 56.1, pp. 79–107.

Surendran, Sajani, Sulochana Gadgil, PA Francis, and M Rajeevan (2015). "Prediction of Indian rainfall during the summer monsoon season on the basis of links with equatorial Pacific and Indian Ocean climate indices". In: *Environmental Research Letters* 10.9, p. 094004.

Šúri, Marcel, Thomas A Huld, Ewan D Dunlop, and Heinz A Ossenbrink (2007). "Potential of solar electricity generation in the European Union member states and candidate countries". In: *Solar energy* 81.10, pp. 1295–1305.

Suzlon (2023). *Suzlon secures order for their 3 MW series turbines from Juniper Green Energy Private Limited of 50.4 MW*. Online. Available at: https://www.suzlon.com/press-release-detail/450/suzlon-secures-order-for-their-3-mw-series-turbines-from-juniper-green-energy-private-limited-of-504-mw. Accessed: 20th November 2023.

Swisher, Philip, Juan Pablo Murcia Leon, Juan Gea-Bermúdez, Matti Koivisto, Helge Aagaard Madsen, and Marie Münster (2022). "Competitiveness of a low specific power, low cut-out wind speed wind turbine in North and Central Europe towards 2050". In: *Applied Energy* 306, p. 118043.

TATA (2017). *Solar today July-September 2017*. Online. Available at: `https://www.tatapowersolar.com/wp-content/uploads/2018/01/02052435/Feature-Solar-Tracker.pdf`. Accessed: 2nd October 2022.

Taylor, James W and Roberto Buizza (2003). "Using weather ensemble predictions in electricity demand forecasting". In: *International Journal of forecasting* 19.1, pp. 57–70.

TERI (2019). *Policy Paper on Solar PV Manufacturing in India: Silicon Ingot and Wafer - PV Cell - PV Module.*

Thornton, Hazel Elizabeth, AA Scaife, BJ Hoskins, DJ Brayshaw, DM Smith, Nick Dunstone, Nicky Stringer, and Philip E Bett (2019). "Skilful seasonal prediction of winter gas demand". In: *Environmental Research Letters* 14.2, p. 024009.

Torralba, Verónica, Francisco J Doblas-Reyes, and Nube Gonzalez-Reviriego (2017a). "Uncertainty in recent near-surface wind speed trends: a global reanalysis intercomparison". In: *Environmental Research Letters* 12.11, p. 114019.

Torralba, Verónica, Francisco J Doblas-Reyes, Dave MacLeod, Isadora Christel, and Melanie Davis (2017b). "Seasonal climate prediction: a new source of information for the management of wind energy resources". In: *Journal of Applied Meteorology and Climatology* 56.5, pp. 1231–1247.

Tourre, Yves M and Warren B White (1995). "ENSO signals in global upper-ocean temperature". In: *Journal of Physical Oceanography* 25.6, pp. 1317–1332.

Trenberth, Kevin E (1997). "The definition of El Niño". In: *Bulletin of the American Meteorological Society* 78.12, pp. 2771–2778.

Trenberth, Kevin E, Toshio Koike, and Kazutoshi Onogi (2008). "Progress and prospects for reanalysis for weather and climate". In: *Eos, Transactions American Geophysical Union* 89.26, pp. 234–235.

Troccoli, Alberto (2010). "Seasonal climate forecasting". In: *Meteorological Applications* 17.3, pp. 251–268.

– (2018). *Weather & Climate Services for the Energy Industry*. Springer Nature.

Troccoli, Alberto, Mike Harrison, David LT Anderson, and Simon J Mason (2008). *Seasonal climate: forecasting and managing risk*. Vol. 82. Springer Science & Business Media.

Ueckerdt, Falko, Robert Brecha, Gunnar Luderer, Patrick Sullivan, Eva Schmid, Nico Bauer, Diana Böttger, and Robert Pietzcker (2015). "Representing power sector variability and the integration of variable renewables in long-term energy-economy models using residual load duration curves". In: *Energy* 90, pp. 1799–1814.

UNFCCC (1992). *United Nations Framework Convention on Climate Change*. Online. Available at: `https://unfccc.int/resource/docs/convkp/conveng.pdf` Accessed: 11th September 2021.

– (2010). *The Cancun Agreements FCCC/CP/2010/7/Add.1.* Online. Available at: `https://unfccc.int/sites/default/files/resource/docs/2010/cop16/eng/07a01.pdf` Accessed: 11th September 2021.

– (2015). *Adoption of the Paris Agreement FCCC/CP/2015/10/Add.1.* Online. Available at: `https://www.un.org/en/development/desa/population/migration/generalassembly/docs/globalcompact/FCCC_CP_2015_10_Add.1.pdf` Accessed: 11th September 2021.

Urraca, Ruben, Thomas Huld, Ana Gracia-Amillo, Francisco Javier Martinez-de-Pison, Frank Kaspar, and Andres Sanz-Garcia (2018). "Evaluation of global horizontal irradiance estimates from ERA5 and COSMO-REA6 reanalyses using ground and satellite-based data". In: *Solar Energy* 164, pp. 339–354.

Van Beek, Lisette, Maarten Hajer, Peter Pelzer, Detlef van Vuuren, and Christophe Cassen (2020). "Anticipating futures through models: the rise of Integrated Assessment Modelling in the climate science-policy interface since 1970". In: *Global Environmental Change* 65, p. 102191.

Van Vuuren, Detlef P, Elke Stehfest, David EHJ Gernaat, Maarten Van Den Berg, David L Bijl, Harmen Sytze De Boer, Vassilis Daioglou, Jonathan C Doelman, Oreane Y Edelenbosch, Mathijs Harmsen, et al. (2018). "Alternative pathways to the 1.5 C target reduce the need for negative emission technologies". In: *Nature Climate Change* 8.5, pp. 391–397.

Vandal, Thomas, Evan Kodra, Sangram Ganguly, Andrew Michaelis, Ramakrishna Nemani, and Auroop R Ganguly (2017). "Deepsd: Generating high resolution climate change projections

through single image super-resolution". In: *Proceedings of the 23rd international conference on knowledge discovery and data mining*, pp. 1663–1672.

Vautard, Robert, Julien Cattiaux, Pascal Yiou, Jean-Noël Thépaut, and Philippe Ciais (2010). "Northern Hemisphere atmospheric stilling partly attributed to an increase in surface roughness". In: *Nature Geoscience* 3.11, pp. 756–761.

VDMA (2022). *International Technology Roadmap for Photovoltaic (ITRPV) 2021 Results*.

Villena-Ruiz, R, F Javier Ramirez, A Honrubia-Escribano, and E Gómez-Lázaro (2018). "A techno-economic analysis of a real wind farm repowering experience: The Malpica case". In: *Energy conversion and management* 172, pp. 182–199.

Vinoj, V, Philip J Rasch, Hailong Wang, Jin-Ho Yoon, Po-Lun Ma, Kiranmayi Landu, and Balwinder Singh (2014). "Short-term modulation of Indian summer monsoon rainfall by West Asian dust". In: *Nature Geoscience* 7.4, pp. 308–313.

Vishnu, S, WR Boos, PA Ullrich, and TA O'brien (2020). "Assessing historical variability of South Asian monsoon lows and depressions with an optimized tracking algorithm". In: *Journal of Geophysical Research: Atmospheres* 125.15, e2020JD032977.

Vitart, Frédéric et al. (2019). "Extended-range prediction". In: *ECMWF Technical Memoranda* 854.

Von Storch, Hans, Eduardo Zorita, and Ulrich Cubasch (1993). "Downscaling of global climate change estimates to regional scales: an application to Iberian rainfall in wintertime". In: *Journal of Climate* 6.6, pp. 1161–1171.

Walker, Dean P, Cathryn E Birch, John H Marsham, Adam A Scaife, Richard J Graham, and Zewdu T Segele (2019). "Skill of dynamical and GHACOF consensus seasonal forecasts of East African rainfall". In: *Climate Dynamics* 53, pp. 4911–4935.

Walker, GT and EW Bliss (1932). "Memoirs of the Royal Meteorological Society". In: *World weather V* 4, pp. 53–84.

Wang, Bin (2006). *The Asian monsoon*. Springer Science & Business Media.

Wang, Bin and Zhen Fan (1999). "Choice of South Asian summer monsoon indices". In: *Bulletin of the American Meteorological Society* 80.4, pp. 629–638.

Wang, Bin, In-Sik Kang, and Jagadish Shukla (2006). "Dynamic seasonal prediction and predictability of the monsoon". In: *The Asian Monsoon*, pp. 585–612.

Wang, Bin, June-Yi Lee, and Baoqiang Xiang (2015a). "Asian summer monsoon rainfall predictability: a predictable mode analysis". In: *Climate Dynamics* 44, pp. 61–74.

Wang, Bin, Renguang Wu, and Xiouhua Fu (2000). "Pacific–East Asian teleconnection: how does ENSO affect East Asian climate?" In: *Journal of Climate* 13.9, pp. 1517–1536.

Wang, Bin, Renguang Wu, and KM Lau (2001). "Interannual variability of the Asian summer monsoon: Contrasts between the Indian and the western North Pacific–East Asian monsoons". In: *Journal of Climate* 14.20, pp. 4073–4090.

Wang, Bin, Renguang Wu, and TIM Li (2003). "Atmosphere–warm ocean interaction and its impacts on Asian–Australian monsoon variation". In: *Journal of Climate* 16.8, pp. 1195–1211.

Wang, Bin, Baoqiang Xiang, and June-Yi Lee (2013). "Subtropical high predictability establishes a promising way for monsoon and tropical storm predictions". In: *Proceedings of the National Academy of Sciences* 110.8, pp. 2718–2722.

Wang, Bin, Baoqiang Xiang, Juan Li, Peter J Webster, Madhavan N Rajeevan, Jian Liu, and Kyung-Ja Ha (2015b). "Rethinking Indian monsoon rainfall prediction in the context of recent global warming". In: *Nature communications* 6.1, p. 7154.

Wang, Bin, Jing Yang, Tianjun Zhou, and Bin Wang (2008). "Interdecadal changes in the major modes of Asian–Australian monsoon variability: Strengthening relationship with ENSO since the late 1970s". In: *Journal of Climate* 21.8, pp. 1771–1789.

Wang, Lei, Mingfang Ting, and PJ Kushner (2017). "A robust empirical seasonal prediction of winter NAO and surface climate". In: *Scientific reports* 7.1, p. 279.

Wang, Pinxian, Steven Clemens, Luc Beaufort, Pascale Braconnot, Gerald Ganssen, Zhimin Jian, Peter Kershaw, and Michael Sarnthein (2005). "Evolution and variability of the Asian monsoon system: state of the art and outstanding issues". In: *Quaternary Science Reviews* 24.5-6, pp. 595–629.

Webster, Peter J, Vo Oo Magana, TN Palmer, J Shukla, RA Tomas, MU Yanai, and T Yasunari (1998). "Monsoons: Processes, predictability, and the prospects for prediction". In: *Journal of Geophysical Research: Oceans* 103.C7, pp. 14451–14510.

Webster, Peter J and Song Yang (1992). "Monsoon and ENSO: Selectively interactive systems". In: *Quarterly Journal of the Royal Meteorological Society* 118.507, pp. 877–926.

Weigel, Andreas P, Mark A Liniger, and Christof Appenzeller (2009). "Seasonal ensemble forecasts: are recalibrated single models better than multimodels?" In: *Monthly Weather Review* 137.4, pp. 1460–1479.

Weisheimer, Antje and Timothy N Palmer (2014). "On the reliability of seasonal climate forecasts". In: *Journal of the Royal Society Interface* 11.96, p. 20131162.

Weisheimer, Antje, Timothy N Palmer, and Francisco J Doblas-Reyes (2011). "Assessment of representations of model uncertainty in monthly and seasonal forecast ensembles". In: *Geophysical Research Letters* 38.16.

White, Christopher J, Henrik Carlsen, Andrew W Robertson, Richard JT Klein, Jeffrey K Lazo, Arun Kumar, Frederic Vitart, Erin Coughlan de Perez, Andrea J Ray, Virginia Murray, et al. (2017). "Potential applications of subseasonal-to-seasonal (S2S) predictions". In: *Meteorological Applications* 24.3, pp. 315–325.

White, Christopher J, Daniela IV Domeisen, Nachiketa Acharya, Elijah A Adefisan, Michael L Anderson, Stella Aura, Ahmed A Balogun, Douglas Bertram, Sonia Bluhm, David J Brayshaw, et al. (2022). "Advances in the application and utility of subseasonal-to-seasonal predictions". In: *Bulletin of the American Meteorological Society* 103.6, E1448–E1472.

Widén, Joakim, Nicole Carpman, Valeria Castellucci, David Lingfors, Jon Olauson, Flore Remouit, Mikael Bergkvist, Mårten Grabbe, and Rafael Waters (2015). "Variability assessment and forecasting of renewables: A review for solar, wind, wave and tidal resources". In: *Renewable and Sustainable Energy Reviews* 44, pp. 356–375.

Wilby, Robert L and Thomas ML Wigley (1997). "Downscaling general circulation model output: a review of methods and limitations". In: *Progress in physical geography* 21.4, pp. 530–548.

Wild, Martin, Hans Gilgen, Andreas Roesch, Atsumu Ohmura, Charles N Long, Ellsworth G Dutton, Bruce Forgan, Ain Kallis, Viivi Russak, and Anatoly Tsvetkov (2005). "From dimming to brightening: Decadal changes in solar radiation at Earth's surface". In: *Science* 308.5723, pp. 847–850.

Wild, Martin, Barbara Trüssel, Atsumu Ohmura, Charles N Long, Gert König-Langlo, Ellsworth G Dutton, and Anatoly Tsvetkov (2009). "Global dimming and brightening: An update beyond 2000". In: *Journal of Geophysical Research: Atmospheres* 114.D10.

Wilks, Daniel S (2011). *Statistical methods in the atmospheric sciences*. Vol. 100. Academic press.

Willson, Richard C (1997). "Total solar irradiance trend during solar cycles 21 and 22". In: *Science* 277.5334, pp. 1963–1965.

WMO (1979). *World Climate Conference - Declaration and supporting documents*. World Meteorological Organization (WMO).

– (2020). *Guidance on operational practices for objective seasonal forecasting. WMO-No. 1246*.

Wohland, Jan, David Brayshaw, Hannah Bloomfield, and Martin Wild (2020). "European multidecadal solar variability badly captured in all centennial reanalyses except CERA20C". In: *Environmental Research Letters* 15.10, p. 104021.

Wohland, Jan, Nour-Eddine Omrani, Dirk Witthaut, and Noel S Keenlyside (2019). "Inconsistent wind speed trends in current twentieth century reanalyses". In: *Journal of Geophysical Research: Atmospheres* 124.4, pp. 1931–1940.

Wu, Jian, Jinlin Zha, Deming Zhao, and Qidong Yang (2018). "Changes in terrestrial near-surface wind speed and their possible causes: an overview". In: *Climate Dynamics* 51.5-6, pp. 2039–2078.

WU, Minmin and Lei Wang (2019). "Enhanced correlation between ENSO and western North Pacific monsoon during boreal summer around the 1990s". In: *Atmospheric and Oceanic Science Letters* 12.5, pp. 376–384.

Wu, Renguang and Ben P Kirtman (2004). "The tropospheric biennial oscillation of the monsoon–ENSO system in an interactive ensemble coupled GCM". In: *Journal of Climate* 17.8, pp. 1623–1640.

Wu, Tongwen, Rucong Yu, Yixiong Lu, Weihua Jie, Yongjie Fang, Jie Zhang, Li Zhang, Xiaoge Xin, Laurent Li, Zaizhi Wang, et al. (2020). "BCC-CSM2-HR: a high-resolution version of the Beijing Climate Center Climate System Model". In: *Geoscientific Model Development Discussions* 2020, pp. 1–64.

Wu, Zhiwei, Bin Wang, Jianping Li, and Fei-Fei Jin (2009). "An empirical seasonal prediction model of the East Asian summer monsoon using ENSO and NAO". In: *Journal of Geophysical Research: Atmospheres* 114.D18.

Xie, Shang-Ping, Kaiming Hu, Jan Hafner, Hiroki Tokinaga, Yan Du, Gang Huang, and Takeaki Sampe (2009). "Indian Ocean capacitor effect on Indo–western Pacific climate during the summer following El Niño". In: *Journal of Climate* 22.3, pp. 730–747.

Xie, Shang-Ping, Yu Kosaka, Yan Du, Kaiming Hu, Jasti S Chowdary, and Gang Huang (2016). "Indo-western Pacific Ocean capacitor and coherent climate anomalies in post-ENSO summer: A review". In: *Advances in Atmospheric Sciences* 33.4, pp. 411–432.

Yadav, Amit Kumar and SS Chandel (2013). "Tilt angle optimization to maximize incident solar radiation: A review". In: *Renewable and Sustainable Energy Reviews* 23, pp. 503–513.

Yang, Jiangyan, Bingqi Yi, Shuai Wang, Yushan Liu, and Yuxiao Li (2022). "Diverse cloud and aerosol impacts on solar photovoltaic potential in southern China and northern India". In: *Scientific Reports* 12.1, p. 19671.

Yang, Jianling, Qinyu Liu, Shang-Ping Xie, Zhengyu Liu, and Lixin Wu (2007). "Impact of the Indian Ocean SST basin mode on the Asian summer monsoon". In: *Geophysical Research Letters* 34.2.

Yang, Song and KM Lau (1998). "Influences of sea surface temperature and ground wetness on Asian summer monsoon". In: *Journal of Climate* 11.12, pp. 3230–3246.

Yang, Song, Zhenning Li, Jin-Yi Yu, Xiaoming Hu, Wenjie Dong, and Shan He (2018). "El Niño–Southern Oscillation and its impact in the changing climate". In: *National Science Review* 5.6, pp. 840–857.

Yang, Xianke and Ping Huang (2021). "Restored relationship between ENSO and Indian summer monsoon rainfall around 1999/2000". In: *The Innovation* 2.2.

Yasunari, Tetsuzo (1979). "Cloudiness fluctuations associated with the Northern Hemisphere summer monsoon". In: *Journal of the Meteorological Society of Japan. Ser. II* 57.3, pp. 227–242.

Yu, Jiang, Tianjun Zhou, and Zhihong Jiang (2020). "Interannual variability of the summer wind energy over China: A comparison of multiple datasets". In: *Wind Energy* 23.8, pp. 1726–1738.

Yu, Lejiang, Shiyuan Zhong, Xindi Bian, and Warren Heilman (2015). "Temporal and spatial variability of wind resources in the United States as derived from the climate forecast system reanalysis". In: *Journal of Climate* 28.3, pp. 1166–1183.

Yu, Shi-Yun, Lei Fan, Yu Zhang, Xiao-Tong Zheng, and Ziguang Li (2021). "Reexamining the Indian summer monsoon rainfall–ENSO relationship from its recovery in the 21st century: Role of the Indian Ocean SST anomaly associated with types of ENSO evolution". In: *Geophysical Research Letters* 48.12, e2021GL092873.

Zeng, Zhenzhong, Shilong Piao, Laurent ZX Li, Philippe Ciais, Yue Li, Xitian Cai, Long Yang, Maofeng Liu, and Eric F Wood (2018). "Global terrestrial stilling: does Earth's greening play a role?" In: *Environmental Research Letters* 13.12, p. 124013.

Zeng, Zhenzhong, Alan D Ziegler, Timothy Searchinger, Long Yang, Anping Chen, Kunlu Ju, Shilong Piao, Laurent ZX Li, Philippe Ciais, Deliang Chen, et al. (2019). "A reversal in global terrestrial stilling and its implications for wind energy production". In: *Nature Climate Change* 9.12, pp. 979–985.

Zhang, Daquan, Gill M Martin, José M Rodríguez, Zongjian Ke, and Lijuan Chen (2020). "Predictability of the Western North Pacific Subtropical high associated with different ENSO phases in GloSea5". In: *Journal of Meteorological Research* 34.5, pp. 926–940.

Zhang, Gangfeng, Cesar Azorin-Molina, Xuejia Wang, Deliang Chen, Tim R McVicar, Jose A Guijarro, Adrian Chappell, Kaiqiang Deng, Lorenzo Minola, Feng Kong, et al. (2022). "Rapid urbanization induced daily maximum wind speed decline in metropolitan areas: A case study in the Yangtze River Delta (China)". In: *Urban Climate* 43, p. 101147.

Zhang, Ting, Bo Tian, Dhritiraj Sengupta, Lei Zhang, and Yali Si (2021). "Global offshore wind turbine dataset". In: *Scientific Data* 8.1, p. 191.

Zhang, Xiaotong, Shunlin Liang, Guoxin Wang, Yunjun Yao, Bo Jiang, and Jie Cheng (2016). "Evaluation of the reanalysis surface incident shortwave radiation products from NCEP, ECMWF, GSFC, and JMA using satellite and surface observations". In: *Remote Sensing* 8.3, p. 225.

Zhao, Mei and Harry H Hendon (2009). "Representation and prediction of the Indian Ocean dipole in the POAMA seasonal forecast model". In: *Quarterly Journal of the Royal Meteorological Society* 135.639, pp. 337–352.

Zhu, Zaichun, Shilong Piao, Ranga B Myneni, Mengtian Huang, Zhenzhong Zeng, Josep G Canadell, Philippe Ciais, Stephen Sitch, Pierre Friedlingstein, Almut Arneth, et al. (2016). "Greening of the Earth and its drivers". In: *Nature Climate Change* 6.8, pp. 791–795.

Zorita, Eduardo and Hans Von Storch (1999). "The analog method as a simple statistical downscaling technique: Comparison with more complicated methods". In: *Journal of Climate* 12.8, pp. 2474–2489.